2019

Substrate Identification of an Oncogenic Kinase: Elucidating the Pathogenesis of a Rare Liver Cancer

Melissa Jarmel

SUBSTRATE IDENTIFICATION OF AN ONCOGENIC KINASE: ELUCIDATING THE PATHOGENESIS OF A RARE LIVER CANCER

A Thesis Presented to the Faculty of

The Rockefeller University

in Partial Fulfillment of the Requirements for

the degree of Doctor of Philosophy

by

Melissa Jarmel

June 2019

SUBSTRATE IDENTIFICATION OF AN ONCOGENIC KINASE: ELUCIDATING THE PATHOGENESIS OF A RARE LIVER CANCER

Melissa Jarmel, Ph.D.

The Rockefeller University 2019

Fibrolamellar Hepatocellular Carcinoma (FLC) is a rare liver cancer with limited treatment options. This cancer primarily affects adolescents and young adults. Our lab has identified a new fusion gene in this cancer called *DNAJB1-PRKACA* that results from a break and re-fusion in chromosome 19. This chimeric gene results in a fusion kinase that acts as the driver of this cancer. While we have shown that the kinase activity of the fusion protein is essential for transformation, it is not currently known whether the oncogenic kinase that results from this fusion event, DNAJB1-PRKACA, phosphorylates the same substrates as PRKACA, the protein product of *PRKACA*. While the total phosphoproteome of a cancer can implicate critical pathway changes in the tumor versus healthy tissue, it cannot provide sufficient information on what kinase is directly responsible for the phosphorylations. Knowing which proteins DNAJB1-PRKACA is directly phosphorylating in the liver could help elucidate a step-wise mechanism for understanding the pathogenesis. Furthermore, it could provide new potential therapeutic options by targeting the downstream pathways of this oncogenic kinase.

In this thesis, I will first describe my work to determine a method of directly identifying proteins that are substrates of DNAJB1-PRKACA and PRKACA. I first tested an approach developed by the Shokat Lab that uses an analog-sensitive (AS) kinase in combination with a selective adenosine triphosphate (ATP) analog to identify unique substrates of a kinase. However, serious concerns of substrate specificity of the AS-kinases were raised as I developed AS versions of DNAJB1-PRKACA and PRKACA. I pivoted to a method that kills the endogenous kinase activity of a lysate using 5'-(4-Fluorosulfonylbenzoyl)adenosine (FSBA); kinase reactions are performed using this kinase-inactive lysate with the purified active kinase of interest and an ATP analog that has a tag on the γ-phosphate. This results in substrates with a specific thiol tag. The ATP-γ-S analog I initially used for this method was effective in visualizing kinase activity changes via western blots, but the thiol-tags were not reliably identified using MS. With the improvement of phosphopeptide enrichment methods and encouragement from the Proteomics Resource Center, a pilot experiment was designed to enrich phosphopeptides from a kinase reaction using regular ATP, FSBA-treated mouse liver lysate, and either PRKACA or DNAJB1-PRKACA. The results of this pilot experiment showed promising differences in substrate specificity between PRKACA and DNAJB1-PRKACA so I moved forward with this assay using human hepatocyte lysate instead of mouse liver lysate.

In the third chapter, I will discuss the results of the assay using kinase-inactive human hepatocyte lysate in kinase reactions to determine substrate differences between three kinases: DNAJB1-PRKACA, PRKACA, and PRKACA (L206R).

PRKACA (L206R) is a PRKACA variant found in adrenal tumors of patients with Cushing's disease. The L206R mutation is thought to block interaction with the regulatory subunit and pathogenesis of the adrenal tumors has been accepted to be the result of constitutive activity of this mutant catalytic subunit. Recently, two papers have suggested that there is an alteration in substrate specificity between PRKACA and PRKACA (L206R). My results demonstrate that there are differences in substrates that are directly phosphorylated by each of the three catalytic subunits: PRKACA, J-PRKACA, and PRKACA (L206R).

Finally, I will discuss how the results of a total phosphome study of FLC patient tumor and normal samples compared against my *in vitro* substrate identification assay. This comparison created a more patient-relevant and focused list of direct substrates of DNAJB1-PRKACA for further study. The thesis will conclude with discussion of the implications for the pathogenesis of FLC based on the direct substrates of interest found in these experiments and future experiments.

To Kay and Gary Jarmel, who guide my every step forward.

I miss you always.

Acknowledgements

I would like to say thank you to my advisor, Sandy, whose love for science and all things curious has been infectious and encouraging to be around. It has been a privilege to work with you on such a motivating topic these last few years. I'll forever be grateful for the support you gave me to take care of my family and for the experiences you've given me to grow into the scientist I am today.

I also want to say thank you to the former and current members of the Simon Lab who have made the last six years at Rockefeller a truly unforgettable experience. I will dearly miss our google searches, secret winter friend gift exchanges, and stimulating conversations. A special shout out to Bassem and Solomon, who have warmed my heart over the last year by keeping me out the cold room by sharing the fruits of your protein labor. And also to Kate and Xiao who provided thoughtful feedback and edits on my dissertation. Y'all are champs.

The Resource Centers at Rockefeller are truly wonderful collaborative experiences. I would specifically like to say thank you to Lavo at the High Throughput Spectroscopy Resource Center. Your brilliance is only matched by your kindness, and it has been a joy to work with you. Also, a huge thank you to Soren Heissel at the Proteomics Resource Center. This thesis work simply could not have happened without you, and I will always be grateful for your contributions. Your thoroughness and thoughtfulness are greatly appreciated. As are your chats and cups of coffee. Rockefeller is really lucky to have you.

Thank you to my thesis committee members, Shai Shaham and Charlie Rice. Your support, guidance, and insight as my project has evolved will always be cherished. A special thank you to Charlie for introducing me to a collaboration with Lefteris and Ype. This really helped take my project to the next level. And to my external examiner, Angus Nairn, thank you for giving of your time and expertise.

Importantly, I would also like to extend my thanks to everyone at the Dean's office. You all care for the graduate students so clearly and make doing a PhD at Rockefeller as easy as grad school could be. Thank you so much for that. A very special thank you to Cris for always going the extra mile to help us out when we're in a jam. You are a gem. And to Andrea: thank you for being someone who has always made me feel heard and seen. You are a gift, to me and to the Rockefeller community.

My undergraduate research experiences at the University of Texas at Austin and the University of Pennsylvania are why I came to graduate school. Thank you to everyone who helped make those experiences truly wonderful. Particularly to Anne Tibbetts and Arnaldo Diaz, who always believed in me.

And, of course, I would like to say thank you to my friends and family. My home team who always has my back and loves me so well. Thank you to Chris and Marie for everything always, but I want to say thanks here for providing me with such a wonderful environment to get the bulk of this dissertation written. And Adam, I think our parents would be proud of where we are today. Thank you for all of your support that has carried me through the end of this chapter. I love you as much as a sister possibly could.

And last, but certainly not least, to my parents. You are both still my inspiration in every minute of every day. Thank you for fostering my curiosity. Who would have guessed it would have led us here?

Table of Contents

LIST OF FIGURES

LIST OF TABLES

LIST OF ABBREVIATIONS

AS	Analog-sensitive
ATP	Adenosine triphosphate
cAMP	cyclic adenosine 3',5'-monophosphate
DNAJB1	Gene of DnaJ heat shock protein family (Hsp40) member B1
DNAJB1-PRKACA	Gene of fusion found in FLC that leads to functional kinase
FLC	Fibrolamellar Hepatocellular Carcinoma
FSBA	5'-(4-Fluorosulfonylbenzoyl)adenosine
GO	Gene Ontology
GST	Glutathione S-transferase
HCC	Hepatocellular Carcinoma
IP	Immunoprecipitation
IPTG	isopropyl β-D-1-thiogalactopyranoside
K-BILDS	Kinase-catalyzed Biotinylation with Inactivated Lysates for Discovery of Substrates
KEGG	Kyoto Encyclopedia of Genes and Genomes
KESTREL	Kinase Substrate Tracking and Elucidation
KISS	Kinase-Interacting Substrate Screening
MIG6	Mitogen-inducible gene 6 (tumor suppressor)
MS	Mass spectrometry
NMR	Nuclear Magnetic Resonance
PDX	Patient Derived Xenograft
PKA	Protein Kinase A, usually referring to the tetrameric holoenzyme
PNBM	p-Nitrobenzyl mesylate
PRKACA (L206R)	Single point mutation PRKACA variant found in adrenal tumors of patients with Cushing's disease
PRKACA	Protein Kinase cAMP-Activated Catalytic Subunit Alpha
PKI	Protein Kinase Inhibitor
RSV	Rous Sarcoma Virus
SEER	Surveillance, Epidemiology, and End Results program
TEV	Tobacco Etch Virus protease
Thio	Thiophosphate Ester Group Identified by MS
TP53	Tumor protein p53
TPE D	Degraded Thiophosphate Ester Group Identified by MS
WHO	World Health Organization

CHAPTER I: INTRODUCTION

Rationale for Thesis Work

In just the last fifty years, our understanding of what causes cancer and how to study and treat it has dramatically changed. One of the paradigm shifts in cancer research came with the discovery of oncogenes, genes that have the potential to transform healthy cells into cancer cells (Stehelin et al. 1976; Shih et al. 1979; Wang et al. 1976; Tabin et al. 1982). Oncogenes can arise because of misregulation of gene expression, mutations within a gene, or chromosomal abnormalities like gene duplications or gene fusions (Esquela-Kerscher and Slack 2006; Croce 2009; Bargmann et al. 1986; Herter-Sprie et al. 2013; Clark et al. 2002; Rowley 1973; Yu et al. 2019; Giam and Rancati 2015).

Since DNA damage increases with age (Freitas and de Magalhães 2011; Soares et al. 2014), it is difficult to find a specific oncogenic driver responsible for an adult cancer because it is likely caused by multiple mutations (Vogelstein et al. 1988; Vogelstein and Kinzler 1993). However, cancers that affect young people, while rarer in occurrence, also have fewer mutations in their DNA due to age. Thus, when a specific genetic driver can be identified in a cancer of a young person, it becomes possible to identify the process of pathogenesis of this cancer due to a more defined genetic event. While each cancer is unique in its pathogenesis, cancers share hallmarks that take advantage of similar pathways to maximize growth and metastasis (Hanahan and Weinberg 2000; Hanahan and Weinberg 2011). By better understanding the players in the pathways that contribute to these hallmarks of cancer, more effective therapeutic

options could be developed that could apply across multiple cancer types that share pathway similarities. In this way, studying a rare cancer that affects young people that has a specific genetic driver provides a unique opportunity to probe at the pathogenesis of not only the rare cancer but also the biology of common pathways critical for the development of other cancers. Fibrolamellar Hepatocellular Carcinoma (FLC) is one of these rare cancers.

FLC is a rare liver cancer that primarily affects adolescents and young adults; there is a single common genetic alteration found in more than 350 confirmed FLC tumors to date since the discovery of this gene fusion in this cancer in 2014 (Honeyman et al. 2014). The fusion event results from a break in chromosome 19. This event links the first exon of a heat shock protein, *DNAJB1,* to exons 2-10 of the catalytic subunit of Protein Kinase A, *PRKACA*. This break occurs in the absence of any other recurrent alterations in the DNA (Darcy et al. 2015). In collaboration with Scott Lowe's lab, we found that FLC-like tumors formed after CRISPR-Cas9 genome editing was used to recreate the fusion event in mice, with similar results found by others in different mouse strains (Engelholm et al. 2017). This indicates that the deletion is sufficient to produce the tumor, but it does not distinguish if this occurs because of the formation of the fusion gene or the loss of genes on the chromosome that results from the fusion event. To address this, *DNAJB1-PRKACA* was overexpressed using transposon-mediated somatic gene transfer. Tumors did not form when *PRKACA* was overexpressed nor when *DNAJB1-PRKACA* was expressed with a point mutation to kill its kinase activity (Kastenhuber et al. 2017), leading us to confidently say that DNAJB1-PRKACA is the oncogenic driver for FLC.

It is not currently known whether the resulting oncogenic kinase, DNAJB1-PRKACA, phosphorylates the same substrates as PRKACA, the protein product of *PRKACA*. Total phosphoproteome studies of FLC could implicate critical pathway changes in the tumor versus healthy tissue, but they could not provide sufficient information to determine what is being directly phosphorylated by a particular kinase. The changes seen could be the result of downstream effects from the primary changes made by DNAJB1-PRKACA. Knowing what DNAJB1-PRKACA is directly phosphorylating in the liver could help elucidate a step-wise mechanism for how the presence of DNAJB1-PRKACA leads to the development of FLC, as well as provide new potential therapeutic options by targeting the downstream pathways of this oncogenic kinase. Our lab has many modes to study FLC, including a repository of over a hundred patient samples, various cell lines expressing the oncogene, relevant genetically-engineered mice, Patient Derived Xenografts (PDX), FLC cells derived from PDX, and organoids; this provides a robust system to further investigate any targets of the oncogenic kinase that are identified. Additionally, identifying specific phosphorylation sites of many substrates is now possible with advancements in molecular biology and mass spectrometry (Dephoure et al. 2013). This thesis describes an effort to identify the direct substrates of DNAJB1-PRKACA that are relevant to the pathogenesis of FLC.

A Brief History of Cancer Biology

Cancer is an umbrella term for a group of diseases linked by the characterization of out of control growth of a cell in one part of the body that can metastasize to surrounding tissues. It is currently the second leading cause of death in the United States, and more than 1.7 million new cancer diagnoses and 600,000 cancer deaths are projected to occur in 2019 in the United States alone (Siegel et al. 2019). While these numbers indicate a still pressing need for further research and treatments, the cancer death rate has dropped 27% between 1991 and 2016 due to improvements in prevention and treatment methods, resulting in more than 2.6 million fewer deaths by cancer than would have been predicted by the death rate at its peak (Siegel et al. 2019).

Our understanding of what causes cancer has solidified considerably since the start of the twentieth century. The first case reported of a possible environmental cancer was by Percival Pott in 1775 who observed scrotal skin cancer in chimney sweeps (Brown and Thornton 1957). However, it was not until 1933 that the chemical responsible for this cancer, benzo(a)pyrene, was identified as the first known carcinogen, or cancer-causing substance. This is also the carcinogen found in cigarette smoke which is clearly linked to lung cancer (Doll and Hill 1950; Wynder and Graham 1950; Cornfield et al. 2009). Public health education campaigns have increased awareness of this established link and likely contributed to the downward trend of new lung cancer cases today (Rodu and Cole 2002; Siegel et al. 2019).

In 1910 and 1911, Rockefeller scientist Peyton Rous published consecutive papers about the results of an experiment where he was able to transmit cancer from a

hen with a tumor to a healthy chicken, hypothesizing that a virus from the cancer in the hen was responsible for the transmission (Rous 1910; Rous 1911). Despite other independent research in Denmark by Ellerman and Bang and in Japan by Fujinami and Inamoto showing cell-free filtrates with transforming capabilities in chickens at the time, the scientific community did not accept this theory for a few decades since Rous' attempts to repeat his results in mammals were unsuccessful (Weiss and Vogt 2011). However, a strain of this Rous Sarcoma Virus (RSV) was shown to be able to produce tumors in rats in the late 1950s (Svet-Moldavsky 1957; Svet-Moldavsky 1958). Soon after, Howard Temin identified the first transformation mutants of RSV and noted that RSV with different mutations determined the various shapes of the cells they infected; this led him to state, "Thus, the virus becomes equivalent to a cellular gene controlling cell morphology" (Temin 1960). Peyton Rous received the Nobel Prize in Physiology or Medicine fifty-six years after his publication for his discovery of tumor-inducing viruses.

Another cause for cancer was suggested in an epidemiological study in the 1960s by Li and Fraumeni on the families of rhabdomyosarcoma patients with siblings or cousins that also had a sarcoma early in life; they hypothesized that cancer could be inherited (Li and Fraumeni 1969). We now know that this syndrome is due to an inheritance of an autosomal dominant mutation in a tumor suppressor known as *TP53* (Malkin et al. 1990). While hereditary cancers are rarer, we are aware of more of them now which allows for better monitoring and preventative options for people at risk (Parkes et al. 2017; Willoughby et al. 2019; Lahiri Batra 2019).

The discovery of oncogenes in the 1970s connected these three theories of what causes cancer (Stehelin et al. 1976; Shih et al. 1979; Wang et al. 1976; Tabin et al.

1982): a gene that has the capability to transform a healthy cell into a tumor cell. Even the oncogenic RSV was found to have a gene of cellular origin that the virus had previously acquired that had the potential to become an oncogene: Src (Stehelin et al. 1977; Ottenhoff-Kalff et al. 1992; Aligayer et al. 2002; Wheeler et al. 2009). We now know that mutations with a gene, faulty gene expression, or chromosomal abnormalities can give rise to oncogenes (Esquela-Kerscher and Slack 2006; Croce 2009; Bargmann et al. 1986; Herter-Sprie et al. 2013; Clark et al. 2002; Rowley 1973; Yu et al. 2019; Giam and Rancati 2015).

We also know that for most adult cancers, multiple genetic changes need to occur for a cancer to develop (Vogelstein et al. 1988; Vogelstein and Kinzler 1993), and that cancers develop more mutations over time, or evolve, which contributes to drug-resistance (Lipinski et al. 2016). The 1990s saw an explosion of cancer research leading to the seminal review of the hallmarks of cancer by Hanahan and Weinberg (Hanahan and Weinberg 2000), which has since been updated (Hanahan and Weinberg 2011). A figure from their latest review is represented here in my thesis as **Figure 1** and shows that there are now different treatment options based on each of these hallmarks of cancer. The more detailed our understanding of the pathways involved in these hallmarks becomes, the more we can develop better targeted therapies for cancer. This is particularly important for cancer as it continues to evolve in a patient's lifetime.

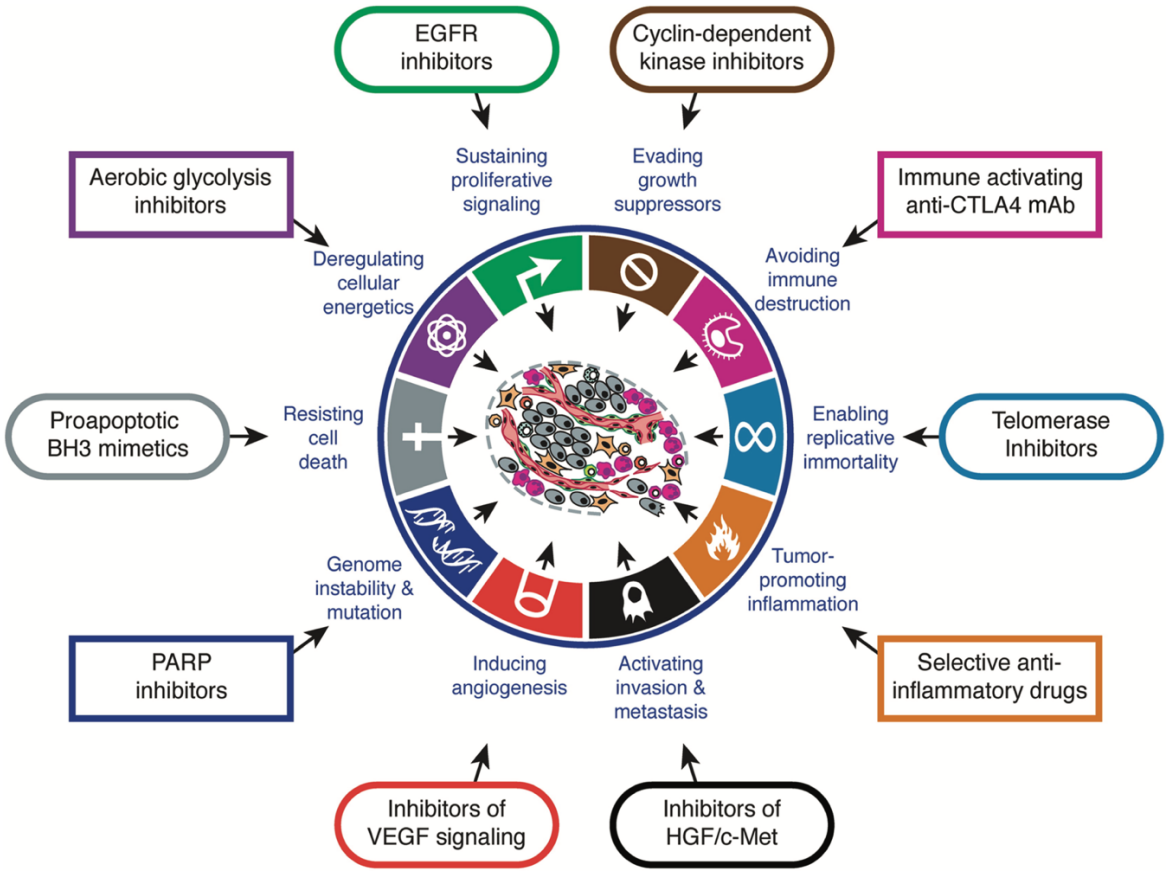

Figure 1. Hallmarks of Cancer with Therapeutic Targets.

This figure appears in the latest version of Hanahan and Weinberg's Hallmarks of Cancer review (Hanahan and Weinberg 2011). Each hallmark of cancer represents an acquired capability that a cancer needs for growth and progression. Drugs have been developed to address each of these hallmarks; some are in clinical trials and some are already approved for use in the clinic to treat cancer. This is by no means a comprehensive list of the many candidate drugs in existence or development.

One of the hallmarks of cancer is genome instability and mutation, a feature that increases in cells with age (Freitas and de Magalhães 2011; Soares et al. 2014). As stated before, adult cancers usually require multiple mutations to develop (Vogelstein et al. 1988; Vogelstein and Kinzler 1993). Cancers that affect young people (the World Health Organization defines young people as aged 10-24) are rarer in occurrence, likely due to fewer mutations in the genome due to age (Siegel et al. 2019). Many of these cancers have oncogenic fusion-genes (Pritchard-Jones 1996), and the defined genetic nature allows for more focused study and treatment. There is extraordinary value in studying these rare cancers, not only for the primary benefit of improving the health of these young people, but to have a simpler model for cancer to study specific pathways that contribute to a hallmark of all cancers. Fibrolamellar Hepatocellular Carcinoma (FLC) is one of these rare cancers and will be the next focus in this chapter.

Fibrolamellar Hepatocellular Carcinoma

Fibrolamellar Hepatocellular Carcinoma (FLC) was first described in 1956 but was not referenced as fibrolamellar carcinoma until 1980 (Edmondson 1956; Craig et al. 1980). The 1980 study was the first to characterize the histology of FLC as showing deeply eosinophilic abnormal hepatocytes with pale bodies surrounded by fibrosis arranged in a lamellar fashion, and it also noted the prevalence of this cancer to affect young people (Craig et al. 1980). The World Health Organization (WHO) only assigned FLC its own WHO classification number distinct from hepatocellular carcinoma (HCC) in 2010 (Bosman FT, World Health Organization, International Agency for Research on Cancer 2010), and prior to 2014 the vast majority of FLC literature was of a clinical and

epidemiological nature. A 2003 epidemiological study looked retrospectively at a cohort of liver cancer patients in the United States from 1986 to 1999 using the Surveillance, Epidemiology, and End Results (SEER) program and determined that only 68 cases were histologically confirmed cases of FLC compared to the 7896 cases of HCC, meaning that FLC only represented 0.85% of all primary liver cancer cases in the United States (El-Serag and Davila 2004).

Based on 275 cases of FLC, the median age of onset for this cancer is 22 years of age, and eighty percent of cases occur between the ages of 10 and 35 with no preference for gender (Torbenson 2012). There is some literature reporting cases in people as young as four months old and as old as 60 years of age, but some of these diagnoses are strongly suspect of truly being FLC (Torbenson 2012; Edmondson 1956; Craig et al. 1980; Katzenstein et al. 2003; Cruz et al. 2008; Lack et al. 1983; Maitra et al. 2000). Patients do not have underlying liver disease, viral infection, or cirrhosis of the liver and often present with nonspecific and vague symptoms like abdominal pain, malaise, and weight loss, making diagnosis difficult until a large abdominal mass is palpable (Craig et al. 1980; El-Gazzaz et al. 2000; Saab and Yao 1996; Berman et al. 1988; El-Serag and Davila 2004; Hemming et al. 1997). The overall 5-year survival rate of FLC is only 30-45%, and treatment options are still limited, with surgery being the mainstay (Katzenstein et al. 2003; Torbenson et al. 2002; Weeda et al. 2013; El-Serag and Davila 2004; Kakar et al. 2005; Mavros et al. 2012). In fact, a leading pathologist in the FLC field stated that the “most important prognostic feature is whether the tumor is resectable” since systemic therapy is not currently an option (Torbenson 2012). The published 5-year survival rate is 100% for FLC patients with resectable tumors restricted

to the liver compared to patients with lymph node involvement, vascular invasion, or multiple tumors (Hemming et al. 1997; Torbenson 2012; Graham and Torbenson 2017). These patients with more advanced disease usually die within five years since most patients do not respond to conventional chemotherapy and have not favored well in clinical trials of current targeted therapies (Hemming et al. 1997; Torbenson 2012; Mavros et al. 2012; Mayo et al. 2014; Chaudhari et al. 2018; Abou-Alfa et al. 2015).

Little was known about the molecular pathogenesis of FLC until the discovery of a new fusion gene present in this cancer in 2014 by our lab (Honeyman et al. 2014). This gene fusion is the result of a single ~400kb deletion on chromosome 19 that fuses the first exon of *DNAJB1,* which codes for a heat shock protein, and exons 2-10 of *PRKACA,* which codes for the catalytic subunit of cAMP-dependent protein kinase A; this new fusion gene yields a functional chimeric kinase present in 15 of 15 of FLC tumors in this study and over 350 more to date (Honeyman et al. 2014).

Our lab also followed up with further genomic and transcriptomic studies that showed there are no other consistent detectable genetic changes common among FLC patients and that the transcriptome of FLC is distinct from normal liver tissue and HCC tissue (Honeyman et al. 2014; Darcy et al. 2015; Simon et al. 2015). Others have confirmed these results (Graham et al. 2015; Malouf et al. 2014; Xu et al. 2015; Cornella et al. 2015; Griffith et al. 2016; Sorenson et al. 2017; Dinh et al. 2017). Our transcriptomic studies implicated several known oncogenes including ErbB2, members of the *Wnt* signaling pathway, and Aurora Kinase A since their transcripts were increased in FLC tumors compared to normal liver tissue and further validated with

qPCR, western blots, and mass spectrometry (Simon et al. 2015). Unpublished results from our lab also notably show that expression of *DNAJB1-PRKACA* is sufficient to produce transcriptomic changes in human hepatoma or HeLa cell lines similar to the changes observed in FLC tumor tissue.

As discussed earlier, our collaboration with the Lowe lab supports that this chimeric kinase drives tumorigenesis in mice and is clearly playing some role in the pathogenesis of FLC (Kastenhuber et al. 2017), and work with different mouse models of FLC supports this same conclusion (Engelholm et al. 2017). However, there is no current data on what this chimeric kinase, DNAJB1-PRKACA, could be directly acting on in FLC.

Another publication from our lab on molecular dynamics simulations (Tomasini et al. 2018) suggested the possibility for differential substrate binding and consequently differential phosphorylation due to different motions seen near the active site in the chimeric kinase that were not observed in PRKACA. Determining whether the chimeric kinase has different substrates from the wild type kinase would inform future directions of study and treatment of this cancer. The total phosphoproteome from an FLC tumor alone would not provide sufficient information to discern the direct substrates of the chimeric kinase in FLC and neither would the phosphome of cell lines or mice expressing this kinase since the phosphoproteomic changes could be the result of secondary changes initially caused by the direct action of DNAJB1-PRKACA. To truly understand the pathogenesis of FLC, we need to understand what DNAJB1-PRKACA is directly acting on in the cells of FLC. It is possible that the main changes between

normal liver tissue and FLC are due to a difference of localization of DNAJB1-PRKACA to PRKACA or that DNAJB1-PRKACA has crucial scaffolding properties inside the cell. Since DNAJB1-PRKACA is a kinase, it warrants further study to determine if its kinase activity differs from PRKACA.

The Biology of DNAJB1, PRKACA, and DNAJB1-PRKACA

The NMR (nuclear magnetic resonance) solution structure of the human *DNAJB1* was solved in 1996 and is depicted in **Figure 2a** (Qian et al. 1996). The NMR structure of the characteristic J-domain and glycine/phenylalanine domains of the bacterial DnaJ was solved in the same year (Pellecchia et al. 1996). This co-chaperone is one of forty-one known members of the DnaJ, or Hsp40, family of heat shock proteins (Kampinga and Craig 2010; Wawrzynow et al. 2018). This family of molecular chaperones contains a highly conserved amino acid stretch known as the J-domain that is encoded in the first exon. The J-domain is known to stimulate the ATPase activity of Hsp70 heat shock proteins to promote proper protein folding and to prevent the aggregation of misfolded proteins (Liberek et al. 1991; Hennessy et al. 2005; Kampinga and Craig 2010; Kityk et al. 2018). The J-domain is comprised of 4 alpha helices and a loop with three conserved amino acids: histidine, proline, and aspartic acid; a point mutation in this loop to a dissimilar amino acid like glutamine abrogates the ability to bind to Hsp70 (Pellecchia et al. 1996; Hennessy et al. 2005). These co-chaperones also have their own intrinsic chaperone activity (Langer et al. 1992).

Since the biochemical activity of their binding partner, Hsp70, itself is highly specific and the number of Hsp70 proteins in a cell is limited, the functional versatility of Hsp70 in the cell is thought to be conferred by the J-domains of the many Hsp40 family members (Hageman and Kampinga 2009; Kampinga and Craig 2010; Hennessy et al. 2005; Caplan 2003). The variety of Hsp40 co-chaperones outnumber Hsp70 proteins four to one in the mitochondria and six to one in the endoplasmic reticulum, though DNAJB1 is thought to operate in the cytosol and nucleus (Kampinga and Craig 2010).

Heat shock proteins have been heavily implicated in cancer biology and some inhibitors are already in clinical trials. Potential anti-cancer therapies for HSP90, another family of heat shock proteins, look promising, while recent Hsp70 clinical trials have been halted due to limited anti-tumor effects and mild nephrotoxicity (Neckers and Workman 2012; Hernández et al. 2002; Karagöz and Rüdiger 2015; Lianos et al. 2015; Murphy 2013; Chatterjee and Burns 2017; Kanazawa et al. 2003; Calderwood and Gong 2016; Wu et al. 2017; Sidera and Patsavoudi 2014; Chunta et al. 2012; Propper et al. 1999).

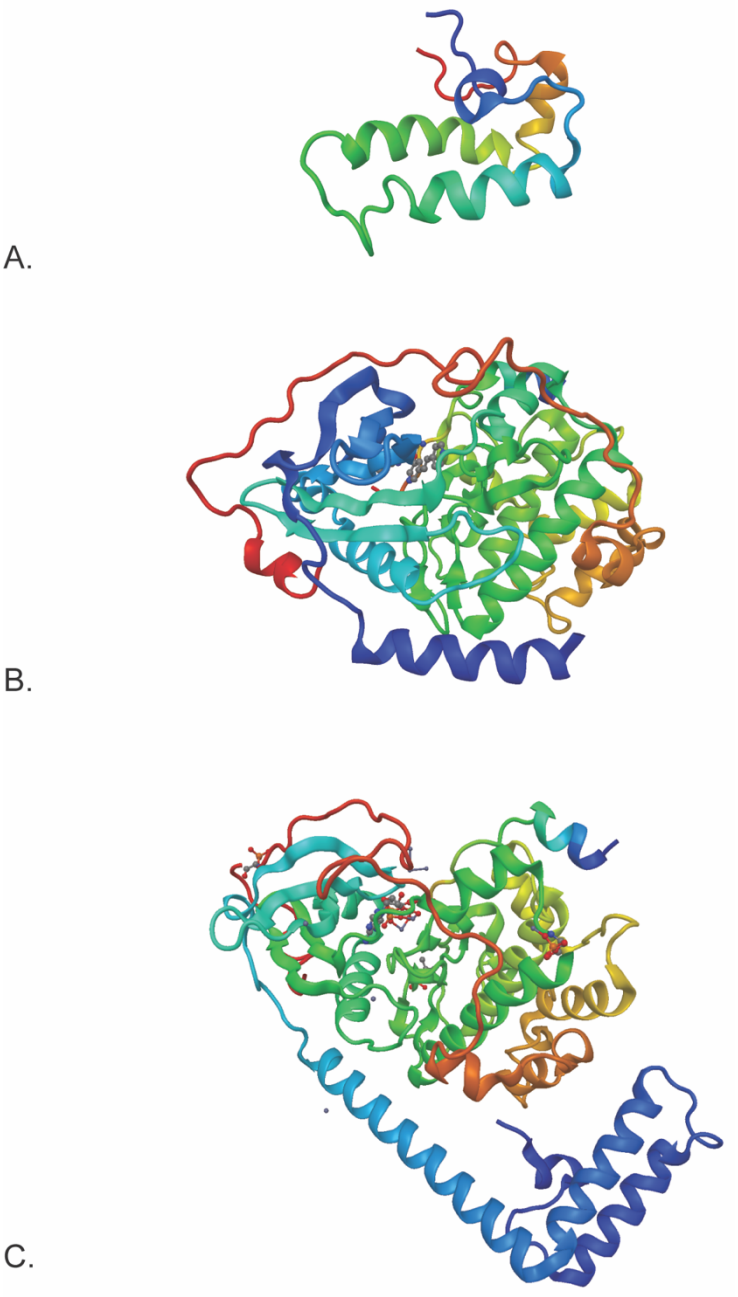

Figure 2. Protein Data Bank (PDB) Structures.

A. J-Domain of DNAJB1; PDB ID 1HDJ.

B. PRKACA; PDB ID 2F7X.

C. DNAJB1-PRKACA; PDB ID 4WB7.

Heat shock proteins have been shown to play a specific role in the sequestering of the well-known tumor suppressor p53. More recent work shows that chaperones may play different roles with this tumor suppressor depending on the context. Because these heat shock proteins cannot distinguish mutant p53 from the wild-type, these chaperones can stabilize the mutant and aid in its aggregation in the cell instead of targeting the mutant protein for degradation (Tracz-Gaszewska et al. 2017; Wawrzynow et al. 2018).

For DNAJB1, the C-terminal end has been implicated to stabilize MDM2, a protein that regulates p53, which inhibits its ability to ubiquitinate and degrade p53. Additionally, it was shown that depletion of DNAJB1 in cancer cells inhibited the activity of p53, leading to cancer cell growth (Qi et al. 2014). This could be relevant to FLC since the C-terminal component of DNAJB1 is lost as a result of the gene fusion. DNAJB1 was also implicated in interacting with another p53 regulator, PDCD5, that promotes p53 mediated apoptosis (Cui et al. 2015). The Cui et al. paper claims that in various cancers DNAJB1 promotes the ubiquitin-dependent proteasomal degradation of PDCD5 which inhibits apoptosis. However, the DNAJB1 domain implicated in this function is not in exon 1, so may not be directly relevant in FLC. DNAJB1 has also been implicated in negatively regulating another tumor suppressor, Mitogen-inducible gene 6 (MIG6). DNAJB1 stabilizes MIG6 and leads to its ubiquitination and proteasomal degradation which leads to the activation of epidermal growth factor receptors (EGFR) (Park et al. 2015). Of course, DNAJB1 is also implicated in FLC since the J-domain is present on the driver, DNAJB1-PRKACA (Honeyman et al. 2014).

The literature on Protein Kinase A (PKA) is even more extensive as it has been studied for over sixty years. Its road to discovery began in the 1950s when Fischer and

Krebs demonstrated that not only was ATP required to activate the protein they were studying, phosphorylase, but that a phosphate group from ATP was being incorporated into a serine in phosphorylase by a phosphorylase kinase that was mediated by cyclic adenosine 3',5'-monophosphate (cAMP) (Krebs and Fischer 1955; Fischer and Krebs 1955; Fischer et al. 1959; Krebs et al. 1959). They next demonstrated that the cAMP effect was mediated by a second kinase leading to the idea of a kinase cascade and the purification of what we now know as cAMP-dependent protein kinase A (PKA) (Walsh et al. 1968).

PKA exists in a tetrameric holoenzyme that is comprised of two catalytic subunits (either PRKACA, PRKACB, or PRKACG) and two regulatory subunits (either RIβ, RIIβ, RIα, or RIIα). The regulatory subunits interact with a highly conserved hydrophobic cleft found in the catalytic subunits (Berthon et al. 2015). The catalytic subunit remains inactive in the holoenzyme until cAMP stimulates the regulatory subunits to release it (Gill and Garren 1970; Tao et al. 1970; Brostrom et al. 1971; Hofmann et al. 1975; Rosen et al. 1975; Brandon et al. 1997). The mechanistic details of this allosteric activation are still an active topic of study (Zhang et al. 2015; Cao et al. 2019). The crystal structure of the PRKACA catalytic subunit revealed the bi-lobe structure of the kinase core, which provided structural insight for studying other kinases (Knighton et al. 1991).

The various isoforms of PKA are involved in a broad range of signaling processes including, but not limited to, protein synthesis, gluconeogenesis, lipogenesis, insulin secretion, cell differentiation, excitation-contraction coupling in the heart, ethanol consumption, and synaptic transmission and memory formation (Colledge and Scott

1999; Wand et al. 2001; Layland et al. 2005; Horiuchi et al. 2008; Smith and Scott 2018). Part of this specificity of function is conferred by the binding of A-kinase-anchoring proteins (AKAPs) to the regulatory subunits of the holoenzyme. These AKAPs compartmentalize PKA in different parts of the cell (Colledge and Scott 1999; Torres-Quesada et al. 2017). Phosphatases and phosphodiesterases also play a critical role in conferring specificity of PKA phosphorylation in the cell (DeSouza et al. 2002; Ahn et al. 2007; Burdyga et al. 2018; Leslie and Nairn 2019; Eiringhaus et al. 2019; Li et al. 2006; Stratakis 2012; Epstein 2017). Additionally, substrates of this kinase have an amino acid motif at the site of serine or threonine phosphorylation that is preferentially recognized by PRKACA (RRxS/T) (Rust and Thompson 2011), as well as a preference for hydrophobic residues.

It should not be surprising that when the activity of a crucial kinase with broad functions in the cell is altered disease states would arise. Impaired or altered PKA activity has been implicated in diabetes, heart disease, neurodegenerative disorders, Carney complex, Cushing's disease, and cancer (Gold et al. 2013; Bockus and Humphries 2015; Dagda and Das Banerjee 2015; Burgers et al. 2016; Caretta and Mucignat-Caretta 2011; Shaikh et al. 2012; Sapio et al. 2014; Honeyman et al. 2014; Berthon et al. 2015; Cheung et al. 2015; Palorini et al. 2016; Patra et al. 2018; Espiard and Bertherat 2015; Beuschlein et al. 2014). Since PKA has been implicated in tumor growth, it has been suggested as a molecular target for cancer therapy. However, because of the highly conserved region of the ATP binding site, exploiting the more specific interaction between PKA and a particular substrate may be a more effective approach (Naviglio et al. 2009; Sapio et al. 2014; de Oliveira et al. 2016).

Our lab studies the PRKACA variant found FLC. The fusion gene found in FLC, *DNAJB1-PRKACA,* yields the fusion kinase: DNAJB1-PRKACA. This kinase has only been identified in FLC tumors and is the driver of this cancer (Honeyman et al. 2014; Darcy et al. 2015; Xu et al. 2015; Cornella et al. 2015; Sorenson et al. 2017; Dinh et al. 2017; Kastenhuber et al. 2017; Engelholm et al. 2017). *DNAJB1-PRKACA* is comprised of the first exon of *DNAJB1,* which contains the characteristic J-domain, and exons 2-10 of *PRKACA,* which preserves the majority of the structure of this kinase, including the active site.

A crystal structure of DNAJB1-PRKACA was published in 2015 (Cheung et al. 2015), and is depicted in Figure 2c. Our lab used molecular dynamics simulations to show that DNAJB1-PRKACA can exist as a structure somewhat similar to the crystal structure with the J-domain tucked under the large lobe of the kinase, but the J-domain can also swing free, away from the core of the kinase. These predictions were confirmed by NMR with a collaborator (Tomasini et al. 2018).

Modeling from our lab has shown that there are no obvious steric interactions of the J-domain with the holoenzyme containing the RIIβ regulatory subunit (Cao et al. 2019). Further collaborations have also determined the crystal structures of DNAJB1-PRKACA in complex with the RIα regulatory subunit, as well as the crystal structure of PRKACA in complex with RIα (Cao et al. 2019). These quaternary holoenzyme structures with RIα differ from the previously reported holoenzyme structures published for PRKACA in complex with RIβ and RIIβ. While DNAJB1-PRKACA and PRKACA showed the same configuration as a holoenzyme when in complex with RIα, a distinct second conformation was identified for DNAJB1-PRKACA. When in complex with RIα,

the J-domains of the chimeric kinase are positioned away from the center of the holoenzyme and are highly dynamic. Despite great advances in the understanding of the structural biology of this kinase, it is not yet known if DNAJB1-PRKACA can phosphorylate different substrates compared to PRKACA. Since DNAJB1-PRKACA is the driver of FLC and kinases have been thoroughly implicated to play a crucial role in cancer biology (citations), determining the phosphorylation pattern of DNAJB1-PRKACA in FLC is critical to understanding the nature of this kinase.

Substrate Identification of Kinases

It is challenging to identify the direct substrates of a particular kinase in a cell since all kinases transfer the gamma-phosphate of ATP to their substrates. Biochemical methods are needed to be able to distinguish between the substrates of the kinase of interest and the substrates of other kinases in the experiment. Most substrate identification methods do not distinguish between direct substrates and substrates that are either phosphorylated by another unrelated kinase or phosphorylated as the consequence of the relevant direct phosphorylations by the kinase of interest. Below, I will highlight five established methods of direct substrate identification.

Kinase substrate tracking and elucidation (KESTREL) is a method that depletes cell lysates of ATP, then introduces an abundance of purified kinase of interest and radiolabeled ATP to favor the kinase reactions of the kinase of interest. Because of the radiolabel, proteins can be separated on a gel and excised to be identified by MS. The substrates are then validated *in vivo* as part of the published protocol for this method

(Cohen and Knebel 2006; Knebel et al. 2001). While the need for *in vivo* validation is acknowledged, it is also worth repeating that all of the kinases in the lysate are still active and can confound the list of proteins that need to be validated as true substrates. This method would also allow for the identification of specific phosphosites of the substrates.

Substrates of a kinase can also be directly identified by creating a peptide array of immobilized substrates and incubating it with the purified kinase of interest and an ATP-analog with a radioactive tag on the gamma phosphate (Ptacek et al. 2005; Boyle et al. 2007). While this method allows for a high throughput screening of potential substrates, it is limited to only identifying substrates in the array, and the dynamics of protein interaction could be altered because of the immobilization of the substrates; these arrays can also be very expensive in time and resources to develop and use. The *in vitro* nature of this experiment also means that spatial and temporal specificity of an interaction is lost so additional *in vivo* work would be required to know if a substrate identified by this method is relevant in a cell.

The Shokat lab developed a chemical genetic approach to identify substrates of kinases by covalent capture of thiophosphopeptides and analysis by mass spectrometry. Kinases have a large gatekeeper residue, like methionine, to help block the hydrophobic region inside the ATP binding pocket. By mutating this gatekeeper reside to a small amino acid, like glycine or alanine, the active site can now utilize a bulky ATP analog. This bulky ATP-analog also has a thiol group on the gamma-phosphate that results in the transfer of a thiophosphate group to the substrate.

Substrates can then be purified and identified by the thiophosphate tag. The thiophosphorylated substrates exist in a population of phosphorylated and unlabeled proteins, but the thiophosphorylated proteins can be specifically alkylated with p-Nitrobenzyl mesylate (PNBM) to generate a bio-orthogonal thiophosphate ester that is recognized by a specific thiophosphate ester specific antibody via western blot. The labeled lysate can also be digested with trypsin to generate peptides to use for mass spectrometry to identify putative substrates. The sample used for mass spectrometry is enriched for the thiol containing peptides. These peptides are then pulled out with iodoacetyl agarose beads and treated with Oxone to release the thiosphosphate ester linked peptides by spontaneous hydrolysis (Hertz et al. 2010; Allen et al. 2007). This method would allow for direct identification of the specific phosphosites of target substrates *in vitro* with minimal background phosphorylation. There is also the possibility of designing *in vivo* experiments with the analog-sensitive kinase and cell-permeable ATP analogs. However, the creation of the analog-sensitive kinases requires mutating the active site of a kinase which could affect the reliability of true substrate identification so *in vivo* validation is still required.

Kinase-Interacting Substrate Screening (KISS) is a more recently developed substrate identification method that washes cell lysate over a glutathione-sepharose affinity column (GST) column coated with a GST-tagged version of the kinase of interest. Kinase-substrate complexes that form on the column are then incubated with ATP to stimulate the phosphorylation of the substrates. The peptides are then digested, subjected to phosphopeptide enrichment, and mass spectrometry for analysis (Amano et al. 2015). This method allows for the identification of specific phosphorylation sites

and enriches for strong substrate-kinase interactions, but more transient phosphorylations of substrates cannot be detected by this method. This method also requires *in vivo* validation.

Kinase-catalyzed Biotinylation with Inactivated Lysates for Discovery of Substrates (K-BILDS) is an even more recently developed method that takes advantage of a nucleotide known as 5'-(4-fluorosulfonylbenzoyl) adenosine hydrochloride (FSBA) that irreversibly inhibits the majority of kinase activity in cell lysates by reacting with the catalytic lysine in the kinase active site. Treating cell lysates with FSBA to knockdown endogenous kinase activity then allows for a more controlled kinase reaction with the addition of the kinase of interest. This method uses an ATP-analog with the gamma-phosphate biotinylated so that putative substrates can be purified using streptavidin beads and analyzed by mass spectrometry (Embogama and Pflum 2017). This method would also allow for direct identification of specific phosphosites of target substrates *in vitro*. However, FSBA does not kill all kinase activity in the cell lysate, so some background biotin-phosphorylation will occur. This method also requires *in vivo* validation.

While all of these methods have their benefits and caveats, one caveat they all share is the requirement of *in vivo* validation of putative substrates. This emphasizes the non-trivial nature of identifying direct substrates of kinases.

Despite decades of research, not all of the substrates of PKA are yet known. There have been a few recent efforts to identify a more encompassing list of PKA substrates (Hu et al. 2014; Hamaguchi et al. 2015; Embogama and Pflum 2017; Imamura et al. 2017; Isobe et al. 2017).

PhosphoNetworks is an online database based on experimentally determined kinase-substrate relationships from a bioinformatics and protein microarray-based strategy that screened 289 human kinases against protein microarrays containing 4,191 different full-length human proteins (Hu et al. 2014); this approach yielded 301 direct putative PRKACA substrates.

Another approach used a PKA-motif antibody to enrich PKA substrates from cells that were treated with chemicals to activate or inhibit PKA; the phosphopeptides that were more enriched when PKA was activated, but not when PKA was inhibited, in the cell were considered putative PKA substrates upon analysis by mass spectrometry (Hamaguchi et al. 2015). This method yielded 45 putative PKA substrates.

A third effort was the K-BILDS method described earlier (Embogama and Pflum 2017); this approach resulted in 279 direct putative PRKACA substrates in HeLa cells, 17 of which they claim are true direct interactors.

Another approach also used drugs to affect PKA activity and quantified the change of the phosphoproteome in HeLa cells. That approach also included a computational model based on known kinase-substrate relationships to characterize the specificity of the kinase sequences and exclude indirect targets (Imamura et al. 2017). The computational model narrowed down the list of reliable PKA candidates to 29, eight of which were previously known substrates. However, for the purpose of comparison, the list of putative substrates identified by their mass spectrometry analysis yielded 1132 potential candidates.

The last approach reviewed here used CRISPR-Cas9 gene editing in vasopressin-responsive mouse epithelial cells to knockout PRKACA and PRKACB. The

phospho-occupancy of these cells were then compared to cells without gene editing which yielded a list of 197 putative direct and indirect PKA substrates (Isobe et al. 2017).

I compared a list of the gene names of the putative substrates from each of these methods using a Venn diagram web tool developed by the Bioinformatics and Evolutionary Genomics group at the Tech Lane Ghent Science Park in Belgium (http://bioinformatics.psb.ugent.be/webtools/Venn/). These lists do not take into account whether these methods identified the exact same phosphosite on the putative substrate, just that the putative substrate was identified in the screen. The resulting Venn diagram and table clearly show that while there is overlap between the putative substrates identified in the different approaches, none of them reveal a single common putative substrate (**Table 1 and Figure 3**). The specific overlaps seen in **Table 1 and Figure 3** demonstrate that the identification of certain putative substrates is favored by different methods. However, each could be identifying a true direct substrate of PRKACA that is not able to be identified by any other and is worthy of study. This comparison emphasizes that each method of substrate identification is limited and definitely requires *in vivo* validation of some kind before moving forward with any experiments or treatments based on a potential specific substrate of the kinase of interest.

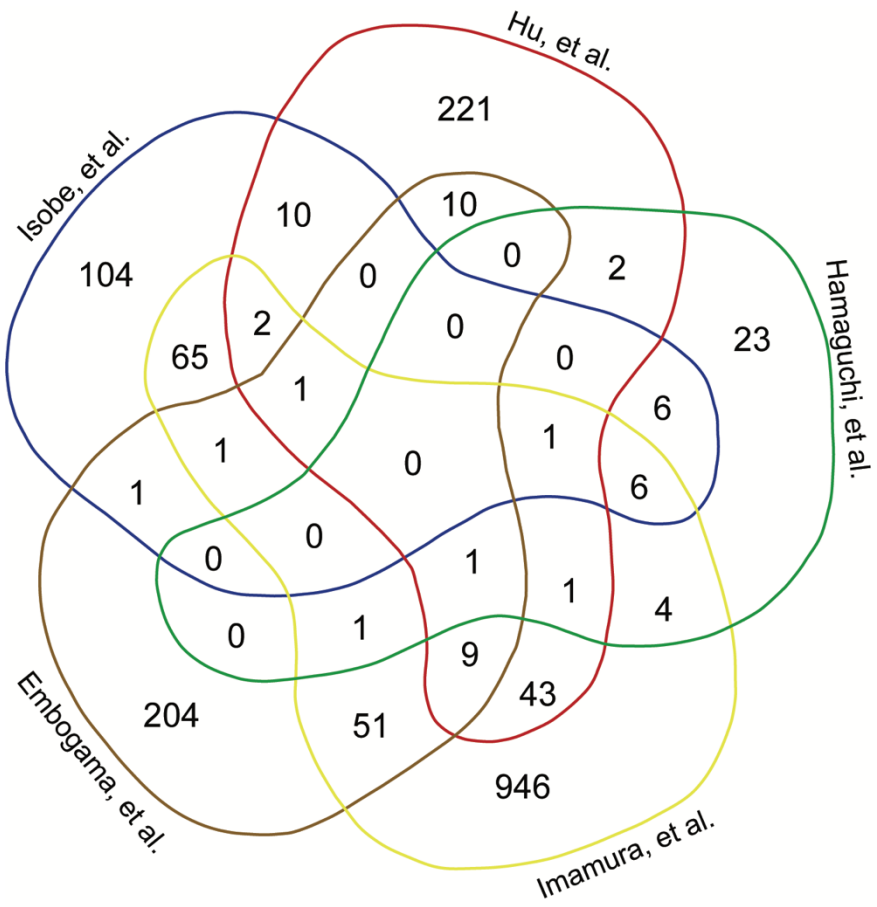

Figure 3. Putative PRKACA Substrate Comparison from Published PKA Substrate Identification Methods.

These substrates were curated from five different sources with various substrate identification methods described above (Hu et al. 2014; Hamaguchi et al. 2015; Embogama and Pflum 2017; Imamura et al. 2017; Isobe et al. 2017). The Venn Diagram was generated by inputting the gene names of the putative substrates from each source into the Bioinformatics and Evolutionary Genomics Venn diagram web tool (http://bioinformatics.psb.ugent.be/webtools/Venn/).

Table 1. Overlap of Putative PRKACA Substrates from Published PKA Substrate Identification Methods.

Overview of Overlap Between Studies		
Study Identifying Substrates	**Total Number of Overlapping Putative PRKACA Substrates**	**Total Number of Putative PRKACA Substrates**
Embogama, et al.	75	279
Hamaguchi, et al.	22	45
Hu, et al.	80	301
Imamura, et al.	186	1132
Isobe, et al.	87	197
Total Number of Unique Putative PRKACA Substrates: 1713		
Specific Overlaps		
Groups of Studies Identifying Substrates	**Number of Overlaps**	**Overlap of Putative PRKACA Substrates**
Hamaguchi, et al. Hu, et al. Imamura, et al. Isobe, et al.	1	CAD
Embogama, et al. Hu, et al. Imamura, et al. Isobe, et al.	1	SPTBN1
Embogama, et al. Hamaguchi, et al. Hu, et al. Imamura, et al.	1	PDE3A
Hu, et al. Imamura, et al. Isobe, et al.	2	PCM1 SMARCAD1
Hamaguchi, et al. Imamura, et al. Isobe, et al.	6	SPECC1L SIK2 LIMCH1 TNKS1BP1 REPS1 DENND4C
Embogama, et al. Imamura, et al. Isobe, et al.	1	LMNA

Hamaguchi, et al. Hu, et al. Imamura, et al.	1	RAF1
Embogama, et al. Hu, et al. Imamura, et al.	9	SMARCC2 NASP ACACA YWHAE YWHAZ ZYX GFPT1 FLNA CTTN
Embogama, et al. Hamaguchi, et al. Imamura, et al.	1	RPLP2
Hu, et al. Isobe, et al.	10	NUP133 CTNNB1 BAD LRRFIP1 MAP2 SRC SUFU LSR ZHX1 NFKB1
Hamaguchi, et al. Isobe, et al.	6	KIAA1522 ARHGEF7 NF1 RPL18A NHSL1 PITPNM3
Imamura, et al. Isobe, et al.	65	COBLL1 MEF2D MYO9B IRF2BP2 TNS3 PI4KB ATG2B ARHGAP17 ARHGAP21 SQSTM1 DCP1A PRKAR2A XRN2 BNIP2 DYNC1H1 ENAH OSBP SORBS2 FAM83H LIMA1 PXN WWC1 PLEKHG3 ARPP19 ARFGEF2 SIPA1L1 IRS2 TJP1 EIF4B RIN1 PKN2 EIF5B PUM2 HECTD1 OPTN CTNNA1 TXLNG AKAP1 RBM14 PRKD2 MAP3K2 MARK2 NCOR1 MICAL3 C2CD2L FBL FKBP15 NSFL1C PRRC2A RAB11FIP1 OSBPL11 CTNND1 TJP2 YBX3 YAP1 HPS5 ABCC1 ARHGAP35 WNK1 DOCK7 LARP4B PARD3 ABLIM1 PUM1 ITPR3
Embogama, et al. Isobe, et al.	1	AGPS
Hamaguchi, et al. Hu, et al.	2	CAMKK1 C19ORF21
Hu, et al. Imamura, et al.	43	ANKS1A CD44 HSPB1 MATR3 PTPN12 LUZP1 TERF2IP SMC3 DNAJC5 NPM1 CDCA7L STUB1 NCOA3 NEDD4L FYN LARP1 VIM PRKAR1A SAFB2 HIRIP3 PYGO2 ARFGAP2 LASP1 TRIP10 STMN1 HSP90AA1 FOXP4 SP100 NDRG1 EMD ATRIP EIF4ENIF1 LIG1 TRIM28 LAS1L TBC1D10B AKAP13 CHAF1B LARP4 DNM1L UHRF1 CEBPB PDE3B
Embogama, et al. Hu, et al.	10	MSN TGM2 YWHAH HLA-A PTBP1 YWHAG XPO1 PSMC5 PRKACA PSMA8
Hamaguchi, et al. Imamura, et al.	4	ZNF318 C2CD5 ACIN1 SAFB
Embogama, et al. Imamura, et al.	51	MAP4 PDHA1 CLUH DPYSL2 PSMA3 ACTL6A PALLD KDM5C YWHAQ SLC1A5 SLC9A3R1 RCC2 INF2 EPRS SPAG9 RANBP1 CAP1 HNRNPK BAG3 FLNB NACA TP53BP1 EIF4G1 LRRC47 MYO1E TK1 HNRNPD SF3A1 EFHD2 EGFR BOD1L1 SSB SLC4A1AP SLC16A3 EDC4 KHSRP PPP6R3 PDIA6 MARCKSL1 PAICS GORASP2 HDAC1 IGF2R SUPT6H MAGED2 MCMBP SERBP1 SRRM2 EIF3G TCOF1 PAK2
Hamaguchi, et al.	23	KLC4 CDC25B CRY2 OFD1 MARK3 PCNX DAPK2 CASP11 PITPNM2 CEP72 KIAA0556 CDK18 PHACTR2

		TMCC1 GLI2 HSPC075 CAMKK2 SIK3 C2ORF55 PDE8B LRCH3 BAT2 EVL
Isobe, et al.	104	CHD9 PDLIM2 CASP6 VEPH1 MAP3K5 TBC1D12 SPIRE2 NEK4 MIB2 PI4KA MYO5B TOMM34 SEC23IP CAMK2D IRS1 ZZEF1 ARHGEF2 CASP8 ITSN2 HSPA4 TIAM1 NULL VILL PSMF1 MTOR OSBPL10 PPM1H PEAK1 EPS8L1 LYST TAB2 HBP1 ATP6V0A2 MAP4K3 MTCH1 CLIP2 WDR4 SLC7A6OS SNX2 MRPS9 PTPN14 CLMN GOLGA5 KLC3 SAYSD1 BLOC1S5 TMEM259 IGSF5 PLEKHF2 MAP4K5 PCYT1B MRPL37 KARS ZNF608 KIAA1109 DOCK1 EIF2AK2 UHRF1BP1L WDTC1 CGNL1 SCYL2 CCS SRP14 KLHDC7A AFAP1L2 WDFY3 TIAM2 ERBB3 SSH1 SLAIN2 ARHGAP29 BORCS6 PURG SHROOM3 ERBIN AP3D1 NFATC2 MPDZ JUP COBL PBXIP1 HERC4 NCK1 CHCHD6 SNX1 ARHGEF17 RTKN FGD3 SNX12 MIA3 CGN VIPAS39 SKT DOPEY1 MAP4K4 RAB18 PHLDB2 KAZN PTPN13 BAIAP2 TNS2 ARHGAP27 PARD6B ZAK
Embogama, et al.	204	TBCB ECHS1 TKT PFKP DECR1 CSPG4 HSD17B10 LMAN1 NT5DC1 DDB1 TLN1 PAIP1 DDX5 USP47 GDA SDHB IPO9 DDOST PUF60 PSMA1 RPL29 RPL35 IMPDH2 PTPN11 DDX47 RTF1 EXOSC2 CYFIP1 USP14 ATP1B1 HYOU1 USP7 NUCB1 SARS UFD1L PRDX4 ARF1 SPG20 NUP88 NOMO1 SMC1A DHX15 HSPA4L FKBP4 SF3A3 FUBP1 AHCYL1 ACO2 UBQLN2 HEXIM1 OXCT1 ETFA MTHFD1 MTHFD2 TPT1 AP2M1 RDX UMPS EHBP1L1 MYOF STOM GPKOW LDLR ITGB1 FKBP10 RPN1 PSMC4 WARS MPI CASP1 CECR5 PSMD12 FKBP5 PRMT1 TYMS MCM5 SFN CSE1L TXNDC5 PFKM ELP3 TES ACAA2 PLS3 PLOD3 PLOD2 RPS24 SH3GL1 PSMC1 ACADS MCCC2 IVD PSME1 PSMD14 SF1 WIBG YWHAB PARP1 DHX9 ANXA2 PSMA4 DUSP12 PRKCSH BUB3 CNN2 WDR61 SERPINH1 CAPZA1 ACY1 PRMT5 RPS10 CLIC4 NHLRC2 FTO PTPRF SEC24C RAB6A SERPINB4 SERPINB1 POLDIP2 POFUT TUBB6 MINPP1 AKAP12 CLU PRPF8 RPL28 IARS ARFIP1 UBE2O MRPL2 PPP2R2A GNB2L1 SF3B1 CKMT1A TUBA1C HMGCL ACAA1 PAAF1 SLC3A2 ASNS PC COPS3 DNM2 VARS CHD4 CDC73 GOLIM4 PSMD4 GDI2 RRM1 PRDX2 DDX17 SBDS TIPRL RNH1 DAK KLC1 GALE DRAP1 DLD LAMP2 CAT NONO SETD7 CPNE1 PLD3 SART3 LAP3 IMPDH1 NMT1 FDXR ST13 UBFD1 RARS POLD1 TRMT10C ACTN1 HSDL2 CLTB PSME3 MGEA5 KPNA6 PDIA4 NAGK RPS14 PGD NME1 RPS16 PYCRL PEBP1 IWS1 CP NANS SF3B3 GPC1 SDHA LANCL1 PNP ANKZF1 ACTR2 PGK1 OAT MPST
Hu, et al.	221	ESPL1 HSPB6 HNRPD HSPB8 PPP1R14A ANXA1 ATP1A3 DSP ALOX5 SERPINF1 PKD1 TRPM8 TTF2 RXRA NFATC4 POU3F4 CENTD2 NFATC1 PLN GRK1

		BIRC5 CIAO1 PLCG1 DAP3 SIP1 C21ORF66 ITGB4 BTBD12 FAM44A RASGRF1 PIN1 GSTA4 EP400 ABCA1 ARID3A PPP1R8 CSDE1 PPP1R9A AICDA BCAM NPR1 AQP2 KCNH2 PDE4C DDX39 LIPE TNNI3 IRF3 TAF10 PLCB3 EZR TFAP2B CIITA CRHR2 RBM19 MAPT GMFB AURKA C14ORF106 KCNJ13 RGS14 CSRP3 ABCB1 KCNA4 PPP1R1B GPBP1L1 RRAD WT1 SNAI1 CTPS MYBPC3 SOX9 ADRB1 CSK NOXA1 TH LCK HAGH CACNA1H PHOX2A DES XRCC4 RDBP NAB2 RNF12 GLI1 GRIA1 ASPSCR1 PCTK1 ACCN2 VTN CCND1 RUNX1T1 POP7 ESR1 KCNN3 SNUPN PFKFB3 NEUROD1 PDE4D NFATC3 PRDX5 U2AF1 SREBF2 BCOR AVPR2 RUVBL2 CSNK1A1 E2F7 APOBEC3F EXOSC5 MDFI GSK3B GNA13 PTPN7 SGK TRPV1 DUOX1 ITGA4 VDR HLCS STK24 CHGB DDEF2 PRKAR2B PPP1R13L H3F3A MC4R PHF17 CSDC2 GATA3 MYOM2 FOXN3 PFKFB2 HIST2H3A CUL5 UTP18 LRP1 MCOLN1 RCHY1 CLDN3 CBL MYLK CAPN2 CREB1 ERBB2 FIP1L1 TFAP2C C20ORF32 AKAP9 TRPV4 NCBP2 PDE5A NR5A2 HDAC8 RBM22 CRIP2 DAXX KCNJ3 HRH1 RYR2 RPS19 NOS3 ID2 RB1 CFTR DHX29 C19ORF2 PDE4B TSC22D4 SEC14L2 SAP30BP PDE11A SOX6 DNAJB2 HNRPK GFAP NRIP2 AQP5 RNUXA PPP2R5D TP53 CBX3 VASP GAS7 CASP9 ZNF496 KCNN2 RBBP5 ETV5 ARHGDIA ARFGEF1 PPP1R1C PPP1R1A LOC51035 CUX1 FXYD1 BMI1 KCND2 TPPP PPP1R14C UNC84B LOC100133382 GSK3A GRK7 TPH2 METTL3 ETV1 NF2 GAD1 SLC4A4 NCOA4 C13ORF15 LOC648998 SRF GATA4 VHL MDM4 PAH HCLS1 CBFA2T3
Imamura, et al.	946	DBNL SLMAP RPTOR TFIP11 BCL2L12 ZHX3 ERCC5 NBAS HIVEP1 TACC2 ATRX BYSL VAMP8 NBN CXCR4 U2SURP WASL EIF6 G3BP1 CHD8 RBM15 NUFIP2 MAST2 SLTM SCAF8 TPX2 EP300 GYS1 MON1B CHORDC1 PACSIN2 C2orf49 ZEB1 TRIM33 TOPBP1 PARN CD2BP2 THRAP3 NUP214 TPD52L2 SOX13 EIF3B MFSD6 SRPK1 USP20 PTCD3 BET1L MCRS1 HMGN1 UBE2E3 UBA1 NMNAT1 SHC1 PRDX6 SAAL1 RAB3GAP1 TAOK3 RIOK1 HERC2 SLC12A4 BASP1 CLCC1 USP6NL BAZ1B SDAD1 PPP1R15B LARP7 ARHGEF12 KPNA2 ATL2 SNRNP70 SLC35F6 RBM17 PTOV1 RALY ZCRB1 KPNA3 PDCD4 TMEM45A CDK12 DDB2 RBM10 JADE3 PHF3 BCLAF1 TRA2B RBM33 RAD23B STK17A MTRR NCOR2 PEX14 PGRMC2 APEH GTF3C3 TBC1D5 MAPKAP1 HIST1H1E THOC2 CEP170 TPI1 MINK1 EZH2 MSH6 MYO1C SRSF6 HDAC7 HSPD1 SLC15A4 SIPA1 OSMR CCDC43 LSM14A ATAD1 NELFE WIZ IMUP RBM4 CSF1 SLC35B2 EDC3 SORT1 CEP170B COPA SETDB1 CARMIL1 SRSF11 PCDH7 TJAP1 PHC3 ORC1

		ACOX1 FAM102B SON PLCL2 USP24 TRAM1 KIAA1143 TWF1 NUP153 MYH9 TTYH3 ATP11C SLC12A6 AVEN C9orf16 URI1 RAP1GAP NOP2 USP42 USP16 RAD9A SCML2 NIPBL POGZ RICTOR USP10 PODXL2 RPS3 PI4K2A RAD18 WDR75 LRRC8A SFSWAP DYNC1LI2 PRRC2B COIL CDK17 ZMYND8 APMAP ZNF687 PTGES3 TSC2 ZNF609 CPSF7 KDM2A EML3 CASC3 TCF12 ATP7A ZNF641 HABP4 NFIL3 DSG2 WDR62 TANC1 DHX16 TBXA2R LEMD2 MIS18BP1 UBXN7 DIDO1 PRKCD LYSMD2 ARAP1 NGDN SAC3D1 ZNF639 PUS1 PPIG ITPRIPL2 UNG DPF2 BCL9L CBARP BRD8 PJA2 DCUN1D5 SMC4 ANKLE2 TMEM230 NOP58 RPRD1B CHMP7 FRYL PTPN2 AP3B1 HCFC1 EPB41L1 AHNAK EXOSC9 UBL7 KRT17 ABCC4 ZFP36L2 RPL4 PBRM1 PPP1R12A VAMP4 PRPF3 CHMP2B DDX24 RNF20 RBM6 USP9X WAPL VAPA SH3PXD2A HNRNPUL2 RBBP6 ARHGEF16 HUWE1 BRF1 TMPO PARG RRAS2 ASAP2 MCM3 PPL CEP131 RPS2 STRIP1 SSRP1 PRPF4B NRBP1 PDAP1 BRD4 CHAF1A RNF113A MYPN TOR1AIP1 PACSIN3 BCKDK CSRP1 ITSN1 SVIL PPHLN1 TBC1D2B AFF4 SUB1 AKAP10 CHAMP1 PRPF6 PCBP1 NSD1 ATP2B2 NCAPD3 PDE8A SH3KBP1 PLA2G4A SYNRG RIF1 UNC13D PROSER2 ABCC2 GPATCH8 DDI2 KIF4A PGM1 CPD MEPCE KIF21A UNK KRT8 SAMD1 SCD MAP7 RBM7 OSBPL3 ANTXR1 TERF2 HASPIN SLC38A2 CD2AP CCDC86 ATN1 SMN2 MPZL1 XPO4 EPS15 TRPT1 GPS1 WIPI2 IFNAR1 SEPT9 EHD2 STX7 SPEN RMDN3 NAP1L4 GPRC5A ANKRD17 UBE2J1 CCNK SZRD1 CDC26 C1orf52 NCKAP5L FAM129B PDS5B CD97 EAF1 MPHOSPH8 NOTCH2 NOC2L TICRR ADD1 PSMD2 CHTF18 ATXN2 MYO18A ZBTB7A MADD PRRC2C SLC4A2 ACLY ARHGAP12 ARHGEF18 SUGP1 ARRB1 HNRNPUL1 VIRMA SIN3A STRN3 POLR3E CHMP3 TXNL1 CEBPZ CCNYL1 OBSCN ANAPC1 SRRT CBX8 MELK RBM3 BMS1 SCFD1 RRBP1 IL1RAP VDAC1 PPP1R10 CDK16 CIR1 FTSJ3 SF3B2 KAT5 FLYWCH2 UTP14A TPD52L1 SLC19A1 XRCC1 SLC4A7 RRP1B EEF1B2 DKC1 PAK1IP1 GNL1 ZNRF2 SLC7A11 NELFB SEC22B PPP1R12C CDS2 AHCTF1 SENP3 ATG9A EEF2K NEDD1 DNAJB6 OCIAD1 TCEAL4 NFIC DDX46 PRPF38B WDR26 ILF3 MUS81 BCL2L13 NUP50 ARFIP2 LEMD3 KRI1 TXLNA BUB1 PIEZO1 GTF3C2 PWWP2A GAL ALDOA RCC1 EIF3H SKIV2L KIF1B DIS3L2 SNTB2 SURF2 PIAS1 ZRANB2 ARGLU1 DOT1L CLASP2 ZC3H14 CNOT2 EIF2AK3 RPRD2 SNW1 RPP30 TRIM16 CDC40 IRF2BPL ATF7IP SEC31A FOXK1 RECQL5 WEE1 ZC3H18 HNRNPC BSG FXR1 NUP210 TIMM8A BIN1 SRRM1 RANBP3 PPAN

		PABPN1 PTDSS1 FMNL1 ACSS2 GLCCI1 BAG6 MMTAG2 SH2D4A SLC7A2 GZF1 DDX55 ARMCX3 QSOX2 FERMT2 NSUN2 YBX1 LRFN4 TPD52 PNISR DTD1 CARHSP1 STK10 SLCO4A1 HERC1 PTPN23 STK11IP DGCR8 ZC3H13 PHACTR4 RTN4 TAX1BP1 GAPVD1 PHRF1 COPB2 CTR9 BRI3BP LMO7 TBC1D4 PPP1R2 HNRNPH1 GIT1 HMOX1 KPNA4 MDC1 CHCHD3 HIST1H1B EPB41 NUP98 INO80B NUCKS1 DFFA RBM34 PAXX RCOR1 U2AF2 SEC16A EBAG9 TRMT1 TMEM51 KMT2D SLU7 DAB2 LEO1 MARCKS TTLL12 TELO2 MAF1 NIFK C7orf50 USP15 PGRMC1 DNAJA2 CCNL1 HDAC4 LYN ZFP91 CDCA3 YAF2 WDR33 AMFR RAI1 NOP56 MAPK1 MPHOSPH10 ATAD2 BPTF DENR HNRNPA2B1 HACD3 TLE3 PHF6 ANAPC2 DNMT1 EPB41L2 TACC1 SLC16A6 PDCL ZC3HC1 DYNC1LI1 PEA15 YRDC VPS4B RREB1 FNBP4 DNMBP FXR2 LIFR ZC3H8 SNAP23 TFDP1 ARHGAP1 CLASP1 EEF1D MGA TFAP4 AFAP1 IRF2BP1 CDK13 SRSF10 BCR TWISTNB UTP3 CLINT1 RTTN PCNP ZFC3H1 RPL15 SMAP RIOK2 KIAA1671 REXO4 MYCBP2 ABCF1 UFD1 SMARCA4 SEPT2 RPS6KA4 LATS1 BRD7 ZBTB21 CEP55 EYA3 HOXC10 NEMF EML4 MED1 ATF2 TMEM245 SRSF1 DIAPH1 ESF1 LAMTOR1 TRAF4 RRM2 CTPS1 NUDC TOP2A SLC20A1 DNAJC2 TOM1L1 IGF1R GOLGA2 TRA2A CAMSAP2 RFC1 NOB1 ABCC5 EIF2A GTF3C4 ASMTL SNAPC5 MOCOS AFDN TTF1 SLC30A1 NCBP1 TBX3 SLC9A1 DNAJC21 HDAC2 NEXN PLEC NRDC IL6ST SART1 MTDH NCAPD2 HSP90AB1 UBAP2L HSPE1 PPP4R3A RBM5 NCL EIF4EBP1 PPP1R9B SLC43A2 TMEM131 WDR44 GPN1 WDHD1 UBE4B MCM2 KRT18 DBN1 TGS1 LRWD1 PTS RPL27A MCM4 TCEA1 SPTBN2 OTUD5 TOMM70 OGFR DDX54 ARHGAP5 DDX21 PWP1 ADAR HTATSF1 ALPI HSF1 POP1 KMT2A PKN1 WTAP MTA1 GPAM ESYT2 BUB1B JMJD1C TIMELESS AKT1S1 DDX10 CCNH SURF6 MTCL1 PHF14 ERCC6 KIF13A KRT7 TMX1 RRP12 PHF8 HSPH1 TMEM87A PLEKHA2 DMAP1 ESCO2 UBA2 SEC62 SRSF2 RAB12 DNTTIP2 DDX51 ZMYM4 PRKAR1B GBF1 HEXIM2 ZC3H11A VCL TCF3 ZNF106 C18orf25 SMN1 RANBP10 MKI67 PANK2 NHS PSMD1 CLSPN DTL EPS8L2 BICD2 SRFBP1 SRSF9 ARL6IP4 RBMX C19orf24 TGFBR2 LRRFIP2 PAXBP1 PURB ACAP2 NAF1 PPP4R2 BUD13 SDE2 SLC39A10 CDCA2 NFX1 MDN1 PPA2 MED24 MAP3K7 OXSR1 EHD1 REEP4 RAB11FIP5 PPIP5K2 GTF2I SLC38A1 PPFIA1 PLCD3 PDS5A CRK NCAPH2 PKM TBC1D15 ADAM17 ZNF830 CDV3 ZFR ZC3H4 HNRNPA3 NOLC1 ELAVL1 HNRNPLL NCOA2 USP5 RPP25 ABCA2 CANX EXO1 DAP CUL4A AJUBA CDC42BPB CIAPIN1 DMD

		STAMBPL1 TMX2 LYSMD1 TCF20 ZNHIT3 PPM1G C9orf40 ELMSAN1 SSH3 TBC1D2 PEX19 RBM39 PRKAB1 RALGAPA1 SHTN1 KIF20A KLC2 SSX2IP EIF2S2 FNDC3B USO1 SIRT1 AREL1 PCBP2 MFAP1 CLIP1 NEK9 UPF3B RPL23A GTF2IRD1 MORC2 ADNP RFFL RBM15B ERICH1 WDR55 DDX39B NUMA1 MIOS HDGF TLE4 WRNIP1 TOP2B CNNM3 GIPC1 FAM117B TAF15 SORBS3 GMPS ZNF592 MED19 EIF4G2 GTF3C1 PAGR1 FAM208A SYNPO POLD3 VAMP7 AMPD2 RSF1 KHDRBS1 MON1A PPP1R18 POU2F1 GAPDH PHF10 CLNS1A PSEN1 APC NUP43 FUNDC2 EPS15L1 SEC61B NMD3 RSL1D1 RBM25 CDC42EP1 TOE1 TPR GATAD2B MAP1S AKAP11 FMNL2 SUPT7L HMGA1 WDR3 YTHDC1 TTC33 RANBP2 LIG3 STK38 TRAFD1 ATP2A2 CTTNBP2NL CAST MGRN1 STRN GAB1 PNN PTDSS2 MTMR3 BMP2K TRIM25 DDX3X SCAF11 USP39 HNRNPU ATXN2L FLII PRCC CLASRP NCAPG CWF19L2 BRAF GOLGA4 RPL14 HNRNPA1 TMOD3 TMF1 RALBP1 CAAP1 GEMIN5 UBR4 FCHO2 DDX20 KTN1 FUNDC1 MYBBP1A PHKB SLC16A1 USP8 SLC17A5 EPHB4 CLN3 MISP STX4 TMEM106B MBD1 NDRG3 TP53BP2 VDAC2 ATP2B1 RPS6KA3 CENPF STT3B SYAP1 BET1 CD3EAP SNX17 HDLBP RANGAP1 PITPNM1 HECW1 SGPP1 DCAF8 RPS27 RLF KLF3 CDCA8 ZNF638 MTFR1

Overview of Thesis Work

In this introduction, I have described the need for more cancer research, even though there have been great strides in knowledge and treatment options in just the last fifty years. I highlighted the advantage of how studying a rare cancer with a defined genetic event in a young person could provide a simpler model for probing at the pathogenesis of a cancer, and further described a particular rare liver cancer that affects adolescents and young adults as a result of a gene fusion: *DNAJB1-PRKACA*. I also described that although there is much known about PKA biology, we still do not have a complete understanding of all substrates of this kinase, let alone its oncogenic variant, DNAJB1-PRKACA. Knowing the direct substrates of this oncogenic kinase found in FLC can inform therapeutic decisions and contribute to a stepwise understanding of the progression of this particular cancer while also furthering our understanding of proteins found in pathways involved in other cancers.

Methods of directly identifying substrates of kinases are non-trivial and each method has its own caveats to consider. However, a desirable method should have two ways of conferring specificity of the readout: part of the method should ensure the amount of activity in the sample is predominately from the kinase of interest and not from other kinases in the sample, and another part of the method should ensure that the detection of the phosphorylation event from the kinase of interest is distinguishable from the phosphorylation event of another kinase in the sample. With this approach in mind, the goal of my thesis work was as follows: ***To specifically identify the direct substrates of DNAJB1-PRKACA that are relevant to the pathogenesis of fibrolamellar hepatocellular carcinoma.***

Chapter II will describe my work to determine a method of substrate identification that would yield a robust list of potential substrates of DNAJB1-PRKACA compared to PRKACA. The approach I first tested was developed by the Shokat lab and uses an analog-sensitive kinase in combination with a selective adenosine triphosphate (ATP) analog. Analog-sensitive kinases have their gate-keeper amino acid in the active pocket of a kinase mutated to open up the pocket in a way that allows for the preferential selection of an ATP analog that has a bulky group attached to the adenosine group. In addition to the bulky group, the ATP analog has a thiol group attached to the γ-phosphate that allows for the identification of substrates with a thiophosphate versus a regular phosphate. Initially, purified kinases of interest were made with a Glutathione S-transferase (GST) tag, but later I switched to a method of purification using beads bound to a specific peptide known as Protein Kinase Inhibitor (PKI) peptide to purifiy the kinase without a tag; a tagless kinase provides more confidence that the kinetics and protein interactions of your purified kinase are reporting the behavior of the kinase *in situ*. We have successfully used this method to purify PRKACA. However, the single mutation of the gatekeeper residue for the analog-sensitive kinases rendered the PKI peptide unable to bind sufficiently to purify the kinases. I could have continued with the GST-tagged versions of the kinases instead, but I was now more concerned about how greatly the mutation of the gatekeeper residue could affect the readout of the potential substrates of interest if a specific binder was significantly affected by the single amino acid change. Indeed, other studies have found that changing this gatekeeper methionine to an alanine or glycine changed the activity of the kinase. Previously, the Shokat lab has also introduced additional

mutations in the active site of their analog-sensitive kinases to retain more activity to more closely resemble the native kinase. Since my goal was to identify the substrates of DNAJB1-PRKACA, this approach could undermine the validity of my results.

As an alternative, I pivoted to a method that kills the endogenous kinase activity of a lysate using 5'-(4-Fluorosulfonylbenzoyl)adenosine (FSBA); this kinase-inactive lysate can then be used in a kinase reaction with your purified kinase of interest and an ATP analog that has a tag on the γ-phosphate to identify direct substrates via MS. The ATP-γ-S analog I initially used for this method was effective in demonstrating kinase activity changes via western blots, but the thiol-tags were not reliably identified using mass spectrometry. With the improvement of phosphopeptide enrichment methods and encouragement from the Proteomics Core, a pilot experiment was done next to enrich phosphopeptides from a kinase reaction using FSBA-treated mouse liver lysate and either PRKACA and DNAJB1-PRKACA with regular ATP. This pilot yielded promising results that showed substrate differences between PRKACA and DNAJB1-PRKACA so a triplicate experiment was designed using human hepatocyte lysate instead of mouse liver lysate.

In Chapter III, I will discuss the results of the assay using FSBA-treated human hepatocyte lysate in kinase reactions to compare the substrate differences of three kinases: DNAJB1-PRKACA, PRKACA, and PRKACA (L206R). The PRKACA (L206R) is a variant of PRKACA that is thought to be constitutively active and is found in adrenal tumors of patients with Cushing's disease. Recent publications probe at potential substrate differences between PRKACA and PRKACA (L206R) (Lubner et al. 2017; Bathon et al. 2019), so this kinase was added to my assay, in part, as a further control

of kinase substrate specificity. The data show that the kinases used for the reactions were all of similar activity and amount and that the phosphopeptide enrichment from each condition was consistent and robust. The raw data was analyzed using MaxQuant, and further analysis was done with Perseus and various bioinformatics software to show that there are differences in substrate preferences between the three kinds of PRKACA.

In Chapter IV, I will discuss how the results of a total phosphome study of FLC patient tumor and normal samples compare against my *in vitro* assay that identifies potential direct substrates of DNAJB1-PRKACA. This comparison allows for the generation of a more focused list of substrates for further study that are capable of being phosphorylated by DNAJB1-PRKACA *in vitro* that also appear phosphorylated in FLC tumors. The thesis will conclude with future directions and discussion of the implications for the pathogenesis of FLC based on the direct substrates of interest.

CHAPTER II: Determining a Method for Substrate Identification of DNAJB1-PRKACA

Background and rationale

In the previous chapter, I described the challenges involved with directly identifying substrates of a particular kinase. Each method that was established at the time I started pursuing this question had its own pros and cons to consider as previously discussed. I chose to start with using the analog-sensitive kinase approach to determine if there were substrate differences between PRKACA and DNAJB1-PRKACA. **Figure 4** depicts the workflow of this analog-sensitive kinase method that was previously described in detail in Chapter I. The paper describing this method claimed that PRKACA could tolerate the mutations necessary to make an analog-sensitive version (Hertz et al. 2010), which meant DNAJB1-PRKACA should also tolerate the necessary mutations; additionally, the first author of this methods paper was at our university and actively collaborating with us at the time.

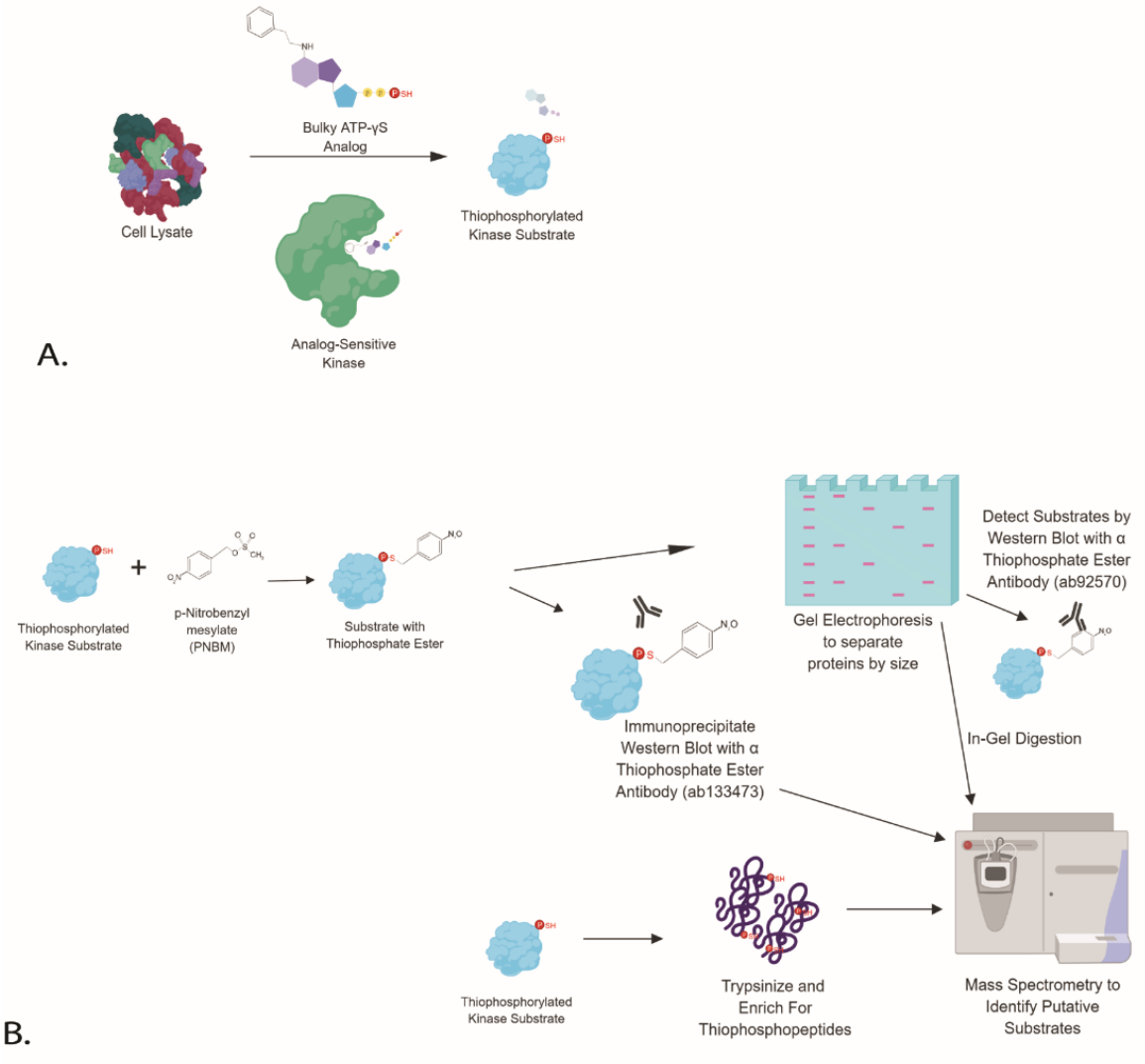

Figure 4. Analog-Sensitive Kinase Approach to Identifying Direct Substrates.
A. Kinase reactions in this method react cell lysate mixtures with analog-sensitive kinases that have their gatekeeper residue mutated to allow for the preferential selection of a bulky-ATP analogy that has thiophosphate in the gamma position.
B. Resulting thiophosphoproteins can be alkylated to create a thiophosphate ester at the site of phosphorylation that can now be recognized by a specific antibody for western blot, immunoprecipitation, and mass spectrometry analysis. Thiophosphoproteins can also be trypsinized and enriched for thiophosphopeptides for mass spectrometry analysis. Created with BioRender and adapted from (Hertz et al. 2010).

Purifying Recombinant DNAJB1-PRAKCA and PRKACA Using a Glutathione S-Transferase Tag

The first step towards attempting the analog-sensitive kinase approach of direct substrate identification was to generate purified kinases. I received pET151 protein expression plasmid constructs that were previously made in the lab for DNAJB1-PRKACA and PRKACA that had a thrombin cleavage site and GST tag at the C-terminal end of each kinase. GST tags allow for a one-step purification of relatively pure protein, has established antibodies that can recognize it via western blot analysis, helps with solubility of proteins, and was suggested as favorable by a collaborator for a different project to try to generate antibodies against DNAJB1-PRKACA.The pET151 plasmids allow for protein expression from the bacterial T7 promoter upon induction with isopropyl β-D-1-thiogalactopyranoside (IPTG) in BL21 (DE3) Competent *E. coli*. These plasmid constructs for the non-analog-sensitive kinases would later serve as templates to introduce the necessary gatekeeper mutations for the analog-sensitive mutants via site-directed mutagenesis.

It was important to first be able to show that I could purify active versions of PRKACA-GST and DNAJB1-PRKACA-GST without the gatekeeper mutation and that the GST tag could be removed so that the kinase used for *in vitro* reactions would structurally resemble what is found *in vivo* as much as possible.

I used these plasmid constructs to express PRKACA-GST with the thrombin cleavage site in BL21 (DE3) Competent *E. coli* and then successfully purified this kinase with glutathione agarose beads. However, when I tested for cleavage of the GST tag from PRKACA with thrombin, the entire kinase was degraded (**Figure 5**).

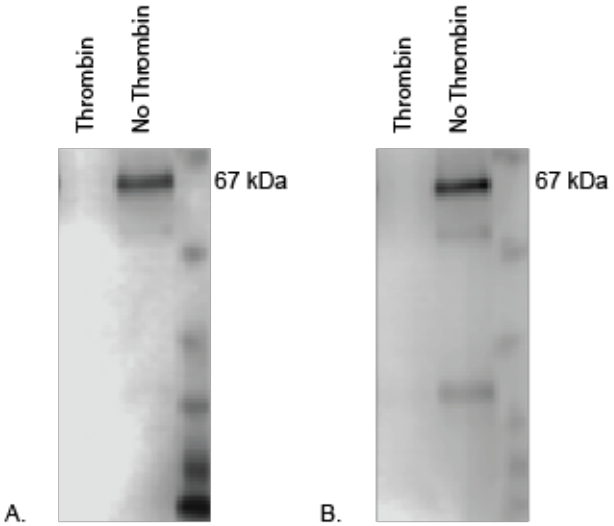

Figure 5. Thrombin Treatment of Purified PRKACA-GST.

For both the (A) anti-PKA western blot and the (B) anti-GST western blot, the first lane contains PRKACA-GST treated with thrombin and the second lane is the negative control of PRKACA in the absence of thrombin.

Table 2. pET151 Constructs with TEV Cleavage Site.

DNAJB1-PRKACA Constructs	**PRKACA Constructs**
DNAJB1-PRKACA-TEV-GST	PRKACA-TEV-GST
DNAJB1-PRKACA-TEV-(GGGGS)-GST	PRKACA -TEV-GGGGS-GST
DNAJB1-PRKACA-TEV-(GGGGS)x2-GST	PRKACA -TEV-(GGGGS)x2-GST

I decided to use site-directed mutagenesis to replace the thrombin cleavage site with a Tobacco Etch Virus (TEV) cleavage site since the sequence is more specific than the sequence cleavage site for thrombin (Waugh 2011). I also took this opportunity to make more constructs that also included a flexible linker to the carboxyl side of the TEV cleavage site in case the cleavage was sterically hindered by the close proximity of the kinase and GST (**Table 2**).

Once I had the constructs in **Table 2,** I expressed and purified DNAJB1-PRKACA-TEV-GST, DNAJB1-PRKACA-TEV-(GGGGS)-GST, and DNAJB1-PRKACA-TEV-(GGGGS)x2-GST. I then tested for cleavage of the GST tag from DNAJB1-PRKACA with TEV protease over the course of four hours. **Figure 6** shows that the flexible linker was indeed necessary for efficient cleavage of GST from DNAJB1-PRKACA with TEV protease. Concurrently, I tested the activity of these three versions of DNAJB1-PRKACA using ADP-Glo (Promega). This method uses two reactions to get a readout of kinase activity. First, a reaction with the kinase of interest and a substrate, in this case a known PKA substrate called Kemptide, is conducted with a consumable amount of ATP for a defined period of time. Then luciferin and luciferase are added to the mixture for a second reaction. In this second reaction, luciferase catalyzes the mono-oxygenation of luciferin to yield oxyluciferin and one photon of light in the presence of ATP. Light will be detected after the second reaction if any ATP is left from the first. The less light that is detected, the more active the kinase was from the first reaction. If no light can be detected, then the kinase consumed all the ATP in the first reaction. Light was only detected in the no kinase control and not detected with all three versions of DNAJB1-PRKACA.

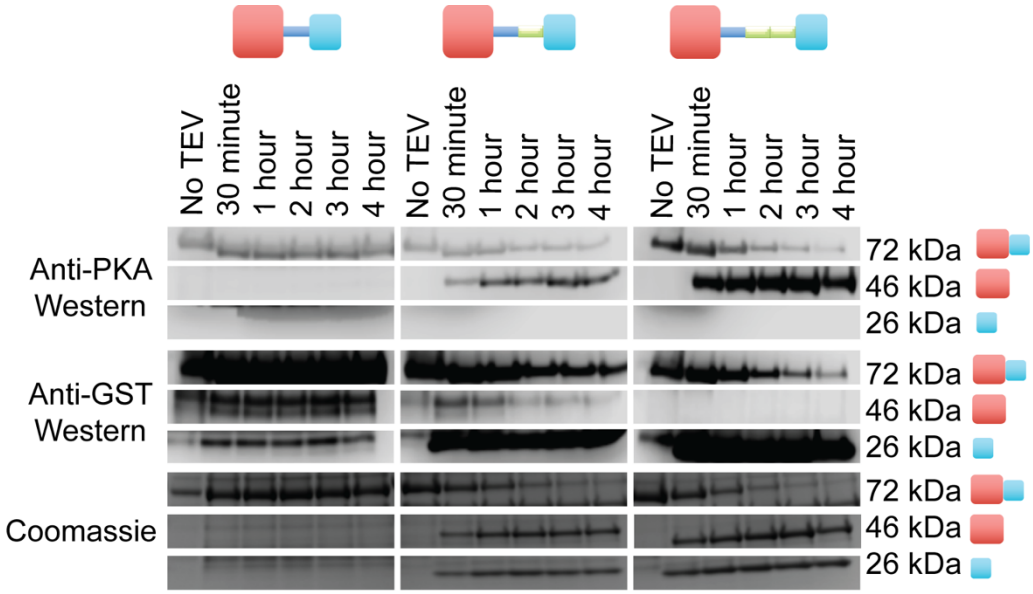

Figure 6. Time-Course of TEV Cleavage of DNAJB1-PRKACA-GST of Varying Linker Length.

The red boxes represent DNAJB1-PRKACA, the blue boxes represent GST, the blue rectangles represent the TEV cleavage site, and the green rectangles represent one GGGGS flexible linker. Each row corresponds to the same molecular weight in the three tested conditions with different linker lengths. The top three rows are western blots probed with an anti-PKA antibody. The middle three rows are western blots probed with anti-GST antibody. And the last three rows are stained with coomassie to visualize total protein at that molecular weight.

At this point, I now knew the conditions needed to produce cleaved and active DNAJB1-PRKACA and was ready to proceed to making the analog-sensitive mutants. However, a collaborator then suggested a different purification method that would allow for tagless purification of PRKACA and perhaps DNAJB1-PRKACA (Olsen and Uhler 1989).

Tagless Purification of Analog-Sensitive Mutant Kinases Reveal a Methodological Concern

A visiting student in our lab at the time, Solomon Levin, tried the tagless purification method for both PRKACA and DNAJB1-PRKACA in pET151 protein expression vectors with great success. This method takes advantage of a well-studied small specific peptide (PKI) that can reversibly bind to the active site of PRKACA (Olsen and Uhler 1989). This peptide is bound to agarose beads, similar to a GST purification, to efficiently and specifically purify PRKACA and DNAJB1-PRKACA. I was able to repeat this kind of purification as shown in **Figure 7.**

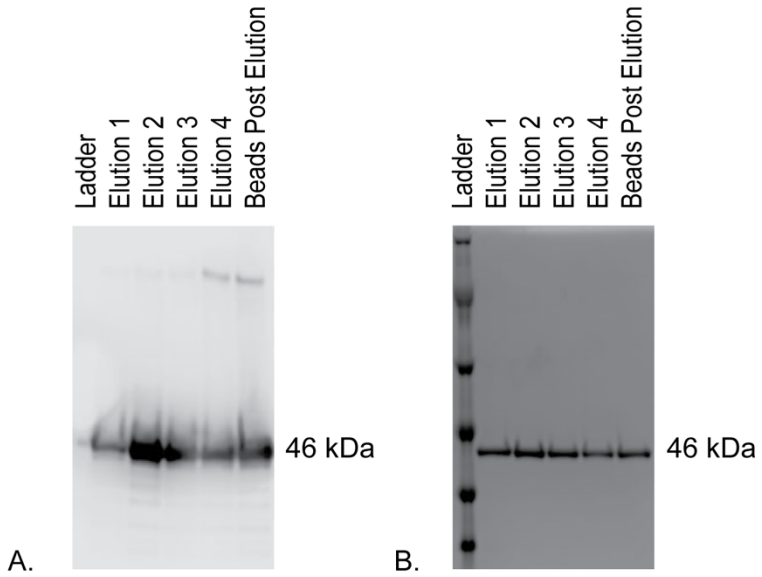

Figure 7. Tagless Purification of DNAJB1-PRKACA.
Both the (A) anti-PKA western blot and the (B) the coomassie, show a robust band around 46kDa, which is the weight of DNAJB1-PRKACA.

Using site-directed mutagenesis on the pET151 constructs for DNAJB1-PRKACA and PRKACA, I changed the gatekeeper residue from methionine to either alanine or glycine to see if one mutation worked more favorably than the other. However, introducing this point mutation rendered the tagless purification method ineffective as shown in **Figure 8**.

I expected some decrease in purification efficiency since the method relied on the specific binding of a small peptide, but to see such a dramatic loss of purification efficiency was alarming. While it was possible to make these analog-sensitive mutants with the GST-tagged constructs I previously showed I could express and purify kinases from, it seemed unfavorable to move forward with a kinase that exhibited such a large change in active site binding capabilities when the goal of my project is to determine whether two similar kinases, DNAJB1-PRKACA and PRKACA, display a difference in substrate specificity. Since I now had a way of purifying the kinases without a tag, I also wanted to use a method that did not require any additional mutations so the structure of the purified kinase would be one less caveat to interpreting any data.

At this time, I learned about 5'-(4-Fluorosulfonylbenzoyl)adenosine (FSBA) from the recently published K-BILDS methods paper (Embogama and Pflum 2017). FSBA irreversibly inhibits many kinases by reacting with a catalytic lysine in the active site. By treating cell lysates with FSBA, it is possible to significantly knockdown kinase activity.

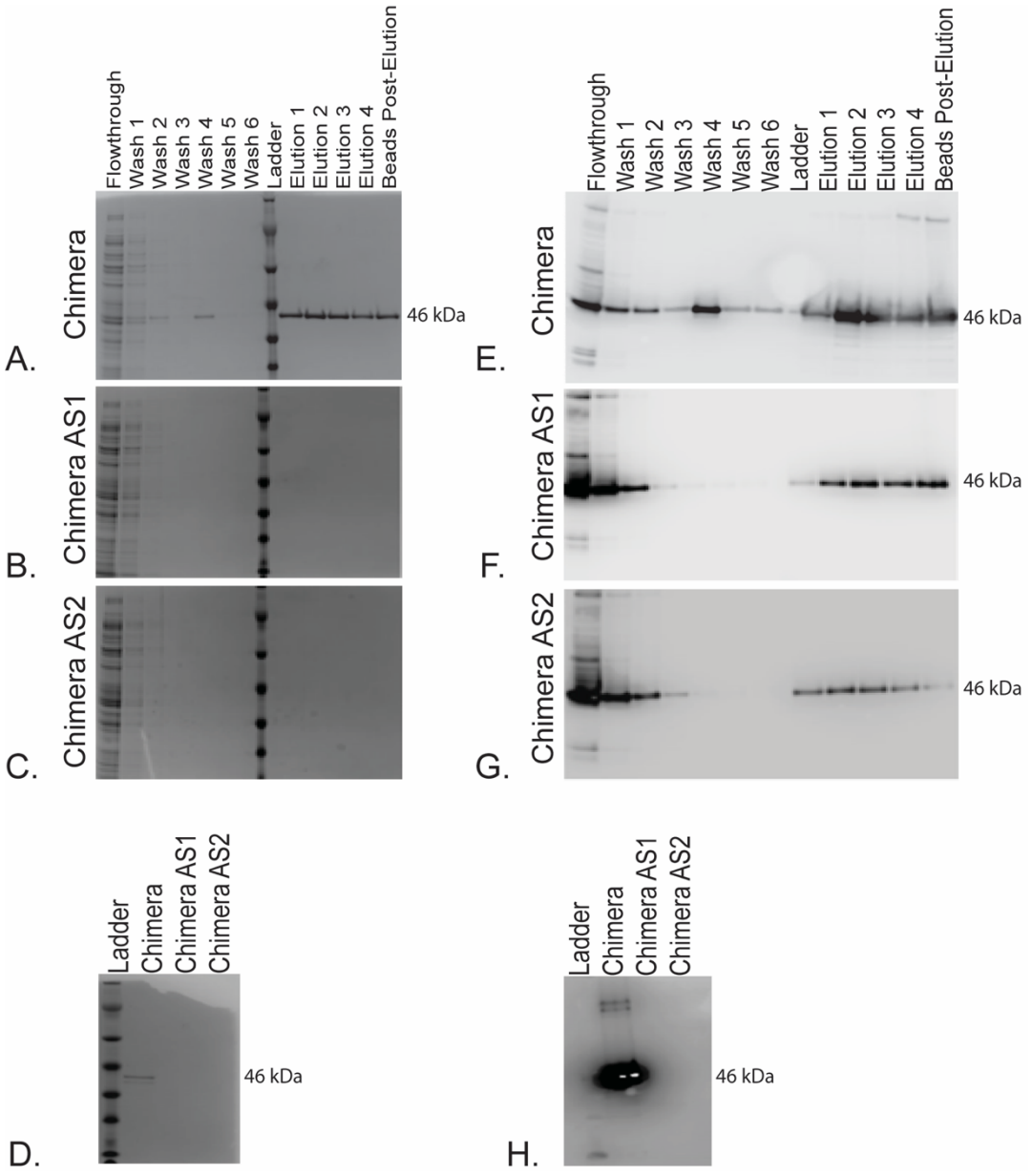

Figure 8. Purification of DNAJB1-PRKACA to Analog-Sensitive DNAJB1-PRKACA. (A-D) are Coomassie stained to visualize total protein content. (E-H) are western blots with an anti-PKA antibody to detect the presence of the DNAJB1-PRKACA, here marked as 'Chimera'. AS1 correlates to changing the gatekeeper methionine to a glycine and AS2 correlates to changing the methionine to an alanine. (A-G) are the results of protein purifications and (D and H) depict the protein detected after a necessary buffer exchange.

FSBA Inhibits Endogenous Kinase Activity in HeLa Cells and Mouse Liver Lysate

I pivoted to this method that knocks down the endogenous kinase activity of a lysate using FSBA. This would allow for the kinase-inactive lysate to be used in a kinase reaction with a purified kinase and an ATP analog that has a tag on the γ-phosphate to identify direct substrates via MS. **Figure 9** graphically summarizes the K-BILDS method discussed in Chapter I. This method uses an ATP with a biotin tag on the gamma phosphate but making this ATP analog is non-trivial.

I chose to modify this approach and use a commercially available ATP-γ-S analog instead; this experimental setup is shown in **Figure 10.** First, a cell lysate would be treated with FSBA to knock down endogenous kinase activity. It is crucial to sufficiently remove unbound FSBA after treatment so that no residual FSBA will inhibit the activity of the added purified kinase. The purified tagless PRKACA or DNAJB1-PRKACA would then be added to the inactive lysates with ATP-γ-S to yield thiophosphorylated substrates. Using purified PRKACA or DNAJB1-PRKACA without a tag allows for kinase reactions with the kinases in as unmodified of a state as possible in an *in vitro* setting. At this point, the thiophosphorylated substrates could either be alkylated to yield a thiophosphate ester that could be recognized by an established antibody (Abcam, ab92570) or, alternatively, these thiophosphorylated substrates could be trypsinized and enriched for thiophosphopeptides to be identified by MS. If the thiophosphorylated substrates are alkylated to produce a thiophosphate ester tag, the samples could be run on a gel to visualize changes in thiophosphorylation patterns by western blot or in-gel digested for MS analysis to identify the substrates. These

thiophosphate esters could also be used to immunoprecipitate the substrates containing the tag with a specific antibody (Abcam, ab133473) for MS analysis.

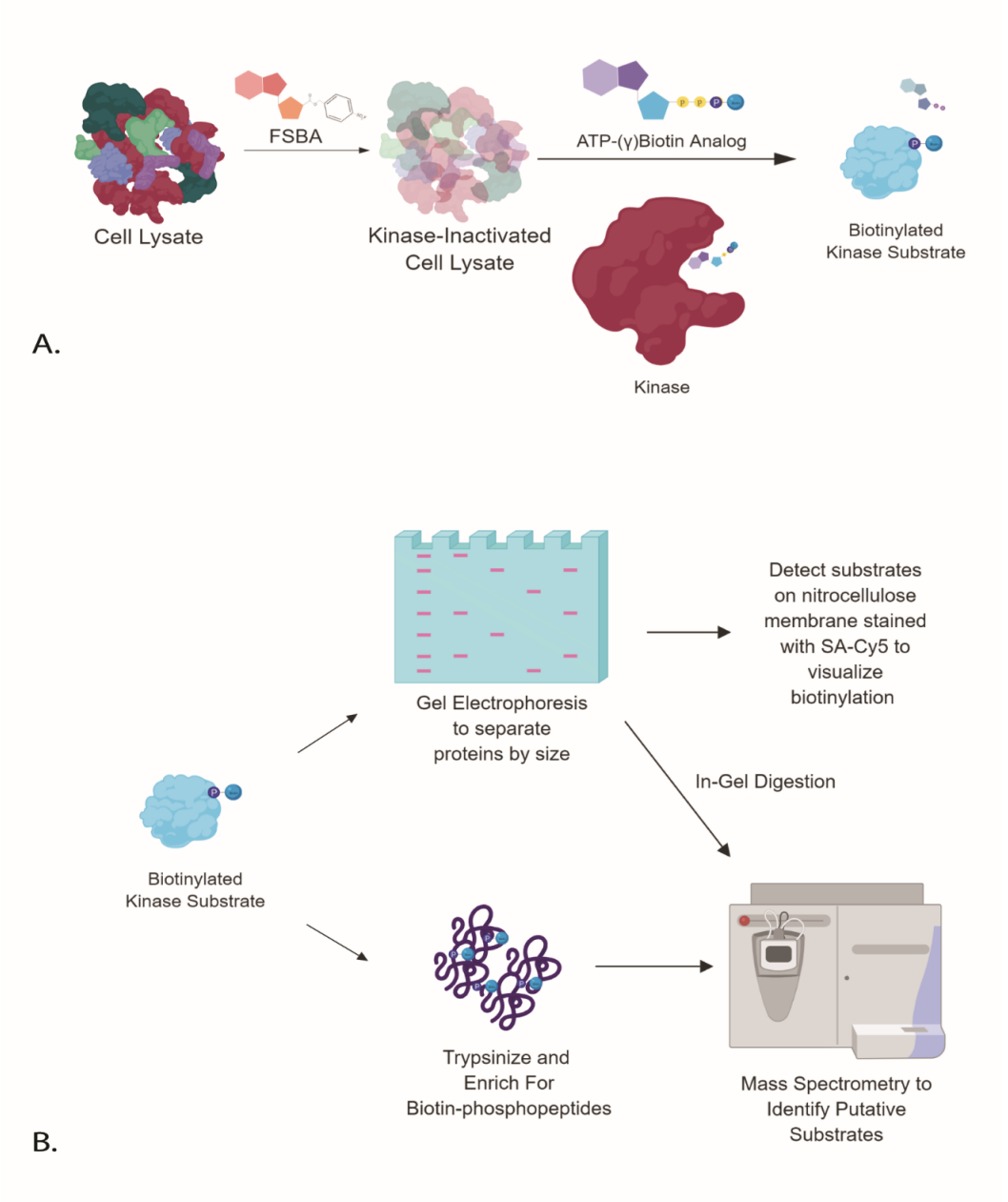

Figure 9. K-BILDS Method Schematic.

Created with BioRender and adapted from (Embogama and Pflum 2017).

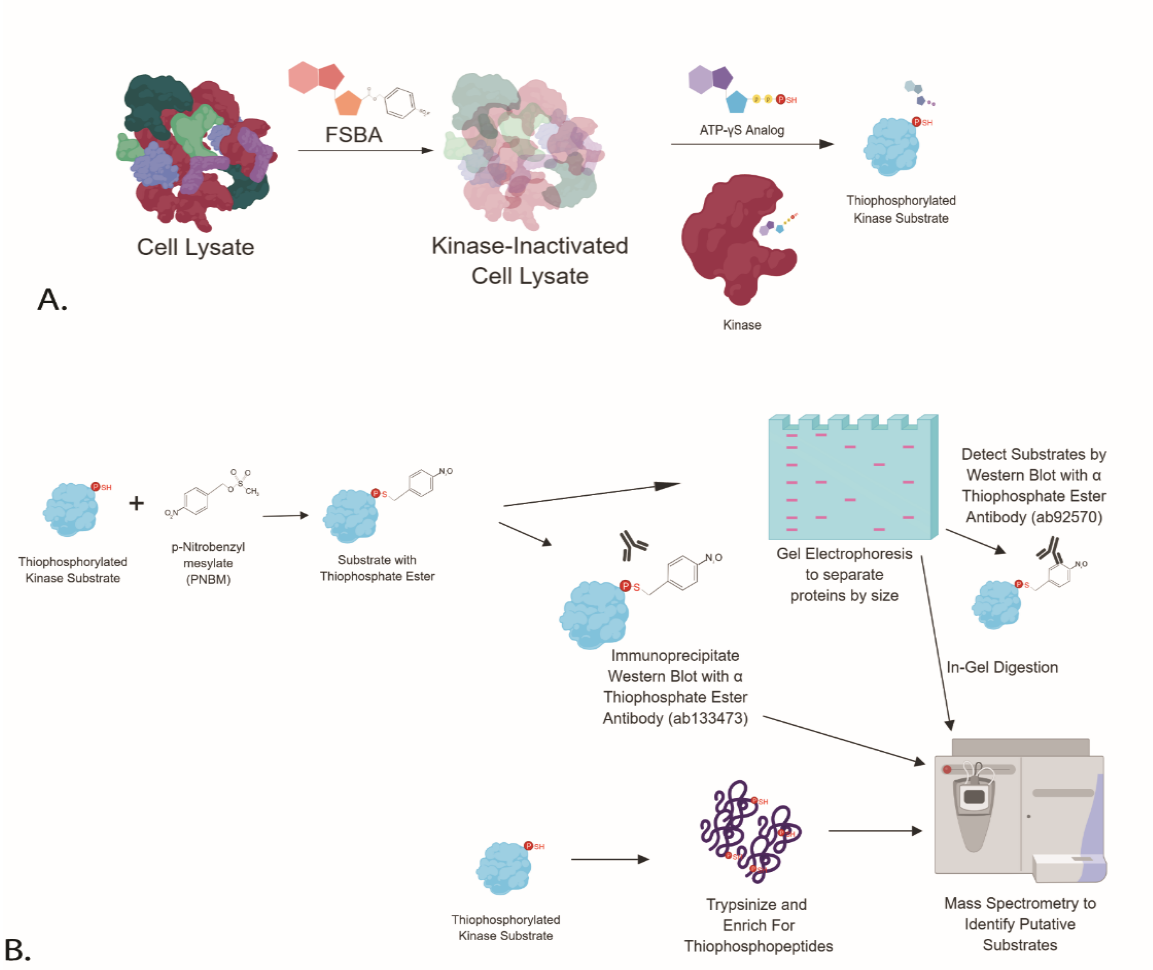

Figure 10. Substrate Identification Method Schematic Combining FSBA and Thiol-Tags.

This method combines aspects of the analog-sensitive kinase work flow with the K-BILDS work flow to maximize available resources. Created with BioRender.

My first step of setting up this pipeline was to show that I could also knock down kinase activity in HeLa lysates with FSBA as I saw in the K-BILDS paper, and to then see if I could visualize increased activity when adding PRKACA or DNAJB1-PRKACA to the inactivated-lysate. FSBA needs to be dissolved in DMSO and the final concentration of DMSO added to the lysates upon FSBA treatment is 20 mM. There was concern that

this high DMSO concentration could be solely responsible for any decrease in kinase activity seen. **Figure 11a** does show that there is a large decrease in activity between untreated and lysates treated with DMSO at 20 mM, but there is a further decrease of activity between the DMSO treated and FSBA treated lysates. Just a reminder that after FSBA treatment, FSBA is thoroughly washed out along with the DMSO so its presence is not directly affecting the kinase reaction. **Figure 11a** also shows that when both PRKACA and DNAJB1-PRKACA are added activity does increase as evidenced by the darker bands; this effect may seem light in western blots but is at least comparable to what is seen in previously published work for this method. Mass spectrometry is more sensitive and should pick up even more than the visible differences. Since FLC is a disease of the liver, I wanted to identify substrates of these kinases from the liver. To do this, I harvested and lysed mouse livers with a technician in the lab to create a large pool of mouse liver proteins to use instead of HeLa cells. Once I obtained this lysate, I also wanted to see if more phosphorylation could be detected by western blot if more kinase was added and indeed more phosphorylation can be detected with increasing amounts of PRKACA (**Figure 11b**). **Figure 11b** also demonstrates that the kinases in mouse liver lysate are not significantly inhibited by 20 mM DMSO, but they are greatly inhibited by 10 mM FSBA.

Interestingly, another lab published a substrate identification paper with a very similar method of FSBA kinase inhibition in a cell lysate and ATP-γ-S to be able to tag substrates for the PNG kinase (Hara et al. 2018). They also first attempted to use the analog-sensitive kinase approach but found that the gatekeeper mutations rendered the PNG inactive. It is possible to introduce other mutations to compensate for this change

in activity, but at the point where you are introducing multiple mutations into a crucial part of the kinase, it is hard to have confidence in the accuracy and specificity of substrates identified using this mutant kinase.

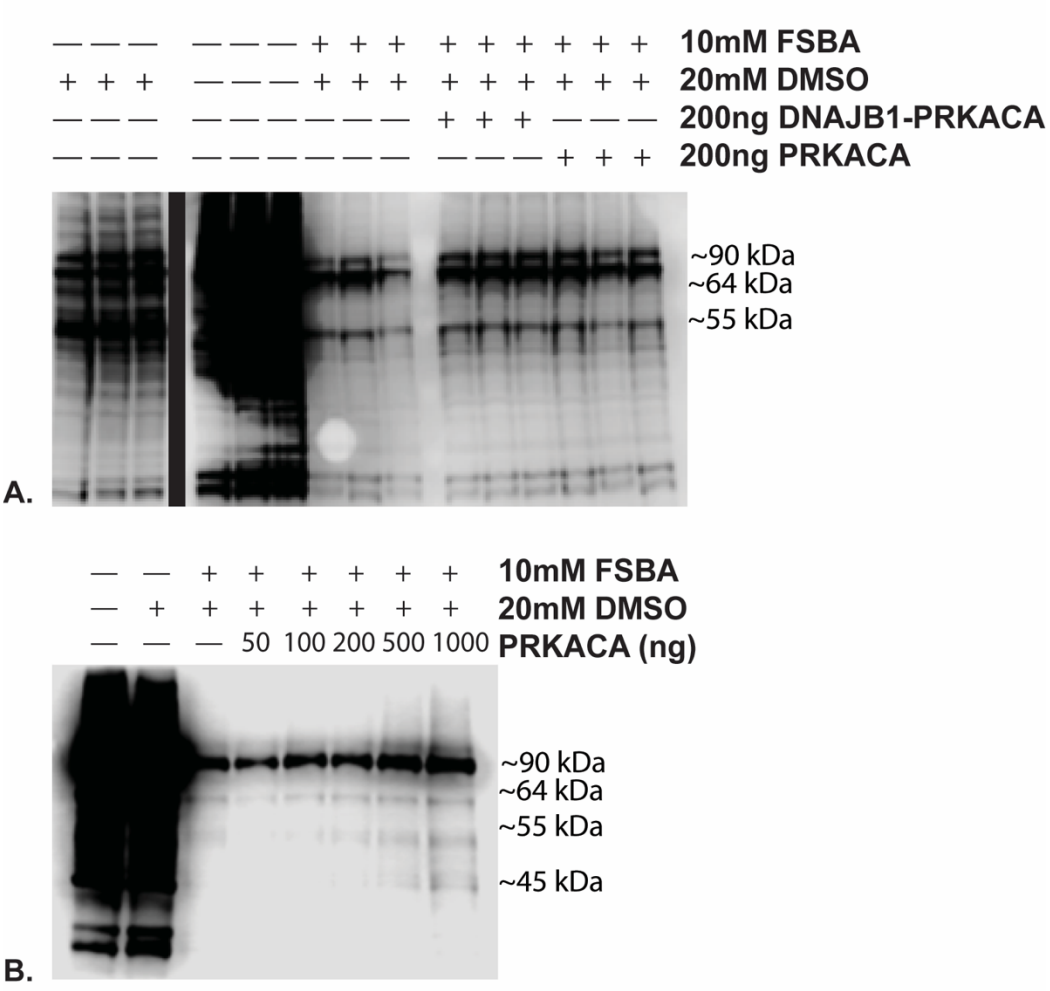

Figure 11. Purified Kinases Phosphorylate FSBA-Treated Lysates.

A. Kinases are inhibited in HeLa lysate by FSBA and DMSO, but more phosphorylation or kinase activity is seen when either kinase is added.

B. Kinases are inhibited in mouse liver lysate by FSBA but not by DMSO. Increasing amounts of PRKACA demonstrate that the increase in phosphorylation is due to the amount of purified kinase added. western blots used thiophosphate ester specific antibody from Abcam (ab92570).

Ineffective Substrate Identification via Mass Spectrometry from Kinase Reactions Using ATP-γ-S

The workflow in **Figure 10** was currently working to the point of being able to visualize activity changes via western blot with the anti-thiophosphate ester antibody. I was initially planning on doing a thiophosphopeptide enrichment by trypsin digesting the initial kinase reaction with FSBA-treated lysate, DNAJB1-PRKACA or PRKACA, and ATP-γ-S, and then pulling out the thiophosphopeptides with iodoacetyl agarose beads. This mixture could then be treated with Oxone to release the thiosphosphate ester linked peptides by spontaneous hydrolysis and identified by mass spectrometry (Hertz et al. 2010; Allen et al. 2007). However, after reading the recent paper identifying substrates of PNG kinase, I learned that they collaborated with Sebastian Lourido, who had a custom fast protein liquid chromatography (FPLC) system that yielded better results (Rothenberg et al. 2016). I put off trying the thiophosphopeptide enrichment in favor of contacting him for a potential collaboration. In the meantime, I attempted to identify the thiophosphopeptides via in-gel digestion or immunoprecipitation (IP).

At this time, I also learned of work being done in the Rice lab by Lefteris Michailidis and Ype de Jong that allows for an efficient method for growing human hepatocytes in mice and harvesting them for experimental use. While there is great homology between mouse and human liver proteins, I wanted to carry out these phosphorylation experiments in as close to the same liver substrate pool as is available to DNAJB1-PRAKCA in patient FLC tumors. It is possible, but unlikely, that the cell of origin of FLC are not hepatocytes, but human hepatocyte lysate would still provide a pool of human substrates from the same organ of disease that I believe could be more

relevant than mouse liver lysate to dissecting possible phosphorylations critical for FLC. I obtained a small aliquot of these cells to lyse and test if endogenous kinase activity could be diminished with FSBA treatment. **Figure 12A** shows that overall activity in the untreated human hepatocyte lysate is significantly less than the activity in the untreated lysate from mouse livers seen in **11B,** but activity is still diminished upon FSBA treatment. Though similar to the mouse liver lysate, the endogenous kinase activity of the human hepatocyte lysate does not seem to be affected by 20 mM DMSO treatment (**Figure 12A**). This makes the human hepatocyte lysate an even more advantageous lysate to use moving forward.

I used the remaining FSBA-treated hepatocyte lysate I had at the time to do a comparison of thiophosphopeptides identified via in-gel digestion between the mouse liver lysate and human hepatocyte lysate. The western blots from these kinase reactions show increased activity in the presence of DNAJB1-PRKACA in mouse liver lysate and human hepatocyte lysate, but only an increased pattern of activity was seen when PRKACA was added to mouse liver lysate and not human hepatocyte lysate (**12B and C**). This was only a single replicate visualized once by western blot, but these same blots were probed with an anti-PKA antibody that showed similar amounts of the kinases were definitely added (**Figure 12D and E**), and the kinases used for these reactions came from the same aliquot, so this was an unexpected result. Working with Soren Heissel in the Proteomics Resource Center, bands were excised from a coomasie stained gel in the places where thiophosphate ester tags were visualized via western blot as indicated by the red (**Figure 12F-H**).

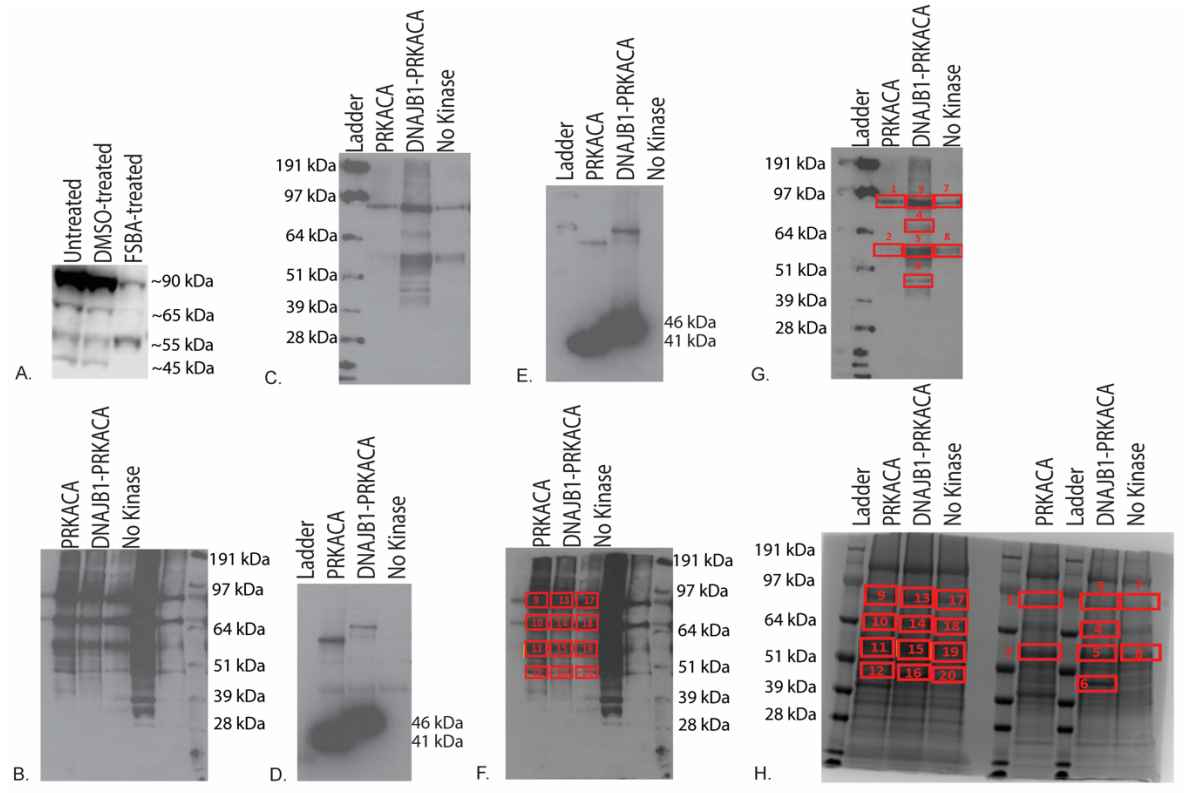

Figure 12. In-Gel Digestion of Kinase Reactions with ATP-γ-S in Mouse Liver Lysate and Human Hepatocyte Lysate.

(A) FSBA-treatment of human hepatocytes. (B, D, and F) western blots of kinase reactions with FSBA-treated mouse liver lysate. (C, E, and G) western blots of kinase reactions with FSBA-treated human hepatocyte lysate. (H) Bands were cut out from this coomassie stained gel for in-gel digestion and MS analysis. The red boxes on this gel match the red boxes on the blots in F and G. (A-C, F, and G) western blot with anti-thiophosphate ester antibody. (D-E) western blot with anti-PKA antibody.

There were more than 7600 peptides identified from MS analysis for this experiment, but only a handful had what could be considered a thiophosphate tag on an amino acid (**Table 4**). When the kinase used ATP-γ-S to phosphorylate a substrate, a thiophosphate group was added to an amino acid, most likely serine or threonine since PRKACA is a Ser/Thr Kinase. This thiophosphate was then alkylated with PNBM to create a thiophosphate ester. As noted in the paper from the Shokat lab (Allen et al. 2007), this structure can fragment, leaving a different signature behind which is denoted as 'TPE D' in **Table 4** and **Table 5**. The non-fragmented thiophosphate ester is denoted as 'Thiop' for these tables. The MS searches for these structures were conducted as previously published (Allen et al. 2007).

To compare the thiophosphopeptides found at the same molecular weight in the different conditions, I grouped the bands that were cut out for the in-gel digestion into 'Band Groups' based on which kinase was present in the initial reaction. These 'Band Groups' are listed in **Table 3** with their corresponding members and used in **Table 4** to easily visualize which 'Band Group' a thiophosphopeptide was identified from. None of the thiophosphopeptides identified in these gel digestions belonged to proteins that were established PKA substrates, and only Krt17 and Canx were also initially identified in the wide-reaching screen from Imamura, et al but not in the other published lists of putative substrates. If a thiophosphopeptide was identified in the 'No Kinase' Band Groups, it should have been identified in all of the corresponding bands for PRKACA and DNAJB1-PRKACA; this was not the case. The minimal detection of thiophosphopeptides and lack of consistency was very discouraging.

Table 3. Band Cut Outs for In-Gel Digestion and MS Identification of Thiophosphopeptides.

Band Groups for Comparison	Corresponding Red Box Label from In-Gel Digestion
PRKACA Band 1	Mouse-9; Human-1
PRKACA Band 2	Mouse-11; Human-2
DNAJB1-PRKACA Band 1	Mouse-13; Human-3
DNAJB1-PRKACA Band 2	Mouse-14; Human-4
No Kinase Band 1	Mouse-17; Human-7
No Kinase Band 2	Mouse-19; Human-8

Table 4. Thiophosphopeptides Identified Using In-Gel Digestion and MS.

Peptides from Human Hepatocyte Lysate	Uniprot #; Gene Name	Thiophosphate Modification	PRKACA Band 1	PRKACA Band 2	DNAJB1-PRKACA Band 1	DNAJB1-PRKACA Band 2	No Kinase Band 1	No Kinase Band 2
SHMLERLYQTK	P52737; Znf136	S1(TPE D)					x	
FKIDASVEK		S6(TPE D)				x		x
KPIHHFLGISTFSQYTVVDENAVAK	P07327; Adh1a	T11(Thiop)	x			x	x	
YQELMNVKLALDIEIATYR	Q6KB66; Krt80	Y1(TPE D)				x		
LIYNSLGGNNR	A0A0C4DGL2; Trpm7	S5(TPE D)	x			x		
IVTNHLYLYEIAR	D6RHD5; Alb	T3(TPE D)				x		
RKPIHHFLGISTFSQYTVVDENAVAK	P07327; Adh1a	S11(TPE D) T12(TPE D)				x		
XFEGEVTKENLLDFIK	H0Y3Z3; P4hb	T7(TPE D)				x		
NKIIAATIENAQPILQIDNAR	P08779; Krt16	T7(TPE D)	x		x	x		
LSLNIDPDAK	H0YIV0/P14625; Hsp90b1	S2(Thiop)	x		x			
RSGEPMVSMQAAEEIR		S2(Thiop)		x				
VGWEQLLTSIARTINEVENQVLTRDAK	Q08043; Actn3	T8(TPE D) (T13(TPE D) T23(TPE D)	x					

Peptides from Mouse Liver Lysate	Uniprot #; Gene Name	Thiophosphate Modification	PRKACA Band 1	PRKACA Band 2	DNAJB1-PRKACA Band 1	DNAJB1-PRKACA Band 2	No Kinase Band 1	No Kinase Band 2
SLAFAYVPVQLSEVGQQVEVELLGKNYPATIIQEPLVLTEPAR	Q9DBT9; Dmgdh	S12(Thiop)	x				x	
LKKSADTLWGIQK	P06151; Ldha	S4(Thiop)			x			
LGTSELLLAK	H3BKD4; Asap1	T3(TPE D)		x		x		
NKILVATVDNASILLQIDNAR	Q9QWL; Krt17	T7(TPE D) S12(TPE D)	x		x			
YLRDAGCPVFLYEFQHTPSSFAK	G5E8K; Ces3b	Y1(Thiop)		x		x		

I also continued with the IP experiment using mouse liver lysate since I already had the materials, and there would be a lag time before I could receive more human hepatocytes to lyse and treat with FSBA. For the IP of substrates with thiophosphate

ester tags, I prepared three 1mg samples of FSBA mouse liver lysate that either had no kinase added, 10ug of DNAJB1-PRKACA added, or 10ug of PRKACA added with ATP-γ-S. The three possible results I was hoping to see from the IP were examples of a thiophosphopeptide in: 1) just the sample treated with DNAJB1-PRKACA, 2) just the sample treated with PRKACA, or 3) both the samples treated with DNAJB1-PRKACA or PRKACA but not the sample without added kinase. Before submitting the IP samples to the Proteomics Core for MS analysis, I took a small aliquot to run on a gel to ensure that increased activity was visualized via western blot in the samples that had kinases added and that protein content was consistent between the samples as visualized by coomassie staining (**Figure 13**). While thiophosphopeptides were also identified in the no kinase control as seen previously, the signal was stronger in the conditions with added kinase which was promising for the mass spectrometry results since the total amount of protein also looked consistent between samples in the Coomassie stained gel.

However, there was only a single potential candidate protein identified in each of the predicted categories as seen in **Table 5**. Only Wipi2 was identified in a previous PKA substrate screen, but again it was the Imamura, et al. screen that initially casted a very wide net of putative substrates. Also, in this experiment, Wipi2 was recognized by DNAJB1-PRKACA and not PRAKCA. Even though this pilot IP experiment with mouse liver lysate only had one sample per condition; these results were very discouraging. It is additionally notable that only the degraded thiophosphate ester structure was able to be identified in this experiment.

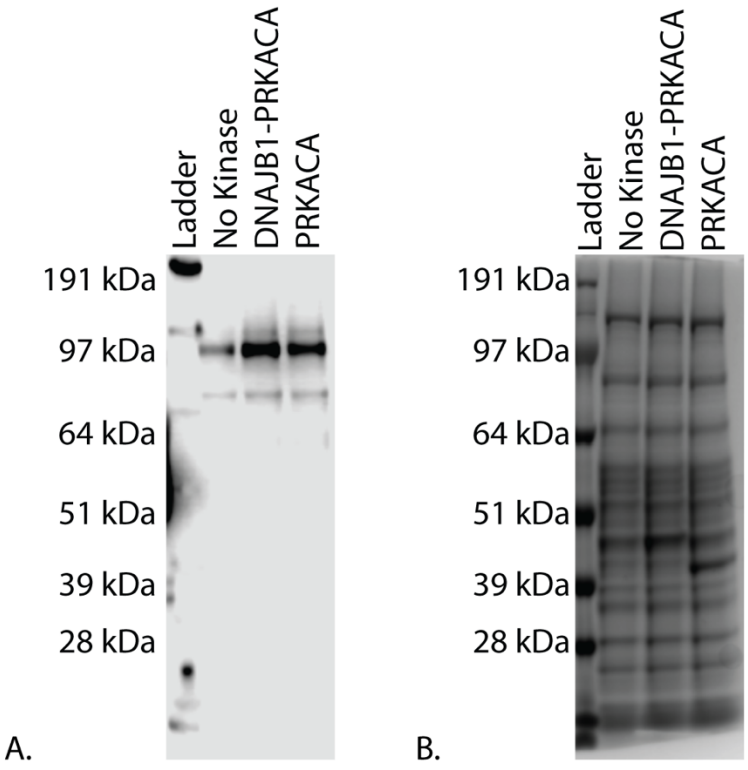

Figure 13. Immunoprecipitated Thiophosphopeptides from Kinase Reactions with FSBA-treated Mouse Liver Lysate and ATP-γ-S.

A. The thiophosphate ester antibody (ab92570) was used to visualize the amounts of thiophosphorylated substrates that were immunoprecipitated from kinase reactions with ATP-γ-S.

B. Coomassie staining shows that the amount of protein loaded from each sample was fairly consistent. It is also possible to see the band at 41kDa for PRKACA that was added. The DNAJB1-PRKACA band at 46kDa seems to be masked by other proteins at the same molecular weight, but the band is slightly darker where this kinase should be as well.

Table 5. Thiophosphopeptides Identified by MS from Proteins Immunoprecipitated with the Anti-Thiophosphate Ester Antibody.

Identified In Sample	Uniprot # Gene Name	Thiophosphate Modification	Peptide Sequence
DNAJB1-PRKACA	D3YWK1 Wipi2	S1(TPE D)	SGYKFFSLSSVDK
DNAJB1-PRKACA & PRKACA	F6RCB2 Cyp2r1	T10(TPE D)	SFESKILEETWSLIDAIETYK
PRKACA	Q9QYB8 Add2	S1(TPE D) S4(TPE D) S8(TPE D)	STESQLMSKGDADTK

The thiophosphopeptide enrichment was never attempted in our lab since there was such difficulty identifying these specific tags with our Proteomics Resource Center using the published mass and structures. We also did not move forward with the collaboration to alternatively enrich thiophosphopeptides using a custom FPLC system. However, the ATP-γ-S and anti-thiophosphate ester antibody have been extremely useful tools to assess the knockdown of endogenous kinase activity in a cell lysate with FSBA.

Phosphopeptide Enrichment from Kinase Reactions with ATP is Sufficient to See Differences in Substrate Specificity in Mouse Liver Lysate

With current phosphopeptide enrichment technology, I was encouraged by members of the Proteomics Resource Center to try kinase reactions with regular ATP to see if we could detect increased phosphorylation upon addition of DNAJB1-PRKACA or PRKACA in FSBA-treated liver lysates. Since at this point, I was still waiting for more human hepatocytes to lyse, I did a pilot experiment using FSBA-treated mouse liver lysate for a kinase reaction with regular ATP in single replicates in three conditions: added PRKACA, added DNAJB1-PRKACA, and no kinase added. Phosphopeptide enrichment was done by Soren Heissel in the Proteomics Resource Center, using in-house constructed titanium dioxide microtips followed by Thermo's High-Select Fe-NTA Phosphopeptide Enrichment Kit. A generalized overview of how this experiment was carried out is depicted in **Figure 14**.

Figure 15 clearly demonstrates that phosphopeptides are more abundant when either the DNAJB1-PRAKCA or PRKACA are added to a kinase reaction. Analysis of the identified phosphosites was performed within the Perseus framework (v. 1.6.1.3). The histograms in **Figure 15C** are not normalized since this pilot experiment was not done in triplicate, but the raw intensity measurements still clearly show that the amount and distribution of phosphopeptides identified in the samples with kinases added is more abundant than when no kinase is added.

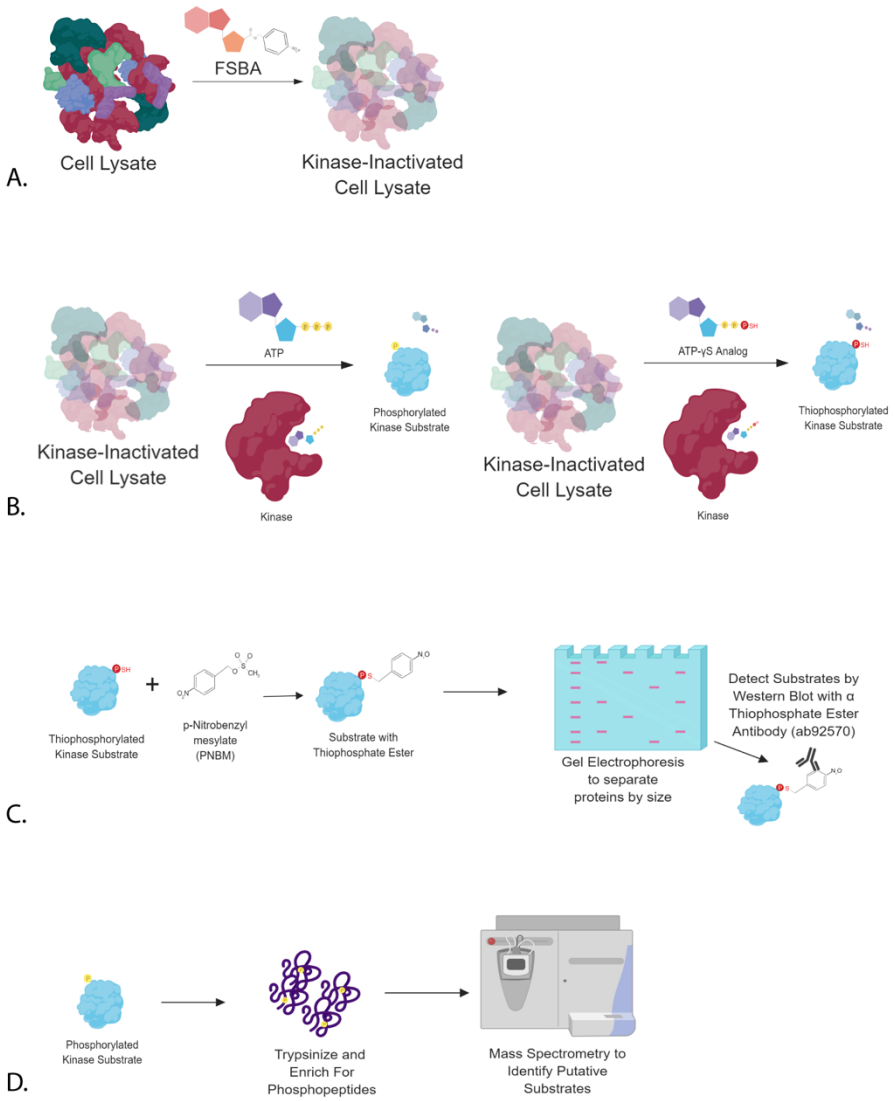

Figure 14. Schematic Overview of a Method to Identify Phosphopeptides Using FSBA-Treated Lysates.

FSBA is still used to knock down endogenous kinase activity in a cellular lysate (A). Then separate kinase reactions are carried out with either ATP or ATP-γ-S and the kinase of interest (B). Thiophosphorylated substrates are then alkylated and run on a gel to be able to visualize FSBA knockdown of endogenous kinases and increased activity upon kinase addition (C). Then the phosphorylated substrates obtained from the kinase reaction in B can be digested and enriched for phosphopeptides and analyzed by MS.

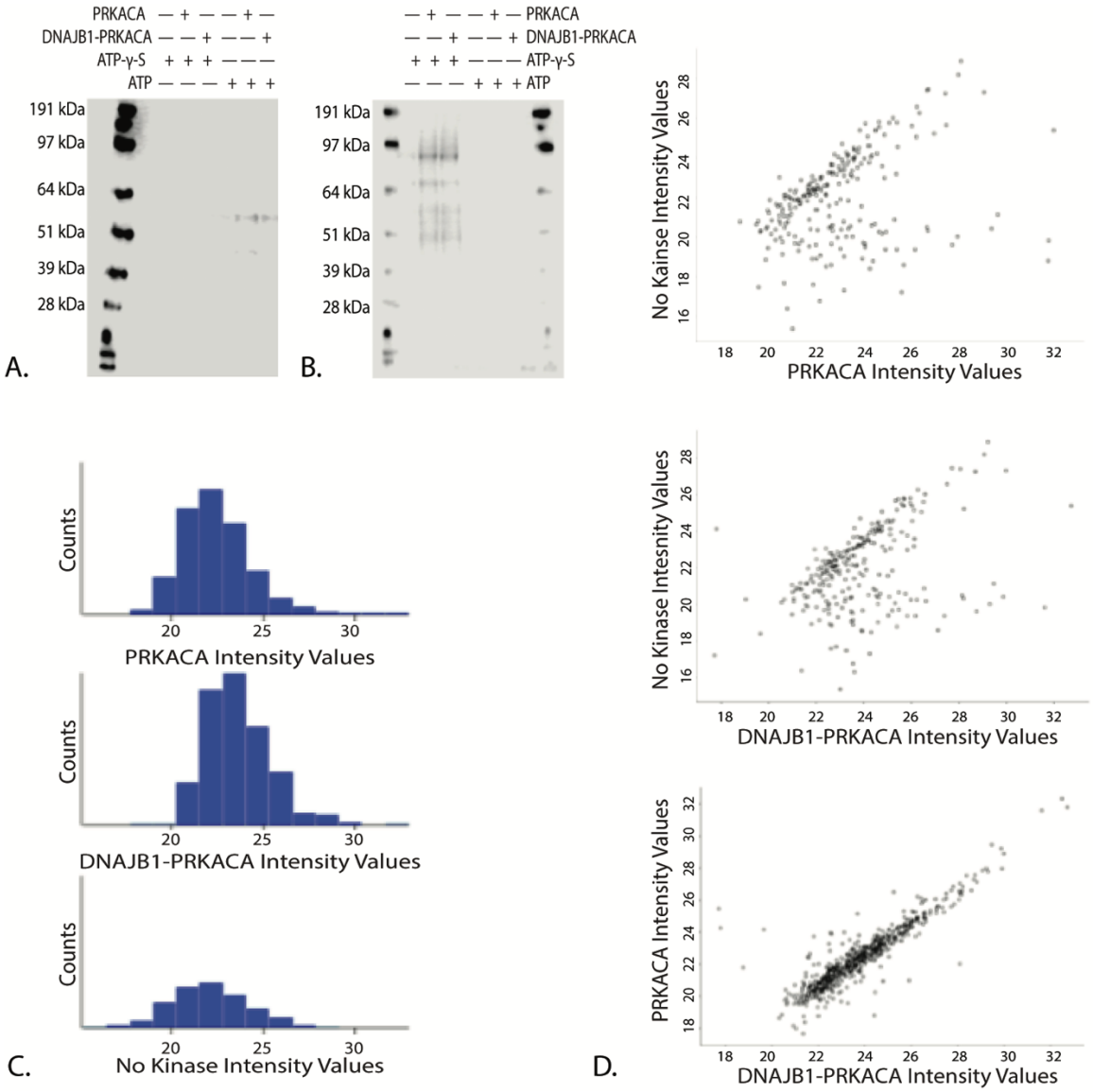

Figure 15. Phosphopeptide Increase in Presence of Added Kinases in FSBA-Treated Mouse Liver Lysate.

Western blots using an (A) anti-thiophosphate ester antibody (ab92570) and a (B) Phospho-(Ser/Thr) Antibody from CST (9631) against different kinase reactions. (C) Histograms of raw intensity measurements of enriched phosphopeptides (x-axes). (D) Scatter plots of raw intensity measurements of enriched phosphopeptides.

Each individual point on the scatter plot in **Figure 15D** represents a unique phosphopeptide that was identified in their respective samples at their particular intensity (or prevalence) in the sample. The scatter plots show that a great portion of the reaction with DNAJB1-PRKACA added or PRKACA added differ in prevalence compared to when no additional kinase was added. Since DNAJB1-PRKACA and PRKACA both have the active site of their kinase encoded by the same exon, it is not surprising that the majority of phosphopeptides identified in both samples are similar to each other. However, it is exciting to see that there are quite a few phosphopeptides that are unique to both of these samples.

To clearly represent this difference seen in potential substrates, the gene names of all unique proteins with phosphopeptides were inputted into the proportional Venn diagram webtool, BioVenn (Hulsen et al. 2008). 360 proteins were identified with phosphorylation sites in the reactions with added kinases that were not present in the reaction with no added kinase. And excitingly, 64 proteins were only identified in the reaction with DNAJB1-PRKACA added. Granted, since this is just a single sample per condition, the possibility of a false positive here is high. However, these were highly encouraging results to move forward and repeat this experiment in triplicate in the human hepatocyte lysate. Especially since in this experiment, many known and suggested PKA substrates were able to be identified (**Table 6**).

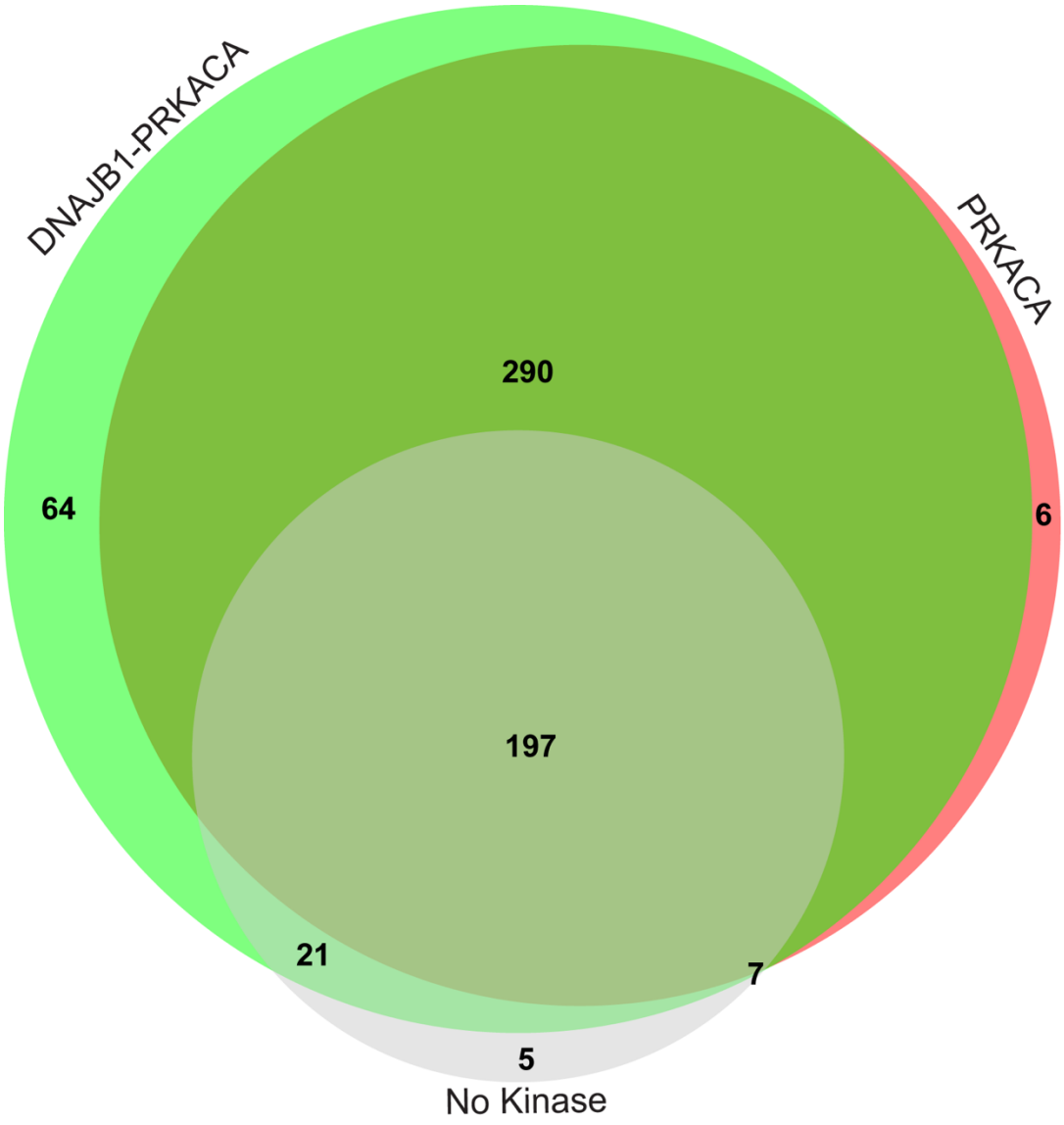

Figure 16. Venn Diagram of the Number of Mouse Proteins with Phosphosites Found in Samples with PRKACA, DNAJB1, or No Kinase Added.

500 unique proteins with identified phosphosites from the sample with PRKACA added is represented in red on the right. 230 unique proteins with identified phosphosites from the no kinase added sample is represented in grey in the middle. 572 unique proteins with identified phosphosites from the sample with DNAJB1-PRKACA added is represented in green on the left. This proportional Venn Diagram was generated using Biovenn (Hulsen et al. 2008).

Table 6 was generated similarly to **Table 1**, but since there are more than five conditions, it is not possible to have this represented in an image with this software. However, the information from the table generated by the same Bioinformatics and Evolutionary Genomics Venn diagram web tool (http://bioinformatics.psb.ugent.be/webtools/Venn/) is more informative. The previous comparison of the five published methods had a total of 1713 putative PKA substrates; this table shows that between DNAJB1-PRKACA and PRKACA in this *in vitro* assay in mouse liver lysate, 339 more putative substrates were added to this list to total 2052 putative substrates of a PKA kinase.

Table 6. Gene Name Overlap of Putative PKA Substrates from Five Published Methods and the *in vitro* Mouse Data.

Overview of Studies		
Study Identifying Substrates	**Total Number of Putative Kinase Substrates**	
Embogama, et al.	279	
Hamaguchi, et al.	45	
Hu, et al.	301	
Imamura, et al.	1132	
Isobe, et al.	197	
DNAJB1-PRKACA *in vitro* Mouse Liver Lysate	454	
PRKACA *in vitro* Mouse Liver Lysate	392	
Total Number of Unique Putative Kinase Substrates: 2052		
Specific Overlaps Between Studies		
Groups of Studies Identifying Substrates	**Number of Overlaps**	**Overlap of Putative Kinase Substrates**
Hamaguchi, et al. Hu, et al. Imamura, et al. Isobe, et al.	1	CAD
Hamaguchi, et al. Imamura, et al. Isobe, et al. PRKACA *in vitro* Mouse Liver Lysate	1	TNKS1BP1
Embogama, et al. Hu, et al. Imamura, et al. Isobe, et al.	1	SPTBN1
Imamura, et al. Isobe, et al. DNAJB1-PRKACA *in vitro* Mouse Liver Lysate PRKACA *in vitro* Mouse Liver Lysate	10	NSFL1C CTNND1 COBLL1 IRF2BP2 ARHGAP17 PRKAR2A ARPP19 EIF4B OPTN YBX3

Embogama, et al. Hamaguchi, et al. Hu, et al. Imamura, et al.	1	PDE3A
Embogama, et al. Imamura, et al. Isobe, et al. DNAJB1-PRKACA *in vitro* Mouse Liver Lysate PRKACA *in vitro* Mouse Liver Lysate	1	LMNA
Hu, et al. Imamura, et al. DNAJB1-PRKACA *in vitro* Mouse Liver Lysate PRKACA *in vitro* Mouse Liver Lysate	7	NPM1 STMN1 NDRG1 TRIM28 ARFGAP2 LASP1 HSP90AA1
Embogama, et al. Hu, et al. DNAJB1-PRKACA *in vitro* Mouse Liver Lysate PRKACA *in vitro* Mouse Liver Lysate	2	YWHAH PRKACA
Embogama, et al. Hamaguchi, et al. Imamura, et al. PRKACA *in vitro* Mouse Liver Lysate	1	RPLP2
Embogama, et al. Imamura, et al. DNAJB1-PRKACA *in vitro* Mouse Liver Lysate PRKACA *in vitro* Mouse Liver Lysate	7	SLC9A3R1 SPAG9 EGFR PDIA6 MARCKSL1 GORASP2 KHSRP
Hu, et al. Imamura, et al. Isobe, et al.	2	SMARCAD1 PCM1
Hu, et al. Isobe, et al. DNAJB1-PRKACA *in vitro* Mouse Liver Lysate	2	CTNNB1 BAD
Hu, et al. Isobe, et al. PRKACA *in vitro* Mouse Liver Lysate	1	LSR

Hamaguchi, et al. Imamura, et al. Isobe, et al.	5	SPECC1L SIK2 REPS1 LIMCH1 DENND4C
Imamura, et al. Isobe, et al. DNAJB1-PRKACA *in vitro* Mouse Liver Lysate	3	TJP1 YAP1 WNK1
Embogama, et al. Isobe, et al. PRKACA *in vitro* Mouse Liver Lysate	1	AGPS
Isobe, et al. DNAJB1-PRKACA *in vitro* Mouse Liver Lysate PRKACA *in vitro* Mouse Liver Lysate	8	CCS SRP14 NCK1 MIA3 HSPA4 SNX2 PLEKHF2 KARS
Embogama, et al. Hu, et al. Imamura, et al.	9	NASP YWHAZ GFPT1 CTTN SMARCC2 ACACA YWHAE ZYX FLNA
Hamaguchi, et al. Hu, et al. Imamura, et al.	1	RAF1
Hu, et al. DNAJB1-PRKACA *in vitro* Mouse Liver Lysate PRKACA *in vitro* Mouse Liver Lysate	8	STK24 LRP1 MYLK CRIP2 CBX3 VASP PRDX5 ARHGDIA
Embogama, et al. Imamura, et al. DNAJB1-PRKACA *in vitro* Mouse Liver Lysate	1	DPYSL2
Imamura, et al. DNAJB1-PRKACA *in vitro* Mouse Liver Lysate PRKACA *in vitro* Mouse Liver Lysate	42	BET1L UBA1 RBM17 HSPD1 ATP11C DDI2 GPS1 ACLY HMOX1 EEF1D PCNP NUDC HSP90AB1 TCEA1 HTATSF1 EPS8L2 PPIP5K2 USP5 SHTN1 GAPDH SEC61B DBNL EIF6 TPD52L2 PRDX6 SNRNP70 VAPA HUWE1 ZNRF2 SEC22B OCIAD1 ALDOA DIS3L2 RANBP3 PHACTR4 MARCKS CANX EIF2S2 MIOS HDGF GMPS CLNS1A
Embogama, et al. DNAJB1-PRKACAc *in vitro* Mouse Liver Lysate PRKACA *in vitro* Mouse Liver Lysate	19	ECHS1 TKT HYOU1 NUCB1 SARS ETFA MTHFD1 ACAA2 SBDS RNH1 CAT CLTB SDHA PGK1 ACADS PSME1 PRKCSH CLU ST13

Hamaguchi, et al. DNAJB1-PRKACA *in vitro* Mouse Liver Lysate PRKACA *in vitro* Mouse Liver Lysate	2	CDK18 DAPK2
Hu, et al. Isobe, et al.	7	NUP133 LRRFIP1 SRC ZHX1 NFKB1 MAP2 SUFU
Imamura, et al. Isobe, et al.	52	MYO9B TNS3 PI4KB ATG2B ARHGAP21 DCP1A XRN2 DYNC1H1 OSBP SORBS2 FAM83H PXN ARFGEF2 IRS2 EIF5B PUM2 HECTD1 CTNNA1 TXLNG RBM14 PRKD2 MARK2 NCOR1 C2CD2L FKBP15 RAB11FIP1 ABCC1 ARHGAP35 DOCK7 ABLIM1 MEF2D SQSTM1 BNIP2 ENAH LIMA1 WWC1 PLEKHG3 SIPA1L1 PKN2 RIN1 AKAP1 MAP3K2 MICAL3 FBL PRRC2A OSBPL11 TJP2 HPS5 LARP4B PARD3 PUM1 ITPR3
Hamaguchi, et al. Isobe, et al.	6	NF1 RPL18A KIAA1522 ARHGEF7 NHSL1 PITPNM3
Isobe, et al. DNAJB1-PRKACA *in vitro* Mouse Liver Lysate	2	SAYSD1 GOLGA5
Isobe, et al. PRKACA *in vitro* Mouse Liver Lysate	1	CASP6
Hu, et al. Imamura, et al.	36	CD44 HSPB1 LUZP1 TERF2IP SMC3 DNAJC5 NCOA3 NEDD4L FYN SAFB2 TRIP10 EIF4ENIF1 LIG1 LARP4 DNM1L PDE3B ANKS1A MATR3 PTPN12 CDCA7L STUB1 LARP1 VIM PRKAR1A HIRIP3 PYGO2 FOXP4 SP100 EMD ATRIP LAS1L TBC1D10B AKAP13 CHAF1B UHRF1 CEBPB
Embogama, et al. Hu, et al.	8	YWHAG PSMC5 MSN TGM2 HLA-A PTBP1 XPO1 PSMA8
Hamaguchi, et al. Hu, et al.	2	CAMKK1 C19ORF21
Hu, et al. PRKACA *in vitro* Mouse Liver Lysate	1	ASPSCR1
Embogama, et al. Imamura, et al.	43	PDHA1 CLUH PALLD YWHAQ RANBP1 HNRNPK BAG3 NACA MYO1E HNRNPD SF3A1 EFHD2 BOD1L1 SSB PPP6R3 HDAC1 IGF2R MCMBP SRRM2 TCOF1

		MAP4 PSMA3 ACTL6A KDM5C SLC1A5 RCC2 INF2 EPRS CAP1 FLNB TP53BP1 EIF4G1 LRRC47 TK1 SLC4A1AP SLC16A3 EDC4 PAICS SUPT6H MAGED2 SERBP1 EIF3G PAK2
Hamaguchi, et al. Imamura, et al.	4	SAFB ZNF318 C2CD5 ACIN1
Imamura, et al. DNAJB1-PRKACA *in vitro* Mouse Liver Lysate	12	PCBP1 EIF3H PRCC WASL APMAP SZRD1 ACSS2 PGRMC1 PEA15 CDV3 DAP CLIP1
Imamura, et al. PRKACA *in vitro* Mouse Liver Lysate	4	TMEM230 BCL2L13 UBA2 STRN
Embogama, et al. DNAJB1-PRKACA *in vitro* Mouse Liver Lysate	3	TLN1 ARFIP1 PSME3
Embogama, et al. PRKACA *in vitro* Mouse Liver Lysate	3	LAP3 AP2M1 CP
Hamaguchi, et al. DNAJB1-PRKACA *in vitro* Mouse Liver Lysate	1	KLC4
DNAJB1-PRKACA *in vitro* Mouse Liver Lysate PRKACA *in vitro* Mouse Liver Lysate	257	CNBP ACOT12 HMGCS2 NDUFS1 SLK CLTA ALDOC HSPA1L VWA5A BHMT DSTN ALDH2 C3 LCMT1 GCLM SCP2 NDUFS4 GPD1 FAM213B CES1F ELAC2 PSMD11 ALAD SNX6 NDUFA2 BTF3 UCHL4 GM20425 RPS21 ATP1A1 PFKL GC CYP2C70 ALDH6A1 PHB2 WDR91 LXN CNGA2 SET ATP5H AKAP2 ACADVL FDX1 TALDO1 SEPHS1 SNRPG SERPINA1B DECR2 CYP2B10 GATD3A EPN1 RPL24 MAVS VCP ALDH5A1 CES3A URAD MOCS1 SNAP29 SDS ASNA1 FCGRT TSSC4 ASL SASH1 ACADM NAMPT TTC36 OXSM CMC2 NECAP1 APOH NDUFV1 GIMAP4 CFL1 F13B AKR1D1 D2HGDH DNAJC8 BCKDHA ACSL1 CDC42EP5 MRPS31 SEMA6D MRPS36 TST CCDC180 NADK H2-KE6 NDUFB11 CPOX EVA1A CYP4F17 PPP1R11 CPS1 MESD LCP1 EIF4H ETFB IDH1 CFDP1 TIMM50 HDGFL2 CALD1 HIBADH ALB AKR1C6 ERRFI1 GPX1 CIDEB FTL1 LBH ACTG1 MTFR1L KEG1 HSD17B6 CYP2A5 TYMP SERPINA1C COMT UQCRC2 ACTR3 GPHN ADH1 CNPY2 JPT1 RIDA ACOT1

		NAXE LDHD DNAJB1 CA14 LYPLA1 ACAT1 TAGLN2 RAPH1 AFG3L2 SULT2A8 MRPL12 PARVA PKLR KIF5B PIGR NT5C GM9774 RAB21 TUBA1B PSMC6 SSR3 CORO1B SERPINA3N EARS2 SELENBP2 UQCRFS1 AKR7A2 CALR SPR SULT2A1 OXR1 SLIRP DHTKD1 CYP2E1 CTH ATP5F1A GYKL1 GSDMDC1 CYP2F2 ALDH7A1 TOM1 DNAJC12 AMACR 9-Sep GOPC PNPLA8 GLYCTK ADCY10 ASGR1 EEF1A1 ATP5PF IDH3A ACSM5 PSMA2 GLUD1 HPD EEF2 HMGN5 DPP3 ISOC2A ATP6V1B2 NSF CYP1A2 SERPINA3K ACAD9 PYGL STARD10 NUBP1 ETFDH HSPA9 ALDH8A1 ENSA ETHE1 PRODH ACAT2 GNMT PPP2R1A GLUL HNRNPAB ALDH1A1 FMO5 HSP90B1 SMOC1 GSTA3 NIT1 GRN SNX3 INMT AFMID ACSF3 THUMPD1 KIF13B UBQLN1 TIMM44 FAM162A MTSS1 SARDH ATP5F1B UGP2 GPRIN3 NNT ANK3 ATP5C1 P4HB ZFP69 COX4I1 AMT HSD11B1 BOLA1 GPT2 ALDOB CYP2D22 CTSZ APOA1 SEPHS2 FTCD AGMAT ECI1 ATIC MUG1 APPL1 LRPAP1 PNPO AARS S100A13 CCDC9 SERHL ACAA1B CBR1
Isobe, et al.	93	CHD9 PDLIM2 SPIRE2 MIB2 TOMM34 SEC23IP IRS1 ZZEF1 TIAM1 PSMF1 OSBPL10 PPM1H TAB2 HBP1 ATP6V0A2 MAP4K3 CLIP2 SLC7A6OS MRPS9 PTPN14 BLOC1S5 TMEM259 PCYT1B MRPL37 ZNF608 KIAA1109 DOCK1 EIF2AK2 WDTC1 CGNL1 KLHDC7A WDFY3 TIAM2 SLAIN2 ARHGAP29 BORCS6 ERBIN JUP PBXIP1 CHCHD6 FGD3 SNX12 VIPAS39 DOPEY1 RAB18 PHLDB2 KAZN BAIAP2 PARD6B VEPH1 MAP3K5 TBC1D12 NEK4 PI4KA MYO5B CAMK2D ARHGEF2 CASP8 ITSN2 NULL VILL MTOR PEAK1 EPS8L1 LYST MTCH1 WDR4 CLMN KLC3 IGSF5 MAP4K5 UHRF1BP1L SCYL2 AFAP1L2 ERBB3 SSH1 PURG SHROOM3 AP3D1 NFATC2 MPDZ COBL HERC4 ARHGEF17 SNX1 RTKN CGN SKT MAP4K4 PTPN13 TNS2 ARHGAP27 ZAK
Hu, et al.	212	HNRPD PPP1R14A SERPINF1 CENTD2 GRK1 BIRC5 CIAO1 SIP1 C21ORF66 RASGRF1 PIN1 EP400 PPP1R9A BCAM NPR1 AQP2 PDE4C DDX39 IRF3 TAF10

		EZR TFAP2B CIITA GMFB AURKA C14ORF106 KCNJ13 RGS14 CSRP3 KCNA4 PPP1R1B GPBP1L1 RRAD SNAI1 SOX9 ADRB1 NOXA1 HAGH CACNA1H XRCC4 NAB2 GLI1 GRIA1 CCND1 RUNX1T1 POP7 ESR1 KCNN3 PDE4D NFATC3 SREBF2 RUVBL2 E2F7 APOBEC3F MDFI GSK3B GNA13 SGK TRPV1 HLCS CHGB DDEF2 PPP1R13L H3F3A MC4R CSDC2 GATA3 FOXN3 PFKFB2 HIST2H3A UTP18 RCHY1 CLDN3 CAPN2 CREB1 ERBB2 TRPV4 PDE5A HDAC8 DAXX KCNJ3 HRH1 ID2 RB1 DHX29 PDE4B SEC14L2 SOX6 DNAJB2 HNRPK NRIP2 RNUXA TP53 CASP9 ZNF496 KCNN2 PPP1R1A FXYD1 BMI1 KCND2 TPPP UNC84B GRK7 TPH2 ETV1 SLC4A4 C13ORF15 LOC648998 CBFA2T3 ESPL1 HSPB6 HSPB8 ANXA1 ATP1A3 DSP ALOX5 PKD1 TRPM8 TTF2 NFATC4 RXRA POU3F4 NFATC1 PLN PLCG1 DAP3 ITGB4 BTBD12 FAM44A GSTA4 ABCA1 ARID3A PPP1R8 CSDE1 AICDA KCNH2 LIPE TNNI3 PLCB3 CRHR2 MAPT RBM19 ABCB1 WT1 CTPS MYBPC3 CSK TH LCK PHOX2A DES RDBP RNF12 PCTK1 VTN ACCN2 SNUPN PFKFB3 NEUROD1 U2AF1 BCOR AVPR2 CSNK1A1 EXOSC5 PTPN7 DUOX1 ITGA4 VDR PRKAR2B PHF17 MYOM2 CUL5 MCOLN1 CBL FIP1L1 TFAP2C C20ORF32 AKAP9 NCBP2 NR5A2 RBM22 RYR2 RPS19 NOS3 CFTR C19ORF2 TSC22D4 SAP30BP PDE11A GFAP AQP5 PPP2R5D GAS7 RBBP5 ETV5 ARFGEF1 PPP1R1C LOC51035 CUX1 PPP1R14C LOC100133382 GSK3A METTL3 NF2 GAD1 NCOA4 SRF GATA4 VHL MDM4 PAH HCLS1
Imamura, et al.	888	SLMAP TFIP11 ZHX3 ERCC5 TACC2 BYSL CXCR4 U2SURP G3BP1 CHD8 RBM15 SCAF8 TPX2 EP300 GYS1 MON1B CHORDC1 C2orf49 ZEB1 TRIM33 PARN CD2BP2 THRAP3 SRPK1 PTCD3 HMGN1 NMNAT1 SHC1 SAAL1 TAOK3 RIOK1 HERC2 SLC12A4 CLCC1 USP6NL BAZ1B SDAD1 PPP1R15B LARP7 KPNA2 ATL2 ZCRB1 KPNA3 PDCD4 DDB2 RBM10 BCLAF1 TRA2B RAD23B STK17A MTRR NCOR2 GTF3C3 HIST1H1E CEP170 TPI1 MSH6 SRSF6 HDAC7 SIPA1 CCDC43

		ATAD1 NELFE IMUP SORT1 SETDB1 CARMIL1 SRSF11 PCDH7 TJAP1 ORC1 SON PLCL2 TRAM1 AVEN C9orf16 USP42 NIPBL POGZ RICTOR RAD18 LRRC8A PRRC2B CDK17 ZNF687 KDM2A EML3 HABP4 NFIL3 WDR62 DHX16 LEMD2 MIS18BP1 UBXN7 DIDO1 LYSMD2 ARAP1 NGDN SAC3D1 ITPRIPL2 UNG DPF2 CBARP BRD8 PJA2 DCUN1D5 ANKLE2 NOP58 RPRD1B CHMP7 FRYL PTPN2 AP3B1 HCFC1 AHNAK UBL7 KRT17 RPL4 PPP1R12A VAMP4 PRPF3 CHMP2B DDX24 RBM6 WAPL SH3PXD2A HNRNPUL2 RBBP6 ARHGEF16 PARG ASAP2 PPL CEP131 STRIP1 SSRP1 PDAP1 BRD4 CHAF1A TOR1AIP1 PACSIN3 BCKDK CSRP1 ITSN1 SVIL CHAMP1 NSD1 ATP2B2 NCAPD3 PROSER2 ABCC2 GPATCH8 KIF4A PGM1 CPD KRT8 MAP7 RBM7 OSBPL3 ANTXR1 TERF2 HASPIN XPO4 EPS15 WIPI2 IFNAR1 EHD2 RMDN3 ANKRD17 UBE2J1 CCNK NCKAP5L FAM129B EAF1 NOTCH2 ADD1 PSMD2 CHTF18 ATXN2 ARHGAP12 VIRMA STRN3 CHMP3 CEBPZ ANAPC1 SRRT MELK RBM3 BMS1 SCFD1 CDK16 SF3B2 KAT5 FLYWCH2 TPD52L1 SLC19A1 XRCC1 PAK1IP1 SLC7A11 CDS2 AHCTF1 SENP3 EEF2K WDR26 MUS81 PWWP2A GAL RCC1 KIF1B PIAS1 ARGLU1 ZC3H14 CNOT2 SNW1 RPP30 TRIM16 CDC40 IRF2BPL RECQL5 WEE1 BSG TIMM8A BIN1 SRRM1 PABPN1 PTDSS1 FMNL1 GLCCI1 MMTAG2 ARMCX3 QSOX2 YBX1 LRFN4 PNISR CARHSP1 STK10 HERC1 PTPN23 DGCR8 COPB2 CTR9 BRI3BP LMO7 HNRNPH1 KPNA4 MDC1 INO80B NUCKS1 RBM34 RCOR1 U2AF2 SEC16A TRMT1 KMT2D LEO1 TELO2 MAF1 C7orf50 USP15 HDAC4 YAF2 WDR33 AMFR MAPK1 MPHOSPH10 HNRNPA2B1 TLE3 TACC1 PDCL ZC3HC1 DYNC1LI1 YRDC VPS4B FXR2 ZC3H8 ARHGAP1 CLASP1 TFAP4 AFAP1 CDK13 BCR TWISTNB RPL15 RIOK2 REXO4 ABCF1 UFD1 SMARCA4 SEPT2 RPS6KA4 BRD7 ZBTB21 CEP55 EYA3 HOXC10 EML4 ATF2 CTPS1 TOM1L1 GOLGA2 TRA2A CAMSAP2 RFC1 ABCC5 ASMTL SNAPC5 MOCOS AFDN SLC30A1 TBX3 DNAJC21

		NRDC SART1 MTDH HSPE1 RBM5 NCL EIF4EBP1 PPP1R9B SLC43A2 WDR44 MCM2 KRT18 TGS1 MCM4 SPTBN2 TOMM70 ARHGAP5 DDX21 PWP1 ADAR POP1 MTA1 GPAM ESYT2 TIMELESS DDX10 KIF13A KRT7 PHF8 TMEM87A PLEKHA2 ESCO2 SEC62 DNTTIP2 ZMYM4 ZNF106 MKI67 PANK2 NHS CLSPN BICD2 ARL6IP4 PAXBP1 PURB ACAP2 PPP4R2 BUD13 SDE2 SLC39A10 CDCA2 PPA2 MED24 MAP3K7 EHD1 RAB11FIP5 GTF2I TBC1D15 ADAM17 ZNF830 ZC3H4 ELAVL1 NCOA2 RPP25 ABCA2 EXO1 AJUBA CIAPIN1 DMD STAMBPL1 TCF20 PPM1G C9orf40 ELMSAN1 SSH3 RBM39 KLC2 FNDC3B USO1 SIRT1 AREL1 PCBP2 MFAP1 NEK9 UPF3B RPL23A ADNP RFFL RBM15B ERICH1 DDX39B TLE4 WRNIP1 TOP2B CNNM3 FAM117B TAF15 SORBS3 MED19 PAGR1 POLD3 VAMP7 AMPD2 RSF1 MON1A POU2F1 APC RSL1D1 RBM25 CDC42EP1 TPR MAP1S AKAP11 WDR3 TTC33 TRAFD1 CTTNBP2NL MGRN1 PTDSS2 BMP2K USP39 HNRNPU ATXN2L FLII CLASRP CWF19L2 BRAF RPL14 HNRNPA1 TMOD3 RALBP1 CAAP1 GEMIN5 UBR4 DDX20 KTN1 MYBBP1A PHKB SLC16A1 USP8 SLC17A5 EPHB4 MBD1 TP53BP2 STT3B SYAP1 CD3EAP HDLBP PITPNM1 HECW1 RLF KLF3 MTFR1 RPTOR BCL2L12 NBAS HIVEP1 ATRX VAMP8 NBN NUFIP2 MAST2 SLTM PACSIN2 TOPBP1 NUP214 SOX13 EIF3B MFSD6 USP20 MCRS1 UBE2E3 RAB3GAP1 BASP1 ARHGEF12 SLC35F6 PTOV1 RALY TMEM45A CDK12 JADE3 PHF3 RBM33 PEX14 PGRMC2 APEH TBC1D5 MAPKAP1 THOC2 MINK1 EZH2 MYO1C SLC15A4 OSMR LSM14A WIZ RBM4 CSF1 EDC3 SLC35B2 CEP170B COPA PHC3 ACOX1 FAM102B KIAA1143 USP24 TWF1 NUP153 MYH9 TTYH3 SLC12A6 RAP1GAP URI1 NOP2 RAD9A USP16 SCML2 USP10 PODXL2 PI4K2A RPS3 WDR75 SFSWAP DYNC1LI2 COIL ZMYND8 PTGES3 TSC2 CPSF7 ZNF609 CASC3 TCF12 ATP7A ZNF641 DSG2 TANC1 TBXA2R PRKCD ZNF639 PUS1 PPIG BCL9L SMC4 EPB41L1 EXOSC9 ABCC4 ZFP36L2 PBRM1 RNF20 USP9X

		BRF1 TMPO RRAS2 MCM3 RPS2 PRPF4B NRBP1 MYPN RNF113A PPHLN1 TBC1D2B AFF4 AKAP10 SUB1 PRPF6 PDE8A SH3KBP1 PLA2G4A SYNRG RIF1 UNC13D MEPCE KIF21A UNK SAMD1 SCD SLC38A2 CD2AP CCDC86 ATN1 MPZL1 SMN2 TRPT1 SEPT9 STX7 SPEN NAP1L4 GPRC5A C1orf52 CDC26 CD97 PDS5B MPHOSPH8 NOC2L TICRR MYO18A ZBTB7A MADD PRRC2C SLC4A2 ARHGEF18 ARRB1 SUGP1 HNRNPUL1 SIN3A POLR3E TXNL1 CCNYL1 OBSCN CBX8 RRBP1 IL1RAP PPP1R10 VDAC1 CIR1 FTSJ3 UTP14A EEF1B2 RRP1B SLC4A7 DKC1 GNL1 NELFB PPP1R12C ATG9A NEDD1 DNAJB6 DDX46 NFIC TCEAL4 PRPF38B ILF3 NUP50 ARFIP2 KRI1 LEMD3 TXLNA BUB1 PIEZO1 GTF3C2 SKIV2L SNTB2 SURF2 ZRANB2 CLASP2 DOT1L EIF2AK3 RPRD2 ATF7IP SEC31A FOXK1 HNRNPC ZC3H18 FXR1 NUP210 PPAN BAG6 SH2D4A SLC7A2 GZF1 DDX55 FERMT2 NSUN2 TPD52 DTD1 SLCO4A1 STK11IP ZC3H13 RTN4 GAPVD1 TAX1BP1 PHRF1 PPP1R2 TBC1D4 GIT1 CHCHD3 HIST1H1B EPB41 NUP98 DFFA PAXX EBAG9 TMEM51 SLU7 DAB2 TTLL12 NIFK DNAJA2 LYN CCNL1 ZFP91 CDCA3 NOP56 RAI1 BPTF ATAD2 DENR HACD3 PHF6 ANAPC2 DNMT1 EPB41L2 SLC16A6 RREB1 FNBP4 LIFR DNMBP SNAP23 TFDP1 MGA IRF2BP1 SRSF10 UTP3 CLINT1 RTTN ZFC3H1 SMAP KIAA1671 MYCBP2 LATS1 NEMF MED1 SRSF1 TMEM245 LAMTOR1 ESF1 DIAPH1 TRAF4 RRM2 SLC20A1 TOP2A DNAJC2 IGF1R NOB1 GTF3C4 EIF2A TTF1 NCBP1 SLC9A1 HDAC2 NEXN PLEC IL6ST NCAPD2 UBAP2L PPP4R3A TMEM131 GPN1 WDHD1 UBE4B DBN1 LRWD1 PTS RPL27A OTUD5 OGFR DDX54 HSF1 ALPI KMT2A PKN1 WTAP BUB1B JMJD1C AKT1S1 CCNH SURF6 MTCL1 PHF14 ERCC6 TMX1 RRP12 HSPH1 DMAP1 SRSF2 RAB12 DDX51 PRKAR1B HEXIM2 GBF1 ZC3H11A VCL TCF3 C18orf25 SMN1 RANBP10 PSMD1 DTL SRFBP1 SRSF9 C19orf24 RBMX TGFBR2 LRRFIP2 NAF1 NFX1 MDN1 OXSR1 REEP4 SLC38A1 PPFIA1 PLCD3 NCAPH2 CRK PDS5A PKM

		ZFR HNRNPA3 NOLC1 HNRNPLL CUL4A CDC42BPB LYSMD1 TMX2 ZNHIT3 TBC1D2 PEX19 PRKAB1 RALGAPA1 KIF20A SSX2IP GTF2IRD1 MORC2 WDR55 NUMA1 GIPC1 ZNF592 EIF4G2 GTF3C1 FAM208A SYNPO KHDRBS1 PPP1R18 PHF10 PSEN1 NUP43 FUNDC2 EPS15L1 NMD3 TOE1 GATAD2B FMNL2 HMGA1 SUPT7L RANBP2 YTHDC1 LIG3 STK38 ATP2A2 CAST GAB1 PNN MTMR3 DDX3X TRIM25 SCAF11 NCAPG GOLGA4 TMF1 FCHO2 FUNDC1 MISP CLN3 STX4 TMEM106B NDRG3 ATP2B1 VDAC2 CENPF RPS6KA3 BET1 SNX17 RANGAP1 SGPP1 DCAF8 RPS27 CDCA8 ZNF638
Embogama, et al.	179	PFKP DECR1 CSPG4 HSD17B10 LMAN1 NT5DC1 DDB1 PAIP1 DDX5 USP47 GDA IPO9 PUF60 RPL35 IMPDH2 RTF1 EXOSC2 USP14 USP7 PRDX4 SPG20 NUP88 NOMO1 DHX15 FKBP4 SF3A3 FUBP1 AHCYL1 ACO2 UBQLN2 HEXIM1 TPT1 RDX UMPS EHBP1L1 LDLR ITGB1 RPN1 PSMC4 CASP1 CECR5 PSMD12 FKBP5 PRMT1 TYMS MCM5 PLS3 PLOD2 RPS24 SH3GL1 WIBG ANXA2 DUSP12 BUB3 CNN2 WDR61 ACY1 PRMT5 RPS10 CLIC4 NHLRC2 FTO PTPRF RAB6A POLDIP2 MINPP1 AKAP12 PRPF8 RPL28 IARS UBE2O PPP2R2A CKMT1A TUBA1C PAAF1 SLC3A2 COPS3 DNM2 VARS PSMD4 DDX17 TIPRL DAK LAMP2 NONO CPNE1 IMPDH1 NMT1 UBFD1 POLD1 ACTN1 HSDL2 NME1 RPS16 PEBP1 SF3B3 PNP ANKZF1 ACTR2 OAT TBCB SDHB DDOST PSMA1 RPL29 PTPN11 DDX47 CYFIP1 ATP1B1 UFD1L ARF1 SMC1A HSPA4L OXCT1 MTHFD2 MYOF STOM GPKOW FKBP10 MPI WARS SFN CSE1L TXNDC5 PFKM ELP3 TES PLOD3 PSMC1 MCCC2 IVD PSMD14 SF1 YWHAB PARP1 DHX9 PSMA4 SERPINH1 CAPZA1 SEC24C SERPINB4 SERPINB1 POFUT TUBB6 MRPL2 GNB2L1 SF3B1 HMGCL ACAA1 ASNS PC CHD4 CDC73 GOLIM4 GDI2 RRM1 PRDX2 KLC1 GALE DRAP1 DLD SETD7 PLD3 SART3 FDXR RARS TRMT10C MGEA5 KPNA6 PDIA4 NAGK RPS14 PGD PYCRL IWS1 NANS GPC1 LANCL1 MPST

Hamaguchi, et al.	20	CDC25B OFD1 MARK3 PITPNM2 CEP72 KIAA0556 PHACTR2 GLI2 HSPC075 BAT2 EVL CRY2 PCNX CASP11 TMCC1 CAMKK2 SIK3 C2ORF55 PDE8B LRCH3
DNAJB1-PRKACA *in vitro* Mouse Liver Lysate	66	MSRB1 PYROXD2 MMGT1 SUGCT SLCO2B1 ACAA1A EIF1 DGLUCY UQCRC1 RCSD1 ACSF2 HS1BP3 NDRG2 PGAM1 CNDP2 DCAF11 TNNT2 B2M ANP32A GLOD4 GPD1L PFAS CR1L CEP290 GBE1 ASPG PDP2 RTRAF CACNB2 PDHX SSR1 HADHA MUSTN1 RUFY3 WIPF1 ADSS PSMA6 ARCN1 TSFM ITIH4 SPHK2 CYP2D11 CDH13 HAL CSMD1 RPS3A1 AADAT PRKAA2 OPLAH PCDH1 WASHC2 NUCB2 EIF5 GM20604 HSPA5 H6PD HNRNPM MMUT FLAD1 IFI35 DOCK5 HAAO CYP2C29 SLCO1B2 KCTD12 C6
PRKACA *in vitro* Mouse Liver Lysate	16	FKBP8 ALDH1L1 SIRT5 FAM50B SCO1 ALDH4A1 MAPRE3 PCX ECI2 ETNPPL IGSF10 ITPA RILP ACBD4 ARID4B ACOX2

Conclusions

In order to try the analog-sensitive kinase approach for direct substrate identification, it was necessary to first obtain purified kinases without the gatekeeper residue mutated to ensure that activity of the kinases was as expected. Additionally, affinity-tags are usually necessary to purify proteins, but these tags can alter the dynamics and activity of the kinase. Thus, it was also necessary to demonstrate that these tags could be cleaved off of the kinases of interest. The original constructs I started working with to express PRKACA-GST or DNAJB1-PRKACA-GST had a thrombin cut site in between the kinase and affinity tag. Upon cleavage with thrombin, the entire PRKACA degraded. It was then necessary to switch to a different protease and corresponding cut site. I used site-directed mutagenesis to replace the thrombin cleavage site with a TEV cleavage site since the TEV sequence is more specific. I also decided to include two different lengths of flexible linkers after the TEV site because I was concerned about whether the TEV protease would be able to access the cut site between the kinase and GST tag. Upon a time-course experiment with TEV cleaving each of with different constructs, I did see that the constructs with the flexible linkers did indeed cleave better, likely to do the increased ease of accessibility to the cut site. I also confirmed that these DNAJB1-PRKACA-GST proteins were active kinases. I was still concerned that the few amino acids left from the TEV cleavage site could affect activity, but before I tested whether the kinases with GST cleaved had similar activity levels to the GST-tagged versions, we learned of a method that would let us purify the kinases without an attached affinity tag at all.

This approach attaches a peptide (PKI) to agarose beads that specifically binds to PRKACA in order to be able to pull out this kinase from a lysate mixture. This method worked more efficiently to purify larger amounts of PRKACA and DNAJB1-PRKACA than with the GST-tag.

I expected some decrease in purification efficiency using this method for the analog-sensitive mutants since PKI specifically binds to the active site of PRKACA, but I did not expect to see such a dramatic decline in binding capacity from the single amino acid change. If this specific peptide that binds to PRKACA experienced such a dramatic change in kinetics, it is likely that other substrates would, too. At this point, I no longer wanted to move forward with the analog-sensitive kinase approach.

I pivoted to an approach that uses FSBA to irreversibly bind to the catalytic lysine of many kinases to render them inactive. I demonstrated that I was able to knock down endogenous kinase activity in HeLa cells, mouse liver lysate, and human hepatocyte lysate. I was also able to show that more phosphorylation occurred in these FSBA-treated lysates upon addition of DNAJB1-PRKACA or PRKACA.

However, in collaboration with Soren Heissel in the Proteomics Resource Center, the thiophosphate ester tags that result from the use of ATP-γ-S in kinase reactions and the following alkylation reaction with PNBM are not able to be reliably identified when following the published methods.

In collaboration with Soren Heissel, kinase reactions with PRKACA and DNAJB1-PRKACA were done with FSBA-treated mouse liver lysate and regular ATP and the resulting phosphopeptides were enriched. Differences between substrate specificity was seen between the three conditions of PRKACA added, DNAJB1-PRAKCA added, and no kinase added; more putative substrates were unique to DNAJB1-PRKACA (64) than PRKACA (6).

Discussion

While using the GST-tagged versions of DNAJB1-PRKACA and PRKACA wound up not being the best option for the assay I used moving forward, these proteins are still helpful tools to have in our lab to study these kinases relevant to FLC. Attaching PRKACA or DNAJB1-PRKACA to the PKI-agarose would make the active site inaccessible for any experiments that would need to be carried out on bead or column; the GST-tagged versions would not have this problem.

However, being able to use the tagless kinases for my *in vitro* assays has greatly improved my confidence in a future read out. A recombinant protein without a tag closely represents the kinases *in vivo* in terms of their intrinsic structure. Any change in substrate preference seen with the *in vitro* assay now should be due to something intrinsic about the kinase or assay and not due to the affinity tag or additional amino acids not found in the kinase *in vivo.*

While it was disappointing to arrive at the conclusion that moving forward with the analog-sensitive kinase approach was no longer desirable, it was validating to learn of other groups who reached the same conclusion. Killing the endogenous kinase activity of a lysate to confer activity specificity of the added kinase of study while keeping the added kinase as close to its native form as possible is an approach with many advantages anyway. While an *in vitro* assay does not allow for the detection of substrate differences that are due to a difference in localization or compartmentalization of the DNAJB1-PRKACA compared to PRKACA, it does allow for the detection of changes in substrate binding partner that are purely affinity based. The J-domain of DNAJB1-PRKACA could attract binding partners that PRKACA could not in such a way to allow for these binding partners of the J domain to now be newly phosphorylated.

The main reason our lab is interested in studying whether DNAJB1-PRAKCA has different phosphorylation targets compared to PRKACA is to better understand FLC, the cancer this oncogenic kinase is driving and also to potentially develop therapeutics against this kinase. Being able to identify which human liver proteins DNAJB1-PRKACA could differentially phosphorylate would be ideal compared to identifying differences with mouse liver proteins or even human proteins in a different cellular context. However, primary hepatocytes have historically been hard to grow, and the cost of purchasing primary hepatocytes can easily become prohibitive to designing large-scale screens. The Rice lab has developed a way to efficiently grow and harvest a large quantity of human hepatocytes; being able to get enough human hepatocytes for this assay is a gamechanger in terms of being able to have human-relevant liver substrate phosphorylation data.

Being able to obtain more human hepatocytes through the collaboration with the Rice lab became even more crucial and exciting after seeing the results of the phosphopeptide enrichment from kinase reactions using regular ATP and FSBA-treated mouse liver lysate. It makes sense that DNAJB1-PRKACA mostly had the same substrates as PRKACA since DNAJB1-PRKACA is only missing one exon of PRKACA. It was exciting to see a noticeable number of substrates appear only in the DNAJB1-PRKACA sample. However, since this was done as a single replicate with mouse liver lysate, I did not want to get ahead of myself with drawing any conclusions about specific proteins from this data. Rather, I wanted to move forward as quickly as possible with obtaining data in triplicate using human hepatocyte lysate to see if a similar result could be obtained.

Chapter III: Phosphopeptide Enrichment of Putative Substrates of PRKACA and Variants from Human Hepatocyte Lysate

Background and Rationale

The pilot experiment of enriching phosphopeptides from kinase reactions using FSBA-treated mouse liver lysate yielded very promising results that there could be multiple substrate differences between DNAJB1-PRKACA and PRKACA. The pilot experiment was only done in single replicates with DNAJB1-PRKACA, PRKACA, and a no kinase condition as the negative control. For the next round of phosphopeptide enrichments, I wanted to repeat these conditions in triplicate to begin to see what changes might be statistically significant. As previously stated, I also wanted to use FSBA-treated human hepatocytes since the phosphorylation sites of human liver proteins could differ from the mouse phosphorylation sites. Additionally, I added another PRKACA variant that is found in the adrenal tumors of Cushing's disease. It is thought that this variant, PRKACA (L206R), cannot properly interact with the regulatory subunits of PKA and thus is constitutively active in the cell. Two recent publications have suggested there could be a difference in substrate specificity for the L206R mutant compared to the native PRKACA (Lubner et al. 2017; Bathon et al. 2019). For my *in vitro* assay, the interaction with the regulatory subunits should not be a contributing factor to substrate specificity since each kinase is being added to the FSBA-treated lysate in its free catalytic form.

Consistency of Kinase Reaction Samples Contributes to Robustness of the Data

It was important to know that the kinases added to the reaction were folded properly, active, and added in the same amount to each kinase reaction. If these conditions are met and as long as your substrate pool is the same, any differences seen in substrate specificity is likely due to an intrinsic aspect of the kinase and not because different amounts of kinase with different activities are being compared against each other. I worked with the High Throughput and Spectroscopy Resource Center at Rockefeller to make sure that the kinases I was using met these conditions. **Figure 17A-C** demonstrates that the same amount of DNAJB1-PRKACA, PRKACA, and PRKACA (L206R) have similar kinase activities when tested using the ADP-Glo Kinase Assay (Promega). Protein quality was measured with the Tycho NT.6 per the manufacturer's protocol to show that the kinases were all properly folded (**Figure 17D**). This technology automatically detects and identifies the inflection temperature of each sample as a function of increasing temperature; a peak in the first derivative view corresponds to the detected inflection temperature of the sample.

The kinase reactions were all carried out for 1 hour at 30°C with 500ug of human hepatocyte lysate from the same FSBA-treated aliquot and 5ug of a kinase in the presence of 1mM ATP; kinase reactions were quenched with 20mM EDTA. The samples were then flash frozen and given to Soren Heissel at the Proteomics Resource Center. He then prepared these samples for phosphopeptiide enrichment as written in the methods.

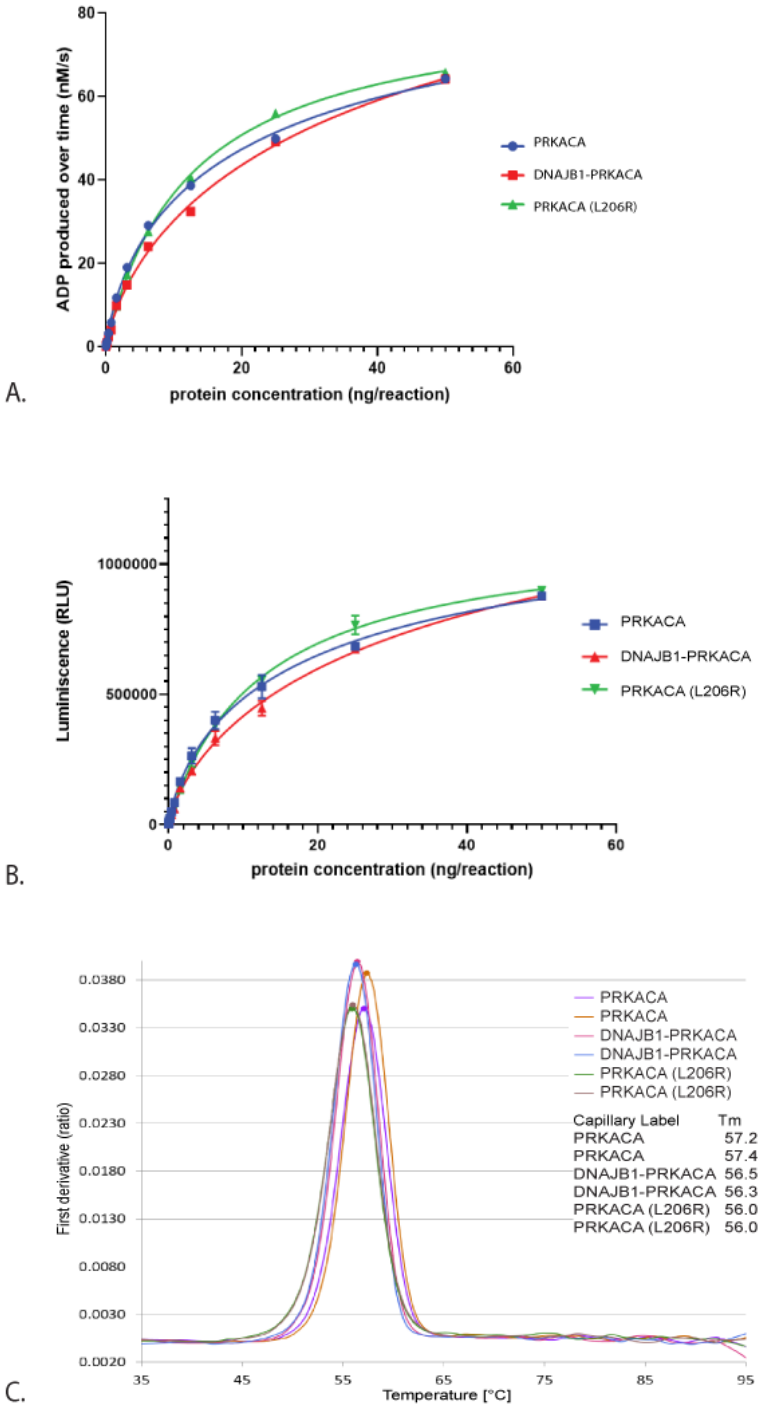

Figure 17. Quality Kinases Used in Triplicate *in vitro* Assay.

(A-B) Kinase Activity as measured with ADP-Glo Kinase Assay (Promega).

(C) Protein quality measured with the Tycho NT.6; a peak in the first derivative view corresponds to the detected inflection temperature of the sample.

The abundance reading of total peptides was normalized to the median abundance in each sample to allow for comparison between the samples. **Figure 18A** shows that the abundance reading in all of the samples across all conditions and triplicate sets were comparable; this suggests that making a single pool of the FSBA-treated human liver lysate to aliquot 500ug for each kinase reaction allowed for consistency and reproducibility across samples. Total peptide was viewed in Proteome Discoverer (ThermoFisher). Only phosphosite data was analyzed using Perseus (Tyanova et al. 2016). The total phosphopeptide amounts were normalized to the median abundance of each sample which showed that more phosphopeptides were enriched from all three triplicate sets that had an added kinase than were enriched from the no kinase added control (**Figure 18B**). The histograms in **Figure 18C** visualize the same point: more phosphopeptides are enriched from the samples that had additional kinases than from the no kinase control.

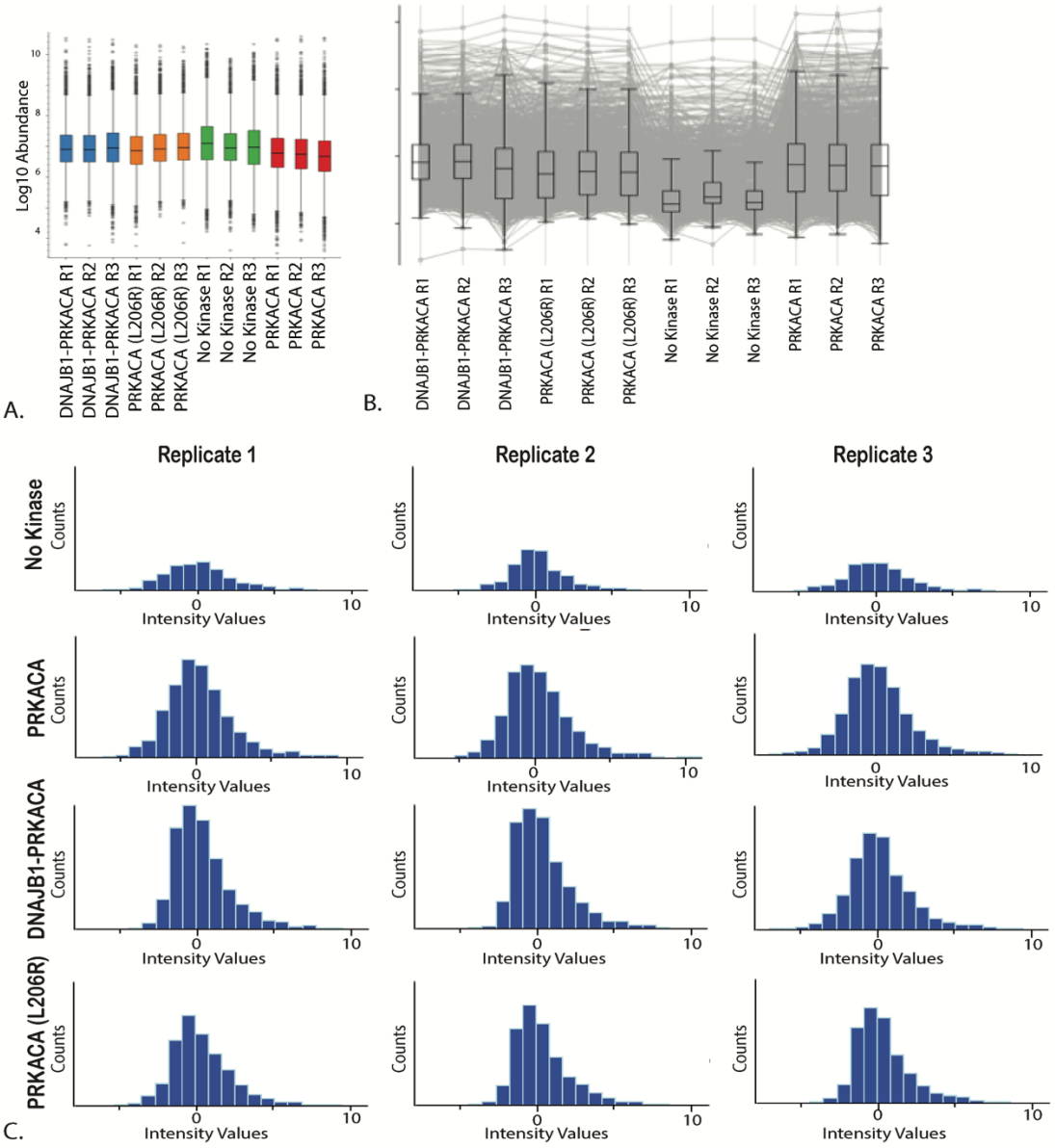

Figure 18. More Phosphopeptides Found in Kinase Reaction Samples Compared to the No Kinase Control.

(A) Total peptides were normalized to the median abundance of each sample in Proteome Discoverer. (B) Total phosphopeptides were normalized to the median abundance of each sample using Perseus. (C) Histograms of the intensity values of enriched phosphopeptides on the x-axes were normalized to the median intensity values of each sample using Perseus.

Differences in Substrate Specificity Between PRKACA, PRKACA (L206R), and DNAJB1-PRKACA

Now that I established that the kinases used in the reactions were of good quality and that the detection of phosphopeptides was consistently more than the no kinase condition for all three kinases tested, I began to look at the differences in which peptides were phosphorylated that could be detected between these samples. A PCA plot clearly depicts that the four conditions in triplicate do cluster separately from each other (**Figure 19A**). This suggests that the substrate specificity for PRKACA, PRKACA (L206R), and DNAJB1-PRKACA are different from each other since these kinases are acting on the same pool of substrates. This is also supported by the heatmap in **Figure 19B** and the Venn diagrams in **Figures 20-22**. The heatmap shows distinct signatures between the four conditions, but the portion of the branch highlighted in aqua blue focuses on a group of proteins whose phosphorylation changes are similar between PRKACA (L206R) and DNAJB1-PRKACA. This could be an interesting group of proteins to focus on since both of these PRKACA variants are found in tumors. **Table 7** lists the proteins and specific phosphosites detected in this region of the heatmap. Inputting the list of gene names in **Table 7** to STRING version 11.0 (Szklarczyk et al. 2019) creates an interactome map that shows a prevalence of proteins that regulate mRNA (**Figure 20** and **Tables 8** and **9**) and proteins involved in a variety of catabolic processes (**Figure 21** and **Table 10**). STRING uses Gene Ontology (GO) Kyoto Encyclopedia of Genes and Genomes (KEGG) databases as part of its analysis.

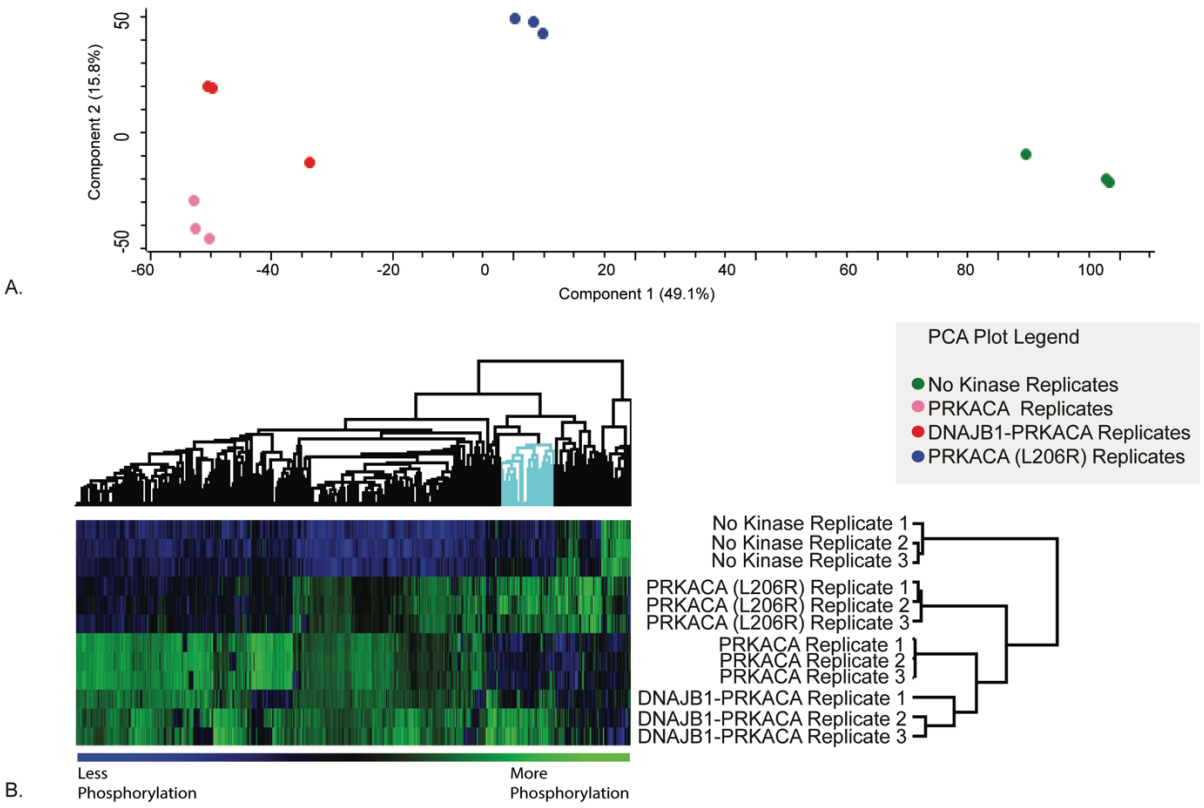

Figure 19. PCA Plot and Heatmap of Phosphopeptide Data Analyzed in Perseus. (A) A principal component analysis (PCA) plot generated in Perseus from the phosphopeptide data depicts each triplicate set as distinct groups. (B) The heatmap was generated in Perseus using a false discovery rate (FDR)-corrected ANOVA test (FDR=0.01). The aqua blue branch of the heatmap highlights the group of proteins with phosphosites detected in the presence of only PRKACA (L206R) and DNAJB1-PRKACA; the proteins in this section are listed in **Table 7**.

Table 7. PRKACA (L206R) and DNAJB1-PRKACA Putative Target Overlap.

Uniprot Number	Phosphosite	Protein names	Gene names
A0A044PY82	233	Uncharacterized protein LOC113230	LOC113230
A0A087WTL4	420	Bcl-2-like protein 13	BCL2L13
A0A087WTS0	169	Glutathione peroxidase;Glutathione peroxidase 2	GPX2
X6RCC3	129	Stromal membrane-associated protein 2	SMAP2
J3KT37	77	Band 4.1-like protein 3;Band 4.1-like protein 3, N-terminally processed	EPB41L3
A0A0A0MSW4	262	Phosphatidylinositol transfer protein beta isoform	PITPNB
E9PMS6	1185	LIM domain only protein 7	LMO7
A0A0C4DGH0	379	CD276 antigen	CD276
H0YMM5	45	Deoxyuridine 5'-triphosphate nucleotidohydrolase, mitochondrial	DUT
A0A0R4J2E8	234	Matrin-3	MATR3
A0A0R4J2E8	188	Matrin-3	MATR3
Q5VTI5	862	Pleckstrin homology domain-containing family A member 6	PLEKHA6
A0A1B0GVJ7	286	Uncharacterized protein KIAA1671	KIAA1671
A0A1W2PPU9	212		
A0A2R8YDF7	246	Lysine-specific demethylase 4A	KDM4A
A3KFL1	124	Exosome complex component RRP4	EXOSC2
A6NDB9	375	Paralemmin-3	PALM3
E9PCT1	464	Serine/arginine repetitive matrix protein 1	SRRM1
E9PCT1	724	Serine/arginine repetitive matrix protein 1	SRRM1
B4DY08	220	Heterogeneous nuclear ribonucleoproteins C1/C2	HNRNPC
G3V1D0	128	Echinoderm microtubule-associated protein-like 3	EML3
B8ZZJ0	2	Small ubiquitin-related modifier 1	SUMO1
C9JGI3	50	Thymidine phosphorylase	TYMP
C9JZZ0	59	Apolipoprotein A-V	APOA5
D6RAS7	117	40S ribosomal protein S3a	RPS3A

E7EPN9	1265	Protein PRRC2C	PRRC2C
S4R3H4	503	Apoptotic chromatin condensation inducer in the nucleus	ACIN1
S4R3H4	767	Apoptotic chromatin condensation inducer in the nucleus	ACIN1
S4R3H4	652	Apoptotic chromatin condensation inducer in the nucleus	ACIN1
E7ET36	19	Transferrin receptor protein 2	TFR2
E7EX73	1022	Eukaryotic translation initiation factor 4 gamma 1	EIF4G1
E7EX17	406	Eukaryotic translation initiation factor 4B	EIF4B
E9PG73	672	Peptidyl-prolyl cis-trans isomerase G	PPIG
E9PN6	14	Tumor protein p53-inducible protein 11	TP53I11
E9PJD9	11	60S ribosomal protein L27a	RPL27A
E9PK91	177	Bcl-2-associated transcription factor 1	BCLAF1
E9PK91	648	Bcl-2-associated transcription factor 1	BCLAF1
E9PQA1	7	Small acidic protein	C11orf58;SMAP
E9PMG1	143	RalBP1-associated Eps domain-containing protein 1	REPS1
F8VSD9	27	tRNA (guanine-N(7)-)-methyltransferase	METTL1
H7BXL1	33	Transmembrane protein 41A	TMEM41A
H3BNA8	21	LYR motif-containing protein 1	LYRM1
H7C113	141	Phospholipid-transporting ATPase IG	ATP11C
H7C1N2	102	Protein cordon-bleu	COBL
M0QXG9	29	BRISC and BRCA1-A complex member 1	BABAM1
K7EM16;P50552	8;239	Vasodilator-stimulated phosphoprotein	VASP
O43493	224	Trans-Golgi network integral membrane protein 2	TGOLN2
O43493	71	Trans-Golgi network integral membrane protein 2	TGOLN2
O43903	282	Growth arrest-specific protein 2	GAS2
O75533	336	Splicing factor 3B subunit 1	SF3B1
P00167	5	Cytochrome b5	CYB5A

P00367	94	Glutamate dehydrogenase 1, mitochondrial	GLUD1
P00918	151	Carbonic anhydrase 2	CA2
P02545	423	Prelamin-A/C;Lamin-A/C	LMNA
P06744	237	Glucose-6-phosphate isomerase	GPI
P07148	56	Fatty acid-binding protein, liver	FABP1
P08238	452	Heat shock protein HSP 90-beta	HSP90AB1
P08240	473	Signal recognition particle receptor subunit alpha	SRPR
P08559	293	Pyruvate dehydrogenase E1 component subunit alpha, somatic form, mitochondrial;Pyruvate dehydrogenase E1 component subunit alpha, testis-specific form, mitochondrial	PDHA1;PDHA2
P09601	229	Heme oxygenase 1	HMOX1
P23284	189	Peptidyl-prolyl cis-trans isomerase B	PPIB
P25685	16	DnaJ homolog subfamily B member 1	DNAJB1
P26368	79	Splicing factor U2AF 65 kDa subunit	U2AF2
P30085	147	UMP-CMP kinase	CMPK1
P30086	13	Phosphatidylethanolamine-binding protein 1;Hippocampal cholinergic neurostimulating peptide	PEBP1
P30533	242	Alpha-2-macroglobulin receptor-associated protein	LRPAP1
P40925	241	Malate dehydrogenase, cytoplasmic	MDH1
P55072	746	Transitional endoplasmic reticulum ATPase	VCP
Q01518	308	Adenylyl cyclase-associated protein 1	CAP1
Q02818	369	Nucleobindin-1	NUCB1
Q08426	189	Peroxisomal bifunctional enzyme;Enoyl-CoA hydratase/3,2-trans-enoyl-CoA isomerase;3-hydroxyacyl-CoA dehydrogenase	EHHADH
Q08495	152	Dematin	DMTN
Q15149	2039	Plectin	PLEC
Q16695	29	Histone H3.1t	HIST3H3

Q3LXA3	545	Bifunctional ATP-dependent dihydroxyacetone kinase/FAD-AMP lyase (cyclizing);ATP-dependent dihydroxyacetone kinase;FAD-AMP lyase (cyclizing)	DAK
Q53EL6	457	Programmed cell death protein 4	PDCD4
Q5JRA6	678	Melanoma inhibitory activity protein 3	MIA3
Q63ZY3	540	KN motif and ankyrin repeat domain-containing protein 2	KANK2
Q6PKG0	1040	La-related protein 1	LARP1
Q8N573	91	Oxidation resistance protein 1	OXR1
Q8NDI1	1035	EH domain-binding protein 1	EHBP1
Q99442	313	Translocation protein SEC62	SEC62
Q9BX68	101	Histidine triad nucleotide-binding protein 2, mitochondrial	HINT2
Q9C0C2	1666	182 kDa tankyrase-1-binding protein	TNKS1BP1
Q9GZT3	102	SRA stem-loop-interacting RNA-binding protein, mitochondrial	SLIRP
Q9H788	51	SH2 domain-containing protein 4A	SH2D4A
Q9HCE5	399	N6-adenosine-methyltransferase subunit METTL14	METTL14
Q9HCN8	55	Stromal cell-derived factor 2-like protein 1	SDF2L1
Q9NSK0	566	Kinesin light chain 4	KLC4
Q9NVD7	19	Alpha-parvin	PARVA
Q9NZN5	22	Rho guanine nucleotide exchange factor 12	ARHGEF12
Q9P2B2	875	Prostaglandin F2 receptor negative regulator	PTGFRN
Q9P2J9	461	[Pyruvate dehydrogenase [acetyl-transferring]]-phosphatase 2, mitochondrial	PDP2
U3KPZ7	859	RNA-binding protein 27	RBM27
Q9UK59	514	Lariat debranching enzyme	DBR1
Q9Y385	266	Ubiquitin-conjugating enzyme E2 J1	UBE2J1
E9PCT1	613	Serine/arginine repetitive matrix protein 1	SRRM1
B0QZK8	51	Heterochromatin protein 1-binding protein 3	HP1BP3

I3L380	5	Monoacylglycerol lipase ABHD12	ABHD12
M0QXU7	179	Mitochondrial import inner membrane translocase subunit TIM44	TIMM44
Q8NHZ8	7	Anaphase-promoting complex subunit CDC26	CDC26
A0A0A0MQU8	49	Interferon alpha-6	IFNA6
E7EX17	450	Eukaryotic translation initiation factor 4B	EIF4B
O43399	166	Tumor protein D54	TPD52L2
O43765	77	Small glutamine-rich tetratricopeptide repeat-containing protein alpha	SGTA
S4R2Y4	87	Chromobox protein homolog 3	CBX3
Q9H307	100	Pinin	PNN
Q9Y2V2	32	Calcium-regulated heat stable protein 1	CARHSP1
Q9UPM8	751	AP-4 complex subunit epsilon-1	AP4E1
Q9UPM8	757	AP-4 complex subunit epsilon-1	AP4E1
Q9UPM8	755	AP-4 complex subunit epsilon-1	AP4E1

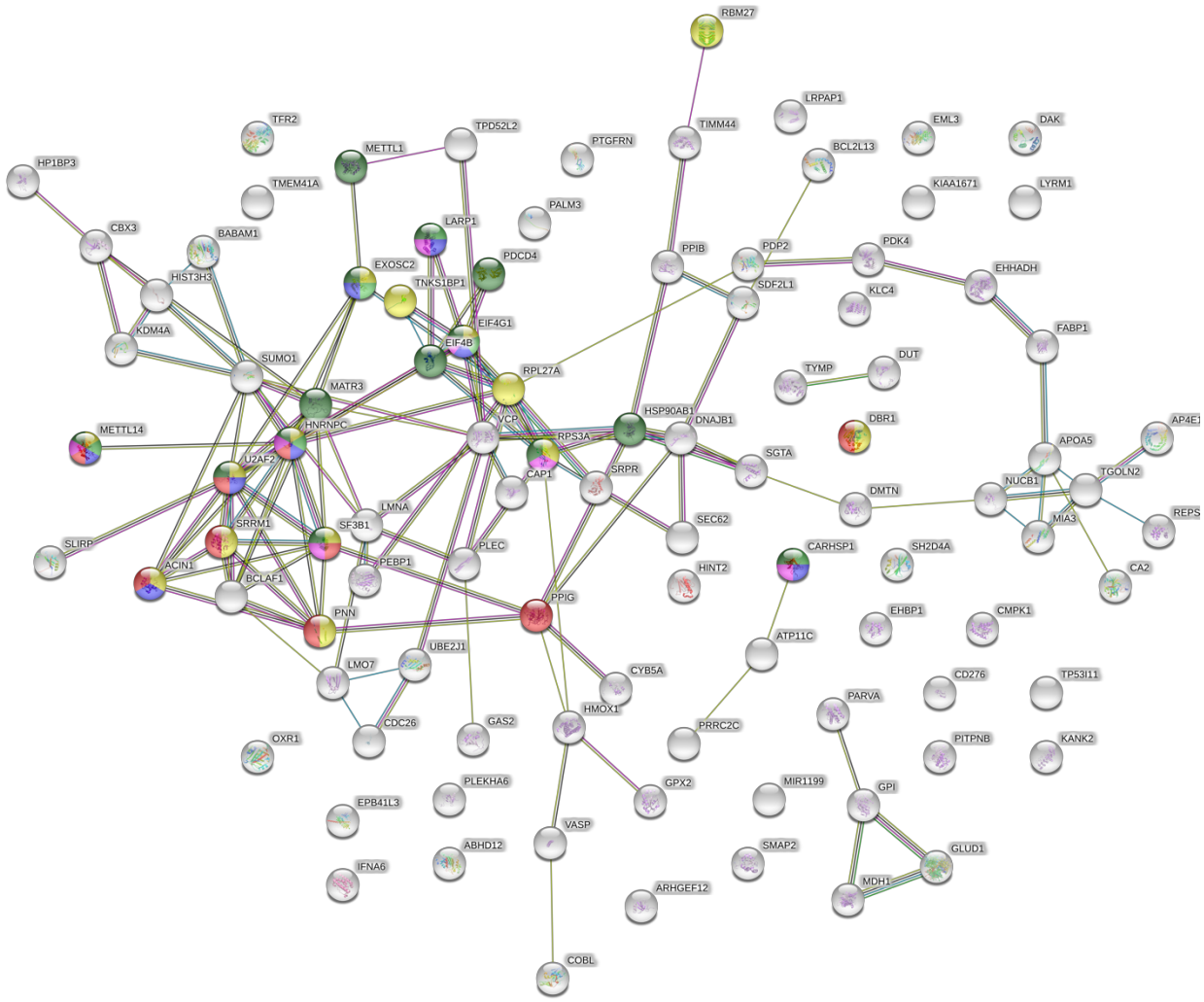

Figure 20. STRING Interactome Map of Proteins with Phosphosites Enriched by PRKACA (L206R) and DNAJB1-PRKACA.

The list of genes used to generate this list comes from **Table 7**. Proteins in this table all contain phosphosites that were enriched in the kinase reactions with PRKACA (L206R) and DNAJB1-PRKACA but not in the PRKACA or No Kinase samples. The colored dots correspond to categories in **Table 8** and **9** as determined by STRING analysis.

Table 8. STRING Analysis of Biological Process (GO) of Proteins with Phosphopeptides Enriched by PRKACA (L206R) and DNAJB1-PRKACA.

Biological Process (GO)			
GO-term	*description*	*count in gene set*	*false discovery rate*
GO:0031329	regulation of cellular catabolic process	16 of 743	0.0027
GO:0031330	negative regulation of cellular catabolic process	9 of 234	0.0044
GO:0016071	mRNA metabolic process	14 of 667	0.0045
GO:1901575	organic substance catabolic process	22 of 1609	0.0061
GO:0046700	heterocycle catabolic process	11 of 440	0.0061
GO:0044270	cellular nitrogen compound catabolic process	11 of 441	0.0061
GO:0019439	aromatic compound catabolic process	11 of 453	0.0061
GO:0043488	regulation of mRNA stability	6 of 113	0.0071
GO:1903311	regulation of mRNA metabolic process	8 of 238	0.0072
GO:1901361	organic cyclic compound catabolic process	11 of 484	0.0072
GO:0034655	nucleobase-containing compound catabolic process	10 of 394	0.0072
GO:0009892	negative regulation of metabolic process	29 of 2762	0.0117
GO:0033554	cellular response to stress	20 of 1553	0.0129
GO:0010605	negative regulation of macromolecule metabolic process	27 of 2558	0.0174
GO:0008380	RNA splicing	9 of 391	0.0217
GO:0044248	cellular catabolic process	20 of 1646	0.0227
GO:0002181	cytoplasmic translation	4 of 57	0.0265
GO:0035966	response to topologically incorrect protein	6 of 172	0.0283
GO:0031331	positive regulation of cellular catabolic process	8 of 343	0.0382
GO:0031324	negative regulation of cellular metabolic process	25 of 2463	0.0434

Table 9. STRING Analysis of Molecular Function (GO) of Proteins with Phosphopeptides Enriched by PRKACA (L206R) and DNAJB1-PRKACA.

Molecular Function (GO)			
GO-term	*description*	*count in gene set*	*false discovery rate*
GO:0003729	mRNA binding	7 of 198	0.0312
GO:0003723	RNA binding	14 of 850	0.0312
GO:0005488	binding	77 of 11878	0.0320
GO:1904288	BAT3 complex binding	2 of 4	0.0362
GO:0019899	enzyme binding	23 of 2197	0.0428
GO:1990226	histone methyltransferase binding	2 of 6	0.0448

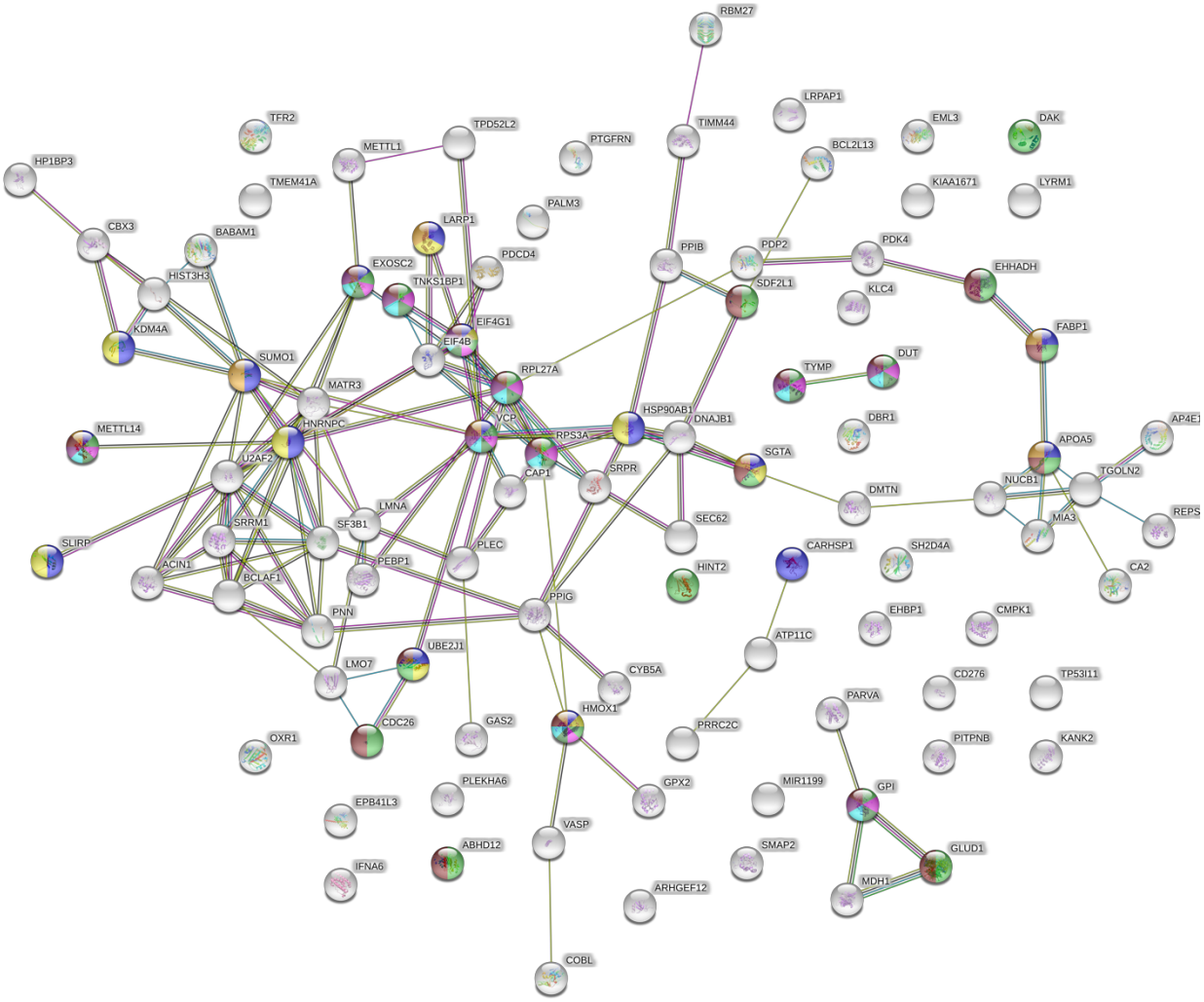

Figure 21. STRING Interactome Map of Proteins with Phosphopeptides Enriched by PRKACA (L206R) and DNAJB1-PRKACA: Highlighting Proteins Involved in Catabolic Processes.

The list of genes used to generate this list comes from **Table 7**. Proteins in this table all contain phosphopeptides that were enriched in the kinase reactions with PRKACA (L206R) and DNAJB1-PRKACA but not in the PRKACA or No Kinase samples. The colored dots correspond to categories in **Table 10** as determined by STRING analysis.

Table 10. STRING Analysis of Biological Process (GO) of Proteins with Phosphopeptides Enriched by PRKACA (L206R) and DNAJB1-PRKACA: Highlighting Proteins Involved in Catabolic Processes.

Biological Process (GO)			
GO-term	*description*	*count in gene set*	*false discovery rate*
GO:0031329	regulation of cellular catabolic process	16 of 743	0.0027
GO:0031330	negative regulation of cellular catabolic process	9 of 234	0.0044
GO:0016071	mRNA metabolic process	14 of 667	0.0045
GO:1901575	organic substance catabolic process	22 of 1609	0.0061
GO:0046700	heterocycle catabolic process	11 of 440	0.0061
GO:0044270	cellular nitrogen compound catabolic process	11 of 441	0.0061
GO:0019439	aromatic compound catabolic process	11 of 453	0.0061
GO:0043488	regulation of mRNA stability	6 of 113	0.0071
GO:1903311	regulation of mRNA metabolic process	8 of 238	0.0072
GO:1901361	organic cyclic compound catabolic process	11 of 484	0.0072
GO:0034655	nucleobase-containing compound catabolic process	10 of 394	0.0072
GO:0009892	negative regulation of metabolic process	29 of 2762	0.0117
GO:0033554	cellular response to stress	20 of 1553	0.0129
GO:0010605	negative regulation of macromolecule metabolic process	27 of 2558	0.0174
GO:0008380	RNA splicing	9 of 391	0.0217
GO:0044248	cellular catabolic process	20 of 1646	0.0227
GO:0002181	cytoplasmic translation	4 of 57	0.0265
GO:0035966	response to topologically incorrect protein	6 of 172	0.0283
GO:0031331	positive regulation of cellular catabolic process	8 of 343	0.0382

The Venn diagrams (**Figures 22-24**) also show that the substrate specificity is more similar between PRKACA and DNAJB1-PRKACA than PRKACA and PRKACA (L206R). **Figures 19B, 23,** and **24** all show that PRKACA (L206R) loses the ability to phosphorylate a large number of substrates that are phosphorylated by PRKACA (and DNAJB1-PRKACA). Despite these differences, it is important to reiterate that these three kinases all share a large majority of substrates (346 potential substrates in my assay).

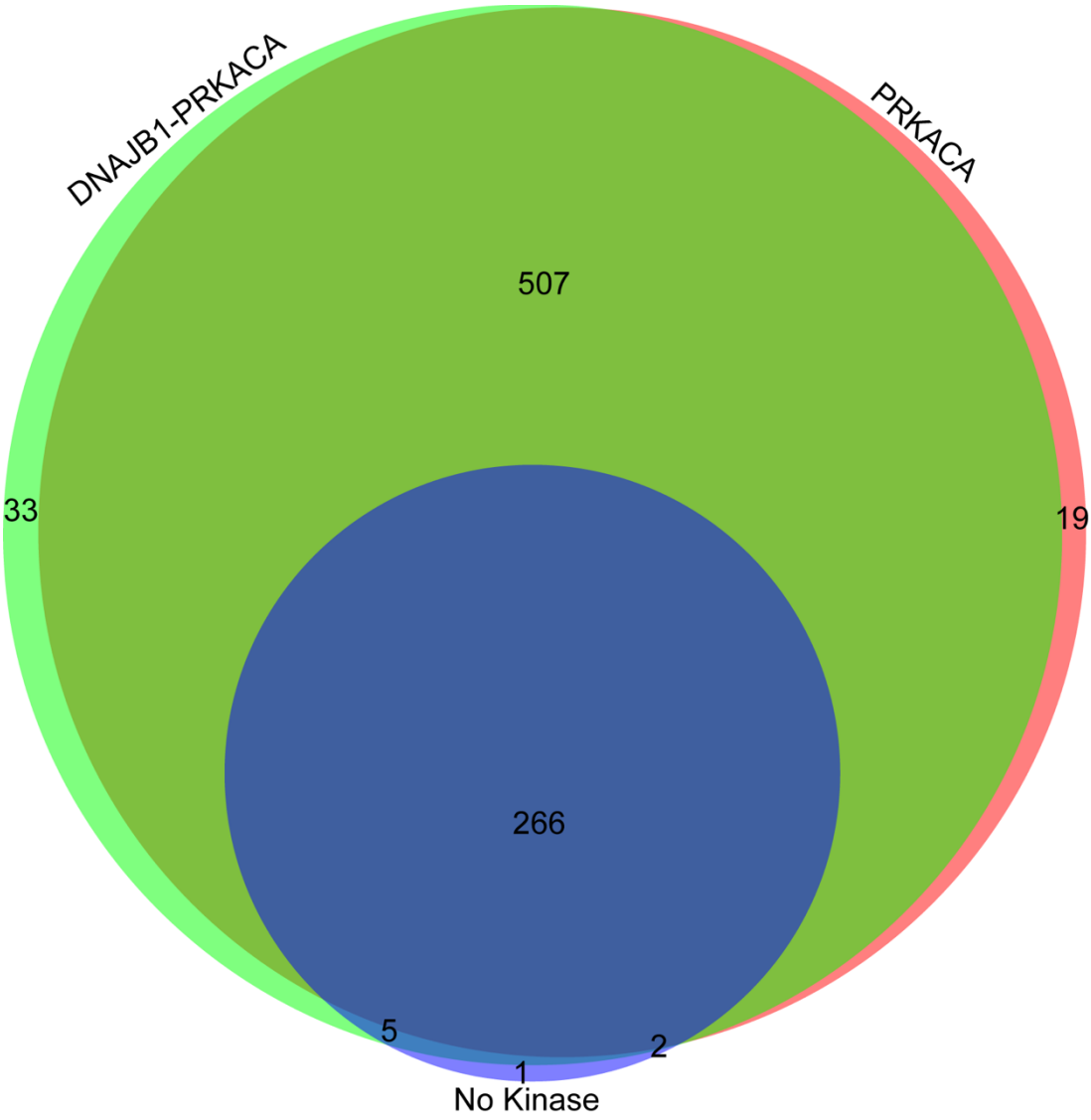

Figure 22. Venn Diagram of the Number of Human Proteins with Phosphosites Found in Samples with DNAJB1-PRKACA, PRKACA, or No Kinase Added.
794 unique proteins with identified phosphosites from the sample with PRKACA added is represented in red on the right. 274 unique proteins with identified phosphosites from the no kinase added sample is represented in blue in the middle. 811 unique proteins with identified phosphosites from the sample with DNAJB1-PRKACA added is represented in green on the left. This proportional Venn Diagram was generated using Biovenn (Hulsen et al. 2008).

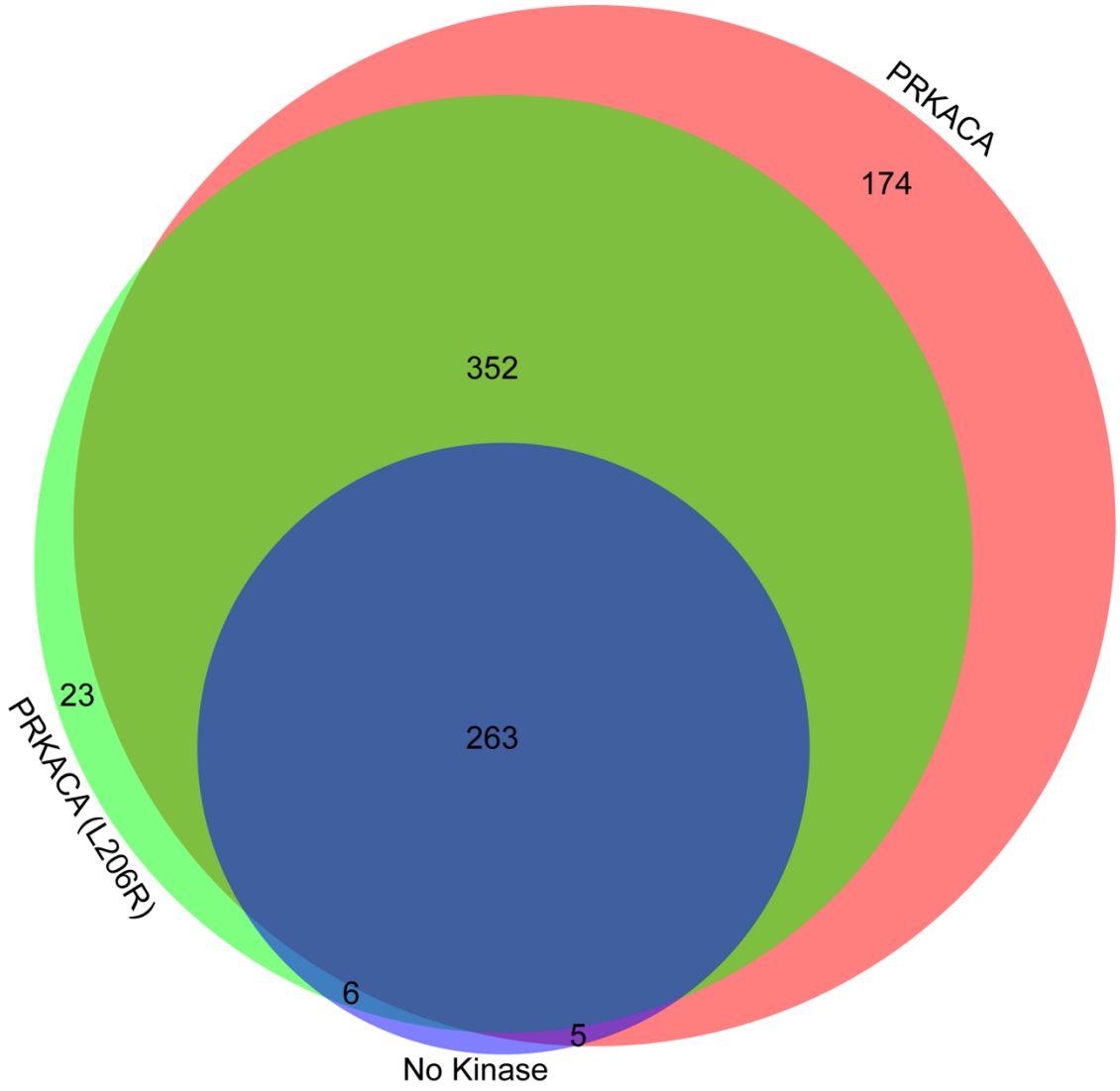

Figure 23. Venn Diagram of the Number of Human Proteins with Phosphosites Found in Samples with PRKACA, PRKACA (L206R), or No Kinase Added.
794 unique proteins with identified phosphosites from the sample with PRKACA added is represented in red on the right. 275 unique proteins with identified phosphosites from the no kinase added sample is represented in blue in the middle. 644 unique proteins with identified phosphosites from the sample with PRKACA (L206R) added is represented in green on the left. This proportional Venn Diagram was generated using Biovenn (Hulsen et al. 2008).

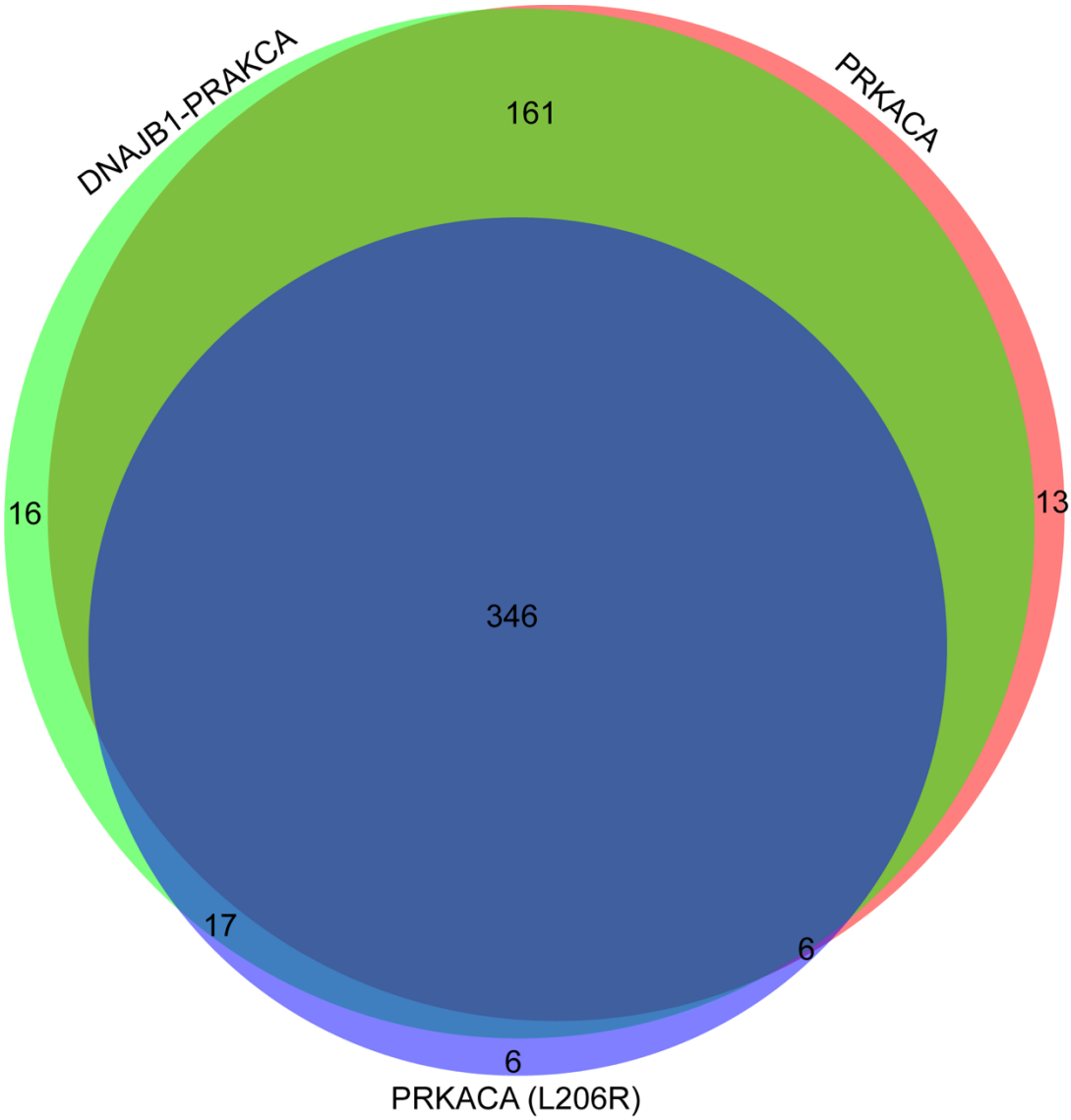

Figure 24. Venn Diagram of the Number of Human Proteins with Phosphosites Found in Samples with PRKACA, PRKACA (L206R), or DNAJB1 Added.

Any gene names that were also identified in the sample with no kinase added were removed from the gene name lists for the kinases in order to draw this comparison. 526 unique proteins with identified phosphosites from the sample with PRKACA added is represented in red on the right. 375 unique proteins with identified phosphosites from the sample with PRKACA (L206R) added sample is represented in blue in the middle. 540 unique proteins with identified phosphosites from the sample with DNAJB1-PRKACA added is represented in green on the left. This proportional Venn Diagram was generated using Biovenn (Hulsen et al. 2008).

Comparison of Putative Substrates Yielded from Mouse Liver in vitro Assay and Human Hepatocyte in vitro Assay

It is not possible to do any meaningful statistical analysis between the pilot experiment using mouse liver lysate and the triplicate experiment using human hepatocyte lysate since the pilot experiment with mouse liver lysate only had one replicate. However, it is possible to compare the list of gene names of proteins that had phosphopeptides enriched in each assay (**Figure 25**). This broad comparison shows that while there are many similarities between proteins that have phosphopeptides enriched in mouse and human liver contexts, far more seem species specific. This is also highlighted with a Venn diagram (**Figure 26)** and corresponding table (**Table 11**). These were generated by inputting the gene names of the putative substrates from each kinase condition from the *in vitro* mouse liver and human hepatocyte assays into the Bioinformatics and Evolutionary Genomics Venn diagram web tool (http://bioinformatics.psb.ugent.be/webtools/Venn/).

Using this list, I took the DNAJB1-PRKACA putative substrates only recognized in mouse liver lysate and the DNAJB1-PRKACA putative substrates only recognized in human hepatocyte lysate and did analysis in STRING (**Figures 27-28** and **Tables 12-15**). For this comparison, I included tables for molecular and cellular function using the GO database and KEGG pathways when these analyses were available. These analyses suggest that the putative DNAJB1-PRKACA substrates unique to mouse liver may not be very interrelated or implicated in critical pathways. However, the DNAJB1-PRKACA putative substrates unique to human hepatocytes seem to be involved in

metabolic pathways and perhaps often localized to the endoplasmic reticulum and mitochondria.

I also did a comparison using the Bioinformatics and Evolutionary Genomics Venn diagram web tool again to see how many of the putative substrates identified from my *in vitro* assays using mouse liver lysate and human hepatocyte lysate were also identified by the sources discussed in Chapter I and listed in **Table 1** (**Table 19**). While there was a great deal of overlap, both *in vitro* assays identified unique putative substrates. This, again, highlights the importance of methodology and source material for identification of phosphosites and the crucial need for further validation to determine a true *in vivo* direct substrate of a kinase.

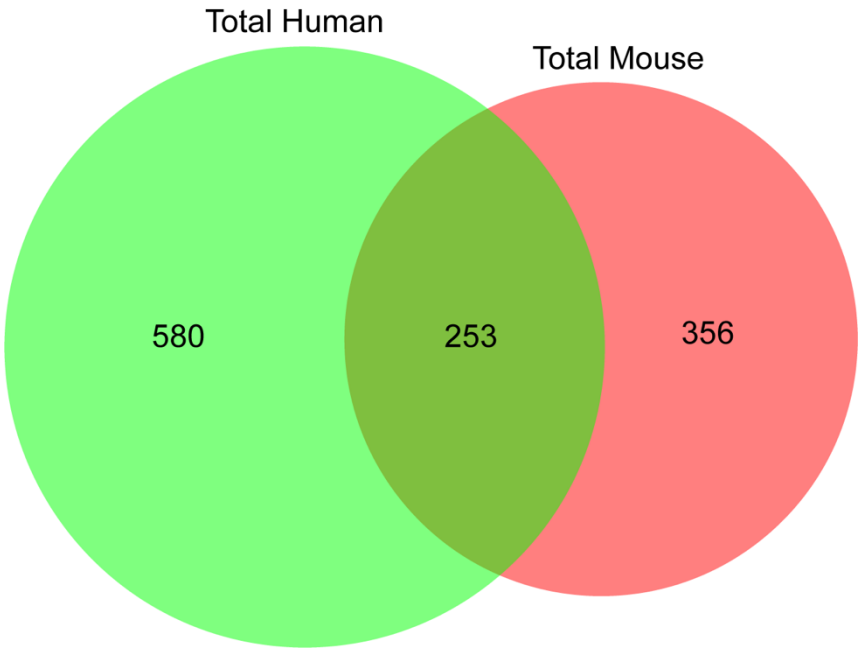

Figure 25. Venn Diagram of the Total Number of Human Proteins Identified with Phosphosites and the Total Number of Mouse Proteins Identified with Phosphosites.

609 unique proteins with identified phosphosites found enriched in the mouse liver *in vitro* experiments are represented in red on the right. 833 unique proteins with identified phosphosites found enriched in human hepatocytes is represented in green on the left. This proportional Venn Diagram was generated using Biovenn (Hulsen et al. 2008).

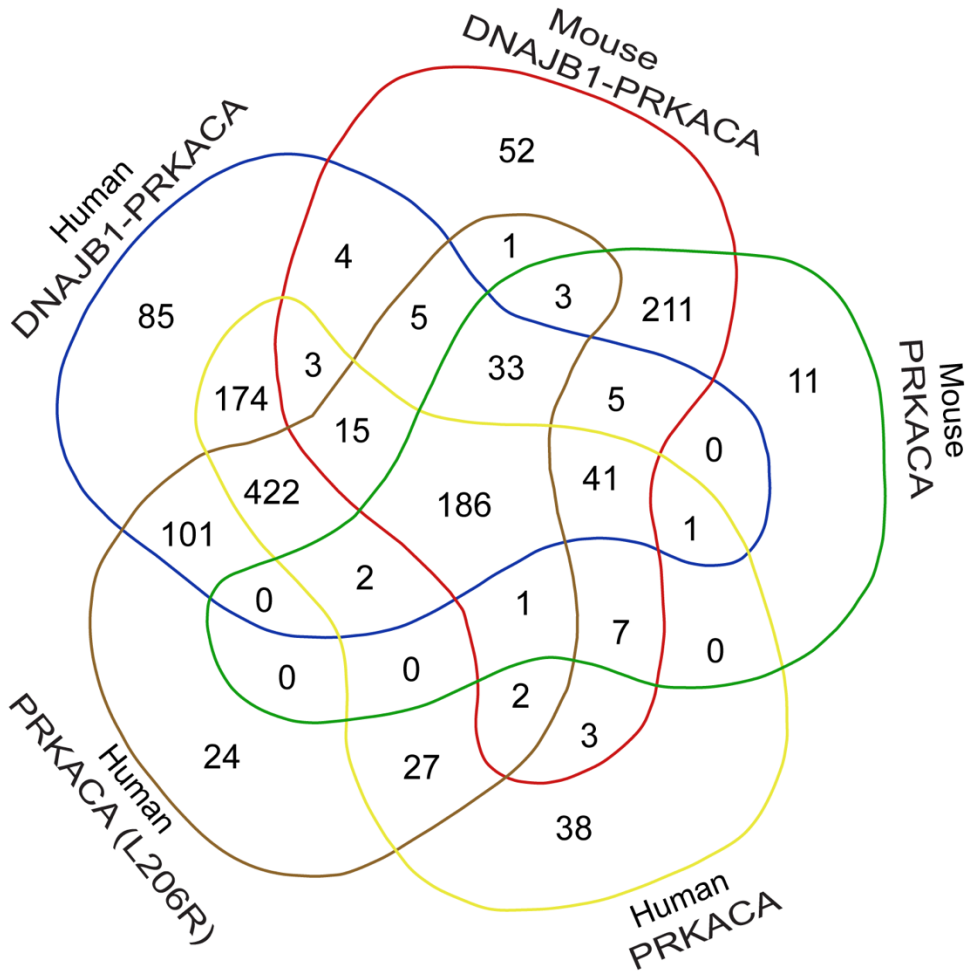

Figure 26. Venn Diagram of Putative Substrates in Mouse Liver and Human Hepatocytes For PRKACA, PRKACA (L206R), DNAJB1-PRKACA.

The Venn Diagram was generated by inputting the gene names of the putative substrates from each condition into the Bioinformatics and Evolutionary Genomics Venn diagram web tool (http://bioinformatics.psb.ugent.be/webtools/Venn/).

Table 11. Overlap of Putative Substrates in Mouse Liver and Human Hepatocytes.

Overview of Studies	
Kinases Used for *in vitro* Reaction	**Total Putative Kinase Substrates Identified**
Human PRKACA	1077
Human DNAJB1-PRKACA	822
Human PRKACA (L206R)	922
Mouse PRKACA	572
Mouse DNAJB1-PRKACA	501
Total Number of Unique Putative Kinase Substrates: 1457	
Specific Overlaps Between Studies	

Kinases Used for *in vitro* Reaction	**Number of Overlaps**	**Overlap of Putative Kinase Substrates**
Human DNAJB1-PRKACA Human PRKACA (L206R) Mouse PRKACA Mouse DNAJB1-PRKACA	186	DBNL COBLL1 ACTR3 PDHA1 TKT TLN1 ACOT1 NDUFS1 TPD52L2 CASP6 IRF2BP2 SLCO2B1 CLTA ACAT1 ALDOC PDCD4 MDH1 PRKAR2A BHMT RAPH1 TPI1 DNAJC5 DSTN ALDH2 C3 HSPD1 HYOU1 ALDH4A1 PARVA SCP2 NPM1 UQCRC1 NUCB1 PIGR BTF3 HSPA4 SLC9A3R1 CDHR5 RAB21 PSMC6 SSR3 ATP1A1 VAPA CORO1B MTHFD1 YWHAH ALDH6A1 PHB2 NDRG2 UQCRFS1 DDI2 PGM1 SET PRKAR1A TALDO1 ARG1 SULT2A1 RMDN3 CTNNB1 NAP1L4 OXR1 SLIRP BAD CYP2E1 SNX2 ANP32A ACLY PRDX5 ALDH7A1 TJP1 TOM1 SEC22B AMACR OCIAD1 ACAA2 BCL2L13 VCP ALDOA RAVER1 LASP1 ALDH5A1 ACADS STMN1 PSME1 HSP90AA1 LRRC47 CARHSP1 PHACTR4 PRKCSH ALDH1L1 HPD NUCKS1 CCS TSSC4 ASL SRP14 ACADM PGRMC1 OPTN CTNNA1 ACAD9 TTC36 PYGL STARD10 LRP1 OXSM PEA15 NDRG1 HSPA9 MYLK SOD1 PCNP APOH NDUFV1 CFL1 ALDH8A1 SGTA CLU ACAT2 TNKS1BP1 NUDC DNAJC8 BCKDHA MTHFS ALDH1A1 MRPS31 HSP90AB1

		TGOLN2 HSP90B1 GSTA3 WDR44 NIT1 TCEA1 KHSRP MRPS36 TRIM28 HTATSF1 TST NSFL1C AFMID ACIN1 VCL TIMM44 CBX3 VASP PDIA6 NCK1 CAT LSR ARHGDIA CETN2 CPS1 CANX DAP UGP2 PRKACA IDH1 CFDP1 MIA3 ST13 CLIP1 P4HB PGLS CALD1 HIBADH ALDOB LMNA CLTB ACOX2 CAST ACTG1 NME1 APPL1 IWS1 CP LRPAP1 PNPO HSD17B6 AARS S100A13 PAK2 SDHA COMT UQCRC2 CBR1 PGK1
Human PRKACA Human DNAJB1-PRKACA Mouse PRKACA Mouse DNAJB1-PRKACA	41	CNPY2 PRDX6 TAGLN2 AFG3L2 PKLR NDUFS4 PSMD11 SNX6 RPS21 AP2M1 PCBP1 CALR SPR AKAP2 ACADVL SEPHS1 SZRD1 ARFGAP2 RPL24 ASGR1 PSMA2 DPP3 ATP6V1B2 NSF NAMPT UGDH PPP2R1A ACSL1 SORD SNX3 THUMPD1 CPOX CTNND1 USP5 PEX19 AHSG COX4I1 ALB CTSZ SEC61B ATIC
Human DNAJB1-PRKACA Human PRKACA (L206R) Mouse PRKACA Mouse DNAJB1-PRKACA	33	GPHN ECHS1 DNAJB1 ATP11C GPD1 ALAD ETFA FDX1 GPS1 GRB14 EPN1 GCLC EEF1A1 EIF4B GLUD1 HMOX1 EEF2 EBAG9 HACL1 FABP1 ETFDH EEF1D H6PD GLUL EPS8L2 GORASP2 EVA1A ETFB EIF2S2 HDGF GAPDH FTCD TYMP
Human PRKACA Human DNAJB1-PRKACA Human PRKACA (L206R) Mouse DNAJB1-PRKACA	15	SUMO1 KLC4 PGRMC2 PGAM1 CNDP2 PFAS HSPA5 HNRNPM ARFIP1 LAD1 YAP1 PSMA6 ARCN1 SYAP1 NADK2
Human PRKACA Human DNAJB1-PRKACA Human PRKACA (L206R) Mouse PRKACA	2	CBS RPLP2
Human PRKACA Human PRKACA (L206R) Mouse PRKACA Mouse DNAJB1-PRKACA	1	CNBP
Human DNAJB1-PRKACA Mouse PRKACA Mouse DNAJB1-PRKACA	5	EIF6 FKBP8 GNMT FMO5 GPX1
Human PRKACA Human DNAJB1-PRKACA Mouse DNAJB1-PRKACA	3	CDH13 PDHX CDV3

Human DNAJB1-PRKACA Human PRKACA (L206R) Mouse DNAJB1-PRKACA	5	EIF1 FAM122A GOLGA5 PDP2 HADHA
Human PRKACA Human DNAJB1-PRKACA Mouse PRKACA	1	AGPS
Human PRKACA Human DNAJB1-PRKACA Human PRKACA (L206R)	422	TFIP11 MAP4 ZHX3 HSPB1 C1ORF53 MACF1 AIFM1 LMAN1 TMEM160 ADD3 HEL-S-117 SLTM RPL19 MYO9B ATP1A3 MESDC2 MATR3 POLI SMARCC1 DSP THRAP3 ST13P5 PDLIM2 LYAR SLCO1B3 PIR AK3 CTAGE5 CYP2D6 TGM2 NASP ARHGEF7 RPL29 SARS2 ARHGEF12 GLUD2 PTPN11 RALY SHROOM1 BCLAF1 RBM33 RAD23B SLC27A3 CAMSAP3 DMTN HIST1H1E GSTA2 ANGPTL3 PIN1 RPS28 NDUFS8 LSM14A YWHAQ PREP DTX3L SCRN2 HSP90AB2P PPM1A PPP1R8 ALCAM TWF1 CCT2 CSDE1 MYH9 ATP5B HSD17B4 TOMM34 XRCC6 TF ASS1 LETM1 SPTBN1 BCAP31 PBDC1 LDHB NME1-NME2 C9ORF142 ACTC1 POTEE UFD1L PRDX4 ABHD12 UFL1 ISOC2 IMMT HIST1H1A SERPINA1 HP1BP3 PPIG OSBP STBD1 ALDH1L2 CYP4F3 NOP58 ALDH1A2 RPRD1B MAMSTR MTTP WIPF3 C17ORF59 AHNAK PPP1R12A CHMP2B BCAP29 SORBS2 PSMF1 HNRNPUL2 YWHAZ SULT1A2 CTAGE15 TMPO LYRM5 ZC3HAV1 ARPC5 PPL ACOT2 CYP2A6 PRPF4B CHMP6 MIA2 MANF CASC4 ANXA6 VAPB LIMA1 CTAGE6 BHMT2 UMPS PRKAB2 PHYKPL UBE2M CTAGE9 SULT1A1 KIN27 PROSER2 LARP1 MARVELD3 LOC113230 ALDH1B1 RANBP1 CBX1 CAP1 SEPT9 WBP11 BABAM1 ADH1C UBE2J1 HNRNPK CLIP2 WDR4 POTEKP VTN HEXB SAFB2 ITGA6 NOC2L PSIP1 ADD1 PRRC2C MVD CYP4F12 HSPA1A SUMF2 CTAGE4 IRS2 C9ORF78 PPIB MXRA5 CYP2A13 SCFD1 RRBP1 HSP90AA5P SPATS2L MAT2B VDAC1 PPP1R10 PPIA RABAC1 RDH16 PRKACB CRAT AK2 ILF3 RPL30 STX16-NPEPL1 SRSF3 NDUFV2 C11ORF58 ATP5EP2 ANXA5 BLVRB CPT2 MYOCD SEC31A ANP32D SSFA2 ZC3H18 HNRNPC SF1 LSM7 TIMM8A SRRM1 PABPN1 NAP1L1 PLIN1 SH2D4A EEF1A2 CD14 PHAX TPD52

		AK1 ACSS3 PGM2 ZC3H13 CGREF1 THOC3 ARPC2 SULT1E1 LMO7 THAP4 MAN1A1 C14ORF166 HIST1H1B CGNL1 NUP98 PGK2 ATP5A1 UROD CD276 NIFK METTL14 EIF1B ATP1A2 UROC1 ACY1 NME2 ATPIF1 PYGB DDRGK1 RPL21 API5 HIST1H1T WIPF2 APOL5 PPM1B POTEF SORBS1 YRDC VPS4B ST13P4 RPL5 CYP4F2 STX12 MRPL39 IGFBP1 SMAP RPS3A ASPDH HINT2 PALM3 CYP2D7 ABCF1 MUT CMPK1 SEPT2 SLC38A3 XPO1 WDR87 SSH1 PALMD HTATIP2 SSB WDR77 PDZK1P1 RPL28 PHACTR2 ATP5J SRP54 DNPH1 SF3B1 MICAL3 ACAA1 STIP1 PLEC CA2 MTDH SLC25A20 NCL ARPC1B AP3D1 PRKACG OGFR SEMA4G ADH1A HSF1 NDUFA7 METAP2 NME2P1 REPS1 KNG1 PHF14 SEC14L2 PA2G4 PRDX2 RPL13 TMX1 HSPH1 ACTB SEC62 PCBD1 MPDZ YLPM1 CYP2C8 KANK2 ALDH1A3 UQCRFS1P1 ACTG2 OXNAD1 COPB1 PRPSAP2 ARHGEF6 DAK POTEI LRRFIP2 COBL PTGFRN SRPR ADH1B CRK SNX1 PKM HSPA1B RBM8A HNRNPA3 NOLC1 PGAM4 TKFC CTAGE8 PDZK1 HSP90AB3P POFUT1 ABCB11 TJP2 SCRIB RBM39 CUX1 GSTA5 ABHD14A-ACY1 ACTA1 TPPP RBM27 SEPT11 LARP4 SNTB1 NUMA1 WRNIP1 RPS25 SDF2L1 ACTA2 SORBS3 EIF3CL TACO1 HIST1H1D STX16 SYNPO CDC5L CTNNA2 AMPD2 CYB5A KIAA1598 PGAM2 DBR1 PSME2 HIST1H1C PLEKHA5 MAP1S ATP5E SERBP1 ZFYVE19 RANBP2 MTCH2 APBB1IP PNN MIEN1 PGM3 ANP32B HEXA AP4E1 NRD1 CASK SMAP2 SRRM2 PEBP1 DTNA HNRNPA1 KTN1 HNRNPA1L2 EEF1A1P5 TCOF1 TTC38 BAIAP2 CES1 PIPOX ADD2 PITPNB BAAT STX4 ARFGAP1 PPP1R7 NDUFA5 PDLIM5 ABLIM1 WASF2 HNRNPUL2-BSCL2 HDLBP SAFB MLLT4 NDUFB9 METTL1 CBFA2T3 IQGAP2 MTFR1
Human PRKACA Mouse PRKACA Mouse DNAJB1-PRKACA	7	HUWE1 BAG6 ASNA1 NUMB SBDS SARDH NNT
Human PRKACA (L206R) Mouse PRKACA Mouse DNAJB1-PRKACA	3	G3BP1 ACBD4 UBA2

Human PRKACA Human PRKACA (L206R) Mouse DNAJB1-PRKACA	2	APMAP PRCC
Human DNAJB1-PRKACA Mouse DNAJB1-PRKACA	4	WASL EIF3H HADH TSFM
Human DNAJB1-PRKACA Mouse PRKACA	174	RAB2A NAPRT QARS RGN RPL17-C18ORF32 SQRDL SPECC1L UGT1A1 LYRM2 CYP2C19 RPL35 PDIA3 ALDH3A2 NEDD4 HIST3H3 HSP90AA4P APOE MYO1C PMM1 ACOX1 HMGN3 SND1 HIST1H2BC PTGES3 APOB HIST1H2BL CS ZNF318 CPSF7 PRDX1 ITGA1 PPP2R1B DKFZP586F0420 PICALM HSPA4L CYP7A1 KHK DNAJC3 MTSS1L ARHGEF16 TARS CDK6 CTSB HIST1H2BN LUC7L SUB1 PCBP3 ALG13 ZYX MAP2K2 CMC1 CD2AP MYH10 HYPK MYH11 UBE2D3 PLRG1 CYP2C9 PRKDC MYO18A DNAJC1 SLCO1B1 SMS HMBOX1 RPL17 ACOT9 TXNDC5 POR CTSD NAA15 RP2 ARFIP2 ADRM1 MCEE PLAA SHMT1 SRP9 HMGB2 IVD ISG15 PROC HSD17B13 PARP1 PRDX3 CHCHD3 SEC16A SCYL2 PML YWHAG MYH14 LEO1 LMNB1 TFAM DUSP3 PSAP ACADSB HGD HMGN2 HIBCH TIMM10 COPE UQCC2 POLDIP2 CFL2 PABPC4 ITFG3 AIMP1 PPIF ABAT SCARB2 PSMA7 SRPRB C2CD2L KRT18 SPECC1L-ADORA2A ATP6V1G1 STOML2 SETSIP HMGB1P1 HIST1H2BK METTL7A CADM1 C21ORF33 TOMM70A ITIH1 OTUB1 NHSL1 CHP1 PSMC5 MLEC PAXBP1 MAP3K7 HTRA2 ZC3H4 IARS2 IGBP1 DDX58 ACACB DMD PABPC1 SERF2 HIST1H2BM RPL8 HSD17B8 PFN1 PCBP2 QRSL1 DDO HIST1H2BD H2BFS XYLB AGXT UBE2V1 HIST2H2BF DCTN2 MECR PMM2 HIST1H2BH HSP90AB4P SSBP1 PDIA4 ANXA4 BMP2K HNRNPL CHCHD4 SNAP91 SUOX SHMT2 ST20-MTHFS PAH LTA4H HMGB1 LBR BAIAP2L1
Human DNAJB1-PRKACA Human PRKACA (L206R)	101	GMPR2 ITGA5 GSTA1 SOS1 NUFIP2 GUCY1A3 GOLM1 FBP2 FASN EXOSC2 RPS4Y2 FRS2 ENOSF1 DENND1A HAO1 GPI STIM1 RPS4X IRS1 LAGE3 EML3 FTH1 KIAA1217 PACSIN3 FETUB GANAB EEPD1 APOA5 EIF3D FHIT EPS15 ARFGEF2 CDC26 FLNB GIGYF2 ECHDC3 GPX2 TRANK1 EPB41L3 RPS4Y1 ABCA12 MIEF1

		EHBP1 ARGLU1 ZC3H14 GCDH EIF4G1 KDM4A GAPVD1 COPB2 HNRNPH1 U2AF2 EIF5B GLRX3 RPS6 C2ORF72 G3BP2 HACD3 AASS FMO3 EIF3A EMC10 FAM134A KIAA1671 FKBP3 EIF3J PPP1R3E EIF2A LRP2 TMEM109 PDHA2 FAH EIF3C RNPEP FBP1 RPL27A DUT FBL HADHB GAS2 ENO3 ENO1 PPFIBP2 TMEM41A REEP4 GTF2I GSTO1 ECHDC2 RSRC2 IFNA6 TCEA3 HNRNPH2 FUNDC2 PLEKHA6 GATM HNRNPU FLNA FCHO2 EHHADH ALPL EEF1G
Mouse PRKACA Mouse DNAJB1-PRKACA	211	ADH1 ACOT12 JPT1 RIDA AGFG1 HMGCS2 NAXE LDHD PI4KB BET1L CXADR UBA1 ATG2B ARHGAP17 SLK CA14 ACSBG2 LYPLA1 SNRNP70 RBM17 HSPA1L ARHGAP39 VWA5A APEH SULT2A8 CCDC43 MRPL12 ADH5 LCMT1 GCLM KIF5B FAM213B CES1F NUDT7 ELAC2 PTMS ANKS1 NDUFA2 DPYD CASP8 SARS UCHL4 HAL GM20425 NT5C GM9774 NKTR TUBA1B CSRP3 TPMT SERPINA3N PFKL EARS2 MCM3 STRIP1 HBA-A1 SELENBP2 GC CYP2C70 WDR91 LXN MAPRE3 AKR7A2 ARPP19 CNGA2 ATP5H SPAG9 PCX ASPSCR1 DPPA3 DHTKD1 CTH ATP5F1A GLOD4 DAPK2 GYKL1 GSDMDC1 CYP2F2 SNRPG CSMD1 DNAJC12 ZNRF2 SERPINA1B 9-Sep DECR2 GOPC PNPLA8 CYP2B10 GLYCTK PLEKHF2 GATD3A MAVS DIS3L2 ADCY10 ECI2 KARS ATP5PF IDH3A URAD CES3A RANBP3 MOCS1 ACSM5 CDK18 SNAP29 STK24 SDS PTMA ETNPPL HEBP1 HMGN5 FCGRT MARCKS ISOC2A PCDH1 SASH1 LDLRAP1 CYP1A2 SERPINA3K CDO1 GSTM1 NUBP1 AKAP1 EFHD2 EGFR SNAP23 CMC2 NECAP1 LNPK GIMAP4 ENSA F13B AKR1D1 ETHE1 PRODH D2HGDH HNRNPAB CDC42EP5 CES2E CRIP2 SEMA6D EIF4EBP1 SMOC1 METTL26 GRN FKBP15 FAM50B INMT CACNB2 SSR1 ACSF3 RILP CCDC180 KIF13B NADK H2-KE6 UBQLN1 NDUFB11 RNH1 FAM162A PPP4R2 HAAO MTSS1 MARCKSL1 PPIP5K2 ATP5F1B SLCO1B2 CYP4F17 PPP1R11 MESD LCP1 EIF4H GPRIN3 LAP3 TIMM50 PRKAB1 YBX3 SHTN1 ANK3 HDGFL2 ATP5C1 2-Sep ZFP69 AMT MIOS HSD11B1 ARID4B KCTD12 BOLA1 GMPS GPT2 CYP2D22

		APOA1 SEPHS2 AKR1C6 CLNS1A ERRFI1 CIDEB AGMAT ECI1 FTL1 STRN LBH MUG1 MTFR1L KEG1 CYP2A5 SERPINA1C CCDC9 SERHL ACAA1B
Human PRKACA Mouse DNAJB1-PRKACA	3	AHCY HS1BP3 AKT1S1
Human PRKACA (L206R) Mouse DNAJB1-PRKACA	1	EIF4EBP2
Human PRKACA (L206R) Human PRKACA	27	DDT LYRM1 PALLD OGDH DOCK8 TSC2 ANXA2P2 SVIL INF2 UGT2A3 CLMN DDX46 BAT3 PRPF40A UCHL3 ANXA2 SH3BP5L HNRNPA2B1 ZDHHC5 MVK PRKAR1B PBXIP1 DDTL CRYL1 MFAP1 SLC4A4 OR51A7
Human DNAJB1-PRKACA	85	GALK1 RPL36A HMGN1 FKBP7 FUBP3 FBXO22 THOC2 YWHAE ERBB2IP TFR2 SDC2 C4A DSG2 GLG1 PCCB GPALPP1 FUBP1 ACO2 TJP3 ECE1 STOM FAM114A2 NEDD4L PLEKHG3 HARS RPS10-NUDT3 RUVBL1 DDAH2 HIRIP3 GRHPR HNRNPUL1 SFN HSD17B7 DMGDH STX5 EEF1B2 PHYH FMO1 PLS3 ELMOD2 RPL36A-HNRNPH2 EPHX2 DDX50 H1F0 ETF1 ARHGEF5 ALS2 YWHAB SEC23A GLYATL1 C4B EIF2AK2 LMAN2 EPB41 DFFA FAM83G GTF2H1 PFKFB2 DENR RPS10 SYMPK DAB2IP ACSM2A FGA GGT7 ESF1 EPHX1 APOO PC PSMD4 COA7 UBXN1 TP53I11 ERP44 ESYT2 SAP30BP GBF1 ENPP1 FAM114A1 FDXR GLB1 ESPN MAT2A ACSM2B S100A9
Mouse DNAJB1-PRKACA	52	MSRB1 PYROXD2 CYP2D11 MMGT1 DPYSL2 SUGCT ACAA1A DGLUCY TJAP1 RCSD1 ACSF2 DCAF11 TNNT2 B2M BAG3 SAYSD1 RPS3A1 GSK3B GPD1L AADAT ACSS2 PRKAA2 OPLAH CR1L CEP290 WASHC2 NUCB2 EIF5 GBE1 GM20604 ASPG RTRAF MMUT GM13889 TOMM70 FLAD1 IFI35 DOCK5 CYP2C29 CUL4A TRAK1 MUSTN1 SIK3 RUFY3 WIPF1 ADSS PSME3 WNK1 GORASP1 ITIH4 SPHK2 C6
Mouse PRKACA	11	CCNY TMEM230 SGK2 BSG IGSF10 SIRT5 ITPA ITIH2 STAB2 SCO1

Human PRKACA	38	ACTN4 RBM15 PNPT1 PDCD5 PLIN2 UBXN4 PLXNB1 NUDT12 PALM2 PALM2-AKAP2 UQCRB NRAP DPYS NACA TNS1 MDH2 VPS53 NUMBL RCC1 ACOX3 UBE2D1 CYP2C18 CYP27A1 CDK5RAP3 PLIN5 ARFGAP3 SLC25A10 CAP2 UBE2D4 RNMTL1 PPM1F USO1 MLXIPL ZNF326 PHYHD1 UBE2D2 UBR4 DAAM1
Human PRKACA (L206R)	24	SMARCC2 EPS8 ERO1L RAF1 GPKOW SLC16A2 PSMD12 KIAA0368 DKC1 ASGR2 YAF2 SAP18 DPP9 MAP2 DR1 PDXDC1 NCKIPSD EXOG ECM29 PAK4 HMGCS1 ARAF PSMB10 FAM21C

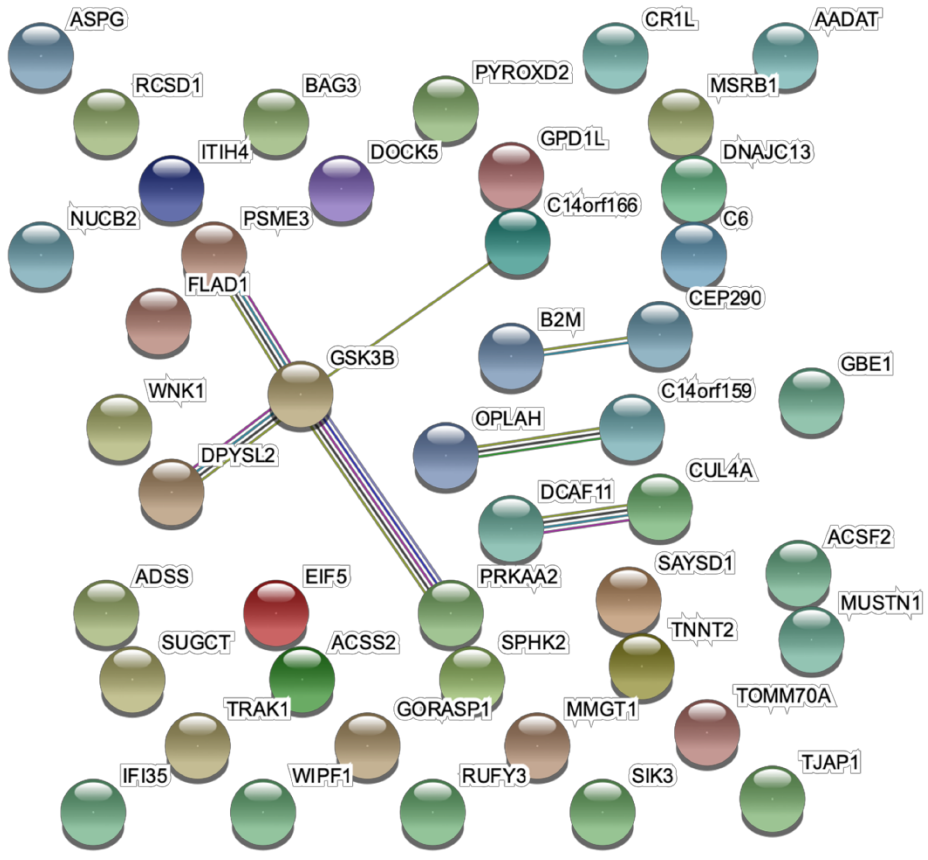

Figure 27. STRING Analysis of Putative Substrates of Only DNAJB1-PRKACA in Mouse from Mouse versus Human Comparison.

Table 12. STRING Cellular Component (GO) Analysis of Putative Substrates of only DNAJB1-PRKACA in Mouse from Mouse versus Human Comparison.

Cellular Component (GO)			
GO-term	*description*	*count in gene set*	*false discovery rate*
GO:0044444	cytoplasmic part	37 of 9377	0.00052
GO:0005829	cytosol	26 of 4958	0.00052
GO:0005622	intracellular	44 of 14286	0.00098
GO:0005737	cytoplasm	39 of 11238	0.0014
GO:0044424	intracellular part	43 of 13996	0.0023
GO:0044464	cell part	45 of 16244	0.0090

Table 13. STRING Molecular Function (GO) Analysis of Putative Substrates of Only DNAJB1-PRKACA in Mouse from Mouse versus Human Comparison.

Molecular Function (GO)			
GO-term	*description*	*count in gene set*	*false discovery rate*
GO:0016812	hydrolase activity, acting on carbon-nitrogen (but not peptide)...	2 of 6	0.0314

Table 14. STRING Cellular Component (GO) analysis of Putative Substrates of Only DNAJB1-PRKACA in Human from Mouse versus Human Comparison.

Cellular Component (GO)			
GO-term	*description*	*count in gene set*	*false discovery rate*
GO:0044444	cytoplasmic part	62 of 9377	0.00082
GO:0043231	intracellular membrane-bounded organelle	66 of 10365	0.00082
GO:0043227	membrane-bounded organelle	69 of 11244	0.00082
GO:0070013	intracellular organelle lumen	41 of 5162	0.0012
GO:0044446	intracellular organelle part	58 of 8882	0.0012
GO:0044422	organelle part	59 of 9111	0.0012
GO:0043229	intracellular organelle	71 of 12193	0.0012
GO:0005737	cytoplasm	67 of 11238	0.0012
GO:0044424	intracellular part	76 of 13996	0.0018
GO:0005829	cytosol	38 of 4958	0.0023
GO:0005739	mitochondrion	17 of 1531	0.0068
GO:0005788	endoplasmic reticulum lumen	7 of 299	0.0079
GO:0044432	endoplasmic reticulum part	15 of 1294	0.0092
GO:0005793	endoplasmic reticulum-Golgi intermediate compartment	4 of 113	0.0321
GO:0005783	endoplasmic reticulum	17 of 1796	0.0321
GO:0005782	peroxisomal matrix	3 of 53	0.0321
GO:0005777	peroxisome	4 of 127	0.0397

Table 15. STRING KEGG Pathways Analysis of Putative Substrates of Only DNAJB1-PRKACA in Human from Mouse versus Human Comparison.

KEGG Pathways			
pathway	*description*	*count in gene set*	*false discovery rate*
hsa00630	Glyoxylate and dicarboxylate metabolism	3 of 28	0.0277
hsa01100	Metabolic pathways	14 of 1250	0.0429

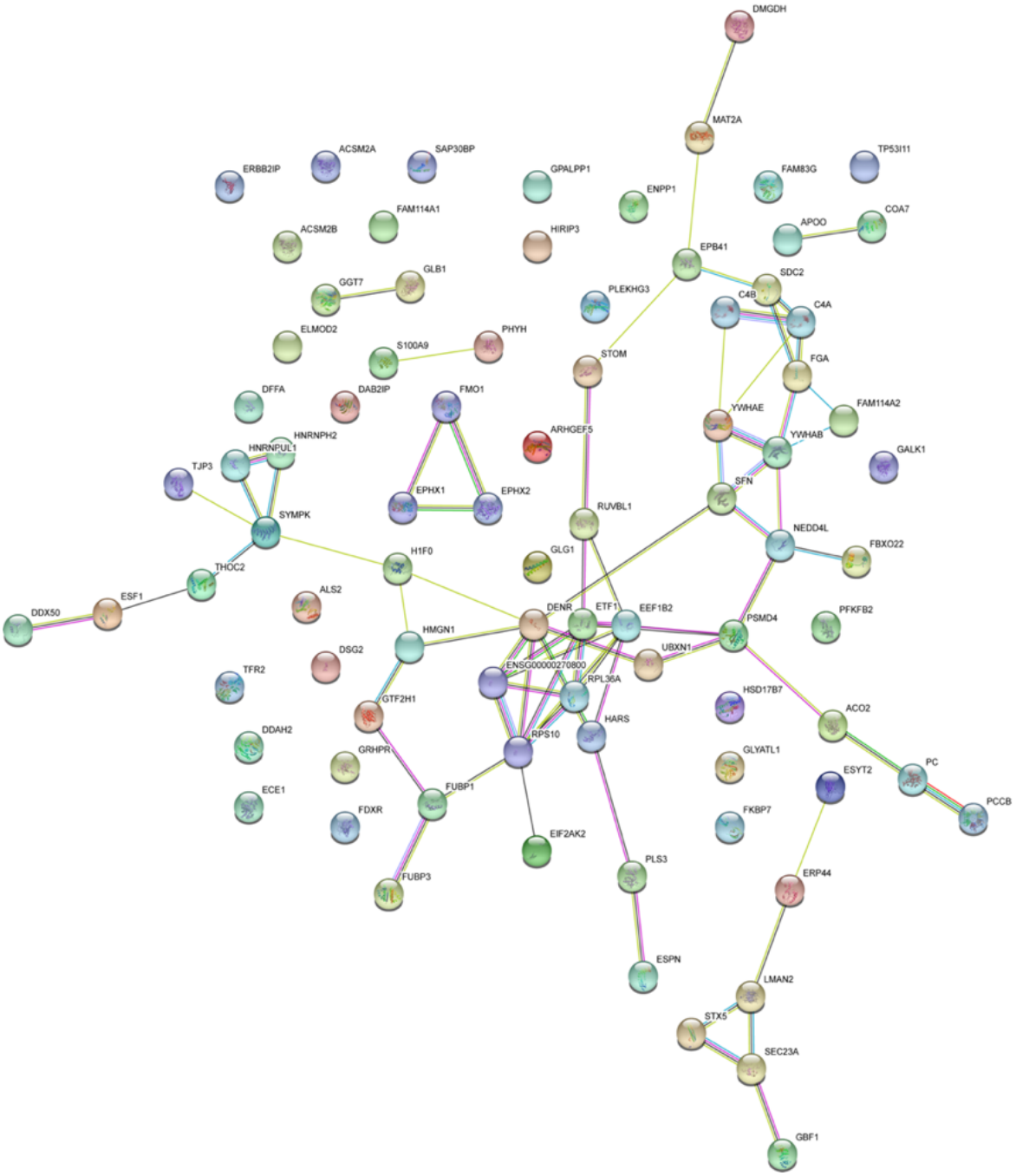

Figure 28. STRING analysis of Putative Substrates of only DNAJB1-PRKACA in Human from Mouse versus Human Comparison.

Table 16. Overlap of Putative Substrates between Mouse and Human *in vitro* Studies and Previously Published PKA Substrate Studies.

Overview of Studies	
Identifying Study	**Total Putative Kinase Substrates Identified**
Embogama, et al.	279
Hamaguchi, et al.	45
Hu, et al.	301
Imamura, et al.	1132
Isobe, et al.	197
DNAJB1-PRKACA *in vitro* Human Hepatocyte Lysate	1077
DNAJB1-PRKACA *in vitro* Mouse Liver Lysate	454
PRKACA (L206R) *in vitro* Human Hepatocyte Lysate	822
PRKACA *in vitro* Human Hepatocyte Lysate	922
PRKACA *in vitro* Mouse Liver Lysate	392
Total Number of Unique Putative Kinase Substrates: 2687	

Specific Overlaps Between Studies		
Identifying Study	**Number of Overlaps**	**Overlap of Putative Kinase Substrates**
Embogama, et al. Imamura, et al. Isobe, et al. DNAJB1-PRKACA *in vitro* Human Hepatocyte Lysate DNAJB1-PRKACA *in vitro* Mouse Liver Lysate PRKACA (L206R) *in vitro* Human Hepatocyte Lysate PRKACA *in vitro* Human Hepatocyte Lysate PRKACA *in vitro* Mouse Liver Lysate	1	LMNA

Embogama, et al. Hu, et al. Imamura, et al. Isobe, et al. DNAJB1-PRKACA *in vitro* Human Hepatocyte Lysate PRKACA (L206R) *in vitro* Human Hepatocyte Lysate PRKACA *in vitro* Human Hepatocyte Lysate	1	SPTBN1
Hamaguchi, et al. Imamura, et al. Isobe, et al. DNAJB1-PRKACA *in vitro* Human Hepatocyte Lysate PRKACA (L206R) *in vitro* Human Hepatocyte Lysate PRKACA *in vitro* Human Hepatocyte Lysate PRKACA *in vitro* Mouse Liver Lysate	1	TNKS1BP1
Imamura, et al. Isobe, et al. DNAJB1-PRKACA *in vitro* Human Hepatocyte Lysate DNAJB1-PRKACA *in vitro* Mouse Liver Lysate PRKACA (L206R) in vitro Human Hepatocyte Lysate PRKACA *in vitro* Human Hepatocyte Lysate PRKACA *in vitro* Mouse Liver Lysate	5	NSFL1C COBLL1 IRF2BP2 PRKAR2A OPTN
Hu, et al. Imamura, et al. DNAJB1-PRKACA *in vitro* Human Hepatocyte Lysate DNAJB1-PRKACA *in vitro* Mouse Liver Lysate PRKACA (L206R) *in vitro* Human Hepatocyte Lysate PRKACA *in vitro* Human Hepatocyte Lysate PRKACA *in vitro* Mouse Liver Lysate	6	NPM1 STMN1 NDRG1 TRIM28 LASP1 HSP90AA1

Embogama, et al. Hu, et al. DNAJB1-PRKACA *in vitro* Human Hepatocyte Lysate DNAJB1-PRKACA *in vitro* Mouse Liver Lysate PRKACA (L206R) *in vitro* Human Hepatocyte Lysate PRKACA i*n vitro* Human Hepatocyte Lysate PRKACA *in vitro* Mouse Liver Lysate	2	YWHAH PRKACA
Embogama, et al. Hamaguchi, et al. Imamura, et al. DNAJB1-PRKACA *in vitro* Human Hepatocyte Lysate PRKACA (L206R) *in vitro* Human Hepatocyte Lysate PRKACA *in vitro* Human Hepatocyte Lysate PRKACA *in vitro* Mouse Liver Lysate	1	RPLP2
Embogama, et al. Imamura, et al. DNAJB1-PRKACA *in vitro* Human Hepatocyte Lysate DNAJB1-PRKACA *in vitro* Mouse Liver Lysate PRKACA (L206R) *in vitro* Human Hepatocyte Lysate PRKACA *in vitro* Human Hepatocyte Lysate PRKACA *in vitro* Mouse Liver Lysate	3	SLC9A3R1 PDIA6 KHSRP
Hu, et al. Isobe, et al. DNAJB1-PRKACA *in vitro* Human Hepatocyte Lysate DNAJB1-PRKACA *in vitro* Mouse Liver Lysate PRKACA (L206R) *in vitro* Human Hepatocyte Lysate PRKACA *in vitro* Human Hepatocyte Lysate	2	CTNNB1 BAD

Hu, et al. Isobe, et al. DNAJB1-PRKACA *in vitro* Human Hepatocyte Lysate PRKACA (L206R) *in vitro* Human Hepatocyte Lysate PRKACA *in vitro* Human Hepatocyte Lysate PRKACA *in vitro* Mouse Liver Lysate	1	LSR
Hamaguchi, et al. Imamura, et al. Isobe, et al. DNAJB1-PRKACA *in vitro* Human Hepatocyte Lysate PRKACA (L206R) *in vitro* Human Hepatocyte Lysate PRKACA *in vitro* Human Hepatocyte Lysate	1	REPS1
Imamura, et al. Isobe, et al. DNAJB1-PRKACA *in vitro* Human Hepatocyte Lysate DNAJB1-PRKACA *in vitro* Mouse Liver Lysate PRKACA *in vitro* Human Hepatocyte Lysate PRKACA *in vitro* Mouse Liver Lysate	1	CTNND1
Imamura, et al. Isobe, et al. DNAJB1-PRKACA *in vitro* Human Hepatocyte Lysate DNAJB1-PRKACA *in vitro* Mouse Liver Lysate PRKACA (L206R) *in vitro* Human Hepatocyte Lysate PRKACA *in vitro* Mouse Liver Lysate	1	EIF4B
Imamura, et al. Isobe, et al. DNAJB1-PRKACA *in vitro* Human Hepatocyte Lysate DNAJB1-PRKACA *in vitro* Mouse Liver Lysate PRKACA (L206R) *in vitro*	2	TJP1 YAP1

Human Hepatocyte Lysate PRKACA *in vitro* Human Hepatocyte Lysate		
Isobe, et al. DNAJB1-PRKACA *in vitro* Human Hepatocyte Lysate DNAJB1-PRKACA *in vitro* Mouse Liver Lysate PRKACA (L206R) *in vitro* Human Hepatocyte Lysate PRKACA *in vitro* Human Hepatocyte Lysate PRKACA *in vitro* Mouse Liver Lysate	6	CCS SRP14 NCK1 MIA3 HSPA4 SNX2
Embogama, et al. Hu, et al. Imamura, et al. DNAJB1-PRKACA *in vitro* Human Hepatocyte Lysate PRKACA (L206R) *in vitro* Human Hepatocyte Lysate PRKACA *in vitro* Human Hepatocyte Lysate	2	NASP YWHAZ
Hu, et al. Imamura, et al. DNAJB1-PRKACA *in vitro* Human Hepatocyte Lysate DNAJB1-PRKACA *in vitro* Mouse Liver Lysate PRKACA *in vitro* Human Hepatocyte Lysate PRKACA *in vitro* Mouse Liver Lysate	1	ARFGAP2
Hu, et al. DNAJB1-PRKACA *in vitro* Human Hepatocyte Lysate DNAJB1-PRKACA *in vitro* Mouse Liver Lysate PRKACA (L206R) *in vitro* Human Hepatocyte Lysate PRKACA *in vitro* Human Hepatocyte Lysate PRKACA *in vitro* Mouse Liver Lysate	6	LRP1 MYLK CBX3 VASP PRDX5 ARHGDIA

Embogama, et al. Imamura, et al. DNAJB1-PRKACA *in vitro* Human Hepatocyte Lysate DNAJB1-PRKACA *in vitro* Mouse Liver Lysate PRKACA (L206R) *in vitro* Human Hepatocyte Lysate PRKACA *in vitro* Mouse Liver Lysate	1	GORASP2
Imamura, et al. DNAJB1-PRKACA *in vitro* Human Hepatocyte Lysate DNAJB1-PRKACA *in vitro* Mouse Liver Lysate PRKACA (L206R) *in vitro* Human Hepatocyte Lysate PRKACA *in vitro* Human Hepatocyte Lysate PRKACA *in vitro* Mouse Liver Lysate	16	HSPD1 DDI2 ACLY PCNP NUDC HSP90AB1 TCEA1 HTATSF1 DBNL TPD52L2 VAPA SEC22B OCIAD1 ALDOA PHACTR4 CANX
Embogama, et al. DNAJB1-PRKACA *in vitro* Human Hepatocyte Lysate DNAJB1-PRKACA *in vitro* Mouse Liver Lysate PRKACA (L206R) *in vitro* Human Hepatocyte Lysate PRKACA *in vitro* Human Hepatocyte Lysate PRKACA *in vitro* Mouse Liver Lysate	14	TKT HYOU1 NUCB1 MTHFD1 ACAA2 CAT CLTB SDHA PGK1 ACADS PSME1 PRKCSH CLU ST13
Hamaguchi, et al. Imamura, et al. Isobe, et al. DNAJB1-PRKACA *in vitro* Human Hepatocyte Lysate PRKACA *in vitro* Human Hepatocyte Lysate	1	SPECC1L
Imamura, et al. Isobe, et al. DNAJB1-PRKACA *in vitro* Human Hepatocyte Lysate PRKACA (L206R) *in vitro* Human Hepatocyte Lysate PRKACA *in vitro*	9	MYO9B OSBP SORBS2 IRS2 CTNNA1 ABLIM1 LIMA1 MICAL3 TJP2

Human Hepatocyte Lysate		
Embogama, et al. Isobe, et al. DNAJB1-PRKACA *in vitro* Human Hepatocyte Lysate PRKACA *in vitro* Human Hepatocyte Lysate PRKACA *in vitro* Mouse Liver Lysate	1	AGPS
Hamaguchi, et al. Isobe, et al. DNAJB1-PRKACA *in vitro* Human Hepatocyte Lysate PRKACA (L206R) *in vitro* Human Hepatocyte Lysate PRKACA *in vitro* Human Hepatocyte Lysate	1	ARHGEF7
Isobe, et al. DNAJB1-PRKACA *in vitro* Human Hepatocyte Lysate PRKACA (L206R) *in vitro* Human Hepatocyte Lysate PRKACA *in vitro* Human Hepatocyte Lysate PRKACA *in vitro* Mouse Liver Lysate	1	CASP6
Embogama, et al. Hu, et al. Imamura, et al. DNAJB1-PRKACA *in vitro* Human Hepatocyte Lysate PRKACA *in vitro* Human Hepatocyte Lysate	1	ZYX
Embogama, et al. Hu, et al. Imamura, et al. DNAJB1-PRKACA *in vitro* Human Hepatocyte Lysate PRKACA (L206R) *in vitro* Human Hepatocyte Lysate	1	FLNA

Hu, et al. Imamura, et al. DNAJB1-PRKACA *in vitro* Human Hepatocyte Lysate PRKACA (L206R) *in vitro* Human Hepatocyte Lysate PRKACA *in vitro* Human Hepatocyte Lysate	7	HSPB1 DNAJC5 SAFB2 LARP4 MATR3 LARP1 PRKAR1A
Embogama, et al. Hu, et al. DNAJB1-PRKACA *in vitro* Human Hepatocyte Lysate PRKACA (L206R) *in vitro* Human Hepatocyte Lysate PRKACA *in vitro* Human Hepatocyte Lysate	2	TGM2 XPO1
Embogama, et al. Imamura, et al. DNAJB1-PRKACA *in vitro* Human Hepatocyte Lysate PRKACA (L206R) *in vitro* Human Hepatocyte Lysate PRKACA *in vitro* Human Hepatocyte Lysate	12	PDHA1 YWHAQ RANBP1 HNRNPK SSB SRRM2 TCOF1 MAP4 CAP1 LRRC47 SERBP1 PAK2
Hamaguchi, et al. Imamura, et al. DNAJB1-PRKACA *in vitro* Human Hepatocyte Lysate PRKACA (L206R) *in vitro* Human Hepatocyte Lysate PRKACA *in vitro* Human Hepatocyte Lysate	2	SAFB ACIN1
Imamura, et al. DNAJB1-PRKACA *in vitro* Human Hepatocyte Lysate DNAJB1-PRKACA *in vitro* Mouse Liver Lysate PRKACA *in vitro* Human Hepatocyte Lysate PRKACA *in vitro* Mouse Liver Lysate	3	USP5 SEC61B PRDX6

Imamura, et al. DNAJB1-PRKACA *in vitro* Human Hepatocyte Lysate DNAJB1-PRKACA *in vitro* Mouse Liver Lysate PRKACA (L206R) *in vitro* Human Hepatocyte Lysate PRKACA *in vitro* Mouse Liver Lysate	8	ATP11C GPS1 HMOX1 EEF1D EPS8L2 GAPDH EIF2S2 HDGF
Imamura, et al. DNAJB1-PRKACA *in vitro* Human Hepatocyte Lysate DNAJB1-PRKACA *in vitro* Mouse Liver Lysate PRKACA (L206R) *in vitro* Human Hepatocyte Lysate PRKACA *in vitro* Human Hepatocyte Lysate	4	PGRMC1 PEA15 DAP CLIP1
Imamura, et al. DNAJB1-PRKACA *in vitro* Human Hepatocyte Lysate PRKACA (L206R) *in vitro* Human Hepatocyte Lysate PRKACA *in vitro* Human Hepatocyte Lysate PRKACA *in vitro* Mouse Liver Lysate	1	BCL2L13
Embogama, et al. DNAJB1-PRKACA *in vitro* Human Hepatocyte Lysate DNAJB1-PRKACA *in vitro* Mouse Liver Lysate PRKACA (L206R) *in vitro* Human Hepatocyte Lysate PRKACA *in vitro* Mouse Liver Lysate	2	ECHS1 ETFA
Embogama, et al. DNAJB1-PRKACA *in vitro* Human Hepatocyte Lysate DNAJB1-PRKACA *in vitro* Mouse Liver Lysate PRKACA (L206R) *in vitro* Human Hepatocyte Lysate PRKACA *in vitro* Human Hepatocyte Lysate	2	TLN1 ARFIP1

Embogama, et al. DNAJB1-PRKACA *in vitro* Human Hepatocyte Lysate PRKACA (L206R) *in vitro* Human Hepatocyte Lysate PRKACA *in vitro* Human Hepatocyte Lysate PRKACA *in vitro* Mouse Liver Lysate	1	CP
Hamaguchi, et al. DNAJB1-PRKACA *in vitro* Human Hepatocyte Lysate DNAJB1-PRKACA *in vitro* Mouse Liver Lysate PRKACA (L206R) *in vitro* Human Hepatocyte Lysate PRKACA *in vitro* Human Hepatocyte Lysate	1	KLC4
DNAJB1-PRKACA *in vitro* Human Hepatocyte Lysate DNAJB1-PRKACA *in vitro* Mouse Liver Lysate PRKACA (L206R) *in vitro* Human Hepatocyte Lysate PRKACA *in vitro* Human Hepatocyte Lysate PRKACA *in vitro* Mouse Liver Lysate	78	NDUFS1 CLTA ALDOC BHMT DSTN ALDH2 C3 SCP2 BTF3 ATP1A1 ALDH6A1 PHB2 SET TALDO1 VCP ALDH5A1 TSSC4 ASL ACADM TTC36 OXSM APOH NDUFV1 CFL1 DNAJC8 BCKDHA MRPS31 MRPS36 TST CPS1 IDH1 CFDP1 CALD1 HIBADH ACTG1 HSD17B6 COMT UQCRC2 ACTR3 ACOT1 ACAT1 RAPH1 PARVA PIGR RAB21 PSMC6 SSR3 CORO1B UQCRFS1 SULT2A1 OXR1 SLIRP CYP2E1 ALDH7A1 TOM1 AMACR HPD ACAD9 PYGL STARD10 HSPA9 ALDH8A1 ACAT2 ALDH1A1 HSP90B1 GSTA3 NIT1 AFMID TIMM44 UGP2 P4HB ALDOB APPL1 LRPAP1 PNPO AARS S100A13 CBR1
Hamaguchi, et al. Hu, et al. Imamura, et al. Isobe, et al.	1	CAD
Imamura, et al. Isobe, et al. DNAJB1-PRKACA *in vitro* Mouse Liver Lysate PRKACA *in vitro* Mouse Liver Lysate	3	ARHGAP17 ARPP19 YBX3

Imamura, et al. Isobe, et al. DNAJB1-PRKACA *in vitro* Human Hepatocyte Lysate PRKACA *in vitro* Human Hepatocyte Lysate	1	C2CD2L
Imamura, et al. Isobe, et al. DNAJB1-PRKACA *in vitro* Human Hepatocyte Lysate PRKACA (L206R) *in vitro* Human Hepatocyte Lysate	3	ARFGEF2 EIF5B FBL
Hamaguchi, et al. Isobe, et al. DNAJB1-PRKACA *in vitro* Human Hepatocyte Lysate PRKACA *in vitro* Human Hepatocyte Lysate	1	NHSL1
Isobe, et al. DNAJB1-PRKACA *in vitro* Human Hepatocyte Lysate DNAJB1-PRKACA *in vitro* Mouse Liver Lysate PRKACA (L206R) *in vitro* Human Hepatocyte Lysate	1	GOLGA5
Isobe, et al. DNAJB1-PRKACA *in vitro* Human Hepatocyte Lysate PRKACA (L206R) *in vitro* Human Hepatocyte Lysate PRKACA *in vitro* Human Hepatocyte Lysate	12	PDLIM2 TOMM34 PSMF1 CLIP2 CGNL1 BAIAP2 WDR4 SSH1 AP3D1 MPDZ COBL SNX1
Embogama, et al. Hamaguchi, et al. Hu, et al. Imamura, et al.	1	PDE3A
Embogama, et al. Hu, et al. Imamura, et al. DNAJB1-PRKACA *in vitro* Human Hepatocyte Lysate	1	YWHAE
Embogama, et al. Hu, et al. Imamura, et al. PRKACA (L206R) *in vitro* Human Hepatocyte Lysate	1	SMARCC2

Hamaguchi, et al. Hu, et al. Imamura, et al. PRKACA (L206R) *in vitro* Human Hepatocyte Lysate	1	RAF1
Embogama, et al. Hu, et al. DNAJB1-PRKACA *in vitro* Human Hepatocyte Lysate PRKACA *in vitro* Human Hepatocyte Lysate	2	YWHAG PSMC5
Hu, et al. DNAJB1-PRKACA *in vitro* Human Hepatocyte Lysate PRKACA (L206R) *in vitro* Human Hepatocyte Lysate PRKACA *in vitro* Human Hepatocyte Lysate	10	PIN1 SEC14L2 TPPP CBFA2T3 ATP1A3 DSP PPP1R8 CSDE1 VTN CUX1
Embogama, et al. Imamura, et al. DNAJB1-PRKACA *in vitro* Mouse Liver Lysate PRKACA *in vitro* Mouse Liver Lysate	3	SPAG9 EGFR MARCKSL1
Embogama, et al. Imamura, et al. PRKACA (L206R) *in vitro* Human Hepatocyte Lysate PRKACA *in vitro* Human Hepatocyte Lysate	2	PALLD INF2
Embogama, et al. Imamura, et al. DNAJB1-PRKACA *in vitro* Human Hepatocyte Lysate PRKACA (L206R) *in vitro* Human Hepatocyte Lysate	2	FLNB EIF4G1
Hamaguchi, et al. Imamura, et al. DNAJB1-PRKACA *in vitro* Human Hepatocyte Lysate PRKACA *in vitro* Human Hepatocyte Lysate	1	ZNF318

Imamura, et al. DNAJB1-PRKACA *in vitro* Mouse Liver Lysate PRKACA *in vitro* Human Hepatocyte Lysate PRKACA *in vitro* Mouse Liver Lysate	1	HUWE1
Imamura, et al. DNAJB1-PRKACA *in vitro* Human Hepatocyte Lysate DNAJB1-PRKACA *in vitro* Mouse Liver Lysate PRKACA *in vitro* Mouse Liver Lysate	1	EIF6
Imamura, et al. DNAJB1-PRKACA *in vitro* Human Hepatocyte Lysate DNAJB1-PRKACA *in vitro* Mouse Liver Lysate PRKACA *in vitro* Human Hepatocyte Lysate	3	PCBP1 SZRD1 CDV3
Imamura, et al. DNAJB1-PRKACA *in vitro* Mouse Liver Lysate PRKACA (L206R) *in vitro* Human Hepatocyte Lysate PRKACA *in vitro* Human Hepatocyte Lysate	2	PRCC APMAP
Imamura, et al. DNAJB1-PRKACA *in vitro* Human Hepatocyte Lysate PRKACA (L206R) *in vitro* Human Hepatocyte Lysate PRKACA *in vitro* Human Hepatocyte Lysate	92	TFIP11 ZHX3 THRAP3 PDCD4 BCLAF1 RAD23B HIST1H1E TPI1 NOP58 RPRD1B AHNAK PPP1R12A CHMP2B HNRNPUL2 PPL PROSER2 PGM1 RMDN3 UBE2J1 ADD1 SCFD1 TIMM8A SRRM1 PABPN1 CARHSP1 LMO7 NUCKS1 YRDC VPS4B ABCF1 SEPT2 MTDH NCL WDR44 SEC62 RBM39 WRNIP1 SORBS3 AMPD2 MAP1S HNRNPA1 KTN1 SYAP1 HDLBP MTFR1 SLTM ARHGEF12 RALY RBM33 PGRMC2 LSM14A TWF1 MYH9 PPIG TMPO PRPF4B SEPT9 NAP1L4 NOC2L PRRC2C RRBP1 PPP1R10 VDAC1 ILF3 SEC31A HNRNPC ZC3H18 SH2D4A TPD52 ZC3H13 HIST1H1B NUP98 NIFK SMAP PLEC OGFR HSF1 PHF14 TMX1 HSPH1 VCL LRRFIP2 CRK PKM HNRNPA3 NOLC1 NUMA1 SYNPO RANBP2 CAST PNN STX4

Embogama, et al. DNAJB1-PRKACA *in vitro* Mouse Liver Lysate PRKACA *in vitro* Human Hepatocyte Lysate PRKACA *in vitro* Mouse Liver Lysate	1	SBDS
Embogama, et al. DNAJB1-PRKACA *in vitro* Human Hepatocyte Lysate PRKACA *in vitro* Human Hepatocyte Lysate PRKACA *in vitro* Mouse Liver Lysate	1	AP2M1
Embogama, et al. DNAJB1-PRKACA *in vitro* Human Hepatocyte Lysate PRKACA (L206R) *in vitro* Human Hepatocyte Lysate PRKACA *in vitro* Human Hepatocyte Lysate	16	LMAN1 PRDX4 UMPS ACY1 RPL28 DAK NME1 PEBP1 RPL29 PTPN11 UFD1L SF1 SF3B1 ACAA1 PRDX2 IWS1
Hamaguchi, et al. DNAJB1-PRKACA *in vitro* Human Hepatocyte Lysate PRKACA (L206R) *in vitro* Human Hepatocyte Lysate PRKACA *in vitro* Human Hepatocyte Lysate	1	PHACTR2
DNAJB1-PRKACA *in vitro* Human Hepatocyte Lysate DNAJB1-PRKACA *in vitro* Mouse Liver Lysate PRKACA *in vitro* Human Hepatocyte Lysate PRKACA *in vitro* Mouse Liver Lysate	29	NDUFS4 PSMD11 SNX6 RPS21 AKAP2 ACADVL SEPHS1 RPL24 NAMPT ACSL1 CPOX ALB CNPY2 TAGLN2 AFG3L2 PKLR CALR SPR ASGR1 PSMA2 DPP3 ATP6V1B2 NSF PPP2R1A SNX3 THUMPD1 COX4I1 CTSZ ATIC
DNAJB1-PRKACA *in vitro* Mouse Liver Lysate PRKACA (L206R) *in vitro* Human Hepatocyte Lysate PRKACA *in vitro* Human Hepatocyte Lysate PRKACA *in vitro* Mouse Liver Lysate	1	CNBP

DNAJB1-PRKACA *in vitro* Human Hepatocyte Lysate DNAJB1-PRKACA *in vitro* Mouse Liver Lysate PRKACA (L206R) *in vitro* Human Hepatocyte Lysate PRKACA *in vitro* Mouse Liver Lysate	15	GPD1 ALAD FDX1 EPN1 EVA1A ETFB TYMP GPHN DNAJB1 EEF1A1 GLUD1 EEF2 ETFDH GLUL FTCD
DNAJB1-PRKACA *in vitro* Human Hepatocyte Lysate DNAJB1-PRKACA *in vitro* Mouse Liver Lysate PRKACA (L206R) *in vitro* Human Hepatocyte Lysate PRKACA *in vitro* Human Hepatocyte Lysate	11	SLCO2B1 UQCRC1 NDRG2 PGAM1 CNDP2 ANP32A PFAS PSMA6 ARCN1 HSPA5 HNRNPM
DNAJB1-PRKACA *in vitro* Human Hepatocyte Lysate PRKACA (L206R) *in vitro* Human Hepatocyte Lysate PRKACA *in vitro* Human Hepatocyte Lysate PRKACA *in vitro* Mouse Liver Lysate	3	ALDH1L1 ALDH4A1 ACOX2
Hu, et al. Imamura, et al. Isobe, et al.	2	SMARCAD1 PCM1
Hu, et al. Isobe, et al. PRKACA (L206R) *in vitro* Human Hepatocyte Lysate	1	MAP2
Hamaguchi, et al. Imamura, et al. Isobe, et al.	3	SIK2 LIMCH1 DENND4C
Imamura, et al. Isobe, et al. DNAJB1-PRKACA *in vitro* Mouse Liver Lysate	1	WNK1
Imamura, et al. Isobe, et al. DNAJB1-PRKACA *in vitro* Human Hepatocyte Lysate	1	PLEKHG3

Isobe, et al. DNAJB1-PRKACA *in vitro* Mouse Liver Lysate PRKACA *in vitro* Mouse Liver Lysate	2	PLEKHF2 KARS
Isobe, et al. DNAJB1-PRKACA *in vitro* Human Hepatocyte Lysate PRKACA *in vitro* Human Hepatocyte Lysate	1	SCYL2
Isobe, et al. PRKACA (L206R) *in vitro* Human Hepatocyte Lysate PRKACA *in vitro* Human Hepatocyte Lysate	2	PBXIP1 CLMN
Isobe, et al. DNAJB1-PRKACA *in vitro* Human Hepatocyte Lysate PRKACA (L206R) *in vitro* Human Hepatocyte Lysate	1	IRS1
Hu, et al. Imamura, et al. DNAJB1-PRKACA *in vitro* Human Hepatocyte Lysate	2	NEDD4L HIRIP3
Hu, et al. DNAJB1-PRKACA *in vitro* Mouse Liver Lysate PRKACA *in vitro* Mouse Liver Lysate	2	STK24 CRIP2
Hu, et al. DNAJB1-PRKACA *in vitro* Human Hepatocyte Lysate PRKACA *in vitro* Human Hepatocyte Lysate	1	PAH
Embogama, et al. Hu, et al. Imamura, et al.	3	GFPT1 CTTN ACACA
Embogama, et al. Imamura, et al. DNAJB1-PRKACA *in vitro* Mouse Liver Lysate	1	DPYSL2
Embogama, et al. Imamura, et al. PRKACA *in vitro* Human Hepatocyte Lysate	1	NACA

Hu, et al. PRKACA (L206R) *in vitro* Human Hepatocyte Lysate PRKACA *in vitro* Human Hepatocyte Lysate	1	SLC4A4
Imamura, et al. DNAJB1-PRKACA *in vitro* Mouse Liver Lysate PRKACA *in vitro* Mouse Liver Lysate	13	BET1L UBA1 RBM17 PPIP5K2 SHTN1 SNRNP70 ZNRF2 DIS3L2 RANBP3 MARCKS MIOS GMPS CLNS1A
Imamura, et al. DNAJB1-PRKACA *in vitro* Human Hepatocyte Lysate DNAJB1-PRKACA *in vitro* Mouse Liver Lysate	2	EIF3H WASL
Imamura, et al. PRKACA (L206R) *in vitro* Human Hepatocyte Lysate PRKACA *in vitro* Mouse Liver Lysate	1	UBA2
Imamura, et al. DNAJB1-PRKACA *in vitro* Human Hepatocyte Lysate PRKACA *in vitro* Human Hepatocyte Lysate	20	ARHGEF16 SEC16A LEO1 KRT18 PAXBP1 MAP3K7 ZC3H4 DMD PCBP2 BMP2K MYO1C ACOX1 PTGES3 CPSF7 SUB1 CD2AP MYO18A ARFIP2 CHCHD3 PEX19
Imamura, et al. PRKACA (L206R) *in vitro* Human Hepatocyte Lysate PRKACA *in vitro* Human Hepatocyte Lysate	6	SVIL HNRNPA2B1 MFAP1 TSC2 DDX46 PRKAR1B
Imamura, et al. DNAJB1-PRKACA *in vitro* Human Hepatocyte Lysate PRKACA (L206R) *in vitro* Human Hepatocyte Lysate	21	EML3 PACSIN3 EPS15 ARGLU1 ZC3H14 COPB2 HNRNPH1 U2AF2 GTF2I HNRNPU NUFIP2 CDC26 GAPVD1 EBAG9 HACD3 KIAA1671 EIF2A RPL27A REEP4 FUNDC2 FCHO2
Embogama, et al. DNAJB1-PRKACA *in vitro* Mouse Liver Lysate PRKACA *in vitro* Mouse Liver Lysate	2	SARS RNH1

Embogama, et al. DNAJB1-PRKACA *in vitro* Human Hepatocyte Lysate PRKACA *in vitro* Human Hepatocyte Lysate	7	RPL35 POLDIP2 HSPA4L TXNDC5 IVD PARP1 PDIA4
Embogama, et al. PRKACA (L206R) *in vitro* Human Hepatocyte Lysate PRKACA *in vitro* Human Hepatocyte Lysate	1	ANXA2
Embogama, et al. DNAJB1-PRKACA *in vitro* Human Hepatocyte Lysate PRKACA (L206R) *in vitro* Human Hepatocyte Lysate	1	EXOSC2
Hamaguchi, et al. DNAJB1-PRKACA *in vitro* Mouse Liver Lysate PRKACA *in vitro* Mouse Liver Lysate	2	CDK18 DAPK2
DNAJB1-PRKACA *in vitro* Mouse Liver Lysate PRKACA *in vitro* Human Hepatocyte Lysate PRKACA *in vitro* Mouse Liver Lysate	3	ASNA1 SARDH NNT
DNAJB1-PRKACA *in vitro* Human Hepatocyte Lysate DNAJB1-PRKACA *in vitro* Mouse Liver Lysate PRKACA *in vitro* Mouse Liver Lysate	3	GPX1 GNMT FMO5
DNAJB1-PRKACA *in vitro* Human Hepatocyte Lysate DNAJB1-PRKACA *in vitro* Mouse Liver Lysate PRKACA *in vitro* Human Hepatocyte Lysate	2	PDHX CDH13
DNAJB1-PRKACA *in vitro* Human Hepatocyte Lysate DNAJB1-PRKACA *in vitro* Mouse Liver Lysate PRKACA (L206R) *in vitro* Human Hepatocyte Lysate	4	EIF1 PDP2 HADHA H6PD

DNAJB1-PRKACA *in vitro* Human Hepatocyte Lysate PRKACA (L206R) *in vitro* Human Hepatocyte Lysate PRKACA *in vitro* Human Hepatocyte Lysate	289	SUMO1 HEL-S-117 RPL19 MESDC2 ST13P5 LYAR PIR CTAGE5 CYP2D6 SHROOM1 SLC27A3 DMTN GSTA2 RPS28 PREP HSP90AB2P PPM1A ALCAM TF ASS1 PBDC1 LDHB NME1-NME2 C9ORF142 ACTC1 ABHD12 UFL1 IMMT HIST1H1A HP1BP3 CDHR5 ALDH1L2 C17ORF59 BCAP29 SULT1A2 ACOT2 CHMP6 MIA2 MANF CASC4 PHYKPL CTAGE9 MARVELD3 CBX1 WBP11 CBS ADH1C POTEKP ITGA6 PSIP1 MVD CYP4F12 CTAGE4 MXRA5 HSP90AA5P SPATS2L RABAC1 PRKACB CRAT RAVER1 SRSF3 NDUFV2 BLVRB MYOCD SSFA2 NAP1L1 EEF1A2 CD14 PHAX AK1 ACSS3 CGREF1 THAP4 MAN1A1 ATP5A1 CD276 METTL14 UROC1 ATPIF1 PYGB API5 APOL5 POTEF ST13P4 SOD1 CYP4F2 RPS3A ASPDH PALM3 MUT SLC38A3 WDR87 PALMD SGTA WDR77 LAD1 ATP5J SRP54 STIP1 SLC25A20 ARPC1B NDUFA7 METAP2 KNG1 PCBD1 KANK2 ALDH1A3 UQCRFS1P1 PRPSAP2 POTEI PTGFRN SRPR CTAGE8 ABCB11 GSTA5 ACTA1 SEPT11 SNTB1 RPS25 SDF2L1 EIF3CL HIST1H1D CYB5A KIAA1598 PGAM2 PSME2 HIST1H1C PLEKHA5 MTCH2 MIEN1 HEXA NRD1 SMAP2 DTNA HNRNPA1L2 PIPOX BAAT ARFGAP1 PPP1R7 NDUFA5 PDLIM5 HNRNPUL2-BSCL2 MLLT4 METTL1 IQGAP2 C1ORF53 MACF1 AIFM1 TMEM160 ADD3 POLI SMARCC1 SLCO1B3 AK3 SARS2 GLUD2 MDH1 CAMSAP3 ANGPTL3 NDUFS8 DTX3L SCRN2 CCT2 ATP5B HSD17B4 XRCC6 LETM1 BCAP31 POTEE ISOC2 SERPINA1 STBD1 CYP4F3 ALDH1A2 MAMSTR MTTP WIPF3 CTAGE15 LYRM5 ZC3HAV1 ARPC5 CYP2A6 ANXA6 VAPB CTAGE6 BHMT2 PRKAB2 UBE2M SULT1A1 KIN27 LOC113230 ALDH1B1 ARG1 BABAM1 HEXB HSPA1A SUMF2 C9ORF78 PPIB CYP2A13 MAT2B PPIA RDH16 AK2 RPL30 STX16-NPEPL1 C11ORF58 ATP5EP2 ANXA5 CPT2 ANP32D LSM7 PLIN1 PGM2 THOC3 ARPC2 SULT1E1 C14ORF166 PGK2 UROD EIF1B ATP1A2 NME2 RPL21 DDRGK1 HIST1H1T WIPF2 PPM1B SORBS1 RPL5 STX12 MRPL39 IGFBP1 HINT2 CYP2D7 CMPK1 HTATIP2 PDZK1P1 DNPH1 MTHFS CA2 TGOLN2 PRKACG SEMA4G ADH1A NME2P1 PA2G4 RPL13 ACTB YLPM1 CYP2C8 ACTG2 OXNAD1 COPB1 ARHGEF6 ADH1B

		HSPA1B RBM8A CETN2 PGAM4 TKFC PDZK1 HSP90AB3P POFUT1 SCRIB ABHD14A-ACY1 RBM27 PGLS ACTA2 TACO1 STX16 CDC5L CTNNA2 DBR1 ATP5E ZFYVE19 APBB1IP PGM3 ANP32B AP4E1 CASK EEF1A1P5 TTC38 CES1 PITPNB ADD2 WASF2 NDUFB9 NADK2
Hu, et al. Isobe, et al.	6	NUP133 LRRFIP1 SRC ZHX1 NFKB1 SUFU
Hamaguchi, et al. Isobe, et al.	4	NF1 RPL18A KIAA1522 PITPNM3
Isobe, et al. DNAJB1-PRKACA *in vitro* Mouse Liver Lysate	1	SAYSD1
Isobe, et al. DNAJB1-PRKACA *in vitro* Human Hepatocyte Lysate	1	EIF2AK2
Hu, et al. Imamura, et al.	27	CD44 LUZP1 TERF2IP SMC3 NCOA3 FYN TRIP10 EIF4ENIF1 LIG1 DNM1L PDE3B ANKS1A PTPN12 CDCA7L STUB1 VIM PYGO2 FOXP4 SP100 EMD ATRIP LAS1L TBC1D10B AKAP13 CHAF1B UHRF1 CEBPB
Embogama, et al. Hu, et al.	4	MSN HLA-A PTBP1 PSMA8
Hamaguchi, et al. Hu, et al.	2	CAMKK1 C19ORF21
Hu, et al. PRKACA *in vitro* Mouse Liver Lysate	1	ASPSCR1
Hu, et al. DNAJB1-PRKACA *in vitro* Human Hepatocyte Lysate	2	PFKFB2 SAP30BP
Embogama, et al. Imamura, et al.	26	CLUH BAG3 MYO1E HNRNPD SF3A1 EFHD2 BOD1L1 PPP6R3 HDAC1 IGF2R MCMBP PSMA3 ACTL6A KDM5C SLC1A5 RCC2 EPRS TP53BP1 TK1 SLC4A1AP SLC16A3 EDC4 PAICS SUPT6H MAGED2 EIF3G
Hamaguchi, et al. Imamura, et al.	1	C2CD5
Imamura, et al. Isobe, et al.	38	TNS3 PI4KB ATG2B ARHGAP21 DCP1A XRN2 DYNC1H1 FAM83H PXN PUM2 HECTD1 TXLNG RBM14 PRKD2 MARK2 NCOR1 FKBP15 RAB11FIP1 ABCC1 ARHGAP35 DOCK7 MEF2D SQSTM1 BNIP2 ENAH WWC1 SIPA1L1 PKN2 RIN1 AKAP1 MAP3K2 PRRC2A OSBPL11 HPS5 LARP4B PARD3 PUM1 ITPR3

Imamura, et al. DNAJB1-PRKACA *in vitro* Mouse Liver Lysate	1	ACSS2
Imamura, et al. PRKACA *in vitro* Mouse Liver Lysate	2	TMEM230 STRN
Imamura, et al. PRKACA *in vitro* Human Hepatocyte Lysate	6	RBM15 RCC1 USO1 UBR4 BAG6 AKT1S1
Imamura, et al. DNAJB1-PRKACA *in vitro* Human Hepatocyte Lysate	11	HMGN1 ESYT2 THOC2 DSG2 HNRNPUL1 EEF1B2 EPB41 DFFA DENR ESF1 GBF1
Imamura, et al. PRKACA (L206R) *in vitro* Human Hepatocyte Lysate	3	G3BP1 YAF2 DKC1
Embogama, et al. DNAJB1-PRKACA *in vitro* Mouse Liver Lysate	1	PSME3
Embogama, et al. PRKACA *in vitro* Mouse Liver Lysate	1	LAP3
Embogama, et al. DNAJB1-PRKACA *in vitro* Human Hepatocyte Lysate	10	FUBP1 ACO2 PLS3 RPS10 PSMD4 STOM SFN YWHAB PC FDXR
Embogama, et al. PRKACA (L206R) *in vitro* Human Hepatocyte Lysate	2	PSMD12 GPKOW
DNAJB1-PRKACA *in vitro* Mouse Liver Lysate PRKACA *in vitro* Human Hepatocyte Lysate	1	HS1BP3
DNAJB1-PRKACA *in vitro* Human Hepatocyte Lysate DNAJB1-PRKACA *in vitro* Mouse Liver Lysate	1	TSFM
DNAJB1-PRKACA *in vitro* Human Hepatocyte Lysate PRKACA *in vitro* Mouse Liver Lysate	1	FKBP8
PRKACA (L206R) *in vitro* Human Hepatocyte Lysate PRKACA *in vitro* Mouse Liver Lysate	1	ACBD4

DNAJB1-PRKACA *in vitro* Mouse Liver Lysate PRKACA *in vitro* Mouse Liver Lysate	128	ACOT12 HMGCS2 SLK HSPA1L VWA5A LCMT1 GCLM FAM213B CES1F ELAC2 NDUFA2 UCHL4 GM20425 PFKL GC CYP2C70 WDR91 LXN CNGA2 ATP5H SNRPG SERPINA1B DECR2 CYP2B10 GATD3A MAVS CES3A URAD MOCS1 SNAP29 SDS FCGRT SASH1 CMC2 NECAP1 GIMAP4 F13B AKR1D1 D2HGDH CDC42EP5 SEMA6D CCDC180 NADK H2-KE6 NDUFB11 CYP4F17 PPP1R11 MESD LCP1 EIF4H TIMM50 HDGFL2 AKR1C6 ERRFI1 CIDEB FTL1 LBH MTFR1L KEG1 CYP2A5 SERPINA1C ADH1 JPT1 RIDA NAXE LDHD CA14 LYPLA1 SULT2A8 MRPL12 KIF5B NT5C GM9774 TUBA1B SERPINA3N EARS2 SELENBP2 AKR7A2 DHTKD1 CTH ATP5F1A GYKL1 GSDMDC1 CYP2F2 DNAJC12 9-Sep GOPC PNPLA8 GLYCTK ADCY10 ATP5PF IDH3A ACSM5 HMGN5 ISOC2A CYP1A2 SERPINA3K NUBP1 ENSA ETHE1 PRODH HNRNPAB SMOC1 GRN INMT ACSF3 KIF13B UBQLN1 FAM162A MTSS1 ATP5F1B GPRIN3 ANK3 ATP5C1 ZFP69 AMT HSD11B1 BOLA1 GPT2 CYP2D22 APOA1 SEPHS2 AGMAT ECI1 MUG1 CCDC9 SERHL ACAA1B
PRKACA (L206R) *in vitro* Human Hepatocyte Lysate PRKACA *in vitro* Human Hepatocyte Lysate	15	DDT OGDH ANXA2P2 UGT2A3 UCHL3 MVK DDTL CRYL1 LYRM1 DOCK8 BAT3 PRPF40A SH3BP5L ZDHHC5 OR51A7
DNAJB1-PRKACA *in vitro* Human Hepatocyte Lysate PRKACA (L206R) *in vitro* Human Hepatocyte Lysate	78	ITGA5 RPS4Y2 FRS2 ENOSF1 DENND1A LAGE3 FTH1 FETUB GANAB EEPD1 EIF3D FHIT FAM122A GIGYF2 ECHDC3 GPX2 TRANK1 EPB41L3 RPS4Y1 ABCA12 GCLC GCDH KDM4A HACL1 RPS6 C2ORF72 G3BP2 AASS FMO3 EIF3A EMC10 FAM134A FKBP3 EIF3J PPP1R3E LRP2 RNPEP FBP1 HADHB GAS2 ENO3 ENO1 TMEM41A IFNA6 PLEKHA6 EHHADH ALPL GMPR2 GSTA1 SOS1 GUCY1A3 GOLM1 FBP2 FASN HAO1 GPI STIM1 RPS4X KIAA1217 APOA5 GRB14 MIEF1 EHBP1 GLRX3 FABP1 TMEM109 PDHA2 FAH EIF3C DUT PPFIBP2 GSTO1 ECHDC2 RSRC2 TCEA3 HNRNPH2 GATM EEF1G
DNAJB1-PRKACA *in vitro* Human Hepatocyte Lysate PRKACA *in vitro* Human Hepatocyte Lysate	142	RAB2A NAPRT RGN RPL17-C18ORF32 UGT1A1 CYP2C19 PDIA3 ALDH3A2 HIST3H3 HSP90AA4P APOE PMM1 HIST1H2BL DKFZP586F0420 PICALM CYP7A1 MTSS1L CTSB PCBP3 HYPK UBE2D3 PLRG1 CYP2C9 PRKDC DNAJC1 SLCO1B1 SMS HMBOX1

		RPL17 ACOT9 POR NAA15 PROC HSD17B13 LMNB1 TFAM DUSP3 HMGN2 COPE CFL2 ITFG3 HIST1H2BK TOMM70A OTUB1 CHP1 IGBP1 ACACB SERF2 RPL8 AHSG DDO HIST1H2BD AGXT UBE2V1 MECR HIST1H2BH SHMT2 ST20-MTHFS LTA4H HMGB1 LBR BAIAP2L1 QARS SQRDL LYRM2 NEDD4 HMGN3 SND1 HIST1H2BC APOB CS PRDX1 ITGA1 PPP2R1B KHK DNAJC3 TARS CDK6 HIST1H2BN LUC7L ALG13 MAP2K2 CMC1 MYH10 MYH11 CTSD RP2 ADRM1 MCEE PLAA SHMT1 SRP9 HMGB2 ISG15 PRDX3 PML MYH14 PSAP ACADSB HGD UGDH HIBCH TIMM10 UQCC2 PABPC4 AIMP1 PPIF ABAT SCARB2 PSMA7 SRPRB SORD SPECC1L-ADORA2A ATP6V1G1 STOML2 SETSIP HMGB1P1 METTL7A CADM1 C21ORF33 ITIH1 MLEC HTRA2 IARS2 DDX58 PABPC1 HIST1H2BM HSD17B8 PFN1 QRSL1 H2BFS XYLB HIST2H2BF DCTN2 PMM2 SSBP1 HSP90AB4P ANXA4 HNRNPL CHCHD4 SNAP91 SUOX
Isobe, et al.	76	CHD9 SPIRE2 MIB2 SEC23IP ZZEF1 TIAM1 OSBPL10 PPM1H TAB2 HBP1 ATP6V0A2 MAP4K3 SLC7A6OS MRPS9 PTPN14 BLOC1S5 TMEM259 PCYT1B MRPL37 ZNF608 KIAA1109 DOCK1 WDTC1 KLHDC7A WDFY3 TIAM2 SLAIN2 ARHGAP29 BORCS6 ERBIN JUP CHCHD6 FGD3 SNX12 VIPAS39 DOPEY1 RAB18 PHLDB2 KAZN PARD6B VEPH1 MAP3K5 TBC1D12 NEK4 PI4KA MYO5B CAMK2D ARHGEF2 CASP8 ITSN2 NULL VILL MTOR PEAK1 EPS8L1 LYST MTCH1 KLC3 IGSF5 MAP4K5 UHRF1BP1L AFAP1L2 ERBB3 PURG SHROOM3 NFATC2 HERC4 ARHGEF17 RTKN CGN SKT MAP4K4 PTPN13 TNS2 ARHGAP27 ZAK
Hu, et al.	198	HNRPD PPP1R14A SERPINF1 CENTD2 GRK1 BIRC5 CIAO1 SIP1 C21ORF66 RASGRF1 EP400 PPP1R9A BCAM NPR1 AQP2 PDE4C DDX39 IRF3 TAF10 EZR TFAP2B CIITA GMFB AURKA C14ORF106 KCNJ13 RGS14 CSRP3 KCNA4 PPP1R1B GPBP1L1 RRAD SNAI1 SOX9 ADRB1 NOXA1 HAGH CACNA1H XRCC4 NAB2 GLI1 GRIA1 CCND1 RUNX1T1 POP7 ESR1 KCNN3 PDE4D NFATC3 SREBF2 RUVBL2 E2F7 APOBEC3F MDFI GSK3B GNA13 SGK TRPV1 HLCS CHGB DDEF2 PPP1R13L H3F3A MC4R CSDC2 GATA3 FOXN3 HIST2H3A UTP18 RCHY1 CLDN3

		CAPN2 CREB1 ERBB2 TRPV4 PDE5A HDAC8 DAXX KCNJ3 HRH1 ID2 RB1 DHX29 PDE4B SOX6 DNAJB2 HNRPK NRIP2 RNUXA TP53 CASP9 ZNF496 KCNN2 PPP1R1A FXYD1 BMI1 KCND2 UNC84B GRK7 TPH2 ETV1 C13ORF15 LOC648998 ESPL1 HSPB6 HSPB8 ANXA1 ALOX5 PKD1 TRPM8 TTF2 NFATC4 RXRA POU3F4 NFATC1 PLN PLCG1 DAP3 ITGB4 BTBD12 FAM44A GSTA4 ABCA1 ARID3A AICDA KCNH2 LIPE TNNI3 PLCB3 CRHR2 MAPT RBM19 ABCB1 WT1 CTPS MYBPC3 CSK TH LCK PHOX2A DES RDBP RNF12 PCTK1 ACCN2 SNUPN PFKFB3 NEUROD1 U2AF1 BCOR AVPR2 CSNK1A1 EXOSC5 PTPN7 DUOX1 ITGA4 VDR PRKAR2B PHF17 MYOM2 CUL5 MCOLN1 CBL FIP1L1 TFAP2C C20ORF32 AKAP9 NCBP2 NR5A2 RBM22 RYR2 RPS19 NOS3 CFTR C19ORF2 TSC22D4 PDE11A GFAP AQP5 PPP2R5D GAS7 RBBP5 ETV5 ARFGEF1 PPP1R1C LOC51035 PPP1R14C LOC100133382 GSK3A METTL3 NF2 GAD1 NCOA4 SRF GATA4 VHL MDM4 HCLS1
Imamura, et al.	729	SLMAP ERCC5 TACC2 BYSL CXCR4 U2SURP CHD8 SCAF8 TPX2 EP300 GYS1 MON1B CHORDC1 C2orf49 ZEB1 TRIM33 PARN CD2BP2 SRPK1 PTCD3 NMNAT1 SHC1 SAAL1 TAOK3 RIOK1 HERC2 SLC12A4 CLCC1 USP6NL BAZ1B SDAD1 PPP1R15B LARP7 KPNA2 ATL2 ZCRB1 KPNA3 DDB2 RBM10 TRA2B STK17A MTRR NCOR2 GTF3C3 CEP170 MSH6 SRSF6 HDAC7 SIPA1 CCDC43 ATAD1 NELFE IMUP SORT1 SETDB1 CARMIL1 SRSF11 PCDH7 TJAP1 ORC1 SON PLCL2 TRAM1 AVEN C9orf16 USP42 NIPBL POGZ RICTOR RAD18 LRRC8A PRRC2B CDK17 ZNF687 KDM2A HABP4 NFIL3 WDR62 DHX16 LEMD2 MIS18BP1 UBXN7 DIDO1 LYSMD2 ARAP1 NGDN SAC3D1 ITPRIPL2 UNG DPF2 CBARP BRD8 PJA2 DCUN1D5 ANKLE2 CHMP7 FRYL PTPN2 AP3B1 HCFC1 UBL7 KRT17 RPL4 VAMP4 PRPF3 DDX24 RBM6 WAPL SH3PXD2A RBBP6 PARG ASAP2 CEP131 STRIP1 SSRP1 PDAP1 BRD4 CHAF1A TOR1AIP1 BCKDK CSRP1 ITSN1 CHAMP1 NSD1 ATP2B2 NCAPD3 ABCC2 GPATCH8 KIF4A CPD KRT8 MAP7 RBM7 OSBPL3 ANTXR1 TERF2 HASPIN XPO4 WIPI2 IFNAR1 EHD2 ANKRD17 CCNK NCKAP5L FAM129B

		EAF1 NOTCH2 PSMD2 CHTF18 ATXN2 ARHGAP12 VIRMA STRN3 CHMP3 CEBPZ ANAPC1 SRRT MELK RBM3 BMS1 CDK16 SF3B2 KAT5 FLYWCH2 TPD52L1 SLC19A1 XRCC1 PAK1IP1 SLC7A11 CDS2 AHCTF1 SENP3 EEF2K WDR26 MUS81 PWWP2A GAL KIF1B PIAS1 CNOT2 SNW1 RPP30 TRIM16 CDC40 IRF2BPL RECQL5 WEE1 BSG BIN1 PTDSS1 FMNL1 GLCCI1 MMTAG2 ARMCX3 QSOX2 YBX1 LRFN4 PNISR STK10 HERC1 PTPN23 DGCR8 CTR9 BRI3BP KPNA4 MDC1 INO80B RBM34 RCOR1 TRMT1 KMT2D TELO2 MAF1 C7orf50 USP15 HDAC4 WDR33 AMFR MAPK1 MPHOSPH10 TLE3 TACC1 PDCL ZC3HC1 DYNC1LI1 FXR2 ZC3H8 ARHGAP1 CLASP1 TFAP4 AFAP1 CDK13 BCR TWISTNB RPL15 RIOK2 REXO4 UFD1 SMARCA4 RPS6KA4 BRD7 ZBTB21 CEP55 EYA3 HOXC10 EML4 ATF2 CTPS1 TOM1L1 GOLGA2 TRA2A CAMSAP2 RFC1 ABCC5 ASMTL SNAPC5 MOCOS AFDN SLC30A1 TBX3 DNAJC21 NRDC SART1 HSPE1 RBM5 EIF4EBP1 PPP1R9B SLC43A2 MCM2 TGS1 MCM4 SPTBN2 TOMM70 ARHGAP5 DDX21 PWP1 ADAR POP1 MTA1 GPAM TIMELESS DDX10 KIF13A KRT7 PHF8 TMEM87A PLEKHA2 ESCO2 DNTTIP2 ZMYM4 ZNF106 MKI67 PANK2 NHS CLSPN BICD2 ARL6IP4 PURB ACAP2 PPP4R2 BUD13 SDE2 SLC39A10 CDCA2 PPA2 MED24 EHD1 RAB11FIP5 TBC1D15 ADAM17 ZNF830 ELAVL1 NCOA2 RPP25 ABCA2 EXO1 AJUBA CIAPIN1 STAMBPL1 TCF20 PPM1G C9orf40 ELMSAN1 SSH3 KLC2 FNDC3B SIRT1 AREL1 NEK9 UPF3B RPL23A ADNP RFFL RBM15B ERICH1 DDX39B TLE4 TOP2B CNNM3 FAM117B TAF15 MED19 PAGR1 POLD3 VAMP7 RSF1 MON1A POU2F1 APC RSL1D1 RBM25 CDC42EP1 TPR AKAP11 WDR3 TTC33 TRAFD1 CTTNBP2NL MGRN1 PTDSS2 USP39 ATXN2L FLII CLASRP CWF19L2 BRAF RPL14 TMOD3 RALBP1 CAAP1 GEMIN5 DDX20 MYBBP1A PHKB SLC16A1 USP8 SLC17A5 EPHB4 MBD1 TP53BP2 STT3B CD3EAP PITPNM1 HECW1 RLF KLF3 RPTOR BCL2L12 NBAS HIVEP1 ATRX VAMP8 NBN MAST2 PACSIN2 TOPBP1 NUP214 SOX13 EIF3B MFSD6 USP20 MCRS1 UBE2E3 RAB3GAP1 BASP1 SLC35F6 PTOV1 TMEM45A CDK12 JADE3 PHF3 PEX14 APEH

		TBC1D5 MAPKAP1 MINK1 EZH2 SLC15A4 OSMR WIZ RBM4 CSF1 EDC3 SLC35B2 CEP170B COPA PHC3 FAM102B KIAA1143 USP24 NUP153 TTYH3 SLC12A6 RAP1GAP URI1 NOP2 RAD9A USP16 SCML2 USP10 PODXL2 PI4K2A RPS3 WDR75 SFSWAP DYNC1LI2 COIL ZMYND8 ZNF609 CASC3 TCF12 ATP7A ZNF641 TANC1 TBXA2R PRKCD ZNF639 PUS1 BCL9L SMC4 EPB41L1 EXOSC9 ABCC4 ZFP36L2 PBRM1 RNF20 USP9X BRF1 RRAS2 MCM3 RPS2 NRBP1 MYPN RNF113A PPHLN1 TBC1D2B AFF4 AKAP10 PRPF6 PDE8A SH3KBP1 PLA2G4A SYNRG RIF1 UNC13D MEPCE KIF21A UNK SAMD1 SCD SLC38A2 CCDC86 ATN1 MPZL1 SMN2 TRPT1 STX7 SPEN GPRC5A C1orf52 CD97 PDS5B MPHOSPH8 TICRR ZBTB7A MADD SLC4A2 ARHGEF18 ARRB1 SUGP1 SIN3A POLR3E TXNL1 CCNYL1 OBSCN CBX8 IL1RAP CIR1 FTSJ3 UTP14A RRP1B SLC4A7 GNL1 NELFB PPP1R12C ATG9A NEDD1 DNAJB6 NFIC TCEAL4 PRPF38B NUP50 KRI1 LEMD3 TXLNA BUB1 PIEZO1 GTF3C2 SKIV2L SNTB2 SURF2 ZRANB2 CLASP2 DOT1L EIF2AK3 RPRD2 ATF7IP FOXK1 FXR1 NUP210 PPAN SLC7A2 GZF1 DDX55 FERMT2 NSUN2 DTD1 SLCO4A1 STK11IP RTN4 TAX1BP1 PHRF1 PPP1R2 TBC1D4 GIT1 PAXX TMEM51 SLU7 DAB2 TTLL12 DNAJA2 LYN CCNL1 ZFP91 CDCA3 NOP56 RAI1 BPTF ATAD2 PHF6 ANAPC2 DNMT1 EPB41L2 SLC16A6 RREB1 FNBP4 LIFR DNMBP SNAP23 TFDP1 MGA IRF2BP1 SRSF10 UTP3 CLINT1 RTTN ZFC3H1 MYCBP2 LATS1 NEMF MED1 SRSF1 TMEM245 LAMTOR1 DIAPH1 TRAF4 RRM2 SLC20A1 TOP2A DNAJC2 IGF1R NOB1 GTF3C4 TTF1 NCBP1 SLC9A1 HDAC2 NEXN IL6ST NCAPD2 UBAP2L PPP4R3A TMEM131 GPN1 WDHD1 UBE4B DBN1 LRWD1 PTS OTUD5 DDX54 ALPI KMT2A PKN1 WTAP BUB1B JMJD1C CCNH SURF6 MTCL1 ERCC6 RRP12 DMAP1 SRSF2 RAB12 DDX51 HEXIM2 ZC3H11A TCF3 C18orf25 SMN1 RANBP10 PSMD1 DTL SRFBP1 SRSF9 C19orf24 RBMX TGFBR2 NAF1 NFX1 MDN1 OXSR1 SLC38A1 PPFIA1 PLCD3 NCAPH2 PDS5A ZFR HNRNPLL CUL4A CDC42BPB LYSMD1 TMX2 ZNHIT3 TBC1D2 PRKAB1 RALGAPA1 KIF20A SSX2IP GTF2IRD1 MORC2 WDR55 GIPC1 ZNF592

		EIF4G2 GTF3C1 FAM208A KHDRBS1 PPP1R18 PHF10 PSEN1 NUP43 EPS15L1 NMD3 TOE1 GATAD2B FMNL2 HMGA1 SUPT7L YTHDC1 LIG3 STK38 ATP2A2 GAB1 MTMR3 DDX3X TRIM25 SCAF11 NCAPG GOLGA4 TMF1 FUNDC1 MISP CLN3 TMEM106B NDRG3 ATP2B1 VDAC2 CENPF RPS6KA3 BET1 SNX17 RANGAP1 SGPP1 DCAF8 RPS27 CDCA8 ZNF638
Embogama, et al.	142	PFKP DECR1 CSPG4 HSD17B10 NT5DC1 DDB1 PAIP1 DDX5 USP47 GDA IPO9 PUF60 IMPDH2 RTF1 USP14 USP7 SPG20 NUP88 NOMO1 DHX15 FKBP4 SF3A3 AHCYL1 UBQLN2 HEXIM1 TPT1 RDX EHBP1L1 LDLR ITGB1 RPN1 PSMC4 CASP1 CECR5 FKBP5 PRMT1 TYMS MCM5 PLOD2 RPS24 SH3GL1 WIBG DUSP12 BUB3 CNN2 WDR61 PRMT5 CLIC4 NHLRC2 FTO PTPRF RAB6A MINPP1 AKAP12 PRPF8 IARS UBE2O PPP2R2A CKMT1A TUBA1C PAAF1 SLC3A2 COPS3 DNM2 VARS DDX17 TIPRL LAMP2 NONO CPNE1 IMPDH1 NMT1 UBFD1 POLD1 ACTN1 HSDL2 RPS16 SF3B3 PNP ANKZF1 ACTR2 OAT TBCB SDHB DDOST PSMA1 DDX47 CYFIP1 ATP1B1 ARF1 SMC1A OXCT1 MTHFD2 MYOF FKBP10 MPI WARS CSE1L PFKM ELP3 TES PLOD3 PSMC1 MCCC2 PSMD14 DHX9 PSMA4 SERPINH1 CAPZA1 SEC24C SERPINB4 SERPINB1 POFUT TUBB6 MRPL2 GNB2L1 HMGCL ASNS CHD4 CDC73 GOLIM4 GDI2 RRM1 KLC1 GALE DRAP1 DLD SETD7 PLD3 SART3 RARS TRMT10C MGEA5 KPNA6 NAGK RPS14 PGD PYCRL NANS GPC1 LANCL1 MPST
Hamaguchi, et al.	19	CDC25B OFD1 MARK3 PITPNM2 CEP72 KIAA0556 GLI2 HSPC075 BAT2 EVL CRY2 PCNX CASP11 TMCC1 CAMKK2 SIK3 C2ORF55 PDE8B LRCH3
DNAJB1-PRKACA *in vitro* Mouse Liver Lysate	47	MSRB1 PYROXD2 MMGT1 SUGCT ACAA1A DGLUCY RCSD1 ACSF2 DCAF11 TNNT2 B2M GLOD4 GPD1L CR1L CEP290 GBE1 ASPG RTRAF CACNB2 SSR1 MUSTN1 RUFY3 WIPF1 ADSS ITIH4 SPHK2 CYP2D11 HAL CSMD1 RPS3A1 AADAT PRKAA2 OPLAH PCDH1 WASHC2 NUCB2 EIF5 GM20604 MMUT FLAD1 IFI35 DOCK5 HAAO CYP2C29 SLCO1B2 KCTD12 C6
PRKACA *in vitro* Mouse Liver Lysate	11	SIRT5 FAM50B SCO1 MAPRE3 PCX ECI2 ETNPPL IGSF10 ITPA RILP ARID4B

PRKACA *in vitro* Human Hepatocyte Lysate	35	ACTN4 PNPT1 PDCD5 PLIN2 UBXN4 NUDT12 PALM2 PALM2-AKAP2 NRAP MDH2 VPS53 ACOX3 CDK5RAP3 NUMB PLIN5 ARFGAP3 SLC25A10 UBE2D4 PLXNB1 AHCY UQCRB DPYS TNS1 NUMBL UBE2D1 CYP2C18 CYP27A1 CAP2 RNMTL1 PPM1F MLXIPL ZNF326 PHYHD1 UBE2D2 DAAM1
DNAJB1-PRKACA *in vitro* Human Hepatocyte Lysate	58	ERBB2IP TFR2 SDC2 GLG1 PCCB TJP3 ECE1 FAM114A2 HARS RPS10-NUDT3 HSD17B7 DMGDH STX5 PHYH RPL36A-HNRNPH2 DDX50 ARHGEF5 ALS2 C4B GTF2H1 APOO COA7 TP53I11 GLB1 GALK1 RPL36A FKBP7 FUBP3 FBXO22 C4A GPALPP1 RUVBL1 DDAH2 GRHPR FMO1 ELMOD2 EPHX2 H1F0 ETF1 SEC23A GLYATL1 LMAN2 FAM83G SYMPK DAB2IP ACSM2A FGA GGT7 HADH EPHX1 UBXN1 ERP44 ENPP1 FAM114A1 ESPN MAT2A ACSM2B S100A9
PRKACA (L206R) *in vitro* Human Hepatocyte Lysate	18	EPS8 ERO1L SLC16A2 KIAA0368 DPP9 PDXDC1 PAK4 HMGCS1 EIF4EBP2 ASGR2 SAP18 DR1 NCKIPSD EXOG ECM29 ARAF PSMB10 FAM21C

Sequence Motif Preferences

One way to look at a group of peptide sequences is to visualize them with a sequence logo (Schneider and Stephens 1990; Crooks et al. 2004). The height of the letters in these graphics is proportional to its frequency at that position in the group of peptides being studied. These logos would obviously reveal the consensus sequence for a group of substrates, but it would also allow for the detection of subtle sequence patterns.

For **Figures 29** and **30,** the peptide sequences identified in the no kinase reaction condition were removed from all conditions to try to truly detect patterns of substrate motifs for these different kinases.

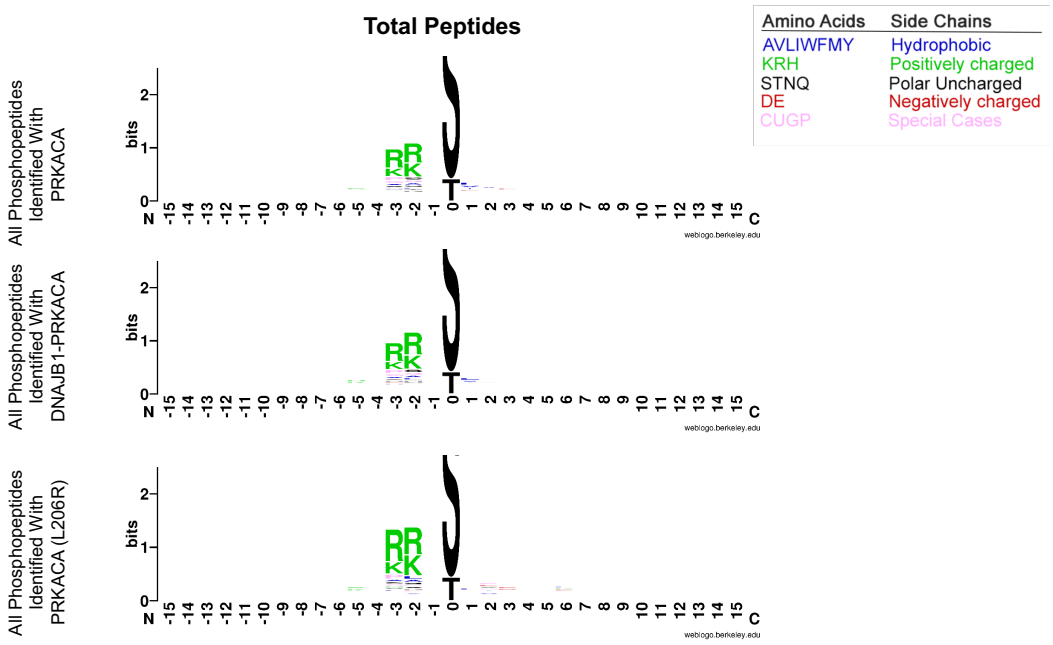

Figure 29. Sequence Logos for Total Peptides Identified in Kinase Reactions in Human Hepatocyte Lysate.

The total number of phosphopeptides identified in each condition were inputted into the sequence logo generator (Crooks et al. 2004) to yield these graphs: 1642 phosphopeptides for PRKACA, 1688 phosphopeptides for DNAJB1-PRKACA, and 1183 phosphopeptides for PRKACA (L206R).

Figure 29 shows very similar sequence logos between the three kinases, but the -3 position for the peptides identified in the PRKACA (L206R) sample show a slight difference in preference compared to the DNAJB1-PRKACA and PRKACA which are very similar. It also looks like there may be subtle differences in the +2 and +3 positions between these three kinases. This matches what was seen in the heatmap and Venn diagram data as well.

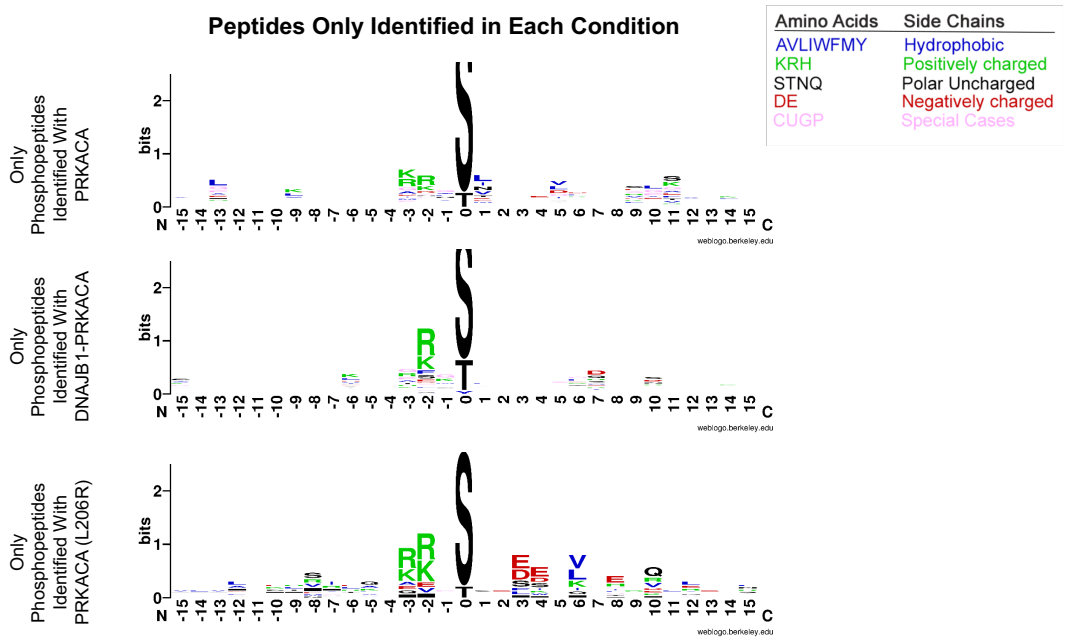

Figure 30. Sequence Logos for Peptides Only Identified in One of the Kinase Reactions in Human Hepatocyte Lysate.

The number of phosphopeptides that were only identified in each condition were inputted into the sequence logo generator (Crooks et al. 2004) to yield these graphs: 43 phosphopeptides for PRKACA, 44 phosphopeptides for DNAJB1-PRKACA, and 20 phosphopeptides for PRKACA (L206R).

Figure 30 is looking at the sequence logos of peptides that were only identified in that particular kinase reaction. These sequence logos may provide more information about substrate preference or specificity of a kinase since it is looking at peptides that were uniquely enriched for phosphorylations in just those samples with that particular kinase. Interestingly, the negatively charged amino acids in the +3 and +4 positions of the peptides found in the PRKACA (L206R) sample match the recently published sequence logo of this kinase from a paper that suggests that this variant has substrate specificity that differs from PRKACA (Bathon et al. 2019). It also looks like PRKACA

may have more of a preference for hydrophobic peptides than DNAJB1-PRKACA. The peptides identified only in the DNAJB1-PRKACA sample also seem to have a preference for a positively charged amino acid in the -6 position and a negatively charged amino acid in the +7. Our lab is following up on these potential differences with computational modeling.

Conclusions

Knocking down the endogenous kinase activity in human hepatocyte lysate with FSBA provides a diverse substrate pool for *in vitro* kinase reactions. Phosphopeptide enrichment from these kinase reactions is sufficient and robust enough to detect hundreds of phosphorylation events above the background phosphorylation detected in the no kinase added control. This method is highly suitable for comparing the potential substrates of multiple kinases on the same lysate.

Since the experiment done in this part of the study was in triplicate, statistical analysis was possible using the Perseus software. A PCA plot and heatmap that was generated using an FDR-corrected ANOVA test (FDR-0.01) show that each of these kinases has a distinct phosphorylation pattern when compared to each other. Interestingly, there is a group of potential substrates of DNAJB1-PRKACA and PRKACA (L206R) that are not enriched from the PRKACA samples. Since both of these PRKACA variants are found in tumors, this may be a key group of proteins to focus on for further studies of tumorigenesis.

STRING analysis based on this interesting list of potential substrates suggests that DNAJB1-PRKACA and PRKACA (L206R) could phosphorylate many human

hepatocyte proteins involved in mRNA regulation or various catabolic processes, both of which could contribute to tumor growth.

A comparison of proteins identified with phosphosites in the mouse liver *in vitro* assay with the proteins identified with phosphosites in the human hepatocyte *in vitro* assay revealed that there are more differences between the two than similarities. A comparison of these same proteins to the proteins identified by the other PKA substrate identification methods in Chapter I also reinforced that the ability to detect certain substrates is affected by the methodology and source material.

Lastly, sequence logo analysis allows for the detection of subtle differences in preference of certain amino acids in particular positions in a peptide favored by a certain kinase. Subtle differences in preference for a particular amino acid can inform a lot about the structure of a kinase.

Discussion

The data from this triplicate experiment is very dense and can continue to be mined for more information. It is an interesting question to consider how to sift through and analyze this data. Just because a potential substrate is highly phosphorylated by DNAJB1-PRKACA in this assay does not necessarily mean it is being phosphorylated in FLC, or even if it is being phosphorylated, it may not be crucially relevant to the pathogenesis of FLC. However, a highly phosphorylated substrate from this *in vitro* assay could provide structural insight into how this kinase favors certain substrates over another. Understanding more about the structure and substrate preference of this kinase could also direct paths to therapeutic discoveries.

It is also interesting that there is a defined overlap between PRKACA (L206R) and DNAJB1-PRKACA phosphorylation targets that is detected in the *in vitro* screen. It is even more interesting that this group of proteins seem to be implicated in mRNA regulation and various catabolic processes. Transcriptional and metabolic changes are crucial to tumor growth and development and both of these kinases were identified in tumors. It is possible that they both have some substrates in common that are crucial to beginning the kinase cascades to trigger tumorigenesis.

I am not surprised that the phosphorylation targets change considerably between mouse liver lysate and human hepatocyte lysate. Having access to human hepatocytes to lyse for this assay is a crucial component for how useful this data set will be in comparing phosphosites of proteins found in FLC tumors to phosphosites of proteins identified in this assay in the condition with DNAJB1-PRKACA.

CHAPTER IV: Comparing Phosphosites of Proteins Enriched in FLC Patient Samples to Phosphosites Enriched in the Presence of DNAJB1-PRKACA in Human Hepatocyte Lysate

Background and Rationale

The data set from the triplicate *in vitro* assay using FSBA-treated human hepatocyte lysate contains a lot of interesting information in its own right as has been discussed, but it cannot tell me which substrates are phosphorylated in an FLC tumor. The total phosphome of a normal and tumor sample from an FLC patient can tell me what is differentially phosphorylated in the tumor and normal tissues and perhaps what pathways are largely being affected, but it cannot tell me what a particular kinase could phosphorylate. However, combining these two data sets can narrow down a list of candidate substrates for DNAJB1-PRKACA that may be relevant to the development or growth of FLC.

FLC is a rare cancer so tissue samples can be hard to come by, but as I mentioned in Chapter I, our lab has a tissue repository of over a hundred patient samples. However, for phosphoproteomics studies, the quality of the sample matters considerably, as does the size. Luckily, members of our lab are very involved in retrieving these samples, so we have some amount of confidence about the time the samples have been outside of the patient until they can be frozen to be preserved.

For this next experiment I designed, I collaborated with Solomon Levin, now an MD/PhD in our lab, to lyse three normal patient liver samples and their corresponding FLC tumors for phosphopeptide enrichment with Soren Heissel in the Proteomics Resource Center.

Phosphopeptides Enriched from FLC Patient Tumor and Normal Liver Samples

The PCA plot generated using Perseus in **Figure 31A** shows that all of the normal patient liver samples are grouping together and that each of the tumors is grouping on its own, meaning that the phosphorylation pattern of the tumor is significantly altered from the phosphorylation pattern of the normal liver tissue. In order to ease my search of comparable phosphosites, the phosphosite intensities were averaged among technical replicates. The PCA plot that resulted after this condensing of data looked very similar as before (**Figure 31A-B**) which was reassuring.

The heatmap of this averaged data also shows a clear signature of phosphorylation for the tumor compared to normal in the same patient (**Figure 32**); all intensity values in the data set comprising the heatmap have a p-value > 0.05. **Figure 33B** shows that of the 316 proteins that have phosphosites that are significantly changed (p-value>0.05) between the tumor and normal liver samples, 108 of these proteins also have phosphosites found enriched in the *in vitro* condition with DNAJB1-PRKACA. **Figure 33A** shows that there is an overlap of 352 proteins that have phosphosites in the total tumor and normal patient data with the proteins that have phosphosites enriched in the DNAJB1-PRKACA added sample in the *in vitro* assay.

This does not mean that they are the same phosphosites, just that they are the same protein that also has phosphosites. We are currently working on a way to be able to quickly identify whether or not a phosphosite matches from the patient data to the *in vitro* data, but for now this is done manually.

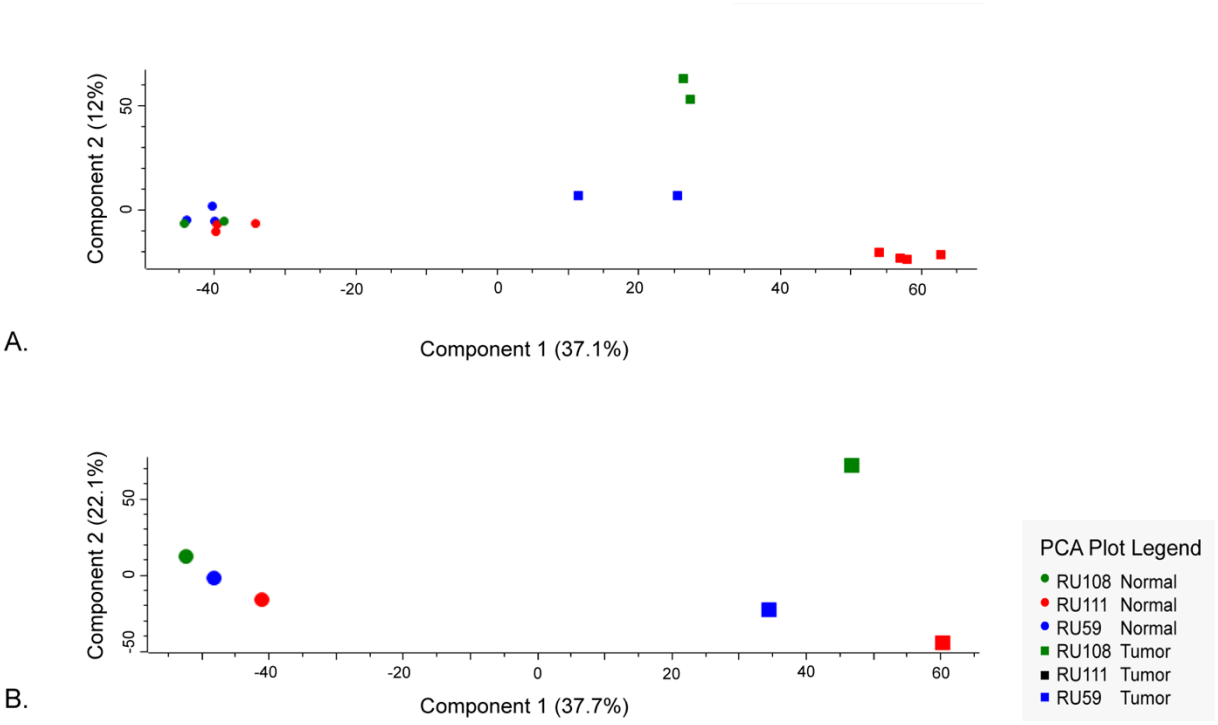

Figure 31. FLC Tumors Have a Distinct Phosphorylation Pattern Compared to Normal Liver Tissue in the Same Patient.

(A) PCA plot generated with Perseus of normal liver tissue compared to FLC tumor tissue from the same patient based on the phosphopeptides enriched from these samples. (B) PCA plot, also generated with Perseus, of averaged phophosite intensities among technical replicates of the FLC tumor and normal liver samples.

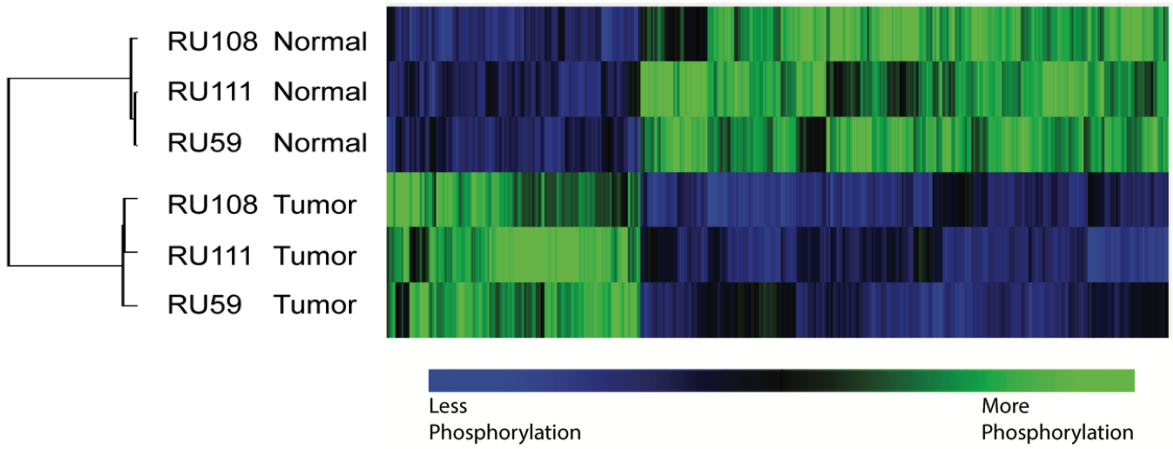

Figure 32. FLC Tumors Have Distinct Phosphorylation Pattern from Normal. Heatmap of the averaged phosphopeptide intensities that significantly change ($p<0.05$) from normal tissue to tumor tissue generated with Perseus.

Using phosphopeptide data exported from Perseus for the patient samples and the *in vitro* kinase reaction for the DNAJB1-PRKACA condition, I manually generated the list of phosphosites that were in common with each other in Excel. I then used this list to manually highlight these points on the plots seen in **Figures 34-36** in red, which are also listed in **Table 17.** Points in orange represent phosphorylation sites present in the patient data and in the *in vitro* data in the DNAJB1-PRAKCA and PRKACA samples; these proteins are also listed in **Table 18.** It is of note that **Figure 36B,** which is a magnified shot of **Figure 34B,** features heat shock proteins, a proteasome subunit, a PKA regulatory subunit, cofilin, and (in red) a 3-keto-steroid reductase as being more phosphorylated in the tumor than the normal patient liver and also being phosphorylated by DNAJB1-PRAKCA in the *in vitro* data.

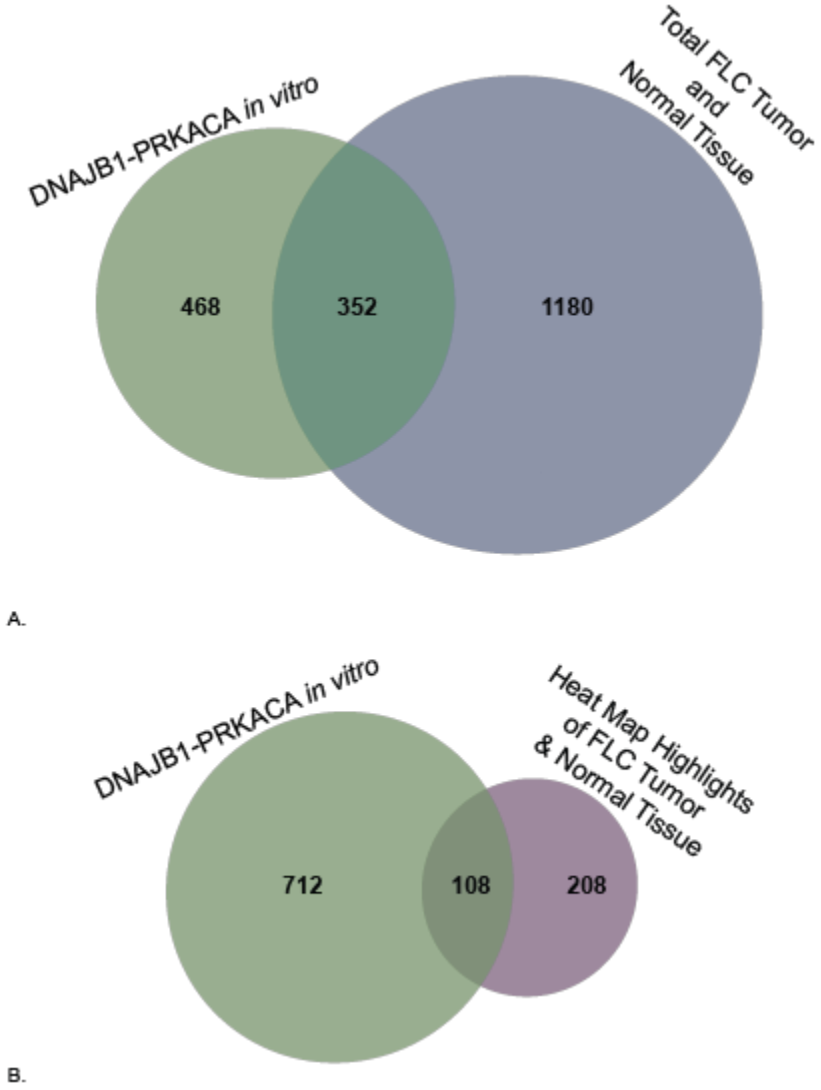

Figure 33. Venn Diagram Comparing Proteins with Phosphosites Found Enriched from the DNAJB1-PRKACA Sample *in vitro* to Patient Data.

(A) Potential DNAJB1-PRKACA targets identified from the *in vitro* assay using FSBA-treated human hepatocyte lysate (in green) overlapped with all of the phoshpoproteins identified in the normal and tumor tissues (in blue). (B) Potential DNAJB1-PRKACA targets identified from the *in vitro* assay using FSBA-treated human hepatocyte lysate (in green) overlapped with the phosphoproteins that show a significant change in phosphorylation between normal and tumor ($p<0.05$) (in purple).

Figure 34. Phosphosites Found in Normal FLC Patient Liver versus FLC Tumor. Intensity values were log2 transformed and normalized by subtraction of the median intensity values in each experiment. Teal represents all phosphosites that are more present in the tumor than the normal and purple represents all phosphosites that are more present in the normal than the tumor. (A) The phosphosites labeled in red are all phosphosites that show up as only phosphorylated in the *in vitro* assay in the DNAJB1-PRKACA condition. (B) Orange represents phosphosites that are also enriched in the samples with DNAJB1-PRKACA and PRKACA in the *in vitro* assay; this list did not take into account if more phosphopeptides with that site were identified in the DNAJB1-PRKACA sample compared to the PRKACA sample

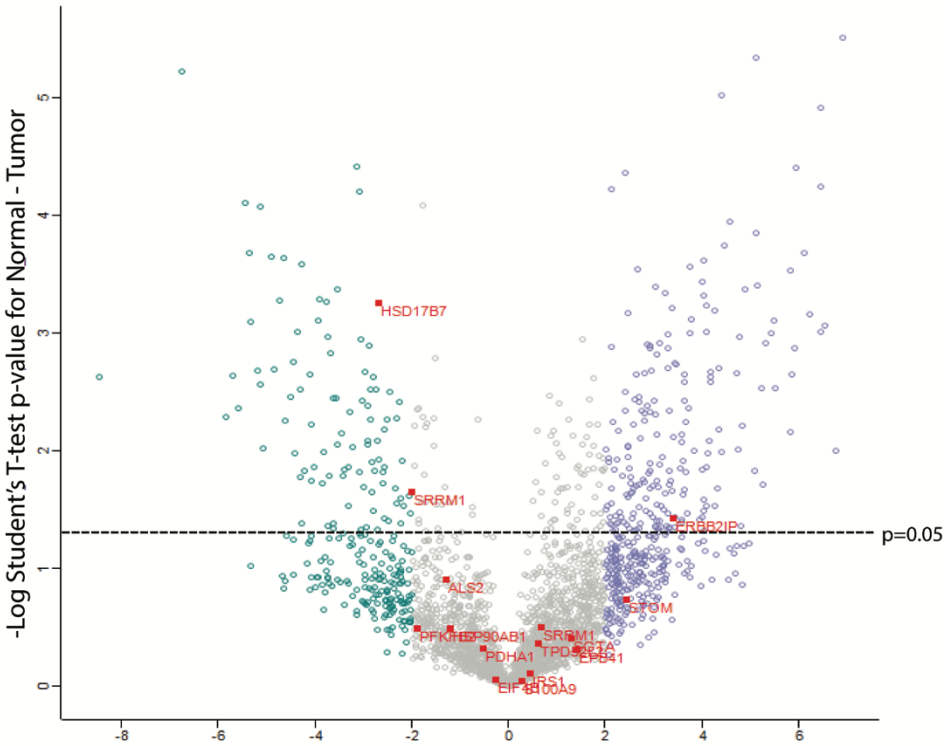
-Log Student's T-test p-value for Normal - Tumor
Student's T-test Difference for Normal - Tumor
p=0.05
HSD17B7
SRRM1
ERBB2IP
ALS2
GTPOM
PFKM
PPP3CB
PDHA1
SRRM1
TPD52
EPB41
EIF4G1
S100A9
-8
-6
-4
-2
0
2
4
6
0
1
2
3
4
5

A.

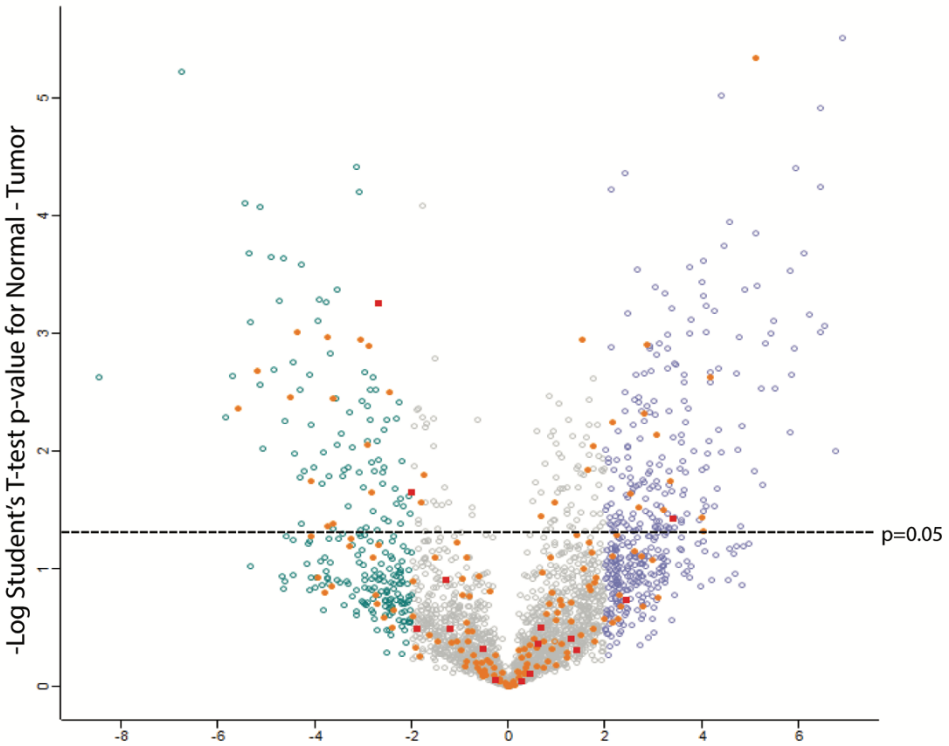
-Log Student's T-test p-value for Normal - Tumor
Student's T-test Difference for Normal - Tumor
p=0.05
-8
-6
-4
-2
0
2
4
6
0
1
2
3
4
5

B.

.

Table 17. Phosphosites Found in Patient Tumor or Normal Liver and Only Identified in DNAJB1-PRKACA Sample in Human *in vitro* Assay.

Phosphosite	Uniprot Number	Gene Name	Protein
500	A0A2R8Y420	EPB41	Protein 4.1
872	Q96RT1	ERBB2IP	Protein LAP2
483	O60825	PFKFB2	6-phosphofructo-2-kinase/fructose-2,6-bisphosphatase 2;6-phosphofructo-2-kinase;Fructose-2,6-bisphosphatase
166	O43399	TPD52L2	Tumor protein D54
353	Q96Q42	ALS2	Alsin
177	P56937	HSD17B7	3-keto-steroid reductase
452	P08238	HSP90AB1	Heat shock protein HSP 90-beta
1100	P35568	IRS1	Insulin receptor substrate 1
293	P08559	PDHA1;PDHA2	Pyruvate dehydrogenase E1 component subunit alpha, somatic form, mitochondrial;Pyruvate dehydrogenase E1 component subunit alpha, testis-specific form, mitochondrial
113	P06702	S100A9	Protein S100-A9
81	O43765	SGTA	Small glutamine-rich tetratricopeptide repeat-containing protein alpha
712	E9PCT1	SRRM1	Serine/arginine repetitive matrix protein 1
637	E9PCT1	SRRM1	Serine/arginine repetitive matrix protein 1
10	F8VSL7	STOM	Erythrocyte band 7 integral membrane protein
450	E7EX17	EIF4B	Eukaryotic translation initiation factor 4B

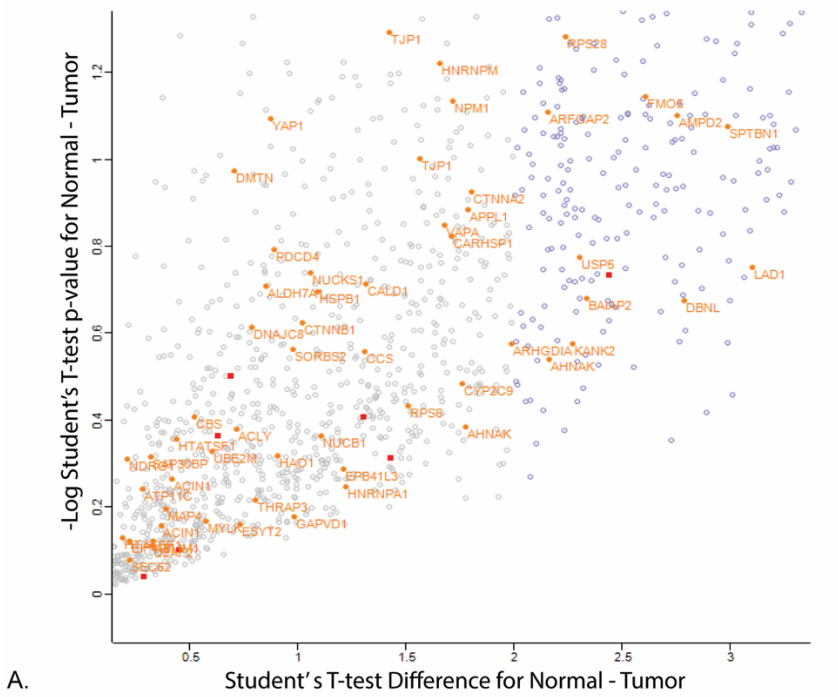

A.

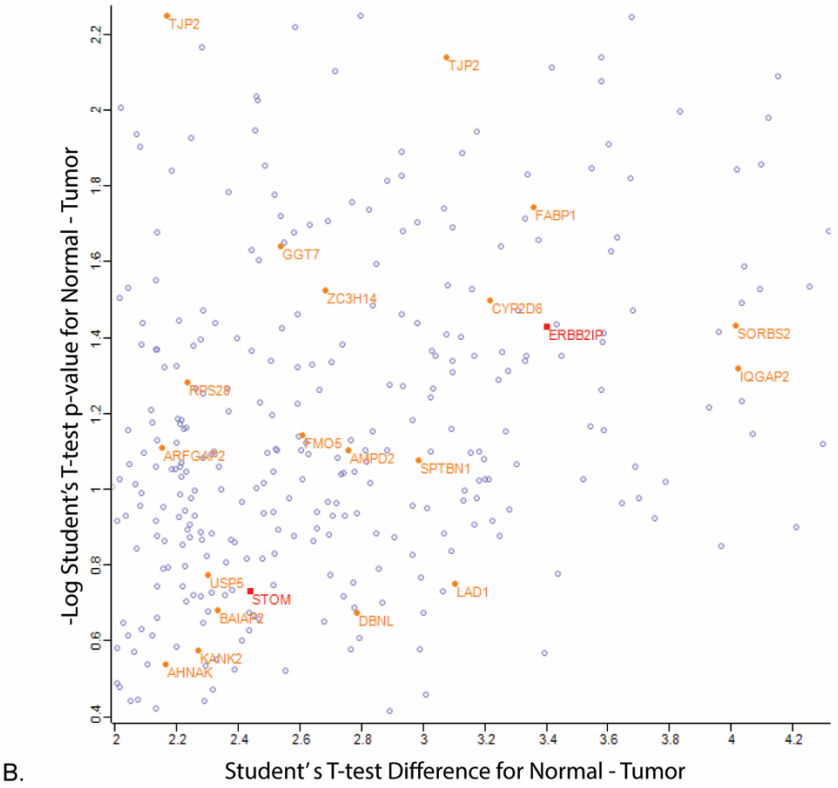

B.

Figure 35. Phosphosites Found More in Normal Patient Liver versus FLC Tumor.

(A) is a magnification of the right side of **Figure 34B**. (B) is a magnification of (**35A**).

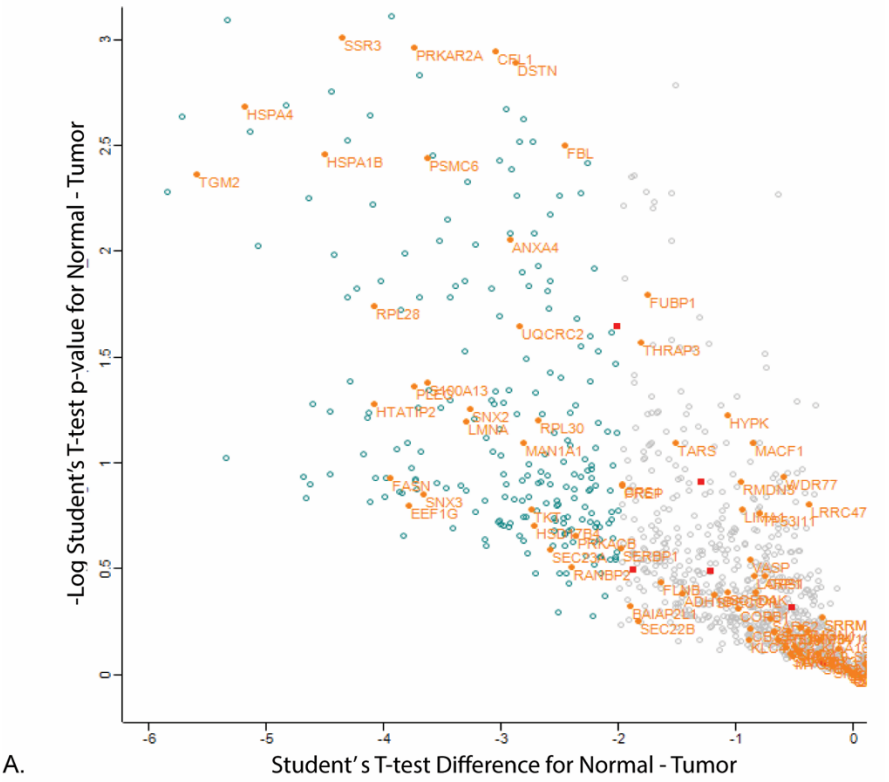

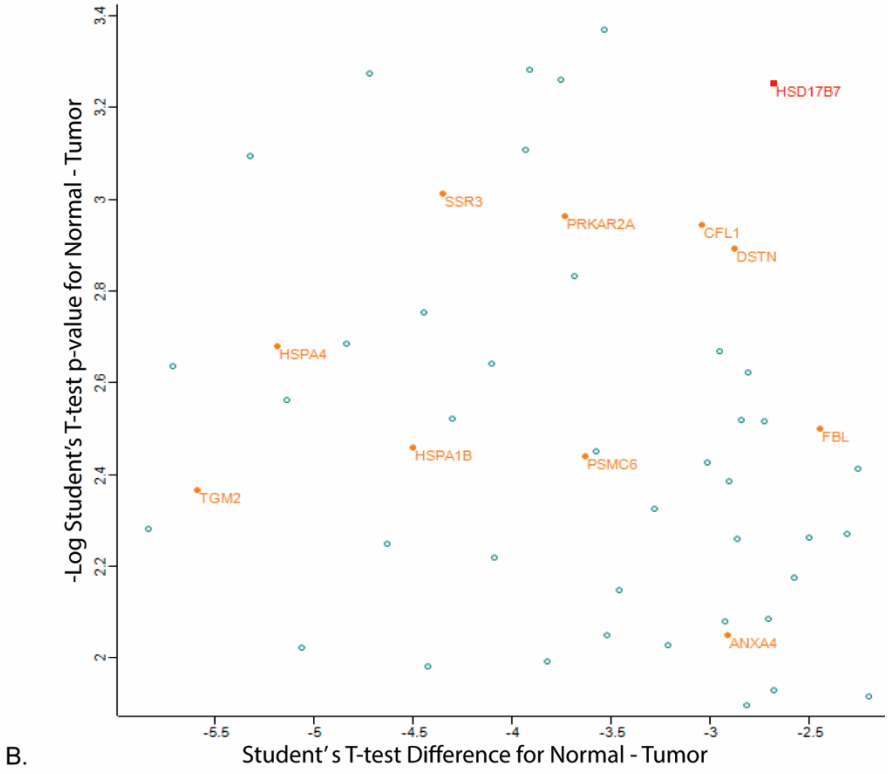

Figure 36. Phosphosites Found More in FLC Tumor versus Normal Patient Liver.

(A) is a magnification of the left side of **Figure 34B**. (B) is a magnification of (**36A**).

Table 18. Total Phosphosites Found in FLC Tumor & Normal Patient Samples Also Found in DNAJB1-PRAKCA & PRAKCA Human Liver Lysate *in vitro* Assay.

Phosphosites	Uniprot Number	Gene Name	Protein
527	F8W8M4	ABLIM1	Actin-binding LIM protein 1
767	S4R3H4	ACIN1	Apoptotic chromatin condensation inducer in the nucleus
503	S4R3H4	ACIN1	Apoptotic chromatin condensation inducer in the nucleus
455	P53396	ACLY	ATP-citrate synthase
9	Q99424	ACOX2	Peroxisomal acyl-coenzyme A oxidase 2;Acyl-coenzyme A oxidase
342	P00325	ADH1B	Alcohol dehydrogenase 1B;Alcohol dehydrogenase 1A
5448	Q09666	AHNAK	Neuroblast differentiation-associated protein AHNAK
135	Q09666	AHNAK	Neuroblast differentiation-associated protein AHNAK
84	A0A1B0GTG2	ALDH7A1	Alpha-aminoadipic semialdehyde dehydrogenase
353	Q96Q42	ALS2	Alsin
139	H0Y360	AMPD2	AMP deaminase 2
125	P09525	ANXA4	Annexin A4;Annexin
400	A0A2R8Y611	AP3D1	AP-3 complex subunit delta-1
410	Q9UKG1	APPL1	DCC-interacting protein 13-alpha
240	Q8N6H7	ARFGAP2	ADP-ribosylation factor GTPase-activating protein 2
34	P52565	ARHGDIA	Rho GDP-dissociation inhibitor 1
141	H7C113	ATP11C	Phospholipid-transporting ATPase IG
68	O75348	ATP6V1G1	V-type proton ATPase subunit G 1
123	I3L0Y9	BAIAP2	Brain-specific angiogenesis inhibitor 1-associated protein 2
331	Q9UHR4	BAIAP2L1	Brain-specific angiogenesis inhibitor 1-associated protein 2-like protein 1
151	P00918	CA2	Carbonic anhydrase 2
283	E7EX44	CALD1	Caldesmon
308	Q01518	CAP1	Adenylyl cyclase-associated protein 1
52	Q9Y2V2	CARHSP1	Calcium-regulated heat stable protein 1
27	P0DN79	CBS	Cystathionine beta-synthase
93	Q13185	CBX3	Chromobox protein homolog 3
95	Q13185	CBX3	Chromobox protein homolog 3
248	J3KNF4	CCS	Copper chaperone for superoxide dismutase
24	P23528	CFL1	Cofilin-1
24	Q9Y281	CFL2	Cofilin-2
933	P53618	COPB1	Coatomer subunit beta
312	P31327	CPS1	Carbamoyl-phosphate synthase [ammonia], mitochondrial
404	P31327	CPS1	Carbamoyl-phosphate synthase [ammonia], mitochondrial
654	P35221	CTNNA2	Catenin alpha-2;Catenin alpha-1
552	A0A2R8Y804	CTNNB1	Catenin beta-1
127	P11712	CYP2C9	Cytochrome P450 2C9;Cytochrome P450 2C19
113	E7ENE7	CYP2D6	Cytochrome P450 2D6;Putative cytochrome P450 2D7

350	Q3LXA3	DAK	Bifunctional ATP-dependent dihydroxyacetone kinase/FAD-AMP lyase (cyclizing);ATP-dependent dihydroxyacetone kinase;FAD-AMP lyase (cyclizing)
51	P51397	DAP	Death-associated protein 1
245	Q9UJU6	DBNL	Drebrin-like protein
251	Q9UJU6	DBNL	Drebrin-like protein
267	Q9UJU6	DBNL	Drebrin-like protein
372	Q08495	DMTN	Dematin
35	O75937	DNAJC8	DnaJ homolog subfamily C member 8
24	P60981	DSTN	Destrin
298	P26641	EEF1G	Elongation factor 1-gamma
450;	E7EX17	EIF4B	Eukaryotic translation initiation factor 4B
1053	E7EUU4	EIF4G1	Eukaryotic translation initiation factor 4 gamma 1
164	A0A087WUT6	EIF5B	Eukaryotic translation initiation factor 5B
649	A0A2U3TZH6	EPB41	Protein 4.1
674	A0A2U3TZH6	EPB41	Protein 4.1
278	A0A0A0MSA4	EPB41L3	Band 4.1-like protein 3;Band 4.1-like protein 3, N-terminally processed
872	Q96RT1	ERBB2IP	Protein LAP2
701	H7BXI1	ESYT2	Extended synaptotagmin-2
56	P07148	FABP1	Fatty acid-binding protein, liver
2236	P49327	FASN	Fatty acid synthase;[Acyl-carrier-protein] S-acetyltransferase;[Acyl-carrier-protein] S-malonyltransferase;3-oxoacyl-[acyl-carrier-protein] synthase;3-oxoacyl-[acyl-carrier-protein] reductase;3-hydroxyacyl-[acyl-carrier-protein] dehydratase;Enoyl-[acyl-carrier-protein] reductase;Oleoyl-[acyl-carrier-protein] hydrolase
39	M0R299	FBL	rRNA 2'-O-methyltransferase fibrillarin
2107	O75369	FLNB	Filamin-B
280	P49326	FMO5	Dimethylaniline monooxygenase [N-oxide-forming] 5
99	Q96AE4	FUBP1	Far upstream element-binding protein 1
881	F8W9S7	GAPVD1	GTPase-activating protein and VPS9 domain-containing protein 1
89	A2A2G5	GGT7	Gamma-glutamyltransferase 7;Gamma-glutamyltransferase 7 heavy chain;Gamma-glutamyltransferase 7 light chain
83	C9JFE4	GPS1	COP9 signalosome complex subunit 1
229	Q9UJM8	HAO1	Hydroxyacid oxidase 1
7	P05114	HMGN1	Non-histone chromosomal protein HMG-14
95	P09651	HNRNPA1	Heterogeneous nuclear ribonucleoprotein A1;Heterogeneous nuclear ribonucleoprotein A1, N-terminally processed;Heterogeneous nuclear ribonucleoprotein A1-like 2
432	A0A087X0X3	HNRNPM	Heterogeneous nuclear ribonucleoprotein M
318	P51659	HSD17B4	Peroxisomal multifunctional enzyme type 2;(3R)-hydroxyacyl-CoA dehydrogenase;Enoyl-CoA hydratase 2
177	P56937	HSD17B7	3-keto-steroid reductase
452	P08238	HSP90AB1	Heat shock protein HSP 90-beta

419	A0A0G2JIW1	HSPA1	Heat shock 70 kDa protein 1B;Heat shock 70 kDa protein 1A
76	P34932	HSPA4	Heat shock 70 kDa protein 4
82	P04792	HSPB1	Heat shock protein beta-1
56	Q9BUP3	HTATIP2	Oxidoreductase HTATIP2
403	O43719	HTATSF1	HIV Tat-specific factor 1
387	O43719	HTATSF1	HIV Tat-specific factor 1
38	Q9NX55	HYPK	Huntingtin-interacting protein K
685	Q13576	IQGAP2	Ras GTPase-activating-like protein IQGAP2
16	Q13576	IQGAP2	Ras GTPase-activating-like protein IQGAP2
1100	P35568	IRS1	Insulin receptor substrate 1
540	Q63ZY3	KANK2	KN motif and ankyrin repeat domain-containing protein 2
1701	Q9BY89	KIAA1671	Uncharacterized protein KIAA1671
566	Q9NSK0	KLC4	Kinesin light chain 4
18	P05783	KRT18	Keratin, type I cytoskeletal 18
408	E9PDI4	LAD1	Ladinin-1
1040	Q6PKG0	LARP1	La-related protein 1
369	Q9UHB6	LIMA1	LIM domain and actin-binding protein 1
423	P02545	LMNA	Prelamin-A/C;Lamin-A/C
429	P02545	LMNA	Prelamin-A/C;Lamin-A/C
431	Q8N1G4	LRRC47	Leucine-rich repeat-containing protein 47
3922	H3BPE1	MACF1	Microtubule-actin cross-linking factor 1, isoforms 1/2/3/5
31	P33908	MAN1A1	Mannosyl-oligosaccharide 1,2-alpha-mannosidase IA
2145	E7EVA0	MAP4	Microtubule-associated protein;Microtubule-associated protein 4
188	D6REM6	MATR3	Matrin-3
747	Q96PC5	MIA2	Melanoma inhibitory activity protein 2;cTAGE family member 6;cTAGE family member 15;cTAGE family member 4;cTAGE family member 8;cTAGE family member 9
1773	Q15746	MYLK	Myosin light chain kinase, smooth muscle;Myosin light chain kinase, smooth muscle, deglutamylated form
1354	M0R300	MYO9B	Unconventional myosin-IXb
330	Q92597	NDRG1	Protein NDRG1
243	P06748	NPM1	Nucleophosmin
148	Q02818	NUCB1	Nucleobindin-1
214	Q9H1E3	NUCKS1	Nuclear ubiquitous casein and cyclin-dependent kinase substrate 1
198	Q9H1E3	NUCKS1	Nuclear ubiquitous casein and cyclin-dependent kinase substrate 1
342	Q96CV9	OPTN	Optineurin
9	P61457	PCBD1	Pterin-4-alpha-carbinolamine dehydratase
457	Q53EL6	PDCD4	Programmed cell death protein 4
293	P08559	PDHA1	Pyruvate dehydrogenase E1 component subunit alpha, somatic form, mitochondrial;Pyruvate dehydrogenase E1 component subunit alpha, testis-specific form, mitochondrial
293	P08559	PDHA2	Pyruvate dehydrogenase E1 component subunit alpha, somatic form, mitochondrial;Pyruvate dehydrogenase E1 component subunit alpha, testis-specific form, mitochondrial
483	O60825	PFKFB2	6-phosphofructo-2-kinase/fructose-2,6-bisphosphatase 2;6-phosphofructo-2-kinase;Fructose-2,6-bisphosphatase
2039	Q15149	PLEC	Plectin

66	Q9H307	PNN	Pinin
667	P48147	PREP	Prolyl endopeptidase
204	P17612	PRKACB	cAMP-dependent protein kinase catalytic subunit beta;cAMP-dependent protein kinase catalytic subunit gamma;cAMP-dependent protein kinase catalytic subunit alpha
58	P13861	PRKAR2A	cAMP-dependent protein kinase type II-alpha regulatory subunit
198	O60256	PRPSAP2	Phosphoribosyl pyrophosphate synthase-associated protein 2
258	A0A087X2I1	PSMC6	26S protease regulatory subunit 10B
14	O00231	PSMD11	26S proteasome non-ATPase regulatory subunit 11
269	Q5VWC4	PSMD4	26S proteasome non-ATPase regulatory subunit 4
1509	P49792	RANBP2	E3 SUMO-protein ligase RanBP2
46	Q96TC7	RMDN3	Regulator of microtubule dynamics protein 3
115	P46779	RPL28	60S ribosomal protein L28
10	P62888	RPL30	60S ribosomal protein L30
23	P62857	RPS28	40S ribosomal protein S28
236	P62753	RPS6	40S ribosomal protein S6
32	Q99584	S100A13	Protein S100-A13
113	P06702	S100A9	Protein S100-A9
221	M0QWZ7	SARS2	Serine--tRNA ligase, mitochondrial
316	Q8WVM8	SCFD1	Sec1 family domain-containing protein 1
681	A0A0U1RQQ9	SCYL2	SCY1-like protein 2
151	E7ESK6	SDC2	Syndecan;Syndecan-2
137	O75396	SEC22B	Vesicle-trafficking protein SEC22b
559	F5H365	SEC23A	Protein transport protein Sec23A
158	Q99442	SEC62	Translocation protein SEC62
85	Q9UHD8	SEPT9	Septin-9
203	Q8NC51	SERBP1	Plasminogen activator inhibitor 1 RNA-binding protein
81	O43765	SGTA	Small glutamine-rich tetratricopeptide repeat-containing protein alpha
188	Q13596	SNX1	Sorting nexin-1
185	O60749	SNX2	Sorting nexin-2
72	O60493	SNX3	Sorting nexin-3
13	C9JI79	SORBS2	Sorbin and SH3 domain-containing protein 2
377	H7BXR3	SORBS2	Sorbin and SH3 domain-containing protein 2
306	H7BXR3	SORBS2	Sorbin and SH3 domain-containing protein 2
832	Q69YQ0	SPECC1L	Cytospin-A
2358	Q01082	SPTBN1	Spectrin beta chain, non-erythrocytic 1
722	A9Z1X7	SRRM1	Serine/arginine repetitive matrix protein 1
647	A9Z1X7	SRRM1	Serine/arginine repetitive matrix protein 1
734	A9Z1X7	SRRM1	Serine/arginine repetitive matrix protein 1
722	A9Z1X7	SRRM1	Serine/arginine repetitive matrix protein 1
645	A9Z1X7	SRRM1	Serine/arginine repetitive matrix protein 1
647	A9Z1X7	SRRM1	Serine/arginine repetitive matrix protein 1
734	A9Z1X7	SRRM1	Serine/arginine repetitive matrix protein 1
5	P84103	SRSF3	Serine/arginine-rich splicing factor 3
105	C9JA28	SSR3	Translocon-associated protein subunit gamma
138	O95210	STBD1	Starch-binding domain-containing protein 1
10	P27105	STOM	Erythrocyte band 7 integral membrane protein

281	P26639	TARS	Threonine--tRNA ligase, cytoplasmic
216	P21980	TGM2	Protein-glutamine gamma-glutamyltransferase 2
928	Q9Y2W1	THRAP3	Thyroid hormone receptor-associated protein 3
444	Q9Y2W1	THRAP3	Thyroid hormone receptor-associated protein 3
605	G3V1L9	TJP1	Tight junction protein ZO-1
163	G3V1L9	TJP1	Tight junction protein ZO-1
245	A0A3B3ITE1	TJP2	Tight junction protein ZO-2
175	A0A3B3ITE1	TJP2	Tight junction protein ZO-2
203	O95049	TJP3	Tight junction protein ZO-3
104	P29401	TKT	Transketolase
376	O60784	TOM1	Target of Myb protein 1
93	Q15785	TOMM34	Mitochondrial import receptor subunit TOM34
14	E9PN66	TP53I11	Tumor protein p53-inducible protein 11
166	O43399	TPD52L2	Tumor protein D54
79	P26368	U2AF2	Splicing factor U2AF 65 kDa subunit
266	Q9Y385	UBE2J1	Ubiquitin-conjugating enzyme E2 J1
28	P61081	UBE2M	NEDD8-conjugating enzyme Ubc12
303	P22695	UQCRC2	Cytochrome b-c1 complex subunit 2, mitochondrial
783	P45974	USP5	Ubiquitin carboxyl-terminal hydrolase 5
164	Q9P0L0	VAPA	Vesicle-associated membrane protein-associated protein A
239	P50552	VASP	Vasodilator-stimulated phosphoprotein
5	Q9BQA1	WDR77	Methylosome protein 50
109	P46937	YAP1	Transcriptional coactivator YAP1
515	Q6PJT7	ZC3H14	Zinc finger CCCH domain-containing protein 14

A Few Proteins of Interest as Potential DNAJB1-PRKACA Targets Relevant to FLC

I was intrigued by the suggestion of RNA regulation from Chapter III and saw the SRRM1 protein in **Table 17** and **18.** SRRM1 is a serine and arginine repetitive matrix 1 protein that is part of the pre- and post-splicing mRNP complexes. In a collaboration with David Requena in our lab, a pilot test was conducted to see if the amount of alternative splicing events were the same in tumor and normal samples from the same patient using previously obtained RNA data from a patient. This analysis was done with SplAdder (Kahles et al. 2016). Nothing seemed significant from this pilot, though that does not mean SRRM1 or RNA splicing is not significant in FLC.

Table 19. SplAdder Analysis.

Alternative_Splicing_Events	59N7	59T5	59T6
Alt_3prime	1439	1481	952
Alt_5prime	1041	1065	621
Exon_skip	2599	2630	1650
Intron_Retention	1885	3313	1653
Multi_Exon_Skip	271	273	163
Mutex_Exons	71	81	60
Total number of reads	32710485	44563838	29536248

PDHA1 also has a phosphosite identified only when DNAJB1-PRKACA or PRKACA-L206R is present; this particular phosphosite has previously been identified to inhibit the function of Pdha1 which can induce cell growth by enhancing glycolysis (Liu et al. 2018). This could be particularly interesting to follow up on since PRKACA-L206R was found in adrenal adenomas in Cushing's syndrome and the DNAJB1-PRKACA results in cancerous tumors in FLC.

Another protein of potential interest to FLC is HSD17B7 which was identified as being highly and significantly phosphorylated in the tumor more than the normal in the patient data. It was also only identified in the DNAJB1-PRKACA condition in the *in vitro* assay. This 3-keto-steroid reductase is involved in the biosynthesis of sex hormones. The role of estrogens in FLC is still unclear, but some male patients present with gynecomastia, or breast growth. This phosphorylated protein could be a contributing factor.

Before getting any results, I was hopeful about seeing phosphorylation of heat shock proteins in the tumor and the *in vitro* assay because of the presence of the J-domain on the fusion kinase. I thought the J-domain of DNAJB1-PRKACA could be

attracting heat shock proteins, like Hsp70 or Hsp90 family members, which would then be phosphorylated. Indeed, Hsp90ab1 was one of the proteins detected with a phosphosite in common between the patient data and the *in vitro* data in the conditions with DNAJB1-PRKACA and PRKACA (L206R). The involvement of heat shock proteins, and also the implication of DNAJB1-PRKACA interaction with proteins involved with catabolism made earlier in Chapter III, prompted me to want to see how much phosphorylation would change when cells were starved in the presence and absence of DNAJB1-PRKACA.

The experiment I designed required the use of two cell lines: Huh7 and Huh7 cells with a plasmid that expresses DNAJB1-PRKACA from the DNAJB1 promoter. In collaboration with a technician in our lab, Harriet Prior, cells from each cell line were either grown as normal or starved for 16 hours. Cells were then harvested and lysed to run on a gel. Western blots were visualized using an antibody against the phosphorylated consensus sequence for PKA (100G7E, Cell Signaling Technology) or an antibody against PRKACA (sc-28315, Santa Cruz Biotechnology). I was expecting to see the change in phosphorylation seen in **Figure 37A,** but I was surprised to see that DNAJB1-PRKACA was not detected in the cell line expressing it under starved conditions. From a literature search, I found a paper that claimed when cells are deprived of amino acids, HSF1, a heat shock transcription factor, loses its DNA binding activity and, as a consequence, DNAJB1 transcript levels sharply decreased (Hensen et al. 2012). If this is what happened in these cell lines, then obtaining an HSF1 inhibitor or using siRNA to knock down HSF1 could be an effective strategy to knockdown DNAJB1-expression, at least experimentally, if not therapeutically.

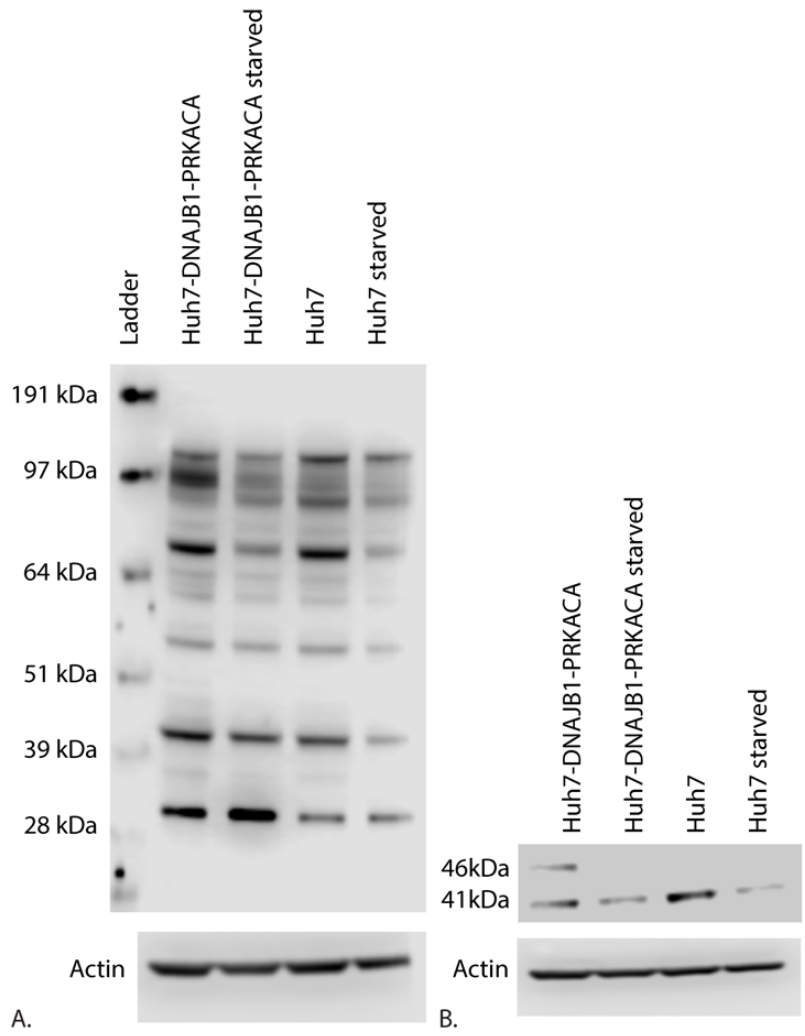

Figure 37. Starved Huh-7 Cells Expressing DNAJB1-PRKACA.

(A) Western blot with an anti-phospho-PKA Substrate antibody (100G7E, CST) and actin control. (B) Western blot with an anti-PKA antibody (sc-28315) and actin control.

Conclusions

The results of the phosphopeptide enrichment from the three patient tumor and normal liver samples showed that the phosphopeptide signature of the tumor is distinctly different from the patient's normal liver. 178 phosphosites were identified in the tumor and normal that were also matched to phosphosites that were increased in the presence of DNAJB1-PRKACA *in vitro*.

Four of these phosphosites belonged to four different heat shock proteins: HSP90AB1, HSP1A1B, HSPA4, and HSPB1. As established in the introduction, heat shock proteins have been implicated to play a role in cancer and disease so these proteins may warrant a further look.

Another three of these phosphosites were found in HSD17B7, PDHA1, and SRRM1. HSD17B7's role in estrogen synthesis, PDHA1's role in cell growth, and SRRM1's role in RNA splicing make them all interesting potential targets to continue to study.

One surprising protein that warrants follow up studies is the heat shock transcription factor, HSF1. This protein was not identified as phosphorylated by either screen, rather it was found as a potential protein of interest to FLC as a consequence of these phosphorylation studies. The implication of DNAJB1-PRKACA's interaction with many metabolic proteins from the phosphorylation studies prompted me to just want to see what changes in phosphorylation could be seen in starvation or normal conditions in the presence or absence of this oncogenic kinase via a western blot with a PKA substrate motif antibody. Under starvation conditions, DNAJB1-PRKACA was no longer detected by western blot. A literature search provided a possible explanation that HSF1

cannot bind DNA in an amino acid depleted environment and thus the transcription of DNAJB1 sharply decreases. It is possible that something else was happening here, but this could be an alternative method to knockdown the oncogenic fusion kinase experimentally, or perhaps therapeutically.

Discussion

It can be enticing to only go after the phosphorylation targets that present as extremely high in the tumor, but perhaps a true and relevant direct target of DNAJB1-PRKACA would only be phosphorylated at low levels due to a regulatory feedback loop, but the activity conferred by the low-level phosphorylation triggers a cascade of events necessary for tumorigenesis or growth. I think it is easy to imagine ways for any protein to be involved with cancer development or progression. So, in that regard, I think a fair argument could be made to follow up with any of the proteins that have phosphosites in common between the two sets of data.

However, this would still be a fairly large endeavor. One way to focus the list even more though would be to only look at phosphosites that are significantly and highly detected in just the tumor samples. You can then compare that list to the phosphosites found in the DNAJB1-PRKACA condition of the *in vitro* assay; you could even make this a more stringent comparison by only considering a match with DNAJB1-PRKACA valid if DNAJB1-PRKACA is the only one detected of the four conditions *in vitro* or if DNAJB1-PRKACA's intensity value is twice that of PRKACA's when they are both detected *in vitro.*

Focusing on proteins that are part of a pathway that seems over-represented among the potential substrates would be another way to let this data guide you to a next step. For instance, probing further at specific catabolic processes that DNAJB1-PRKACA could affect or delving deeper into RNA splicing mechanisms that may be important to FLC.

Chapter V: Concluding Remarks

The work presented in this thesis focused on addressing the open question of whether or not the oncogenic kinase DNAJB1-PRKACA has different substrates than PRKACA that are relevant in FLC. Establishing a known substrate-kinase interaction with pathological effects that is specific to DNAJB1-PRKACA would provide a different avenue for therapeutic development. There is no current way to inhibit the activity of DNAJB1-PRKACA without inhibiting the activity of the crucial native PRKACA. Understanding more about the structure of this oncogenic kinase and the biochemical functions of any slight structural differences would create avenues to exploit for therapeutic options.

My studies show that when PRKACA, DNAJB1-PRKACA, and PRKACA (L206R) have the same pool of substrates for the same amount of time at the same temperature, these kinases exhibit reproducible preferences for certain substrates over others. It is still possible that inside the cell the crucial component to differential phosphorylation is differential subcellular localization of DNAJB1-PRKACA and PRKACA. However, after seeing these results, I would be surprised if the pathology was only due to a difference in localization. I think it is likely a synergistic effect of intrinsic specificity and subcellular localization. It is also possible that the J-domain on the kinase is acting as a scaffold and this scaffold is providing a platform for carcinogenesis. Again, I am not ruling this out. However, I do feel confident that my data, which eliminates any localization variations, rules out the hypothesis that there are no differences in substrate specificity between PRKACA and DNAJB1-PRKACA intrinsic to their structure.

It is also possible that part of the reason this cancer is slow growing is that maybe the kinase isn't initially expressed at a level to be harmful because the *DNAJB1* promoter is tightly regulated. It may remain this way until a physical stressor or even a normal change in development hyperactives the DNAJB1 promoter. This hyperactivation would then release this oncogenic kinase to wreak havoc on the cell. Or maybe this PRKACA variant is the cell stressor that overtime activates the heat shock response due to some action it has that causes protein aggregates to form, but by activating the heat shock response, the consequence is actually upregulation of this kinase. Maybe part of the oncogenic nature of this kinase is dose dependent in some way that is specific to DNAJB1-PRKACA since overexpression of PRKACA did not result in FLC like tumors in our collaboration with the Lowe lab. Maybe the upregulation of multiple heat shock proteins we see in the transcriptomic data of FLC tumors is a clue that heat shock factors in general are getting elevated and increasing the levels of DNAJB1-PRKACA as an unintended consequence.

While there is plenty to still analyze and mine from the data I already have, I am keen to get back to some experiments. In the immediate future, I would like to repeat this triplicate *in vitro* FSBA-treated human hepatocyte assay with an additional kinase: a kinase-dead version of DNAJB1-PRKACA. This condition should yield the same results as the no kinase condition, but it would be surprising and interesting if it was significantly different. I also would like to try this assay using what we are calling normal liver from an FLC patient that we receive with their tumor samples. It is possible that there is something different about the normal livers of FLC patients that is shown on a protein level that is not detected by genomic analysis. Total MS analysis of this liver

sample may bury the key protein difference, but if a key difference is a certain substrate population present in normal FLC patient livers not found in the livers of non-FLC patients, then lysing the FLC patient's normal liver and subjecting it to this assay could reveal a new substrate population. Now that our lab has FLC cells robustly growing in a dish, it is also possible to consider doing this assay with the lysate of FLC cells.

The substrate specificity of DNAJB1-PRAKCA and PRKACA seen in the sequence logos of my data has already informed computational biology projects in the lab that will continue to investigate the subtle changes in the active pocket that could confer substrate specificity.

Appendix I: Materials and Methods

Mouse Liver Lysate

Livers were harvested from mice and homogenized in Lysis Buffer (150mM NaCl, 0.5% Triton X-100, 10% glycerol, 50mM Tris HCl pH 8.0, 1x Protease inhibitor) until sample mixture was consistent. These mixtures were then sonicated five times with brief one second pulses on ice followed by incubation on ice for 15-30 minutes. Then the mixtures were centrifuged at max speed for 20-30 minutes and supernatants were collected in a manner to avoid the fatty layer; this step may need to be repeated to sufficiently remove the fatty layer. The protein amount was then measured by Bradford (ThermoFisher). The samples were flash frozen or immediately treated with FSBA.

FSBA Treatment

As published for HeLa cells (Embogama and Pflum 2017).

Kinase Reactions with FSBA-Treated Lysates

Thoroughly exchange buffer of at least 100ug of FSBA-treated lysate to wash out any residual FSBA using 3kDa Ultracel Concentrators (Amicon) using a buffer optimal for the kinase to be optimally active. Reactions carried out with 1mM ATP of choice and 1ug of purified kinase for every 100ug of FSBA-treated lysate. Make sure to add PhosSTOP to desired concentration to maximize phosphorylation signal. Incubate at 30°C for 30min-2hr. Quench with 20mM EDTA.

In Vitro Assay with Mouse Liver Lysate

Digestion

Proteins were precipitated by ice-cold acetone (HPLC-grade, Sigma) overnight at -20C. Pellets were dissolved in 8M urea (GE Healthcare), 50 mM ammonium bicarbonate (AMBIC. Fluka Chemicals), 10mM dithiothreitol (EMD Chemicals) in water, and disulfide bonds were reduced for 1 hour at room temperature with vigorous shaking. Iodoaceamide (Sigma) was added to 20mM and alkylation proceeded for 1 hour at room temperature in the dark. Samples were diluted with 50 mM AMBIC and digested with lysyl endopeptidase (Wako) overnight at room temperature. The concentration of urea was adjusted to 1.5M using 50mM AMBIC, and the samples were further digested for six hours at room temperature, using sequencing grade modified trypsin (Promega). Digestion was stopped by acidification using either formic acid (FA, Fluka) or trifluoroacetic acid (TFA, Thermo), and peptides were purified using high-capacity 30 mg Oasis HLB cartridges (Waters), according to manufactorer specifications.

Phosphopeptide Enrichment

Peptides were subjected to a two-step phosphopeptide enrichment, first by in-house constructed titanium dioxide microtips as described by Larsen *et al* in 2005[1] with minor modifications followed by High-Select Fe-NTA Phosphopeptide Enrichment Kit (Thermo Scientific), according to manufacturer specifications.

LC-MS/MS

Solvent A was 0.1% formic acid in water and solvent B was 0.1% formic acid, 80 % acetonitrile (ACN) in water. All LC-MS solvents are of HPLC grade and purchased from Sigma.

Enriched phosphopeptides were separated using a Dionex 3000 Ultimate HPLC equipped with a NCS3500RS nano- and microflow pump (Dionex). Peptides were loaded onto a 100 µm*20mm Acclaim PepMap C18 trap column (Thermo Scientific) at 3µL/min. Separation was achieved using a 75µm*120mm pulled-emitter nanocolumn (Nikkyo Technos). Solvent B went from 1% to 5 % over 6 minutes, increased to 40% over 80 minutes followed by a sharp 1-minute increase to 90% where it was kept for 22 minutes. Peptides were analyzed using a Q-Exactive HF mass spectrometer (Thermo Scientific). Data was recorded in positive mode with Top 20 DDA acquisition. MS1 resolution was set to 60 000 and an MS2 resolution of 30 000. AGC targets of 3e6 (MS1) and 2e5 (MS2) were applied.

Database searching

RAW files were searched using MASCOT (Mass Matrix) through Proteome Discoverer v. 1.4 (Thermo Scientific) with the Percolator function enabled. The False Discovery Rate (FDR) was set to 1%. Data was queried against the *Mus musculus* proteome, concatenated with common contaminants. Oxidation of M, acetylation of protein N-terminus and phosphorylation of S and T were allowed as dynamic modifications. Carbamidomethylation of C was set as static modification. A maximum of 3 missed cleavages was allowed.

Thiophosphopeptides from Gel Bands

In-gel digestion

Bands were excised from the gel using a scalpel, cut into small pieces (roughly 2*2mm) and destained using a solution of 40% ACN, 100mM AMBIC in water. In-gel digestion was performed as described by Shevchenko *et. al*[5] using the same chemical suppliers as described in the section *In Vitro Assay with Mouse Liver Lysate*.

LC-MS/MS

The same solvents were used as described in the section *In Vitro Assay with Mouse Liver Lysate*.

Peptides were separated using a Dionex 3000 Ultimate HPLC equipped with a NCS3500RS nano- and microflow pump. Peptides were loaded onto a 100 µm*20mm Acclaim PepMap C18 trap column at 3µL/min. Separation was achieved using a 75µm*120mm pulled-emitter nanocolumn. Solvent B went from 1% to 5 % over 1 minute, increased to 38% over 20 minutes followed by a sharp 1-minute increase to 90% where it was kept for 15 minutes. Peptides were analyzed using a Q-Exactive HF mass spectrometer. Data was recorded in positive mode with Top 15 DDA acquisition. MS1 resolution was set to 60 000 and an MS2 resolution of 30 000. AGC targets of 3e6 (MS1) and 2e5 (MS2) were applied.

Database searching

RAW files were searched using MASCOT through Proteome Discoverer v. 1.4 with the Percolator function enabled. The False Discovery Rate (FDR) was set to 1%. Data was queried against the *Mus musculus* proteome, concatenated with common contaminants. Oxidation of M, acetylation of protein N-terminus, phosphorylation of S and T and thiophospho esterification of S and T were allowed as dynamic modifications. Carbamidomethylation of C was set as static modification. A maximum of 3 missed cleavages was allowed.

Human Hepatocyte Lysate

Hepatocytes were isolated from chimeric livers as described (de Jong et al. 2014; Vercauteren et al. 2016). Briefly, mice were anesthetized with ketamine/xylazine and a 24G angiocath was inserted into the inferior vena cava. Then the portal vein was cut, and the mouse liver was perfused sequentially with PBS-/- supplemented with heparin, Hanks buffered saline solution (HBSS) supplemented with 5mM EDTA and 50mM HEPES, and finally HBSS supplemented with 0.05% Type IV collagenase (Sigma Aldrich) and 1U/ml DNAse (Thermo Fisher, Waltham, MA). After perfusion, the liver was disrupted over a 70mm cell strainer, washed in PBS-/- and live hepatocytes enriched by Percoll density centrifugation. Hepatocytes were resuspended in 54% Percoll (GE Healthcare, Chicago, IL) and centrifuged at 100g for 5 minutes. After washing with PBS, cells were pelleted and kept at -20^{o}C until ready for lysis. Lysis requires the use of 1mL The mixtures were incubated with Lysis Buffer (150 mM NaCl, 0.5% Triton X-100, 10% glycerol, 50mM Tris HCl pH 8.0, 1x protease inhibitor) on ice for 15 minutes (1 mL Lysis

Buffer for every 20x10^6 cells) After incubation, the samples were centrifuged for 10 min at 4°C at 13.5 rpm and supernatant was collected. The protein amount was measured by Bradford (ThermoFisher), and the samples were flash frozen or immediately treated with FSBA.

In Vitro Assay with Human Hepatocyte Lysate

Digestion

Samples were digested and purified as described in the section *In Vitro Assay with Mouse Liver Lysate*.

Phosphopeptide Enrichment

Phosphopeptides were enriched as described in the section *In Vitro Assay with Mouse Liver Lysate*.

LC-MS/MS

Solvent A was 0.1% formic acid in water and solvent B was 0.1% formic acid, 80 % acetonitrile (ACN) in water. All LC-MS solvents are of HPLC grade and purchased from Sigma.

Enriched phosphopeptides were separated using a Dionex 3000 Ultimate HPLC equipped with a NCS3500RS nano- and microflow pump. Peptides were loaded onto a 100 µm*20mm Acclaim PepMap C18 trap column at 3µL/min. Separation was achieved using a 75µm*120mm pulled-emitter nanocolumn. Solvent B went from 1% to 4 % over 1 minute, increased to 38% over 60 minutes followed by a sharp 1-minute increase to 90% where it was kept for 15 minutes. Peptides were analyzed using a Q-Exactive HF mass spectrometer. Data was recorded in

positive mode with Top 20 DDA acquisition. MS1 resolution was set to 60 000 and an MS2 resolution of 30 000. AGC targets of 3e6 (MS1) and 2e5 (MS2) were applied.

Database Searching

Acquired RAW files were analyzed in the MaxQuant[3] framework (v. 1.6.0.13). Spectra were queried against the human proteome and searched with a 1% false discovery rate on both PSM and protein level. Carbamidomethylation of C was applied as a static modification and oxidation (M), acetylation (Protein N-terminus) and phosphorylation (S, T or Y) were applied as variable modifications. A maximum of 5 modifications was allowed on each peptide. Matching between runs was enabled.

Data analysis

Statistical analysis of the phosphosites was performed within the Perseus[4] framework (v. 1.6.1.3).

Intensities were log2 transformed and normalized by subtraction of the median in each experiment. Observed values in at least 2/3 replicates in at least one condition was required. Missing values were imputed by low-abundant random signals. Significant differences in phosphosite abundances were determined by Student's t-tests (p=0.05) and a permutation FDR truncated ANOVA test (FDR=0.01). Heatmaps were generated by performing hierarchical clustering with Euclidian distances of z-scored ANOVA-significant phosphosites.

FLC Patient Tumor and Normal Liver Tissue Processing

Liver samples were placed on dry ice immediately after resection and stored at -80 C. For tissue lysis, small pieces (2-5 mm in diameter) were cut from the specimen and placed in ice cold lysis buffer (5mM EGTA, 1mM EDTA, 1% Triton X-100, 150 mM NaCl, 50mM Tris pH 7.5) supplemented with cOmplete EDTA-free protease inhibitor (Roche), and PhosSTOP phosphatase inhibitor (Roche) tablets. Samples were sonicated on ice for 20-30 seconds and spun at 1,100 x RCF for 10 minutes. The supernatant was transferred to another tube and spun at 30,000 x RCF for 30 minutes. To avoid the lipid layer, the Eppendorf tube was punctured near the bottom (above the pellet) and the supernatant flowed into another tube until the lipid layer reached the level of the hole. Spins were performed at 4 C. The lysate was assayed for protein concentration using the BCA assay (Pierce).

Total Phosphoproteomics of FLC Patient Tumor versus Normal Liver Tissue

Digestion

Based on optical concentration measurements, 390 µg protein was withdrawn from all samples which were precipitated by acetone. Proteins were digested and peptides were purified as described in the section *In Vitro Assay with Mouse Liver Lysate*.

Phosphopeptide Enrichment

Peptides were again subjected to a two-step phosphopeptide enrichment, first by titanium dioxide batch enrichment as described by Thingholm and Larsen in 2016[2] The flow through was enriched by High-Select Fe-NTA Phosphopeptide

Enrichment Kit, according to manufacturer specifications and the two fractions were combined.

LC-MS/MS Analysis

Solvent A was 0.1% formic acid in water and solvent B was 0.1% formic acid, 80 % acetonitrile (ACN) in water. All LC-MS solvents are of LC/MS purity and purchased from Fisher Chemical.

Enriched phosphopeptides were separated using an Easy 1200 nLC (Thermo Scientific). Separation was achieved directly using a 75µm*120mm pulled-emitter nanocolumn without trap column loading. Solvent B went from 0% to 30% over 70 minutes and to 60 % over 10 minutes followed by a sharp 5-minute increase to 90% where it was kept for 15 minutes. Peptides were analyzed using a Orbitrap Fusion Lumos mass spectrometer (Thermo Scientific). Data was recorded in positive mode with Top 20 DDA acquisition and quadrupole isolation and HCD fragmentation (30% CE). MS1 resolution was set to 60 000 and an MS2 resolution of 30 000. AGC targets of 1e6 (MS1) and 8e4 (MS2) were applied.

Database searching

Acquired RAW files were analyzed as described in the section In Vitro Assay with Human Hepatocyte Lysate

Data Analysis

All phosphosite intensities were averaged among technical replicates. It was required that a site must be observed in at least 50% of technical replicates within each biological replicate, or the average would be replaced by “NaN”.

Statistical analysis of the average intensity values for the 3 patients was performed within the Perseus framework. Intensities were log2 transformed and normalized by subtraction of the median in each experiment. Observed values in at least 2/3 replicates in at least one condition was required. Missing values were imputed by low-abundant random signals. Significant differences in phosphosite abundances were determined by Student's t-tests (p=0.05).

Splicing with SplAdder

RNA was extracted from OCT embedded frozen tissue using the miRNeasy Mini Kit (Qiagen). Two samples from the primay tumor and 1 sample from the adjacent normal liver tissue. Paired-end RNA sequencing libraries (2x150 bp) were generated using the TruSeq Stranded Total RNA Sample Prep Kit, including ribosomal RNA depletion using Ribo-Zero (Illumina). These libraries were sequenced in an Illumina MiSeq system. Quality control of the resulting sequencing files was performed using FastQC and MultiQC (Ewels et al. 2016), followed by adapter trimming using BBDuk (included in BBMap v37.47). The trimmed reads were mapped to the annotated Human Genome GRCh38.92 using STAR v2.6.1 (Dobin et al. 2013). Alternative splicing events were quantified on the alignment files using splAdder (Raetsch & Kahles, version March-2019), including exon skip, intron retention, alternative 3'/5' splice site, multiple exon skip and mutually exclusive exons.

Huh7 Starvation Experiment

Huh7 and Huh7-chimera cell lines were grown in Dulbecco's Modified Eagle's medium (DMEM, Gibco) supplemented with 1X non-essential amino acids (NEAA, Gibco) and 10% fetal bovine serum (FBS, Sigma). ~16 hours prior to harvesting, one dish for each cell line was then starved in media containing only DMEM and 1X NEAA. Cells were then harvested by trypsinization, and samples were subjected to total protein concentration normalization using a DC Assay (Bio-Rad). Samples were then lysed in a solution containing RIPA (Alfa Aesar) with cOmplete protease inhibitors (Sigma) and phosSTOP (Sigma), run on a NuPAGE 4-12% Bis-Tris protein gel, transferred to a membrane, blocked in 5% milk in TBS-T, and incubated with the relevant primary antibodies. Each blot was incubated with either PKAα cat Antibody (sc-28315, Santa Cruz Biotechnology) or phospho-PKA substrate (100G7E, Cell Signaling Technology) at a 1:1000 dilution. Secondary antibodies were then added at a 1:50,000 dilution, developed with Amersham ECL Prime (GE Life Sciences), and imaged using a LI-COR chemiluminescent gel imager. All blots were then stripped and incubated with an antibody against actin at a dilution of 1:5000 as a control to ensure equal loading. Blots were then developed and visualized using the same Amersham ECL developing solution and LI-COR system.

Antibodies and Proteins and Constructs

pET151DNAJB1-PRAKCA-GST with thrombin cut site gift from Sergio Botero

pET151PRAKCA-GST with thrombin cut site gift from Sergio Botero

pET151DNAJB1-PRKACA tagless gift from Sergio Botero

pET151PRKACA tagless gift from Sergio Botero

PKAα cat antibody (sc-28315, Santa Cruz Biotechnology)

GST antibody (GE 27457701)

Thrombin (GE 27084601)

AcTEV (ThermoFisher 12575015)

Thiophosphate ester antibody for WB (ab92570, abcam)

Thiophosphate ester antibody for IP (ab133473, abcam)

Kinase Purifications and Assays

GST-tagged protein purification using Glutathione Sepharose 4B beads (GE), per manufacturer's protocol.

Kinase-Glo (Promega) per the manufacturer's protocol

Tycho for protein quality per the manufacturer's protocol

ADP-Glo (Promega):

Customized Assay Buffer not included in kit: (40 mM Tris (pH 7.5); 20 mM $MgCl_2$; 0.1% Tween 20; 2mM TCEP). Compounds are dispensed in 384-well plate with 10 µL/well Assay Buffer with ATP (final concentration of 10, 50, or 100 µM) The following reagents are added: 3 µL/well kemptide (final concentration of 50 or 250 µM depending on ATP concentration) and 2 µL/well DNAJB1-PRKACA (final concentration of 1 nM). The plates were sealed, centrifuged, and incubated at room temperature for 10 min when the kinase reactions had 10 µM ATP and for 15 minutes when the reactions had 50 µM or higher ATP. After incubation, 5 µL of ADP-Glo reagent were added to each well. These plates were centrifuged, sealed, shaken, and incubated for 60 min at room temperature. Then 10 µL of

kinase detection reagent were added to each well. Then the plates were again centrifuged, sealed, shaken, and incubated for 60 min at room temperature. The plates were then read, and luminescence was measured.

Kinase reactions with ATP-γ-S and subsequent alkylation and immunoprecipitation were conducted per the manufacturer's protocol (abcam).

Appendix II: Rights and Permissions

Figure 6. Reprinted by permission from Elsevier: Cell. Hanahan D, Weinberg RA. (2011). Hallmarks of Cancer: The Next Generation. Cell, *144,* 646-674., copyright (2011).

References

Abou-Alfa, G.K., Mayer, R.J., Cosgrove, D., et al. 2015. Randomized phase II study of everolimus (E), leuprolide + letrozole (LL), and E + LL (ELL) in patients (pts) with unresectable fibrolamellar carcinoma (FLC). *Journal of Clinical Oncology* 33(15_suppl), pp. e15149–e15149.

Ahn, J.-H., McAvoy, T., Rakhilin, S.V., Nishi, A., Greengard, P. and Nairn, A.C. 2007. Protein kinase A activates protein phosphatase 2A by phosphorylation of the B56delta subunit. *Proceedings of the National Academy of Sciences of the United States of America* 104(8), pp. 2979–2984.

Aligayer, H., Boyd, D.D., Heiss, M.M., Abdalla, E.K., Curley, S.A. and Gallick, G.E. 2002. Activation of Src kinase in primary colorectal carcinoma: an indicator of poor clinical prognosis. *Cancer* 94(2), pp. 344–351.

Allen, J.J., Li, M., Brinkworth, C.S., et al. 2007. A semisynthetic epitope for kinase substrates. *Nature Methods* 4(6), pp. 511–516.

Amano, M., Hamaguchi, T., Shohag, M.H., et al. 2015. Kinase-interacting substrate screening is a novel method to identify kinase substrates. *The Journal of Cell Biology* 209(6), pp. 895–912.

Bargmann, C.I., Hung, M.C. and Weinberg, R.A. 1986. Multiple independent activations of the neu oncogene by a point mutation altering the transmembrane domain of p185. *Cell* 45(5), pp. 649–657.

Bathon, K., Weigand, I., Vanselow, J.T., et al. 2019. Alterations in protein kinase A substrate specificity as a potential cause of cushing syndrome. *Endocrinology* 160(2), pp. 447–459.

Berman, M.A., Burnham, J.A. and Sheahan, D.G. 1988. Fibrolamellar carcinoma of the liver: an immunohistochemical study of nineteen cases and a review of the literature. *Human Pathology* 19(7), pp. 784–794.

Berthon, A.S., Szarek, E. and Stratakis, C.A. 2015. PRKACA: the catalytic subunit of protein kinase A and adrenocortical tumors. *Frontiers in cell and developmental biology* 3, p. 26.

Beuschlein, F., Fassnacht, M., Assié, G., et al. 2014. Constitutive activation of PKA catalytic subunit in adrenal Cushing's syndrome. *The New England Journal of Medicine* 370(11), pp. 1019–1028.

Bockus, L.B. and Humphries, K.M. 2015. cAMP-dependent Protein Kinase (PKA) Signaling Is Impaired in the Diabetic Heart. *The Journal of Biological Chemistry* 290(49), pp. 29250–29258.

Bosman FT, World Health Organization, International Agency for Research on Cancer 2010. WHO classification of tumours of the digestive system. In: Bosman, F. T. ed. *Classification of tumours of the digestive system*. Lyon: IARC Press, p. 417.

Boyle, S.N., Michaud, G.A., Schweitzer, B., Predki, P.F. and Koleske, A.J. 2007. A critical role for cortactin phosphorylation by Abl-family kinases in PDGF-induced dorsal-wave formation. *Current Biology* 17(5), pp. 445–451.

Brandon, E.P., Idzerda, R.L. and McKnight, G.S. 1997. PKA isoforms, neural pathways, and behaviour: making the connection. *Current Opinion in Neurobiology* 7(3), pp. 397–403.

Brostrom, C.O., Corbin, J.D., King, C.A. and Krebs, E.G. 1971. Interaction of the subunits of adenosine 3':5'-cyclic monophosphate-dependent protein kinase of muscle.

Proceedings of the National Academy of Sciences of the United States of America 68(10), pp. 2444–2447.

Brown, J.R. and Thornton, J.L. 1957. Percivall Pott (1714-1788) and chimney sweepers' cancer of the scrotum. *British journal of industrial medicine* 14(1), pp. 68–70.

Burdyga, A., Surdo, N.C., Monterisi, S., et al. 2018. Phosphatases control PKA-dependent functional microdomains at the outer mitochondrial membrane. *Proceedings of the National Academy of Sciences of the United States of America* 115(28), pp. E6497–E6506.

Burgers, P.P., Bruystens, J., Burnley, R.J., et al. 2016. Structure of smAKAP and its regulation by PKA-mediated phosphorylation. *The FEBS Journal* 283(11), pp. 2132–2148.

Calderwood, S.K. and Gong, J. 2016. Heat shock proteins promote cancer: it's a protection racket. *Trends in Biochemical Sciences* 41(4), pp. 311–323.

Cao, B., Lu, T.-W., Martinez Fiesco, J.A., et al. 2019. Structures of the PKA RIα Holoenzyme with the FLHCC Driver J-PKACα or Wild-Type PKACα. *Structure*.

Caplan, A.J. 2003. What is a co-chaperone? *Cell Stress & Chaperones* 8(2), pp. 105–107.

Caretta, A. and Mucignat-Caretta, C. 2011. Protein kinase a in cancer. *Cancers* 3(1), pp. 913–926.

Chatterjee, S. and Burns, T.F. 2017. Targeting heat shock proteins in cancer: A promising therapeutic approach. *International Journal of Molecular Sciences* 18(9).

Chaudhari, I.A., Khobragade, K., Bhandare, M. and Shrikhande, S.V. 2018. Management of fibrolamellar hepatocellular carcinoma. *Chinese clinical oncology* 7(5),

p. 51.

Cheung, J., Ginter, C., Cassidy, M., et al. 2015. Structural insights into mis-regulation of protein kinase A in human tumors. *Proceedings of the National Academy of Sciences of the United States of America* 112(5), pp. 1374–1379.

Chunta, J.L., Vistisen, K.S., Yazdi, Z. and Braun, R.D. 2012. Uptake rate of cationic mitochondrial inhibitor MKT-077 determines cellular oxygen consumption change in carcinoma cells. *Plos One* 7(5), p. e37471.

Clark, J., Edwards, S., John, M., et al. 2002. Identification of amplified and expressed genes in breast cancer by comparative hybridization onto microarrays of randomly selected cDNA clones. *Genes, Chromosomes and Cancer* 34(1), pp. 104–114.

Cohen, P. and Knebel, A. 2006. KESTREL: a powerful method for identifying the physiological substrates of protein kinases. *The Biochemical Journal* 393(Pt 1), pp. 1–6.

Colledge, M. and Scott, J.D. 1999. AKAPs: from structure to function. *Trends in Cell Biology* 9(6), pp. 216–221.

Cornella, H., Alsinet, C., Sayols, S., et al. 2015. Unique genomic profile of fibrolamellar hepatocellular carcinoma. *Gastroenterology* 148(4), p. 806–18.e10.

Cornfield, J., Haenszel, W., Hammond, E.C., Lilienfeld, A.M., Shimkin, M.B. and Wynder, E.L. 2009. Smoking and lung cancer: recent evidence and a discussion of some questions. 1959. *International Journal of Epidemiology* 38(5), pp. 1175–1191.

Craig, J.R., Peters, R.L., Edmondson, H.A. and Omata, M. 1980. Fibrolamellar carcinoma of the liver: a tumor of adolescents and young adults with distinctive clinico-pathologic features. *Cancer* 46(2), pp. 372–379.

Croce, C.M. 2009. Causes and consequences of microRNA dysregulation in cancer.

Nature Reviews. Genetics 10(10), pp. 704–714.

Crooks, G.E., Hon, G., Chandonia, J.M. and Brenner, S.E. 2004. WebLogo: a sequence logo generator. *Genome Research* 14(6), pp. 1188–1190.

Cruz, O., Laguna, A., Vancells, M., Krauel, L., Medina, M. and Mora, J. 2008. Fibrolamellar hepatocellular carcinoma in an infant and literature review. *Journal of Pediatric Hematology/Oncology* 30(12), pp. 968–971.

Cui, X., Choi, H.-K., Choi, Y.-S., et al. 2015. DNAJB1 destabilizes PDCD5 to suppress p53-mediated apoptosis. *Cancer Letters* 357(1), pp. 307–315.

Dagda, R.K. and Das Banerjee, T. 2015. Role of protein kinase A in regulating mitochondrial function and neuronal development: implications to neurodegenerative diseases. *Reviews in the neurosciences* 26(3), pp. 359–370.

Darcy, D.G., Chiaroni-Clarke, R., Murphy, J.M., et al. 2015. The genomic landscape of fibrolamellar hepatocellular carcinoma: whole genome sequencing of ten patients. *Oncotarget* 6(2), pp. 755–770.

Dephoure, N., Gould, K.L., Gygi, S.P. and Kellogg, D.R. 2013. Mapping and analysis of phosphorylation sites: a quick guide for cell biologists. *Molecular Biology of the Cell* 24(5), pp. 535–542.

DeSouza, N., Reiken, S., Ondrias, K., Yang, Y.-M., Matkovich, S. and Marks, A.R. 2002. Protein kinase A and two phosphatases are components of the inositol 1,4,5-trisphosphate receptor macromolecular signaling complex. *The Journal of Biological Chemistry* 277(42), pp. 39397–39400.

Dinh, T.A., Vitucci, E.C.M., Wauthier, E., et al. 2017. Comprehensive analysis of The Cancer Genome Atlas reveals a unique gene and non-coding RNA signature of

fibrolamellar carcinoma. *Scientific reports* 7, p. 44653.

Dobin, A., Davis, C.A., Schlesinger, F., et al. 2013. STAR: ultrafast universal RNA-seq aligner. *Bioinformatics* 29(1), pp. 15–21.

Doll, R. and Hill, A.B. 1950. Smoking and carcinoma of the lung; preliminary report. *British medical journal* 2(4682), pp. 739–48.

Edmondson, H.A. 1956. Differential diagnosis of tumors and tumor-like lesions of liver in infancy and childhood. *Archives of Pediatrics & Adolescent Medicine* 91(2), p. 168.

Eiringhaus, J., Herting, J., Schatter, F., et al. 2019. Protein kinase/phosphatase balance mediates the effects of increased late sodium current on ventricular calcium cycling. *Basic Research in Cardiology* 114(2), p. 13.

El-Gazzaz, G., Wong, W., El-Hadary, M.K., et al. 2000. Outcome of liver resection and transplantation for fibrolamellar hepatocellular carcinoma. *Transplant International* 13(0), pp. S406–S409.

El-Serag, H.B. and Davila, J.A. 2004. Is fibrolamellar carcinoma different from hepatocellular carcinoma? A US population-based study. *Hepatology* 39(3), pp. 798–803.

Embogama, D.M. and Pflum, M.K.H. 2017. K-BILDS: A Kinase Substrate Discovery Tool. *Chembiochem* 18(1), pp. 136–141.

Engelholm, L.H., Riaz, A., Serra, D., et al. 2017. CRISPR/Cas9 Engineering of Adult Mouse Liver Demonstrates That the Dnajb1-Prkaca Gene Fusion Is Sufficient to Induce Tumors Resembling Fibrolamellar Hepatocellular Carcinoma. *Gastroenterology* 153(6), p. 1662–1673.e10.

Epstein, P.M. 2017. Different phosphodiesterases (PDEs) regulate distinct

phosphoproteomes during cAMP signaling. *Proceedings of the National Academy of Sciences of the United States of America* 114(30), pp. 7741–7743.

Espiard, S. and Bertherat, J. 2015. The genetics of adrenocortical tumors. *Endocrinology and Metabolism Clinics of North America* 44(2), pp. 311–334.

Esquela-Kerscher, A. and Slack, F.J. 2006. Oncomirs - microRNAs with a role in cancer. *Nature Reviews. Cancer* 6(4), pp. 259–269.

Ewels, P., Magnusson, M., Lundin, S. and Käller, M. 2016. MultiQC: summarize analysis results for multiple tools and samples in a single report. *Bioinformatics* 32(19), pp. 3047–3048.

Fischer, E.H., Graves, D.J., Crittenden, E.R.S. and Krebs, E.G. 1959. Structure of the site phosphorylated in the phosphorylase b to a reaction. *The Journal of Biological Chemistry* 234(7), pp. 1698–1704.

Fischer, E.H. and Krebs, E.G. 1955. Conversion of phosphorylase b to phosphorylase a in muscle extracts. *The Journal of Biological Chemistry* 216(1), pp. 121–132.

Freitas, A.A. and de Magalhães, J.P. 2011. A review and appraisal of the DNA damage theory of ageing. *Mutation Research* 728(1–2), pp. 12–22.

Giam, M. and Rancati, G. 2015. Aneuploidy and chromosomal instability in cancer: a jackpot to chaos. *Cell Division* 10, p. 3.

Gill, G.N. and Garren, L.D. 1970. A cyclic-3',5'-adenosine monophosphate dependent protein kinase from the adrenal cortex: comparison with a cyclic AMP binding protein. *Biochemical and Biophysical Research Communications* 39(3), pp. 335–343.

Gold, M.G., Gonen, T. and Scott, J.D. 2013. Local cAMP signaling in disease at a glance. *Journal of Cell Science* 126(Pt 20), pp. 4537–4543.

Graham, R.P., Jin, L., Knutson, D.L., et al. 2015. DNAJB1-PRKACA is specific for fibrolamellar carcinoma. *Modern Pathology* 28(6), pp. 822–829.

Graham, R.P. and Torbenson, M.S. 2017. Fibrolamellar carcinoma: A histologically unique tumor with unique molecular findings. *Seminars in diagnostic pathology* 34(2), pp. 146–152.

Griffith, O.L., Griffith, M., Krysiak, K., et al. 2016. A genomic case study of mixed fibrolamellar hepatocellular carcinoma. *Annals of Oncology* 27(6), pp. 1148–1154.

Hageman, J. and Kampinga, H.H. 2009. Computational analysis of the human HSPH/HSPA/DNAJ family and cloning of a human HSPH/HSPA/DNAJ expression library. *Cell Stress & Chaperones* 14(1), pp. 1–21.

Hamaguchi, T., Nakamuta, S., Funahashi, Y., et al. 2015. In vivo screening for substrates of protein kinase A using a combination of proteomic approaches and pharmacological modulation of kinase activity. *Cell Structure and Function* 40(1), pp. 1–12.

Hanahan, D. and Weinberg, R.A. 2011. Hallmarks of cancer: the next generation. *Cell* 144(5), pp. 646–674.

Hanahan, D. and Weinberg, R.A. 2000. The hallmarks of cancer. *Cell* 100(1), pp. 57–70.

Hara, M., Lourido, S., Petrova, B., et al. 2018. Identification of PNG kinase substrates uncovers interactions with the translational repressor TRAL in the oocyte-to-embryo transition. *eLife* 7.

Hemming, A.W., Langer, B., Sheiner, P., Greig, P.D. and Taylor, B.R. 1997. Aggressive surgical management of fibrolamellar hepatocellular carcinoma. *Journal of*

Gastrointestinal Surgery 1(4), pp. 342–346.

Hennessy, F., Nicoll, W.S., Zimmermann, R., Cheetham, M.E. and Blatch, G.L. 2005. Not all J domains are created equal: implications for the specificity of Hsp40-Hsp70 interactions. *Protein Science* 14(7), pp. 1697–1709.

Hensen, S.M.M., Heldens, L., van Enckevort, C.M.W., van Genesen, S.T., Pruijn, G.J.M. and Lubsen, N.H. 2012. Heat shock factor 1 is inactivated by amino acid deprivation. *Cell Stress & Chaperones* 17(6), pp. 743–755.

Hernández, M.P., Chadli, A. and Toft, D.O. 2002. HSP40 binding is the first step in the HSP90 chaperoning pathway for the progesterone receptor. *The Journal of Biological Chemistry* 277(14), pp. 11873–11881.

Herter-Sprie, G.S., Greulich, H. and Wong, K.-K. 2013. Activating mutations in ERBB2 and their impact on diagnostics and treatment. *Frontiers in oncology* 3, p. 86.

Hertz, N.T., Wang, B.T., Allen, J.J., et al. 2010. Chemical genetic approach for kinase-substrate mapping by covalent capture of thiophosphopeptides and analysis by mass spectrometry. *Current protocols in chemical biology* 2(1), pp. 15–36.

Hofmann, F., Beavo, J.A., Bechtel, P.J. and Krebs, E.G. 1975. Comparison of adenosine 3':5'-monophosphate-dependent protein kinases from rabbit skeletal and bovine heart muscle. *The Journal of Biological Chemistry* 250(19), pp. 7795–7801.

Honeyman, J.N., Simon, E.P., Robine, N., et al. 2014. Detection of a recurrent DNAJB1-PRKACA chimeric transcript in fibrolamellar hepatocellular carcinoma. *Science* 343(6174), pp. 1010–1014.

Horiuchi, J., Yamazaki, D., Naganos, S., Aigaki, T. and Saitoe, M. 2008. Protein kinase A inhibits a consolidated form of memory in Drosophila. *Proceedings of the National*

Academy of Sciences of the United States of America 105(52), pp. 20976–20981.

Hu, J., Rho, H.-S., Newman, R.H., Zhang, J., Zhu, H. and Qian, J. 2014. PhosphoNetworks: a database for human phosphorylation networks. *Bioinformatics* 30(1), pp. 141–142.

Hulsen, T., de Vlieg, J. and Alkema, W. 2008. BioVenn – a web application for the comparison and visualization of biological lists using area-proportional Venn diagrams. *BMC Genomics* 9, p. 488.

Imamura, H., Wagih, O., Niinae, T., Sugiyama, N., Beltrao, P. and Ishihama, Y. 2017. Identifications of Putative PKA Substrates with Quantitative Phosphoproteomics and Primary-Sequence-Based Scoring. *Journal of Proteome Research* 16(4), pp. 1825–1830.

Isobe, K., Jung, H.J., Yang, C.-R., et al. 2017. Systems-level identification of PKA-dependent signaling in epithelial cells. *Proceedings of the National Academy of Sciences of the United States of America* 114(42), pp. E8875–E8884.

de Jong, Y.P., Dorner, M., Mommersteeg, M.C., et al. 2014. Broadly neutralizing antibodies abrogate established hepatitis C virus infection. *Science Translational Medicine* 6(254), p. 254ra129.

Kahles, A., Ong, C.S., Zhong, Y. and Rätsch, G. 2016. SplAdder: identification, quantification and testing of alternative splicing events from RNA-Seq data. *Bioinformatics* 32(12), pp. 1840–1847.

Kakar, S., Burgart, L.J., Batts, K.P., Garcia, J., Jain, D. and Ferrell, L.D. 2005. Clinicopathologic features and survival in fibrolamellar carcinoma: comparison with conventional hepatocellular carcinoma with and without cirrhosis. *Modern Pathology*

18(11), pp. 1417–1423.

Kampinga, H.H. and Craig, E.A. 2010. The HSP70 chaperone machinery: J proteins as drivers of functional specificity. *Nature Reviews. Molecular Cell Biology* 11(8), pp. 579–592.

Kanazawa, Y., Isomoto, H., Oka, M., et al. 2003. Expression of heat shock protein (Hsp) 70 and Hsp 40 in colorectal cancer. *Medical Oncology* 20(2), pp. 157–164.

Karagöz, G.E. and Rüdiger, S.G.D. 2015. Hsp90 interaction with clients. *Trends in Biochemical Sciences* 40(2), pp. 117–125.

Kastenhuber, E.R., Lalazar, G., Houlihan, S.L., et al. 2017. DNAJB1-PRKACA fusion kinase interacts with β-catenin and the liver regenerative response to drive fibrolamellar hepatocellular carcinoma. *Proceedings of the National Academy of Sciences of the United States of America* 114(50), pp. 13076–13084.

Katzenstein, H.M., Krailo, M.D., Malogolowkin, M.H., et al. 2003. Fibrolamellar hepatocellular carcinoma in children and adolescents. *Cancer* 97(8), pp. 2006–2012.

Kityk, R., Kopp, J. and Mayer, M.P. 2018. Molecular Mechanism of J-Domain-Triggered ATP Hydrolysis by Hsp70 Chaperones. *Molecular Cell* 69(2), p. 227–237.e4.

Knebel, A., Morrice, N. and Cohen, P. 2001. A novel method to identify protein kinase substrates: eEF2 kinase is phosphorylated and inhibited by SAPK4/p38delta. *The EMBO Journal* 20(16), pp. 4360–4369.

Knighton, D.R., Zheng, J.H., Ten Eyck, L.F., et al. 1991. Crystal structure of the catalytic subunit of cyclic adenosine monophosphate-dependent protein kinase. *Science* 253(5018), pp. 407–414.

Krebs, E.G. and Fischer, E.H. 1955. Phosphorylase activity of skeletal muscle extracts.

The Journal of Biological Chemistry 216(1), pp. 113–120.

Krebs, E.G., Graves, D.J. and Fischer, E.H. 1959. Factors affecting the activity of muscle phosphorylase b kinase. *The Journal of Biological Chemistry* 234, pp. 2867–2873.

Lack, E.E., Neave, C. and Vawter, G.F. 1983. Hepatocellular carcinoma. Review of 32 cases in childhood and adolescence. *Cancer* 52(8), pp. 1510–1515.

Lahiri Batra, S. 2019. Management of gynecologic cancers in relation to genetic predisposition. *Seminars in oncology nursing*.

Langer, T., Lu, C., Echols, H., Flanagan, J., Hayer, M.K. and Hartl, F.U. 1992. Successive action of DnaK, DnaJ and GroEL along the pathway of chaperone-mediated protein folding. *Nature* 356(6371), pp. 683–689.

Layland, J., Solaro, R.J. and Shah, A.M. 2005. Regulation of cardiac contractile function by troponin I phosphorylation. *Cardiovascular Research* 66(1), pp. 12–21.

Leslie, S.N. and Nairn, A.C. 2019. cAMP regulation of protein phosphatases PP1 and PP2A in brain. *Biochimica et biophysica acta. Molecular cell research* 1866(1), pp. 64–73.

Li, F.P. and Fraumeni, J.F. 1969. Soft-tissue sarcomas, breast cancer, and other neoplasms. A familial syndrome? *Annals of Internal Medicine* 71(4), pp. 747–752.

Li, X., Huston, E., Lynch, M.J., Houslay, M.D. and Baillie, G.S. 2006. Phosphodiesterase-4 influences the PKA phosphorylation status and membrane translocation of G-protein receptor kinase 2 (GRK2) in HEK-293beta2 cells and cardiac myocytes. *The Biochemical Journal* 394(Pt 2), pp. 427–435.

Lianos, G.D., Alexiou, G.A., Mangano, Alberto, et al. 2015. The role of heat shock

proteins in cancer. *Cancer Letters* 360(2), pp. 114–118.

Liberek, K., Marszalek, J., Ang, D., Georgopoulos, C. and Zylicz, M. 1991. Escherichia coli DnaJ and GrpE heat shock proteins jointly stimulate ATPase activity of DnaK. *Proceedings of the National Academy of Sciences of the United States of America* 88(7), pp. 2874–2878.

Lipinski, K.A., Barber, L.J., Davies, M.N., Ashenden, M., Sottoriva, A. and Gerlinger, M. 2016. Cancer evolution and the limits of predictability in precision cancer medicine. *Trends in cancer* 2(1), pp. 49–63.

Liu, Z., Yu, M., Fei, B., Fang, X., Ma, T. and Wang, D. 2018. miR-21-5p targets PDHA1 to regulate glycolysis and cancer progression in gastric cancer. *Oncology Reports* 40(5), pp. 2955–2963.

Lubner, J.M., Dodge-Kafka, K.L., Carlson, C.R., Church, G.M., Chou, M.F. and Schwartz, D. 2017. Cushing's syndrome mutant PKAL205R exhibits altered substrate specificity. *FEBS Letters* 591(3), pp. 459–467.

Maitra, A., Ramnani, D.M., Margraf, L.R. and Gazdar, A.F. 2000. Synchronous wilms tumor and fibrolamellar hepatocellular carcinoma: report of a case. *Pediatric and developmental pathology : the official journal of the Society for Pediatric Pathology and the Paediatric Pathology Society* 3(5), pp. 492–496.

Malkin, D., Li, F.P., Strong, L.C., et al. 1990. Germ line p53 mutations in a familial syndrome of breast cancer, sarcomas, and other neoplasms. *Science* 250(4985), pp. 1233–1238.

Malouf, G.G., Job, S., Paradis, V., et al. 2014. Transcriptional profiling of pure fibrolamellar hepatocellular carcinoma reveals an endocrine signature. *Hepatology*

59(6), pp. 2228–2237.

Mavros, M.N., Mayo, S.C., Hyder, O. and Pawlik, T.M. 2012. A systematic review: treatment and prognosis of patients with fibrolamellar hepatocellular carcinoma. *Journal of the American College of Surgeons* 215(6), pp. 820–830.

Mayo, S.C., Mavros, M.N., Nathan, H., et al. 2014. Treatment and prognosis of patients with fibrolamellar hepatocellular carcinoma: a national perspective. *Journal of the American College of Surgeons* 218(2), pp. 196–205.

Murphy, M.E. 2013. The HSP70 family and cancer. *Carcinogenesis* 34(6), pp. 1181–1188.

Naviglio, S., Caraglia, M., Abbruzzese, A., et al. 2009. Protein kinase A as a biological target in cancer therapy. *Expert Opinion on Therapeutic Targets* 13(1), pp. 83–92.

Neckers, L. and Workman, P. 2012. Hsp90 molecular chaperone inhibitors: are we there yet? *Clinical Cancer Research* 18(1), pp. 64–76.

de Oliveira, P.S.L., Ferraz, F.A.N., Pena, D.A., Pramio, D.T., Morais, F.A. and Schechtman, D. 2016. Revisiting protein kinase-substrate interactions: Toward therapeutic development. *Science Signaling* 9(420), p. re3.

Olsen, S.R. and Uhler, M.D. 1989. Affinity purification of the C alpha and C beta isoforms of the catalytic subunit of cAMP-dependent protein kinase. *The Journal of Biological Chemistry* 264(31), pp. 18662–18666.

Ottenhoff-Kalff, A.E., Rijksen, G., van Beurden, E.A., Hennipman, A., Michels, A.A. and Staal, G.E. 1992. Characterization of protein tyrosine kinases from human breast cancer: involvement of the c-src oncogene product. *Cancer Research* 52(17), pp. 4773–4778.

Palorini, R., Votta, G., Pirola, Y., et al. 2016. Protein kinase A activation promotes cancer cell resistance to glucose starvation and anoikis. *PLoS Genetics* 12(3), p. e1005931.

Park, S.-Y., Choi, H.-K., Seo, J.S., et al. 2015. DNAJB1 negatively regulates MIG6 to promote epidermal growth factor receptor signaling. *Biochimica et Biophysica Acta* 1853(10 Pt A), pp. 2722–2730.

Parkes, A., Arun, B.K. and Litton, J.K. 2017. Systemic Treatment Strategies for Patients with Hereditary Breast Cancer Syndromes. *The Oncologist* 22(6), pp. 655–666.

Patra, K.C., Kato, Y., Mizukami, Y., et al. 2018. Mutant GNAS drives pancreatic tumourigenesis by inducing PKA-mediated SIK suppression and reprogramming lipid metabolism. *Nature Cell Biology* 20(7), pp. 811–822.

Pellecchia, M., Szyperski, T., Wall, D., Georgopoulos, C. and Wüthrich, K. 1996. NMR structure of the J-domain and the Gly/Phe-rich region of the Escherichia coli DnaJ chaperone. *Journal of Molecular Biology* 260(2), pp. 236–250.

Pritchard-Jones, K. 1996. Genetics of childhood cancer. *British Medical Bulletin* 52(4), pp. 704–723.

Propper, D.J., Braybrooke, J.P., Taylor, D.J., et al. 1999. Phase I trial of the selective mitochondrial toxin MKT077 in chemo-resistant solid tumours. *Annals of Oncology* 10(8), pp. 923–927.

Ptacek, J., Devgan, G., Michaud, G., et al. 2005. Global analysis of protein phosphorylation in yeast. *Nature* 438(7068), pp. 679–684.

Qi, M., Zhang, J., Zeng, W. and Chen, X. 2014. DNAJB1 stabilizes MDM2 and contributes to cancer cell proliferation in a p53-dependent manner. *Biochimica et*

Biophysica Acta 1839(1), pp. 62–69.

Qian, Y.Q., Patel, D., Hartl, F.U. and McColl, D.J. 1996. Nuclear magnetic resonance solution structure of the human Hsp40 (HDJ-1) J-domain. *Journal of Molecular Biology* 260(2), pp. 224–235.

Rodu, B. and Cole, P. 2002. Impact of the American anti-smoking campaign on lung cancer mortality. *International Journal of Cancer* 97(6), pp. 804–806.

Rosen, O.M., Rubin, C.S. and Erlighman, J. 1975. Properties of the cyclid AMP-dependent protein kinase from bovine and porcine heart. *Advances in enzyme regulation* 13, pp. 173–185.

Rothenberg, D.A., Gordon, E.A., White, F.M. and Lourido, S. 2016. Identification of Direct Kinase Substrates Using Analogue-Sensitive Alleles. *Methods in Molecular Biology* 1355, pp. 71–84.

Rous, P. 1911. A sarcoma of the fowl transmissible by an agent separable from the tumor cells. *The Journal of Experimental Medicine* 13(4), pp. 397–411.

Rous, P. 1910. A transmissible avian neoplasm. (sarcoma of the common fowl.). *The Journal of Experimental Medicine* 12(5), pp. 696–705.

Rowley, J.D. 1973. Letter: A new consistent chromosomal abnormality in chronic myelogenous leukaemia identified by quinacrine fluorescence and Giemsa staining. *Nature* 243(5405), pp. 290–293.

Rust, H.L. and Thompson, P.R. 2011. Kinase consensus sequences: a breeding ground for crosstalk. *ACS Chemical Biology* 6(9), pp. 881–892.

Saab, S. and Yao, F. 1996. Fibrolamellar hepatocellular carcinoma. Case reports and a review of the literature. *Digestive Diseases and Sciences* 41(10), pp. 1981–1985.

Sapio, L., Di Maiolo, F., Illiano, M., et al. 2014. Targeting protein kinase A in cancer therapy: an update. *EXCLI journal* 13, pp. 843–855.

Schneider, T.D. and Stephens, R.M. 1990. Sequence logos: a new way to display consensus sequences. *Nucleic Acids Research* 18(20), pp. 6097–6100.

Shaikh, D., Zhou, Q., Chen, T., Ibe, J.C.F., Raj, J.U. and Zhou, G. 2012. cAMP-dependent protein kinase is essential for hypoxia-mediated epithelial-mesenchymal transition, migration, and invasion in lung cancer cells. *Cellular Signalling* 24(12), pp. 2396–2406.

Shih, C., Shilo, B.Z., Goldfarb, M.P., Dannenberg, A. and Weinberg, R.A. 1979. Passage of phenotypes of chemically transformed cells via transfection of DNA and chromatin. *Proceedings of the National Academy of Sciences of the United States of America* 76(11), pp. 5714–5718.

Sidera, K. and Patsavoudi, E. 2014. HSP90 inhibitors: current development and potential in cancer therapy. *Recent patents on anti-cancer drug discovery* 9(1), pp. 1–20.

Siegel, R.L., Miller, K.D. and Jemal, A. 2019. Cancer statistics, 2019. *CA: A Cancer Journal for Clinicians* 69(1), pp. 7–34.

Simon, E.P., Freije, C.A., Farber, B.A., et al. 2015. Transcriptomic characterization of fibrolamellar hepatocellular carcinoma. *Proceedings of the National Academy of Sciences of the United States of America* 112(44), pp. E5916-25.

Smith, F.D. and Scott, J.D. 2018. Protein kinase A activation: Something new under the sun? *The Journal of Cell Biology* 217(6), pp. 1895–1897.

Soares, J.P., Cortinhas, A., Bento, T., et al. 2014. Aging and DNA damage in humans: a

meta-analysis study. *Aging* 6(6), pp. 432–439.

Sorenson, E.C., Khanin, R., Bamboat, Z.M., et al. 2017. Genome and transcriptome profiling of fibrolamellar hepatocellular carcinoma demonstrates p53 and IGF2BP1 dysregulation. *Plos One* 12(5), p. e0176562.

Stehelin, D., Fujita, D.J., Padgett, T., Varmus, H.E. and Bishop, J.M. 1977. Detection and enumeration of transformation-defective strains of avian sarcoma virus with molecular hybridization. *Virology* 76(2), pp. 675–684.

Stehelin, D., Varmus, H.E., Bishop, J.M. and Vogt, P.K. 1976. DNA related to the transforming gene(s) of avian sarcoma viruses is present in normal avian DNA. *Nature* 260(5547), pp. 170–173.

Stratakis, C.A. 2012. Cyclic AMP, protein kinase A, and phosphodiesterases: proceedings of an international workshop. *Hormone and Metabolic Research* 44(10), pp. 713–715.

Svet-Moldavsky, G.J. 1957. Development of Multiple Cysts and of Hæmorrhagic Affections of Internal Organs in Albino Rats treated during the Embryonic or New-born Period with Rous Sarcoma Virus. *Nature* 180(4597), pp. 1299–1300.

Svet-Moldavsky, G.J. 1958. Sarcoma in Albino Rats treated during the Embryonic Stage with Rous Virus. *Nature* 182(4647), pp. 1452–1453.

Szklarczyk, D., Gable, A.L., Lyon, D., et al. 2019. STRING v11: protein-protein association networks with increased coverage, supporting functional discovery in genome-wide experimental datasets. *Nucleic Acids Research* 47(D1), pp. D607–D613.

Tabin, C.J., Bradley, S.M., Bargmann, C.I., et al. 1982. Mechanism of activation of a human oncogene. *Nature* 300(5888), pp. 143–149.

Tao, M., Salas, M.L. and Lipmann, F. 1970. Mechanism of activation by adenosine 3':5'-cyclic monophosphate of a protein phosphokinase from rabbit reticulocytes. *Proceedings of the National Academy of Sciences of the United States of America* 67(1), pp. 408–414.

Temin, H.M. 1960. The control of cellular morphology in embryonic cells infected with rous sarcoma virus in vitro. *Virology* 10, pp. 182–197.

Tomasini, M.D., Wang, Y., Karamafrooz, A., et al. 2018. Conformational Landscape of the PRKACA-DNAJB1 Chimeric Kinase, the Driver for Fibrolamellar Hepatocellular Carcinoma. *Scientific reports* 8(1), p. 720.

Torbenson, M. 2012. Fibrolamellar carcinoma: 2012 update. *Scientifica* 2012, p. 743790.

Torbenson, M., Wang, J., Choti, M., et al. 2002. Hepatocellular carcinomas show abnormal expression of fibronectin protein. *Modern Pathology* 15(8), pp. 826–830.

Torres-Quesada, O., Mayrhofer, J.E. and Stefan, E. 2017. The many faces of compartmentalized PKA signalosomes. *Cellular Signalling* 37, pp. 1–11.

Tracz-Gaszewska, Z., Klimczak, M., Biecek, P., et al. 2017. Molecular chaperones in the acquisition of cancer cell chemoresistance with mutated TP53 and MDM2 up-regulation. *Oncotarget* 8(47), pp. 82123–82143.

Tyanova, S., Temu, T., Sinitcyn, P., et al. 2016. The Perseus computational platform for comprehensive analysis of (prote)omics data. *Nature Methods* 13(9), pp. 731–740.

Vercauteren, K., Hoffman, B.E., Zolotukhin, I., et al. 2016. Superior In vivo Transduction of Human Hepatocytes Using Engineered AAV3 Capsid. *Molecular Therapy* 24(6), pp. 1042–1049.

Vogelstein, B., Fearon, E.R., Hamilton, S.R., et al. 1988. Genetic alterations during colorectal-tumor development. *The New England Journal of Medicine* 319(9), pp. 525–532.

Vogelstein, B. and Kinzler, K.W. 1993. The multistep nature of cancer. *Trends in Genetics* 9(4), pp. 138–141.

Walsh, D.A., Perkins, J.P. and Krebs, E.G. 1968. An adenosine 3',5'-monophosphate-dependant protein kinase from rabbit skeletal muscle. *The Journal of Biological Chemistry* 243(13), pp. 3763–3765.

Wand, G., Levine, M., Zweifel, L., Schwindinger, W. and Abel, T. 2001. The cAMP-protein kinase A signal transduction pathway modulates ethanol consumption and sedative effects of ethanol. *The Journal of Neuroscience* 21(14), pp. 5297–5303.

Wang, L.H., Duesberg, P.H., Kawai, S. and Hanafusa, H. 1976. Location of envelope-specific and sarcoma-specific oligonucleotides on RNA of Schmidt-Ruppin Rous sarcoma virus. *Proceedings of the National Academy of Sciences of the United States of America* 73(2), pp. 447–451.

Waugh, D.S. 2011. An overview of enzymatic reagents for the removal of affinity tags. *Protein Expression and Purification* 80(2), pp. 283–293.

Wawrzynow, B., Zylicz, A. and Zylicz, M. 2018. Chaperoning the guardian of the genome. The two-faced role of molecular chaperones in p53 tumor suppressor action. *Biochimica et biophysica acta. Reviews on cancer* 1869(2), pp. 161–174.

Weeda, V.B., Murawski, M., McCabe, A.J., et al. 2013. Fibrolamellar variant of hepatocellular carcinoma does not have a better survival than conventional hepatocellular carcinoma--results and treatment recommendations from the Childhood

Liver Tumour Strategy Group (SIOPEL) experience. *European Journal of Cancer* 49(12), pp. 2698–2704.

Weiss, R.A. and Vogt, P.K. 2011. 100 years of Rous sarcoma virus. *The Journal of Experimental Medicine* 208(12), pp. 2351–2355.

Wheeler, D.L., Iida, M. and Dunn, E.F. 2009. The role of Src in solid tumors. *The Oncologist* 14(7), pp. 667–678.

Willoughby, A., Andreassen, P.R. and Toland, A.E. 2019. Genetic Testing to Guide Risk-Stratified Screens for Breast Cancer. *Journal of personalized medicine* 9(1).

Wu, J., Liu, T., Rios, Z., Mei, Q., Lin, X. and Cao, S. 2017. Heat shock proteins and cancer. *Trends in Pharmacological Sciences* 38(3), pp. 226–256.

Wynder, E.L. and Graham, E.A. 1950. Tobacco smoking as a possible etiologic factor in bronchiogenic carcinoma; a study of 684 proved cases. *Journal of the American Medical Association* 143(4), pp. 329–336.

Xu, L., Hazard, F.K., Zmoos, A.-F., et al. 2015. Genomic analysis of fibrolamellar hepatocellular carcinoma. *Human Molecular Genetics* 24(1), pp. 50–63.

Yu, Y.-P., Liu, P., Nelson, J., et al. 2019. Identification of recurrent fusion genes across multiple cancer types. *Scientific reports* 9(1), p. 1074.

Zhang, P., Kornev, A.P., Wu, J. and Taylor, S.S. 2015. Discovery of allostery in PKA signaling. *Biophysical reviews* 7(2), pp. 227–238.